Combination Surface Strategies that Improve the Longevity, Tunability, and Antifouling Properties of Nitric Oxide-Releasing Platforms

By

Megan Douglass

(Under the Direction of Hitesh Handa)

ABSTRACT

Blood-contacting medical devices are routinely impacted by two clinical complications: infection and device-induced thrombosis. Due to nitric oxide (NO)'s endogenous role as an antimicrobial and antithrombotic agent, NO-releasing platforms have gained tremendous popularity for combatting both clotting and infection. However, NO-releasing materials have three major shortcomings that limit commercial applications: (1) a limited NO reservoir, (2) a lack of NO release tunability, and (3) an inability to prevent biofouling.

In this dissertation work, NO-releasing materials were combined with different surface strategies to improve the longevity, tunability, and antifouling properties of NO-releasing platforms. In the first approach, a novel polymeric platform that could explicitly release NO from the material's NO reservoir as well as generate NO from interaction with endogenous NO donors was demonstrated using an *S*-nitroso-*N*-acetylpenicillamine (SNAP)-doped polymer with a selenium interface. The SNAP-Se platform exhibited potent antimicrobial activity (>99% reduction in *Staphylococcus aureus* and *Escherichia coli*) and reduced *in vitro* platelet adhesion by 85.5% compared to controls.

In the second approach, polymeric coatings containing the NO donor S-nitrosoglutathione (GSNO) and a copper nanoparticle catalyst were applied to commercial poly(vinyl chloride) tubing for the tunable, elevated release of NO. The addition of copper increased the NO flux up to five times higher, resulting in superior *in vitro* antimicrobial activity (96-99.9% reduction in *S. aureus* and *Pseudomonas aeruginosa*) and *in vivo* hemocompatibility in a 4 h extracorporeal rabbit model, maintaining 89.3% of baseline platelet counts while controls only maintained 67.6%.

In the third approach, SNAP-based silicone rubber platforms were infused with silicone oil (Si) to combine the multifunctional properties of NO with an antifouling, liquid-infused interface. The combined platform demonstrated potent antibacterial activity against methicillin-resistant *S. aureus* and *P. aeruginosa* for up to 28 d. Moreover, SNAP-Si cannulas evaluated in a 14- and 21-d subcutaneous mouse model enhanced material biocompatibility by reducing the thickness of the fibrous encapsulation by ~60.9% and cell density around the implant by ~60.8% after 3 weeks.

The combined surface strategies significantly improved the properties of existing NO-releasing platforms, demonstrating excellent potential in reducing rates of infection and thrombosis commonly associated with medical device applications.

INDEX WORDS: Medical devices, Hemocompatible, Antimicrobial, Surface modification, Nitric oxide

Combination Surface Strategies that Improve the Longevity, Tunability, and Antifouling Properties of Nitric Oxide (NO)-Releasing Platforms

By

MEGAN DOUGLASS

B.S., The University of Georgia, 2017

A Dissertation Submitted to the Graduate Faculty of The University of Georgia in Partial Fulfillment of the Requirements for the Degree

DOCTOR OF PHILOSOPHY

ATHENS, GEORGIA

2021

Combination Surface Strategies that Improve the Longevity, Tunability, and Antifouling Properties of Nitric Oxide (NO)-Releasing Platforms

by

Megan Douglass

Major Professor: Hitesh Handa

Committee: William Kisaalita
Elizabeth J. Brisbois
Ramana Pidaparti

Electronic Version Approved:

Ron Walcott
Vice Provost for Graduate Education and Dean of the Graduate School
The University of Georgia
December 2021

DEDICATION

This research work is dedicated to my parents, Don and Jennifer Douglass. Thank you for your endless love, encouragement, and prayers.

ACKNOWLEDGEMENTS

I have had the privilege of working with many individuals who have assisted me throughout my PhD. I would like to thank my mentor, Dr. Hitesh Handa, for his continuous support for both my dissertation work as well as my development as an independent researcher. Dr. Handa's guidance was paramount to my accomplishments and growth as an engineer and scientist. I also would like to thank my committee members Dr. William Kisaalita, Dr. Elizabeth Brisbois, and Dr. Ramana Pidaparti, for their helpful recommendations for my PhD work. Thank you to Dr. Averett for your support and guidance during my PhD. Thank you to Dr. Chad Schmiedt, Dr. Gina Kim, and their teams for their surgical expertise used to better understand material compatibility in mouse and rabbit models. Thank you to Margaret Sapp and Victoria Martinez for your steadfast dedication to creating a positive, stress-free environment for graduate students and streamlining the PhD process. I would also like to thank my lab members and colleagues for their helpful collaborations and perspectives: Dr. Sean Hopkins, Dr. Marcus Goudie, Dr. Priya Singha, Dr. Jitendra Pant, Mark Garren, Morgan Ashcraft, Arnab Mondal, Ryan Devine, Lori Estes, Sama Ghalei, Manjyot Kaur Chug, Divine Francis, Rashmi Pandey, Lauren Griffin, Sarah Wilson, Elaine Wu, Stephen Thompson, Patrick Maffe, Ekrem Ozkan, Dani Workman, Katie Homeyer, Jianwen Li, Megan Norman, Thao Nguyen, Martin Tran, Nicole Tayag, and Tia Shorter. It has been a privilege collaborating with such an inspiring and exciting group. I would like to thank my project and PhD funding sources (CDC, NIH, DOD, JDRF, UGA, ARCS Foundation, and Baxter) for their research support. Lastly, I would like to thank my family and friends: my parents, Clay, Kelley, Aaron, Daniel, Caitlyn, Jenny, and Na Ai. God has truly blessed me by surrounding me

with such a loving and encouraging group of people who were vital not only for the successful completion of my studies, but my personal growth as well.

TABLE OF CONTENTS

Page

LIST OF TABLES

LIST OF FIGURES

CHAPTER 1

INTRODUCTION - BIOINSPIRED HEMOCOMPATIBLE & ANTIMICROBIAL SURFACES FOR MEDICAL DEVICE APPLICATIONS[1]

[1] Portions of this chapter were submitted as: Douglass, M., Garren, M., Devine, R., Mondal, A., and Handa H. Bio-inspired Hemocompatible Surface Modifications for Biomedical Applications. Submitted to *Progress in Materials Science*, 8/13/2020.

1.1 Current Clinical Complications with Medical Devices

Blood-contacting medical devices act as a mainstay for intravenous drug administration, tissue engineering, extracorporeal circulation (ECC), and disease management (**Figure 1.1**). Despite decades of development, two of the most common clinical complications associated with indwelling medical devices are infection and device-induced thrombosis. Between 50-70% of healthcare-associated infections in the US are related to medical devices(1). Moreover, incidences of device-induced thrombosis frequently disrupt medical device use and have direct implications on patient outcome; the rate of thrombosis of some of the most commonly utilized blood-contacting medical devices are shown in **Table 1.1**. As a result of both infection and thrombosis, patients face further complications including loss of device function, additional treatment and surgeries, increased hospital stay, and higher rates of morbidity and mortality. Therefore, methods to reduce both the rate of infection and device-induced thrombosis are needed.

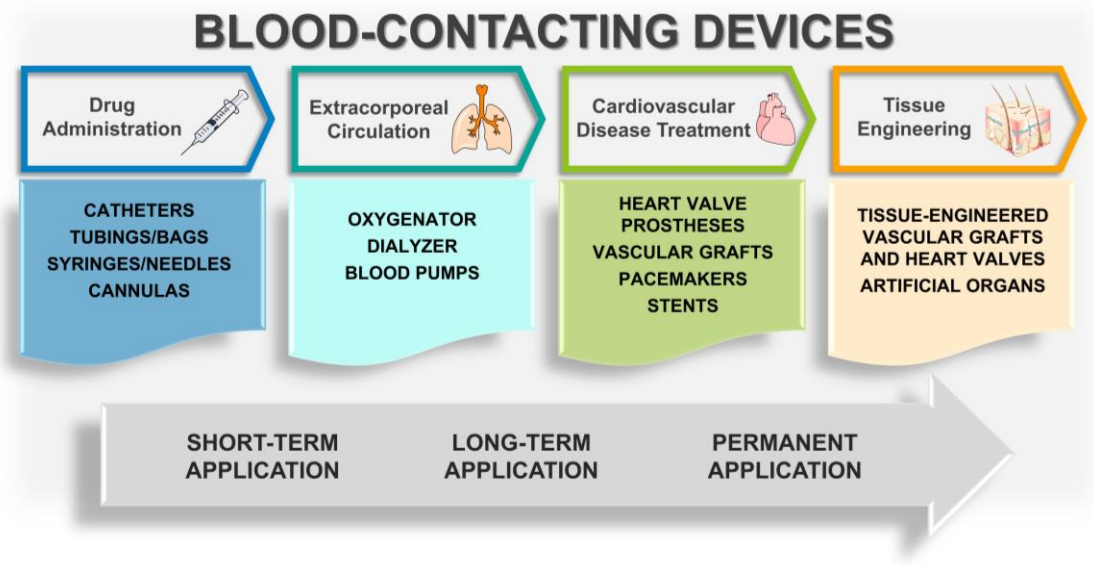

Figure 1.1 - Blood-contacting devices are used for various clinical applications including drug administration, extracorporeal circulation, cardiovascular disease treatment, and tissue engineering. Devices used for clinical use range from short-term application to permanent exposure to the body.

Table 1.1 - Reported incidence rates of thrombosis or occlusion and infection in commonly utilized blood-contacting medical devices.

Medical Device	Rate of thrombosis or occlusion	Rate of nosocomial infection	Citations
Peripherally Inserted Central Catheters	**7-40%**	**5-15%**	**(2-5)**
Extracorporeal Membrane Oxygenation	**8-13%**	**8-64%**	**(6-10)**
Cardiac Implantable Devices	**2-37%**	**1-20%**	**(11-15)**
Central Venous Ports	**1-13%**	**1-8%**	**(16-18)**

1.1.1 Medical Device-Induced Thrombosis

1.1.1.1 Overview of Medical Device-Induced Thrombosis

Regulating host response upon exposure remains the leading challenge related to many blood-contacting devices. A major determining factor in the success of blood-contacting devices is their compatibility with blood, namely hemocompatibility. Preventing thrombus formation on the surface of devices is crucial for maintaining device functionality and patient safety. Despite the intensive research and development surrounding these devices, blood coagulation and thrombosis remain the largest limitation of many medical devices. Without anticoagulant or antiplatelet therapies, when foreign devices are exposed to blood, clinical manifestation of thrombus formation can occur spontaneously and abruptly, ultimately leading to device failure. Device-induced blood clots can impede device functionality, occlude vessels, or break off and move downstream, causing further complications such as pulmonary embolism, kidney failure, deep vein thrombosis, heart attack, or stroke. While systemic anticoagulation helps reduce the occurrence of device-induced thrombosis, these events still occur. The administration of anticoagulants can also lead to hemorrhaging. Thrombosis and bleeding have been linked to decreased survival rates by 33% and 40% in ECMO patients, respectively(19). Therefore, the use of systemic anticoagulation and antiplatelet therapies requires careful monitoring to prevent device-induced thrombosis while minimizing the risk of bleeding.

1.1.1.2 Mechanisms of Device-Induced Thrombosis

When exposed to blood, foreign surfaces are subjected to various complex reactions which can compromise the lifetime and usability of the device **(Figure 1.2)**. Under normal conditions, due to its antithrombotic properties, the endothelium can interact with blood without triggering clot formation(20). However, when devices are introduced to the blood, the adsorption of physiological proteins initiates the activation of a number of biological processes including the coagulation cascade and inflammation. Overall, medical device-induced thrombosis is the result of fXIIa-mediated thrombin formation and platelet adhesion and aggregation which are both initiated by protein adsorption(21).

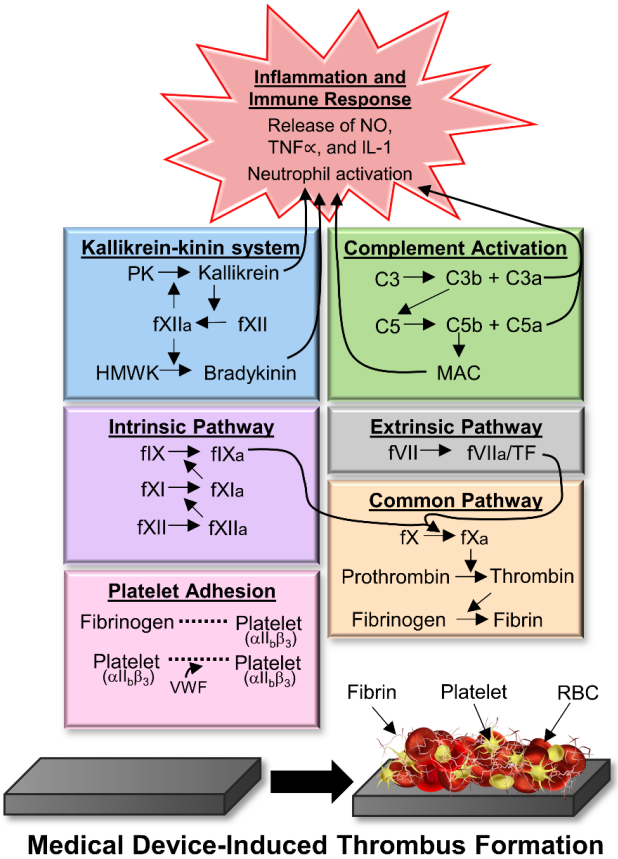

Figure 1.2 - Schematic representing major biochemical reactions including the intrinsic and extrinsic coagulation pathways, complement activation, and the common pathway of coagulation as a result of the exposure of medical devices. VWF, von Willebrand factor; NO, nitric oxide; TNFα, tumor necrosis factor; IL-1, interleukin 1; HMWK, high molecular weight kininogen; TF, tissue factor; MAC, membrane attack complex; RBC, red blood cell. Red dotted line represents binding.

Proteins, which constitute a major part of plasma, are considered to initiate thrombosis by rapidly adsorbing to the foreign surface immediately after entering the blood(21). Surface chemistry and physical properties of the device modulates which proteins are attracted to the surface and the strength at which they adsorb. Furthermore, proteins can be displaced by other proteins over time based on their relative affinity, size, and charge, a phenomenon recognized as the Vroman effect(21). Generally, smaller proteins absorb quickly to the surface and are eventually replaced by larger proteins or proteins with greater affinity(22). Blood is composed of different plasma proteins, several of which play key roles in mediating platelet, leukocyte, and red blood cell attachment.

Platelets are essential for the maintenance of hemostasis, responsible for forming hemostatic plugs and the release of pro-coagulant signals which ultimately assist in the transformation of prothrombin to thrombin(23). Platelets interact with fibrinogen attached to the foreign surface by the integrin aII_bb_3 present on platelets(21). Due to their high affinity to fibrinogen, platelets can adhere at adsorbed fibrinogen concentrations as small as 7 ng cm^{-2}(21, 24). After adhering to fibrinogen, platelets begin to form dendritic pseudopodia and release agonists that further promote aggregation and adhesion of platelets(22). Von Willebrand factor joins together activated platelets through the aII_bb_3 complex(25). Adhered leukocytes can degranulate, releasing platelet-activating factor, interleukins, and TNFα, which further progress platelet activation. Red blood cells adhere independently from the protein monolayer and release adenosine diphosphate (ADP), which further promotes platelet aggregation(21).

Key factors composing the contact-phase system can also bind to the device surface and displace fibrinogen including factor XII (fXII),) HMWK, prekallikrein (PK), and factor XI (fXI)(21, 26). Bound fXII can autoactivate into fXIIa, which activates PK into active kallikrein

and HMWK into bradykinin, both of which stimulate coagulation and inflammatory responses(21). Through the intrinsic pathway, fXIIa begins a series of reactions that result in the activation of factor X, ultimately triggering thrombin generation and inflammation(21, 26). Both the extrinsic and intrinsic pathways of coagulation, which share the activation of factor X, begin the conversion of prothrombin to thrombin and the transformation of fibrinogen to fibrin and platelet aggregation, resulting in a dense network of clot formation(21, 26).

Exposure of artificial surfaces to blood can also induce the complement system, a key pathway for immune response as the initial line of defense against foreign bodies. The complement system is initiated by three different pathways: classical, alternative, and mannose-binding lection (MBL) pathway. Ultimately, these three pathways result in C3 convertase, which by cleaving C3 into C3a and C3b, promotes inflammation to the site. The generation of C5 convertase also cleaves C5 into C5a and C5b(26). Together C3a and C5a increase recruitment, attachment, and activation of leukocytes(21). Moreover, C5b can subsequently bind to the surface and initiate the production of the membrane attack complex (MAC), triggering a series of inflammatory reactions(26).

1.1.1.3 Current Clinical Standard: Systemic Anticoagulation

Systemic administration of anticoagulants, mainly systemic heparinization, remains the most widely used technique to control clot formation. However, anticoagulant therapies are among the most common causes of adverse-drug-related events and deaths in hospitalized patients. A surveillance study examining adverse drug events with hospitalized Medicare patients found that 13.6% of patients administered heparin and 8.2% of patients administered warfarin experienced an adverse drug event(27). According to a comprehensive study conducted at Brigham and Women's Hospital, of the nearly 500 anticoagulant-associated adverse drug events, 48.8% were due to medication errors, 30.5% were due to adverse drug reactions, and 20.7% were due to both

medication errors and adverse drug reactions; as a result, death within 30 days of the adverse event occurred in 11% of patients(28). Patients receiving anticoagulants are likely to have medical conditions (eg., heart failure, ischemic heart disease, chronic kidney disease, stroke) that increase the patient's vulnerability to adverse drug events, increasing the likelihood of longer hospital stay, more complicated treatment requirements, and risk of death(28).

All forms of anticoagulants have been associated with the development of acute hemorrhaging(29). Incidence rates of major bleeding events during systemic heparinization are reported to occur 7.3 to 16.7 per 100 person-years(30). Moreover, systemic heparization has led to side effects including drug intolerance, thrombocytopenia, and osteopenia(31). Even after discontinuation of systemic heparinization, 50% of patients that develop heparin-induced thrombocytopenia experience a thrombotic event, and thrombotic complications associated with heparin-induced thrombocytopenia are associated with a mortality rate between 20-30%(32, 33). In response, researchers have set out to develop improved hemocompatible devices, averting the need for additional systemic administration of anticoagulants or antiplatelet therapies(34).

1.1.2 Medical Device-Associated Infection

1.1.2.1 Overview of Medical Device-Associated Infection

Medical device-associated infections compose over half of all nosocomial infections in the US, presenting a major threat to patient outcome(1, 35). The current clinical standard to treat device-related infections is antibiotic therapy, but several complications have arisen that significantly limits successful treatment. First, infections caused by antibiotic-resistant pathogens are responsible for 68,000 deaths in the US and EU combined(36). Regardless of the pathogen, antibiotic resistance is significantly more prevalent in device-associated infections including urinary and vascular catheters and ventilators(35). Moreover, the surfaces of medical devices

provide an interface for bacteria to attach and form a biofilm, which decreases antibiotic susceptibility by 500-5000-fold(37). Therefore, new methods of preventing and combatting bacterial colonization and biofilm formation are needed to reduce device-associated infection.

1.1.2.2 Biofilm Formation on Medical Devices

Biofilm formation occurs in four steps: 1) bacterial adhesion, 2) monolayer formation and extracellular polymeric substance (EPS) production, 3) microcolony formation, and 4) maturation and dispersal (**Figure 1.3**)(38). In the first step, bacteria attach to the surface of the device through physical forces (van der Waals forces, steric interactions, and electrostatic interactions) or bacterial appendages(39). Plasma proteins including fibrinogen and fibronectin that adsorb to the surface of the device can also facilitate bacterial adhesion(40). Bacteria begin to multiply and produce an EPS matrix, a stable, protective barrier between the bacteria and its surrounding environment(41, 42). As the colonized bacteria continues to grow, formation of different micro-communities begin to emerge, forming a complex, coordinated network capable of supporting microbial cross-feeding(42). The maturing biofilm exhibits a distinct three-dimensional structure composed of

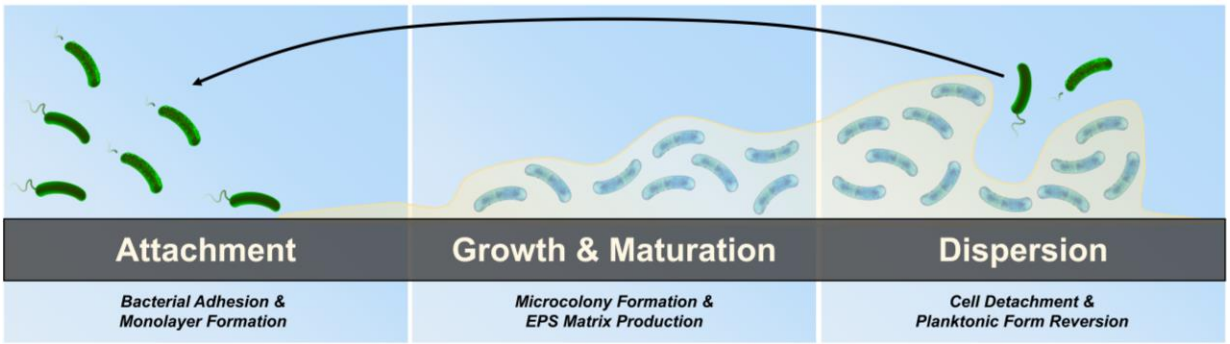

Figure 1.3 – Biofilm formation on the surface of medical devices, which includes bacterial attachment and monolayer formation, microcolony formation and EPS matrix production, and cell detachment and dispersion to a new site.

small channels for nutrient, water, and waste transportation(43). Finally, portions of the biofilm begin to disperse, releasing bacteria that revert to their planktonic form, spreading the infection to a new site(39). When the released bacteria attach to a new surface, the process begins again.

1.1.2.3 Current Clinical Standard: Antibiotic Therapy

The current clinical standard for treating medical device-related infections is to remove and replace the device and treatment with antibiotics(44). Rapid diagnosis and choice of antibiotic therapy have direct implications on morbidity and mortality rates. In intensive care units, depending on the device that was infected, antibiotic regimes may vary: antibiotics used to treat central line-associated bloodstream infections (CLABSIs) should be effective against Gram-positive and non-fermentative pathogens; antibiotics used to treat ventilator-associated pneumonia (VAP) should be broad-spectrum; antibiotics used to treat catheter-associated urinary tract infections (CAUTIs) should be effective against *Enterobacteriaceae* and non-fermentative pathogens(44). Moreover, immunocompromised patients are also often advised to receive antifungal therapy(44).

Despite these practices, due to the emergence of antibiotic tolerance and resistance combined with the formation of biofilms, treatment of medical device-related infections is difficult. Currently, approximately 2.8 million antibiotic-resistance infections and 35,000 related deaths occur in the US each year(45). Several different bacterial and biofilm mechanisms have been indicated to promote antibiotic resistance and tolerance (**Table 1.2**). The rapid emergence of resistance combined with the limited discovery of new antibiotic therapies underlines the need for alternate antimicrobial methods to prevent and treat infections.

Table 1.2 - Bacterial (blue) and biofilm (green) mechanisms that promote antibiotic resistance and tolerance, limiting treatment efficacy.

Mechanism	Citation
Efflux pumps that extrude antibiotics from the cell	(46)
Drug-modifying or degrading enzymes	(46)
Altered antibiotic target sites	(47)
Drug-neutralizing proteins	(48)
Reduced cell permeability (eg., outer membrane of Gram-negative bacteria)	(49)
Slow nutrient uptake, mediating antibiotic penetration	(37)
Increased plasmid transfer efficiency containing antibiotic resistance genes	(50)
Environmental adaptability due to quorum sensing	(51)
Protective EPS matrix	(51)
Development of persister cells that resist antibiotic treatment	(48)

1.2 Current Hemocompatible and Antimicrobial Surfaces

1.2.1 Biopassive and Bioactive Surface Strategies

The fate of a biomaterial directly depends on its ability to mitigate protein adsorption and thrombosis and prevent infection. Surface modifications used to avoid these clinical complications fall into two different categories: biopassive surface strategies and bioactive surface strategies. Biopassive strategies aim to minimize triggering large adverse reactions, effectively evading surface-induced coagulation by preventing protein adsorption and platelet adhesion and preventing infection by reducing bacterial adhesion. These modifications invoke a low immune response from the body, but the effectiveness of these devices over long periods of exposure time is still a concern, limiting their use almost exclusively to short-term or single-use applications. **Table 1.3** includes a brief description, advantages, and disadvantages of different biopassive surface strategies to minimize surface fouling from proteins, bacteria, and/or platelets.

Another method of mitigating infection and/or clot formation can be achieved through the incorporation of bioactive molecules. Such agents present on or locally released from biomaterials can react with the surrounding environment, directly inhibiting vital players in clot formation (eg.,

platelets, fibrinogen, thrombin) or combatting bacterial pathogens adhered to the surface or in the surrounding environment. Although these surfaces can exhibit potent antithrombotic and/or antimicrobial activity, many active agents lose efficacy once immobilized or incorporated into a surface and have limited storage within or on the surface of the material. **Tables 1.4** and **1.5** include a brief description, advantages, and disadvantages of different bioactive hemocompatible and antimicrobial surface strategies, respectively.

Table 1.3 - Common biopassive surface modifications applied to medical devices to repel protein adsorption, protein adhesion, and/or bacterial adhesion

Common Biopassive Surface Modifications

Surface Modification	Description	Advantages	Disadvantages	Citations
Superhydrophobic Surfaces	Non-wetting micro/nanostructured surface with contact angle > 150º; commonly bioinspired (eg., Lotus plant)	• Broadly antifouling • Can be self-cleaning • Extended to other applications (water/oil separation, antifogging, etc)	• Unstable air pocket layer • Subject to mechanical degradation • Time-sensitive	(52-56)
Liquid-Infused Surfaces	Tethers an intermediate antifouling, 'slippery' liquid to the polymer surface; inspired by the *Nepenthes* pitcher plant	• Broadly antifouling • Self-cleaning • Self-healing • Shear tolerant	• Subject to lubricant depletion • Long-term clinical efficacy and stability not yet determined	(57-63)
Passive Protein-Coated Surfaces	Biomimetic interface that decreases secondary protein adsorption	• Prevents protein adsorption needed for thrombus formation and/or bacterial colonization • Albumin nanocarriers are ready on the market	• Subject to Vroman effect • Uncontrollable conformational changes • Storage & sterilization instability	(64-72)
Hydrophilic Interfaces	Forms hydration layer through innate surface properties or through immobilization of hydrophilic molecules (eg., PEG), creating steric hinderance to surrounding proteins	• Broadly antifouling • Low cost • Easy manufacturing • Commercially available	• Can be less effective compared to zwitterionic surfaces • Protein interaction and denaturation can still occur	(73-78)
Zwitterionic Surfaces	Contains both positive and negative charges, leading to a strongly bound antifouling hydration layer	• Broadly antifouling • Some are easily synthesized • Commercially available • Very stable hydration layer	• Insolubility issues • Moisture sensitive • Demonstrated effectiveness *in vivo* only for short-term thus far • Costly	(79-87)

Inorganic Hemocompatible Coatings	Chemically inert interface; includes metal oxides, nitrides, silicon carbide, and diamond-like carbon coatings	• Decreased protein adsorption • High specific strength to weight ratio • Protective against corrosion • Can be easily alloyed • Commercially available	• Subject to interface defects • Does not prevent thromboembolism, infection, and restenosis • Unpredictable oxide layer thickness	(22, 88-96)

.

Table 1.4 - Common bioactive hemocompatible surface modifications applied to medical devices to minimize thrombus formation

Common Bioactive Hemocompatible Surface Modifications

Surface Modification	Description	Advantages	Disadvantages	Citations
Thrombin-Inhibiting Peptide Immobilization	Directly binds to the reactive site (univalent) or to the reactive site and exosite 1 (bivalent) of thrombin	• Does not depend on the presence of other cofactors • Potent antithrombotic properties	• Can lose efficacy over time due to saturation • Elevated inflammatory response • Reduced efficacy once immobilized • Does not broadly prevent surface fouling	(97-105)
Heparin Immobilization	Enhances antithrombin activity, preventing thrombin and factor X activation	• Some products already FDA approved • Extensively tested *in vivo* for short- and long-term applications • Does not inhibit endothelial cell proliferation	• Reduced efficacy once immobilized • Depends on the presence of antithrombin • Costly • Does not broadly prevent surface fouling	(106-110)
Dermatan Sulfate Immobilization	Increases heparin cofactor II activity on thrombin	• Promising antithrombotic activity • Moderately reduces non-specific cellular adhesion and protein adsorption	• Limited research • Difficult to manufacture • Sterilization & storage stability concerns	(111-113)
Dextran Immobilization	Enhances fibrinolysis, reduces platelet adhesion, and decreases platelet activation	• Extends clotting times • Exhibits antifouling properties against cells, protein, and platelet adhesion	• Limited long-term stability *in vivo* • Limited long-term storage stability evaluation • Difficult to manufacture • Mode of action is unclear	(114-117)
NO-Releasing/ Generating Platforms	Multifunctional endogenous molecule that attenuates platelet adhesion, activation, and aggregation	• Dual antithrombotic and antimicrobial surface properties • Moderately stable • NO-releasing materials extensively evaluated *in vivo* • Many fabrication methods (blending, solvent swelling, covalent immobilization)	• Does not prevent surface fouling • Limited NO donor storage • Efficacy determined by level of release or generation • Limited *in vivo* evaluation of NO-generating surfaces	(109, 118-121)

		• Does not require NO donor elution for activity • Potentially tunable release kinetics	• Can be temperature-sensitive • High levels of NO can be cytotoxic	

Table 1.5 - Common bioactive antimicrobial surface modifications applied to medical devices to combat invading pathogens

Common Bioactive Antimicrobial Surface Modifications

Surface Modification	Description	Advantages	Disadvantages	Citations
Antimicrobial Peptide-Immobilized Surfaces	Disrupts bacterial membrane through electrostatic interaction with phospholipids	• Reduces bacteria-surface interactions • Low toxicity • Effective against bacteria, fungi, and virus • Effective at relatively low concentrations	• Difficult to produce • Loss in efficacy once immobilized • Costly • Some resistance has been reported • Subject to protein adsorption	(122-127)
Antibiotic-Incorporated Surfaces	Isolated antimicrobial compounds that can inhibit bacterial growth or directly eliminate pathogens	• Retains good antimicrobial activity • Already commercialized • Can be broad-spectrum	• Contributes to development of antibiotic resistance • Limited reservoir • Not effective against biofilms	(128-131)
NO-Releasing/ Generating Platforms	Multifunctional endogenous molecule exhibiting potent antimicrobial activity including amine and thiol nitrosation, lipid peroxidation, and DNA cleavage	• Effective against bacteria, fungi, and virus • Multifunctional (antithrombotic, wound healing, antimicrobial) • Low bacterial resistance • Effective against antibiotic-resistant bacteria • Effective against Gram-positive and Gram-negative pathogens	• Does not prevent fouling • Limited NO donor storage • Efficacy determined by level of release or generation • Limited *in vivo* evaluation of NO-generating surfaces • Can be temperature-sensitive • High levels of NO can be cytotoxic	(61, 118, 128, 132-134)
Silver Coatings	Induces loss in membrane potential, protein dysfunction, and oxidative stress	• Already commercialized • Broad spectrum • Cost effective • Ability to be alloyed	• Can be cytotoxic • Mixed clinical efficacy • Rapid depletion	(128, 135-138)
Chlorohexidine Coatings	Antiseptic that exhibits bacteriostatic and bactericidal activity through membrane disruption	• Already commercialized • Effective against bacteria and fungi • Slower development of bacterial resistance	• Limited reservoir • Subject to protein adsorption • Mixed clinical efficacy • Concentration-dependent	(128, 135, 139-142)
Quaternary Ammonium Immobilization	Cationic antimicrobial that disrupts the bacterial membrane and	• Already used in commercial applications • Broad-spectrum • Effective at different pH	• Only contact-based killing • Costly	(143-147)

	replaces metal cations (Ca^{2+}, Mg^{2+})		• Subject to protein adsorption • Potentially cytotoxic	
Bacteriophage-Incorporated Materials	Viruses that infect bacteria, replicate, and cause cell lysis	• Host specific • Self-replicating • Nontoxic • Effective against antibiotic-resistant bacteria	• Not stable • Moisture-sensitive • Some resistance can be developed • Difficult to isolate and manufacture	(128, 148-150)
Antimicrobial Enzyme Immobilization	Isolated enzymes from living organisms that can degrade the structure and components of bacterial cells or inhibit quorum sensing	• Can be pathogen-specific (if desired) • Lower bacterial resistance • Low cytotoxicity • Effective against antibiotic-resistant bacteria	• Can denature • Difficult to purify • Lower efficacy once immobilized • Storage and sterilization instability • Costly • Subject to protein adsorption	(128, 151-154)
Photobactericidal Coatings	Generates reactive oxygen species that induce DNA, RNA, protein, and lipid damage	• Broad-spectrum • Tunable generation • Relatively simple fabrication • Effective against bacteria and virus	• At higher doses, can be cytotoxic • Light-sensitive • Low coating durability • Subject to protein adsorption	(155-159)
Triclosan Coatings	Antimicrobial agent that inhibits fatty acid synthesis and disrupts bacterial membrane	• Antibacterial and antifungal • Already commercialized	• Can be cytotoxic • Mixed clinical efficacy • Some antimicrobial resistance	(128, 160-162)

1.3 Overview of NO-Releasing and NO-Generating Surfaces

NO is a gaseous free radical secondary messenger that attenuates the binding of platelets to adsorbed plasma proteins such as fibrinogen and vWF, thereby preventing their activation(163-165). The endothelial lining of blood vessels consists of a monolayer of cells that continuously synthesize NO from L-arginine at an estimated flux ranging between $0.5 – 4.0 \times 10^{-10}$ cm^{-2} min^{-1}, whereby NO and its metabolic byproducts reduce platelet activation by the downregulation of P-selectin expression(166-169). To improve the hemocompatibility of blood-contacting materials, biomimetic NO-functionalized surfaces aim to sustain NO fluxes comparable to the native endothelium and have been developed via two main strategies (**Figure 1.4**): (1) release from

materials containing an NO donor reservoir and (2) catalytic surface generation of NO from a supplemented or endogenous NO donor.

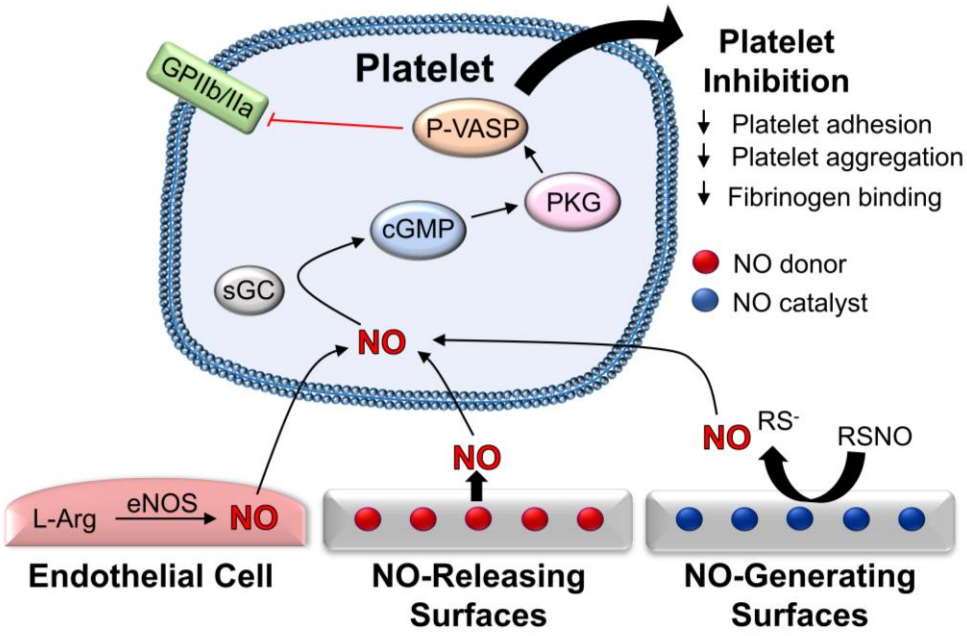

Figure 1.4 - NO-releasing and NO-generating surfaces inspired by the native endothelium designed for blood-contacting applications

In addition to its antithrombotic capabilities, NO exhibits broad-spectrum antimicrobial activity on both Gram-positive and Gram-negative bacterial and fungal cells(170). Neutrophils produce potent levels of NO, which can directly combat invading pathogens by inducing DNA mutations, enzyme alterations, and lipid peroxidation(170). As a result, NO donor molecules have been incorporated into polymeric platforms to reduce bacterial colonization and biofilm formation both *in vitro* and *in vivo*(171, 172).

1.3.1 Current State of NO-Releasing Materials

Materials are rendered NO-releasing through the incorporation of NO donor molecules, which spontaneously deliver NO to the surrounding environment. NO donors are generally classified as directly or physiologically activated, with some of the most synonymous being

diazeniumdiolates (NONOates), S-nitrosothiols (RSNOs) such as S-nitrosocysteine (CysNO), S-nitrosoglutathione (GSNO), and S-nitroso-N-acetyl-DL-penicillamine (SNAP), organic nitrates/nitrites, and metal nitrosyls. Due to their ability to spontaneously release NO under physiological conditions, substantial research has gone into developing NO-releasing materials using NONOates and RSNOs to achieve stable, long-term NO release. Many polymers and inorganic nanoparticles have been infused with NO donors via blending, solvent swelling, solvent evaporation, and covalent immobilization(173, 174).

One of the most widely utilized NO donors, NONOates are known to release NO via enzymatic, chemical, or thermal decomposition with kinetics tunable by environmental acidity (**Figure 1.5**)(175). The NO release profile derived from NONOates is directly related to the pH and temperature of the environment as well as the structure of the molecule(176). NONOate-incorporated materials have been extensively examined *in vivo*, showing great promise in improving both hemocompatibility (reduced thrombus formation, preserved platelet count), antimicrobial efficacy, and wound healing properties(175, 177-181). However, toxicity concerns with NONOates remain, which can form carcinogenic nitrosamine compounds(182, 183).

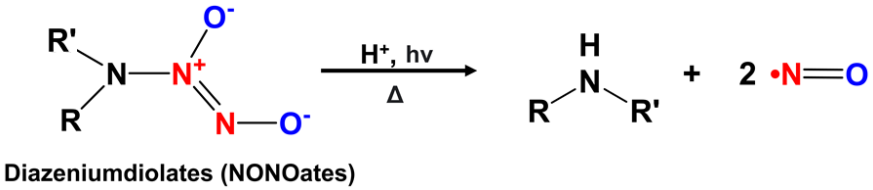

Figure 1.5 - NO release mechanism of diazeniumdiolates (NONOates), which is directly related to the pH, temperature of the environment, and structure of the molecule.

Another widely used NO donor class, RSNOs are synthesized from a nitrosation reaction with a sulfhydryl-containing compound, attaching a nitroso group to the sulfur of a thiol(184). RSNOs have variable long-term stability based on steric effects, with NO release mediated by thermal decomposition(185), photolysis(186), and metal ion catalysis (**Figure 1.6**)(187).

Endogenous RSNOs (GSNO, CysNO) are responsible for the transportation and delivery of NO in the body(183, 188). As a result of their superior stability, tunability, inherent biocompatibility, and potent antimicrobial and antiplatelet properties, both synthetic and endogenous RSNOs have been synthesized and incorporated into different polymeric platforms to deliver NO(176, 189). Multiple recent reports have shown improvements in both the antithrombotic and antimicrobial efficacy of different medical-grade polymers and devices both *in vitro* and *in vivo*. Brisbois et al. developed extended antithrombotic surface functionalization Elast-eon E2As with SNAP, which showed a three-fold reduction in thrombus area and 90% reduction in bacterial adhesion in a 7-d intravascular catheter sheep model(118). Further work developed SNAP-doped silicone tubing which showed a 67% platelet preservation relative to controls in a 4 h rabbit extracorporeal circulation (ECC) model, while multi-lumens filled with a SNAP-PEG blend showed a 55% reduction in thrombus formation over an extended 11-d rabbit model and >97% reduction in viable *S. aureus* and *E. coli* adhesion in a 3-d CDC biofilm bioreactor(190, 191). Wo et al. blended SNAP into novel silicone-PCU films under the tradename CarboSil 2080 A^{TM} and achieved a six-fold reduction in thrombus area in a 7 d rabbit intravascular catheter model and 2-2.5 log reduction in viable *S. epidermidis* and *P. aeruginosa* in a 14-d CDC biofilm bioreactor(120, 192). Other hybrid strategies have considered copper (193, 194), selenium(133), and zinc oxide(195) nanoparticle topcoats to catalyze the NO release from RSNO incorporated within the CarboSil matrix. Further work with CarboSil composites of GSNO and copper nanoparticles applied to PVC tubing has demonstrated its viability for ECC applications, wherein for a 4 h rabbit model the combination of copper and GSNO maintained almost 90% of the baseline platelet count (this work is a portion of this dissertation)(194). Although early work incorporated NO donors via blending into the polymer matrix, potential issues of extruding NO-releasing polymers due to the thermal sensitivity of the

NO-releasing functionalities remained a concern. However, recent studies have shown that RSNOs can be impregnated through a solvent swelling method, presenting a simple, straightforward fabrication strategy and circumventing thermal decomposition during synthesis(61, 191).

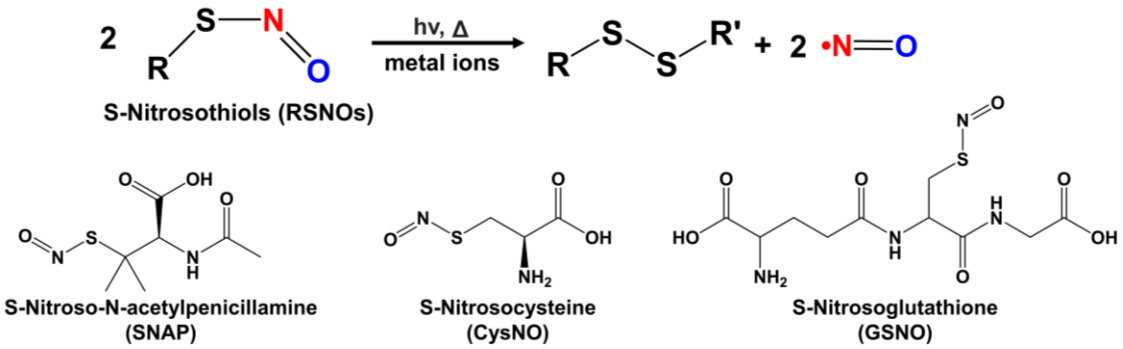

Figure 1.6 - NO release mechanism of S-Nitrosothiols (RSNOs) and common RSNO examples (SNAP, CysNO, GSNO).

1.3.2 Short-Comings of NO-Releasing Materials and Potential Solutions

Although NO-releasing materials have been synthesized to minimize infection and improve blood-material interactions, several shortcomings remain: (1) donor leaching can be cytotoxic and delocalizes the NO release downstream from the material interface (190, 196); (2) NO-releasing materials alone lack NO flux tunability, and increasing donor concentration does not directly correlate to higher stabilized NO fluxes (191, 196); (3) NO-releasing materials have a limited reservoir of NO for long-term applications; and (4) NO-releasing devices do not prevent surface fouling from blood proteins or bacteria.

To stabilize NO release profiles and prevent cytotoxicity, topcoats composed of hydrophobic polymers have been added to NO-releasing polymers to modulate diffusion of water into NO-doped layers and subsequent leaching of NO donors (192), while other strategies that covalently attach NO donors to polymer matrices have also shown success(196, 197). One such strategy involves covalently attaching SNAP to silicone rubber, wherein doing so almost 125 d of

stabilized NO release was achieved alongside a ~36% improvement in platelet count in a 4 h rabbit model(186, 198). Most recently, Goudie et al. incorporated alkylamine spacers with a methacrylate brancher onto PDMS to enable denser SNAP attachment with stabilized NO release over 25 d as well as a three-fold reduction in fibrinogen adsorption and a nine-fold reduction in platelet adherence over unmodified PDMS(61, 199). Ongoing work with covalently attached SNAP and other NO moieties show promise for the increased efficacy of NO-releasing materials.

One advantage of RSNOs as NO donors is that their release can be mediated through heat, light, or the presence of metal ions. Although heat and light catalysis are more limited for many medical device applications, metal nanoparticles can be incorporated into NO-releasing polymeric materials, catalyzing the release of NO from incorporated RSNOs. This strategy can be particularly useful for applications requiring higher levels of NO release, potentially improving antimicrobial and hemocompatible efficacy. Hybrid strategies have considered copper (192, 196), selenium (133), and zinc oxide (195) nanoparticle topcoats to catalyze the NO release from RSNO-infused CarboSil (including work that is included in this dissertation). Further work with CarboSil composites of GSNO and copper nanoparticles applied to PVC tubing has demonstrated its viability for ECC applications, wherein for a 4 h rabbit model the combination of copper and GSNO maintained almost 90% of the baseline platelet count (which is later introduced in Chapter 3)(194).

To improve the longevity of NO production at a material interface, NO-generating materials have been developed from the premise that the NO release from endogenous and supplemented RSNOs is catalyzed by copper ions (200) and other metal ions(195, 201, 202). More recently, work with metal-organic frameworks (MOFs) has improved the stability of metal ions in materials and invigorated interest in developing long-term, self-sustaining materials that can

generate NO from endogenous RSNOs(203). In 2012, Harding et al. demonstrated that the MOF $Cu_3(BTC)_2$ (BTC: 1,3,5-benzentricarboxylate) shows catalytic activity with CysNO but is limited by its instability under physiological conditions(203). Follow-up work addressed this structural instability with the alternative MOF Cu (II) 1,3,5-Benzene-tris-triazole (CuBTTri) which generated NO both in a heterogeneous state and when composited with PUs(204). Newly reported hemocompatibility studies have demonstrated that CuBTTri with supplemented GSNO reduces thrombus formation in human whole blood and inhibited platelet aggregation in PRP(121). Moreover, MOF-incorporated materials and other NO-generating platforms have shown promising antimicrobial efficacy *in vitro* against *S. aureus*, *S. epidermidis*, and *E. coli*, although most rely on the metal ion elution as the antimicrobial agent(183, 205-207). Despite promising *in vitro* capability to achieve antithrombotic and antimicrobial activity, one major shortcoming of NO-generating materials is that NO-generating surfaces rely on high, local endogenous RSNO concentrations to generate substantial levels of NO. NO-generating surfaces produce lower levels of NO compared to NO-releasing surfaces, which may not suffice to prevent initial infection or platelet activation(61, 208). Moreover, surface fouling can potentially block catalytic sites, limiting the material's ability to effectively generate NO. To overcome issues presented by both NO-releasing and generating surfaces, these strategies can be combined into a single platform (discussed and presented in Chapter 2 of this dissertation).

Finally, NO functionalization as an active strategy for preventing platelet activation cannot attenuate blood plasma protein adsorption onto polymeric surfaces, such that multi-defense strategies are required(209). One such strategy is to mask the surface of hydrophobic NO donor-containing films with a hydration layer, whereby hydrophobic proteins have shown decreased adsorption(210, 211). SNAP-doped CarboSil 2080A base layers top-coated with hydrophilic

polymers (e.g., SP60D60 and SG80A) (212) as well as grafted zwitterions (213, 214) have shown resistance to biofouling. Other work has used immobilized heparin (215) or methods that confer an enhanced anti-platelet and anti-biofouling effect through hydrophobin protein top coating (71) or liquid infusion via the fabrication of silicone oil-infused, SNAP-doped silicone(61, 208).

To reduce fouling by protein, bacteria, and platelets, one promising strategy to combine with NO-releasing surfaces is a liquid-infused (LI) interface. Inspired by *Nepenthes* pitcher plants, Wong et al. at the Harvard Wyss Institute reported the first bioinspired LI surface in 2011(216). Unlike superhydrophobic surfaces which rely on hierarchical structure to repel liquids, slippery liquid-infused porous surface (SLIPS) utilizes nanoscale porosity and capillary forces to tether an intermediate liquid to a polymer surface(217). Once tethered, the intermediate liquid layer provides an anti-fouling, incompressible homogeneous layer capable of self-healing and self-cleaning(218). Demonstrating the physiological efficacy of LI surfaces, Yuan et al. developed a fluorocarbon-infused surface by merging photografting polymerization with osmotically-driven wrinkling to create a rough surface morphology, reducing fibrinogen adsorption by 96%, minimizing platelet adhesion, and decreasing *S. aureus* and *E. coli* attachment after 24 h of incubation(219). Similarly, Yao et al. fabricated omniphobic fluorogel elastomers using perfluorinated alkyl acrylate monomers and a fluorinated macromolecular crosslinker capable of broad antifouling capabilities including decreased protein adsorption and whole blood repellency(220). Using a more robust infection model, LI polytetrafluoroethylene (PTFE) surfaces showed minimal *P. aeruginosa* contamination on the surface after 7 d of exposure under flow conditions (99.6% reduction in biofilm mass compared to controls)(221). However, like other passive surfaces, LI surfaces do not prevent blood component activation. LI surfaces are capable of overcoming this limitation through the incorporation of bioactive agents(222, 223). Work by

Goudie et al. was the first to combine LI surfaces and NO-releasing surfaces (LINOrel) into a silicone oil-infused polymer, resulting in a significant reduction in platelet adhesion and viable adhered bacteria(61). However, long-term antimicrobial efficacy and *in vivo* capabilities of this combination have yet to be explored (work performed in Chapters 4 and 5 of this dissertation).

1.4 *In Vitro* and *In Vivo* Assessment of Hemocompatible and Antimicrobial Surfaces

1.4.1 Hemocompatibility Assessments

To increase hemocompatibility, researchers are now modifying surfaces to prevent or disrupt pathways that lead to device-induced thrombosis described in Section 1.1. Hemocompatibility assessment guidelines provided by ISO 10993-4 are comprised of five distinct categories: thrombosis, coagulation, platelets, hematology, and immunology (**Table 1.6**)(26, 224, 225). Therefore, to evaluate the entire picture of hemocompatibility for biomaterials, each category should be examined.

Table 1.6 - Hemocompatibility assessment categories of biomaterials based on ISO 10993-4 standards

Category	Measurement Target
Thrombosis	Platelet, leukocyte, and red blood cell adhesion; fibrin formation
Coagulation	PTT; FPA; Factor XIIa, TAT; F1+2
Platelets	Platelet count; P-selectin; activated GPIIb/IIIa; PF4
Hematology	Leukocyte count; hemolysis (free hemoglobin); CD11b expression
Immunology	Complement activation (C3a, C5a, Bb, iC3b, C4d, C5b-9)

Prior to evaluating materials *in vivo*, hemocompatibility measurements can be performed by incubating the materials in static, agitated, or flow conditions. Material thrombogenicity is commonly predicted *in vitro* or *ex vivo* through platelet adhesion and aggregation measurements, leukocyte adhesion, and plasma protein adsorption(26). A simple, cost-effective method of analyzing materials is through static platelet-rich plasma (PRP) or whole blood incubation to gain a preliminary understanding of the blood-material interactions; however, cell sedimentation,

interactions with non-test materials, and platelet activation at the blood-air interface significantly impact the reliability of static testing(26, 226). Models that agitate the incubated material through gentle rocking or shaking help prevent cell sedimentation, but fail to mimic vascular blood flow. Therefore, the most accurate models for evaluating the hemocompatibility of materials *ex vivo* emulate flow conditions found in the body. Several different models (flat-plate flow chamber, parallel-plate and cone-platelet viscometer, Chandler loop, roller pump) have been developed to mimic arterial shear rates, but several shortcomings still exist. In the Chandler loop setup, which involves rotating a loop filled with whole blood and an air pocket through a water bath maintained at 37° C, proteins can become denatured and platelets can be activated at the air-blood interface(26). Moreover, pumps used to induce blood flow can cause hemolysis and platelet activation. Finally, all of these systems fail to capture endothelium interactions with the material(26).

To evaluate material hemocompatibility *in vivo*, several different models (rabbit, pig, rat, ewes, feline, bovine, canine, baboons, etc.) have been developed for devices including catheters, extracorporeal tubing, stents, vascular grafts, and patches(112, 119, 227-233). Extracorporeal circulation in both a rabbit and pig model has been used to determine thrombogenicity, measuring platelet consumption, thrombus formation, protein adhesion, and device failure rate(234, 235). However, several limitations of these models still exist. For example, if thrombus that forms on the inside of the device is dislodged into the bloodstream, these models may fail to account for that. Moreover, since several different models exist, comparisons between research findings remain difficult.

1.4.2 Antimicrobial Assessments

Materials can exhibit anti-infection properties by locally releasing antimicrobial agents, through direct contact killing, or by preventing bacterial fouling(236). Depending on the method, different *in vitro* tests may be more appropriate while determining the antimicrobial efficacy of a material (**Table 1.7**). The antimicrobial efficacy of a material is commonly measured by taking the difference between the logarithmic value of viable bacteria cells adhered to the test material and control materials after bacterial exposure(236) Materials can be evaluated against Gram-positive and Gram-negative bacteria as well as fungi to determine if the antimicrobial properties are broad-spectrum.

Table 1.7 - Common methods of determining antimicrobial efficacy of biomaterials *in vitro.*

Testing Method	Description	Material Design		
		Antimicrobial-Releasing	Antifouling Surfaces	Contact Killing
Zone of Inhibition	Qualitative analysis where test materials cut into uniform disc shapes are placed on inoculated agar plates and incubated for 24 h. The "zone of inhibition" refers to the area around the test material where bacterial viability and growth is inhibited.	x		
Bacterial Adhesion	Quantitative analysis where samples are suspended in a bacterial solution. After incubation, the samples are homogenized/ vortexed to detach the adhered bacteria and the number of viable bacteria is measured. This study can be conducted in a well-plate or in a bioreactor (eg., CDC biofilm reactor, dripflow bioreactor)	x	x	x
Bacterial Viability in Suspension	Quantitative analysis where samples are suspended in a bacterial solution. After incubation, the viability of the bacteria in solution is measured.	x		
Live/Dead Staining	Qualitative or quantitative analysis where bacteria exposed to a sample are stained with fluorescent markers to determine viability. Live and dead cells can be separated and quantified using flow cytometry.	x		x

In vivo determination of antimicrobial efficacy can vary depending on the intended application of the material. Medical devices such as central venous catheters, urinary catheters, or stents have been developed either through the direct modification of an existing device or by

fabricating novel materials (e.g., dip-coating a polymer solution onto a mandrel) and have been evaluated in several different animals including mice, rats, rabbits, and pigs(237-240). Moreover, the antimicrobial efficacy and foreign body response of materials intended for medical devices or wound healing applications are also most commonly studied subcutaneously using mouse and rat models(241, 242). Understanding the antimicrobial efficacy of the material *in vivo* can help better predict clinical performance, which may be more limited due to protein adsorption, fibrous encapsulation, and degradative reactive oxygen species compared to results found during *in vitro* evaluations(243).

1.5 Summary

Despite decades of development, two common clinical complications associated with indwelling medical devices remain: infection and thrombosis. The fate of medical devices largely depends on their ability to minimize protein adsorption, thrombosis, and infection. To increase the lifetime of the device and improve patient outcome, biopassive and bioactive surface modifications can be applied. Biopassive surfaces mitigate protein adsorption, platelet adhesion, and bacterial adhesion, but the long-term efficacy of these surfaces is still a concern. Bioactive surfaces directly interfere with bacterial viability and biofilm formation and/or thrombosis, but common complications with these materials include a limited bioactive agent reservoir, limitations due to protein adsorption, and depreciated bioactivity due after incorporation. One promising class of materials, NO-releasing surfaces, exhibit multifunctional activity, inhibiting platelet activation and adhesion and reducing the viability of adhered pathogens. However, these surfaces: (1) lack of NO release tunability; (2) have a limited NO reservoir; and (3) are still subject to biofouling. Therefore, other surface modifications can be combined with NO-releasing surfaces to help overcome these shortcomings and are presented in this dissertation. Standard, robust antimicrobial

and hemocompatible evaluations can be conducted both *in vitro* and *in vivo* to compare different surface modifications while predicting clinical performance.

1.6 Statement of Dissertation Research

Clinical manifestations of thrombosis and infection have plagued medical device use in healthcare settings. NO-releasing materials have been routinely documented to inhibit platelet activation and adhesion and reduce the viability of adhered bacterial pathogens. Although NO-releasing materials have been synthesized to minimize infection and improve blood-material interactions, three shortcomings remain: (1) NO-releasing materials have a limited reservoir of NO for long-term applications; (2) NO-releasing materials lack NO flux tunability; and (3) NO-releasing materials do not prevent surface fouling from blood proteins or bacteria. The primary objective of this dissertation was to address these critical issues by combining different surface modification strategies. The efficacy of each surface strategy was evaluated (NO-generating surfaces, metal nanoparticle coatings, liquid-infused surfaces) in combination with NO-releasing technology by its ability to reduce bacterial colonization and thrombus formation *in vitro* and/or *in vivo* (**Table 1.8**). This dissertation was prepared using a manuscript-style format, where each chapter is derived from publications already accepted or to submitted to peer-reviewed scientific journals. The introductory Chapter 1 also has sections taken from a review article under review with *Progress in Materials Science.*

In Chapter 2, a SNAP-doped polymer with a blended selenium (Se) - polymer interface was fabricated, and the unique capability of the SNAP-Se polymer composites to explicitly release NO from the SNAP reservoir as well as generate NO via the Se-based interface is reported for the first time. The antimicrobial efficacy, antiplatelet activity, and cytotoxicity of the fabricated

materials were evaluated *in vitro*. This work has been published in *ACS Applied Materials & Interfaces*(133).

In Chapter 3, the efficacy of a copper nanoparticle (Cu NP) catalyst for the tunable release of NO from a GSNO coating applied to commercial Tygon S3^{TM} E-3603 poly(vinyl chloride) tubing was evaluated. The effect of the increased NO release on antimicrobial efficacy and cytotoxicity was measured *in vitro*. Finally, extracorporeal circuits were coated and exposed to 4 h of blood flow in an *in vivo* rabbit model, and platelet consumption and animal survival were monitored. This work has been published in *ACS Applied Bio Materials*(119).

In Chapters 4 & 5, NO-releasing surfaces were modified to create an antifouling, liquid-infused interface, and the efficacies of the combined surface strategies were monitored *in vitro* and *in vivo*. In Chapter 4, the covalent attachment of a common synthetic NO donor, SNAP, onto medical-grade polydimethylsiloxane (PDMS) was combined with a liquid-infused interface to achieve sustained NO-releasing and antifouling surface properties. Robust antimicrobial evaluations were measured after 24 h, 7 d, 14 d, and 28 d against both Gram-positive methicillin-resistant *Staphylococcus aureus* (MRSA) and Gram-negative *Pseudomonas aeruginosa* (*P. aeruginosa*), and hemocompatibility measurements were conducted *in vitro*. In Chapter 5, SNAP-impregnated PDMS with a similar liquid-infused interface was fabricated, and the antimicrobial efficacy was determined after 7 d *in vitro* in a CDC biofilm reactor. The foreign body response of the fabricated materials implanted subcutaneously was monitored in a 14-d and 28-d mouse model. This work has been published in *ACS Applied Materials & Interfaces*.(244)

Finally, in Chapter 6, a summary of the work as well as future directions are discussed. This includes a summary of the findings from each chapter, as well as highlighting the need for

defining specific NO release profiles desired for individual applications to better optimize clinical efficacy while minimizing potential costs.

Table 1.8 - Surface modification strategies combined with NO-releasing surfaces explored in this dissertation work.

Goal	Surface Modification Strategy	NO-Releasing Strategy	Chapter
Long-term NO production	NO-generating surfaces	Blended SNAP	2
Tunable NO release	Metal nanoparticle coatings	Blended GSNO	3
Reduce surface fouling	Liquid-infused surfaces	SNAP Impregnation (Swelling)	4 & 5

1.7 References

1. VanEpps JS, Younger JG. Implantable Device-Related Infection. Shock. 2016;46(6):597-608.

2. Parada G, Yu Y, Riley W, Lojovich S, Tshikudi D, Ling Q, et al. Ultrathin and Robust Hydrogel Coatings on Cardiovascular Medical Devices to Mitigate Thromboembolic and Infectious Complications. Adv Healthc Mater. 2020;9(20):e2001116.

3. Johnston AJ, Streater CT, Noorani R, Crofts JL, Del Mundo AB, Parker RA. The effect of peripherally inserted central catheter (PICC) valve technology on catheter occlusion rates--the 'ELeCTRiC' study. J Vasc Access. 2012;13(4):421-5.

4. Seckold T, Walker S, Dwyer T. A comparison of silicone and polyurethane PICC lines and postinsertion complication rates: a systematic review. J Vasc Access. 2015;16(3):167-77.

5. Grau D, Clarivet B, Lotthe A, Bommart S, Parer S. Complications with peripherally inserted central catheters (PICCs) used in hospitalized patients and outpatients: a prospective cohort study. Antimicrob Resist Infect Control. 2017;6:18.

6. Biffi S, Di Bella S, Scaravilli V, Peri AM, Grasselli G, Alagna L, et al. Infections during extracorporeal membrane oxygenation: epidemiology, risk factors, pathogenesis and prevention. Int J Antimicrob Agents. 2017;50(1):9-16.

7. Raffini L. Anticoagulation with VADs and ECMO: walking the tightrope. Hematology Am Soc Hematol Educ Program. 2017;2017(1):674-80.

8. Olson SR, Murphree CR, Zonies D, Meyer AD, McCarty OJT, Deloughery TG, et al. Thrombosis and Bleeding in Extracorporeal Membrane Oxygenation (ECMO) Without Anticoagulation: A Systematic Review. ASAIO J. 2021;67(3):290-6.

9. Schmidt M, Brechot N, Hariri S, Guiguet M, Luyt CE, Makri R, et al. Nosocomial infections in adult cardiogenic shock patients supported by venoarterial extracorporeal membrane oxygenation. Clin Infect Dis. 2012;55(12):1633-41.

10. Allou N, Lo Pinto H, Persichini R, Bouchet B, Braunberger E, Lugagne N, et al. Cannula-Related Infection in Patients Supported by Peripheral ECMO: Clinical and Microbiological Characteristics. ASAIO Journal. 2019;65(2):180-6.

11. Grammes JA, Schulze CM, Al-Bataineh M, Yesenosky GA, Saari CS, Vrabel MJ, et al. Percutaneous pacemaker and implantable cardioverter-defibrillator lead extraction in 100 patients with intracardiac vegetations defined by transesophageal echocardiogram. J Am Coll Cardiol. 2010;55(9):886-94.

12. Wilhelm BJ, Thone M, El-Scheich T, Livert D, Angelico R, Osswald B. Complications and Risk Assessment of 25 Years in Pediatric Pacing. Ann Thorac Surg. 2015;100(1):147-53.

13. Li X, Ze F, Wang L, Li D, Duan J, Guo F, et al. Prevalence of venous occlusion in patients referred for lead extraction: implications for tool selection. Europace. 2014;16(12):1795-9.

14. Lonyai A, Dubin AM, Feinstein JA, Taylor CA, Shadden SC. New insights into pacemaker lead-induced venous occlusion: simulation-based investigation of alterations in venous biomechanics. Cardiovasc Eng. 2010;10(2):84-90.

15. Tompkins C, McLean R, Cheng A, Brinker JA, Marine JE, Nazarian S, et al. End-stage renal disease predicts complications in pacemaker and ICD implants. J Cardiovasc Electrophysiol. 2011;22(10):1099-104.

16. Tabatabaie O, Kasumova GG, Kent TS, Eskander MF, Fadayomi AB, Ng SC, et al. Upper extremity deep venous thrombosis after port insertion: What are the risk factors? Surgery. 2017;162(2):437-44.

17. Teichgraber UK, Pfitzmann R, Hofmann HA. Central venous port systems as an integral part of chemotherapy. Dtsch Arztebl Int. 2011;108(9):147-53; quiz 54.

18. Hsieh CC, Weng HH, Huang WS, Wang WK, Kao CL, Lu MS, et al. Analysis of risk factors for central venous port failure in cancer patients. World J Gastroenterol. 2009;15(37):4709-14.

19. Dalton HJ, Garcia-Filion P, Holubkov R, Moler FW, Shanley T, Heidemann S, et al. Association of bleeding and thrombosis with outcome in extracorporeal life support. Pediatr Crit Care Med. 2015;16(2):167-74.

20. Gorbet MB, Sefton MV. Biomaterial-associated thrombosis: roles of coagulation factors, complement, platelets and leukocytes. Biomaterials. 2004;25(26):5681-703.

21. Jaffer IH, Fredenburgh JC, Hirsh J, Weitz JI. Medical device-induced thrombosis: what causes it and how can we prevent it? J Thromb Haemost. 2015;13 Suppl 1:S72-81.

22. Werner C, Maitz MF, Sperling C. Current strategies towards hemocompatible coatings. J Mater Chem. 2007;17(32):3376-84.

23. Johnson SA, Vanhorn DL, Pederson HJ, Marr J. Function of Platelets - a Review. Transfusion. 1966;6(1):3-+.

24. Tsai WB, Grunkemeier JM, Horbett TA. Human plasma fibrinogen adsorption and platelet adhesion to polystyrene. J Biomed Mater Res. 1999;44(2):130-9.

25. Chen Z, Mondal NK, Ding J, Koenig SC, Slaughter MS, Wu ZJ. Paradoxical Effect of Nonphysiological Shear Stress on Platelets and von Willebrand Factor. Artif Organs. 2016;40(7):659-68.

26. Weber M, Steinle H, Golombek S, Hann L, Schlensak C, Wendel HP, et al. Blood-Contacting Biomaterials: In Vitro Evaluation of the Hemocompatibility. Front Bioeng Biotechnol. 2018;6:99.

27. Classen DC, Jaser L, Budnitz DS. Adverse drug events among hospitalized Medicare patients: epidemiology and national estimates from a new approach to surveillance. Jt Comm J Qual Patient Saf. 2010;36(1):12-21.

28. Piazza G, Nguyen TN, Cios D, Labreche M, Hohlfelder B, Fanikos J, et al. Anticoagulation-associated adverse drug events. Am J Med. 2011;124(12):1136-42.

29. Harter K, Levine M, Henderson SO. Anticoagulation drug therapy: a review. West J Emerg Med. 2015;16(1):11-7.

30. van Rein N, Biedermann JS, van der Meer FJM, Cannegieter SC, Wiersma N, Vermaas HW, et al. Major bleeding risks of different low-molecular-weight heparin agents: a cohort study in 12 934 patients treated for acute venous thrombosis. J Thromb Haemost. 2017;15(7):1386-91.

31. Nelson-Piercy C. Hazards of heparin: allergy, heparin-induced thrombocytopenia and osteoporosis. Baillieres Clin Obstet Gynaecol. 1997;11(3):489-509.

32. Ahmed I, Majeed A, Powell R. Heparin induced thrombocytopenia: diagnosis and management update. Postgrad Med J. 2007;83(983):575-82.

33. Pollak U. Heparin-induced thrombocytopenia complicating extracorporeal membrane oxygenation support: Review of the literature and alternative anticoagulants. Journal of Thrombosis and Haemostasis. 2019;17(10):1608-22.

34. Ashcraft M, Douglass M, Chen Y, Handa H. Combination strategies for antithrombotic biomaterials: an emerging trend towards hemocompatibility. Biomater Sci. 2021;9(7):2413-23.

35. Weiner-Lastinger LM, Abner S, Edwards JR, Kallen AJ, Karlsson M, Magill SS, et al. Antimicrobial-resistant pathogens associated with adult healthcare-associated infections: Summary of data reported to the National Healthcare Safety Network, 2015-2017. Infect Control Hosp Epidemiol. 2020;41(1):1-18.

36. Avershina E, Shapovalova V, Shipulin G. Fighting Antibiotic Resistance in Hospital-Acquired Infections: Current State and Emerging Technologies in Disease Prevention, Diagnostics and Therapy. Front Microbiol. 2021;12:707330.

37. Khatoon Z, McTiernan CD, Suuronen EJ, Mah TF, Alarcon EI. Bacterial biofilm formation on implantable devices and approaches to its treatment and prevention. Heliyon. 2018;4(12):e01067.

38. Crouzet M, Le Senechal C, Brozel VS, Costaglioli P, Barthe C, Bonneu M, et al. Exploring early steps in biofilm formation: set-up of an experimental system for molecular studies. BMC Microbiol. 2014;14:253.

39. Gupta P, Sarkar S, Das B, Bhattacharjee S, Tribedi P. Biofilm, pathogenesis and prevention—a journey to break the wall: a review. Archives of Microbiology. 2016;198(1):1-15.

40. Herrmann M, Vaudaux PE, Pittet D, Auckenthaler R, Lew PD, Schumacher-Perdreau F, et al. Fibronectin, fibrinogen, and laminin act as mediators of adherence of clinical staphylococcal isolates to foreign material. J Infect Dis. 1988;158(4):693-701.

41. Flemming HC, Neu TR, Wozniak DJ. The EPS matrix: the "house of biofilm cells". J Bacteriol. 2007;189(22):7945-7.

42. Jamal M, Ahmad W, Andleeb S, Jalil F, Imran M, Nawaz MA, et al. Bacterial biofilm and associated infections. J Chin Med Assoc. 2018;81(1):7-11.

43. Roy R, Tiwari M, Donelli G, Tiwari V. Strategies for combating bacterial biofilms: A focus on anti-biofilm agents and their mechanisms of action. Virulence. 2018;9(1):522-54.

44. Zingg W, Harbarth S. Oxford Textbook of Critical Care. Diagnosis, prevention, and treatment of device-related infection in the ICU: Oxford University Press; 2016.

45. Kadri SS. Key Takeaways From the U.S. CDC's 2019 Antibiotic Resistance Threats Report for Frontline Providers. Critical care medicine. 2020;48(7):939-45.

46. Peterson E, Kaur P. Antibiotic Resistance Mechanisms in Bacteria: Relationships Between Resistance Determinants of Antibiotic Producers, Environmental Bacteria, and Clinical Pathogens. Frontiers in Microbiology. 2018;9(2928).

47. Lambert PA. Bacterial resistance to antibiotics: modified target sites. Adv Drug Deliv Rev. 2005;57(10):1471-85.

48. Sharma D, Misba L, Khan AU. Antibiotics versus biofilm: an emerging battleground in microbial communities. Antimicrobial Resistance & Infection Control. 2019;8(1):76.

49. Delcour AH. Outer membrane permeability and antibiotic resistance. Biochim Biophys Acta. 2009;1794(5):808-16.

50. Ma H, Bryers JD. Non-invasive determination of conjugative transfer of plasmids bearing antibiotic-resistance genes in biofilm-bound bacteria: effects of substrate loading and antibiotic selection. Appl Microbiol Biotechnol. 2013;97(1):317-28.

51. Yi L, Jin M, Li J, Grenier D, Wang Y. Antibiotic resistance related to biofilm formation in Streptococcus suis. Appl Microbiol Biotechnol. 2020;104(20):8649-60.

52. Cho E, Kim SH, Kim M, Park J-S, Lee S-J. Super-hydrophobic and antimicrobial properties of Ag-PPFC nanocomposite thin films fabricated using a ternary carbon nanotube-Ag-PTFE composite sputtering target. Surface and Coatings Technology. 2019;370:18-23.

53. Tripathy A, Kumar A, Sreedharan S, Muralidharan G, Pramanik A, Nandi D, et al. Fabrication of Low-Cost Flexible Superhydrophobic Antibacterial Surface with Dual-Scale Roughness. Acs Biomater Sci Eng. 2018;4(6):2213-23.

54. Ozkan E, Mondal A, Singha P, Douglass M, Hopkins SP, Devine R, et al. Fabrication of Bacteria- and Blood-Repellent Superhydrophobic Polyurethane Sponge Materials. ACS Appl Mater Interfaces. 2020;12(46):51160-73.

55. Bartlet K, Movafaghi S, Dasi LP, Kota AK, Popat KC. Antibacterial activity on superhydrophobic titania nanotube arrays. Colloids Surf B Biointerfaces. 2018;166:179-86.

56. Pan Q, Cao Y, Xue W, Zhu D, Liu W. Picosecond Laser-Textured Stainless Steel Superhydrophobic Surface with an Antibacterial Adhesion Property. Langmuir. 2019;35(35):11414-21.

57. Jenkins J, Mantell J, Neal C, Gholinia A, Verkade P, Nobbs AH, et al. Antibacterial effects of nanopillar surfaces are mediated by cell impedance, penetration and induction of oxidative stress. Nat Commun. 2020;11(1):1626.

58. Bhadra CM, Truong VK, Pham VT, Al Kobaisi M, Seniutinas G, Wang JY, et al. Antibacterial titanium nano-patterned arrays inspired by dragonfly wings. Sci Rep. 2015;5:16817.

59. Ivanova EP, Hasan J, Webb HK, Gervinskas G, Juodkazis S, Truong VK, et al. Bactericidal activity of black silicon. Nature Communications. 2013;4(1):2838.

60. Wang C, Yan Y, Du D, Xiong X, Ma Y. WO3-Based Slippery Liquid-Infused Porous Surfaces with Long-Term Stability. ACS Appl Mater Interfaces. 2020;12(26):29767-77.

61. Goudie MJ, Pant J, Handa H. Liquid-infused nitric oxide-releasing (LINORel) silicone for decreased fouling, thrombosis, and infection of medical devices. Sci Rep. 2017;7(1):13623.

62. Peppou-Chapman S, Hong JK, Waterhouse A, Neto C. Life and death of liquid-infused surfaces: a review on the choice, analysis and fate of the infused liquid layer. Chem Soc Rev. 2020;49(11):3688-715.

63. Leslie DC, Waterhouse A, Berthet JB, Valentin TM, Watters AL, Jain A, et al. A bioinspired omniphobic surface coating on medical devices prevents thrombosis and biofouling. Nature Biotechnology. 2014;32(11):1134-40.

64. Yamazoe H, Tanabe T. Drug-carrying albumin film for blood-contacting biomaterials. J Biomater Sci Polym Ed. 2010;21(5):647-57.

65. Hlady V, Andrade JD, Ho CH, Feng L, Tingey K. Plasma-Protein Adsorption on Model Biomaterial Surfaces. Clinical Materials. 1993;13(1-4):85-93.

66. Schottler S, Becker G, Winzen S, Steinbach T, Mohr K, Landfester K, et al. Protein adsorption is required for stealth effect of poly(ethylene glycol)- and poly(phosphoester)-coated nanocarriers. Nat Nanotechnol. 2016;11(4):372-7.

67. Krajewski S, Neumann B, Kurz J, Perle N, Avci-Adali M, Cattaneo G, et al. Preclinical evaluation of the thrombogenicity and endothelialization of bare metal and surface-coated neurovascular stents. AJNR Am J Neuroradiol. 2015;36(1):133-9.

68. Kinnari TJ, Peltonen LI, Kuusela P, Kivilahti J, Kononen M, Jero J. Bacterial adherence to titanium surface coated with human serum albumin. Otol Neurotol. 2005;26(3):380-4.

69. von Vacano B, Xu R, Hirth S, Herzenstiel I, Ruckel M, Subkowski T, et al. Hydrophobin can prevent secondary protein adsorption on hydrophobic substrates without exchange. Analytical and Bioanalytical Chemistry. 2011;400(7):2031-40.

70. Weickert U, Wiesend F, Subkowski T, Eickhoff A, Reiss G. Optimizing biliary stent patency by coating with hydrophobin alone or hydrophobin and antibiotics or heparin: an in vitro proof of principle study. Advances in Medical Sciences. 2011;56(2):138-44.

71. Devine R, Singha P, Handa H. Versatile biomimetic medical device surface: hydrophobin coated, nitric oxide-releasing polymer for antimicrobial and hemocompatible applications. Biomater Sci. 2019;7(8):3438-49.

72. Artini M, Cicatiello P, Ricciardelli A, Papa R, Selan L, Dardano P, et al. Hydrophobin coating prevents Staphylococcus epidermidis biofilm formation on different surfaces. Biofouling. 2017;33(7):601-11.

73. Damodaran VB, Murthy NS. Bio-inspired strategies for designing antifouling biomaterials. Biomaterials Research. 2016;20(1):18.

74. Wang C, Feng R, Yang F. Enhancing the hydrophilic and antifouling properties of polypropylene nonwoven fabric membranes by the grafting of poly(N-vinyl-2-pyrrolidone) via the ATRP method. J Colloid Interface Sci. 2011;357(2):273-9.

75. Sawada I, Fachrul R, Ito T, Ohmukai Y, Maruyama T, Matsuyama H. Development of a hydrophilic polymer membrane containing silver nanoparticles with both organic antifouling and antibacterial properties. Journal of Membrane Science. 2012;387-388:1-6.

76. Bekale L, Agudelo D, Tajmir-Riahi HA. The role of polymer size and hydrophobic end-group in PEG-protein interaction. Colloids Surf B Biointerfaces. 2015;130:141-8.

77. Dimitriou MD, Zhou Z, Yoo H-S, Killops KL, Finlay JA, Cone G, et al. A General Approach to Controlling the Surface Composition of Poly(ethylene oxide)-Based Block Copolymers for Antifouling Coatings. Langmuir. 2011;27(22):13762-72.

78. Singha P, Pant J, Goudie MJ, Workman CD, Handa H. Enhanced antibacterial efficacy of nitric oxide releasing thermoplastic polyurethanes with antifouling hydrophilic topcoats. Biomaterials Science. 2017;5(7):1246-55.

79. Ye S-H, Chen Y, Mao Z, Gu X, Shankarraman V, Hong Y, et al. Biodegradable Zwitterionic Polymer Coatings for Magnesium Alloy Stents. Langmuir. 2019;35(5):1421-9.

80. Tang S-H, Domino MY, Venault A, Lin H-T, Hsieh C, Higuchi A, et al. Bioinert Control of Zwitterionic Poly(ethylene terephtalate) Fibrous Membranes. Langmuir. 2019;35(5):1727-39.

81. Xiang T, Zhang L-S, Wang R, Xia Y, Su B-H, Zhao C-S. Blood compatibility comparison for polysulfone membranes modified by grafting block and random zwitterionic copolymers via surface-initiated ATRP. Journal of Colloid and Interface Science. 2014;432:47-56.

82. Plegue TJ, Kovach KM, Thompson AJ, Potkay JA. Stability of Polyethylene Glycol and Zwitterionic Surface Modifications in PDMS Microfluidic Flow Chambers. Langmuir. 2018;34(1):492-502.

83. Ye S-H, Hong Y, Sakaguchi H, Shankarraman V, Luketich SK, D'Amore A, et al. Nonthrombogenic, Biodegradable Elastomeric Polyurethanes with Variable Sulfobetaine Content. ACS Applied Materials & Interfaces. 2014;6(24):22796-806.

84. Chou Y-N, Venault A, Wang Y-H, Chinnathambi A, Higuchi A, Chang Y. Surface zwitterionization on versatile hydrophobic interfaces via a combined copolymerization/self-assembling process. Journal of Materials Chemistry B. 2018;6(30):4909-19.

85. Cai X, Yuan J, Chen S, Li P, Li L, Shen J. Hemocompatibility improvement of poly(ethylene terephthalate) via self-polymerization of dopamine and covalent graft of zwitterions. Materials Science and Engineering: C. 2014;36:42-8.

86. Surman F, Riedel T, Bruns M, Kostina NY, Sedláková Z, Rodriguez-Emmenegger C. Polymer Brushes Interfacing Blood as a Route Toward High Performance Blood Contacting Devices. Macromolecular Bioscience. 2015;15(5):636-46.

87. Venault A, Ye C-C, Lin Y-C, Tsai C-W, Jhong J-F, Ruaan R-C, et al. Zwitterionic fibrous polypropylene assembled with amphiphatic carboxybetaine copolymers for hemocompatible blood filtration. Acta Biomaterialia. 2016;40:130-41.

88. Huang N, Yang P, Leng YX, Chen JY, Sun H, Wang J, et al. Hemocompatibility of titanium oxide films. Biomaterials. 2003;24(13):2177-87.

89. Jiang L, Yao H, Luo X, Zou D, Han C, Tang C, et al. Copper-mediated synergistic catalytic titanium dioxide nanofilm with nitric oxide generation and anti-protein fouling for enhanced hemocompatibility and inflammatory modulation. Applied Materials Today. 2020;20:100663.

90. Chen JY, Leng YX, Tian XB, Wang LP, Huang N, Chu PK, et al. Antithrombogenic investigation of surface energy and optical bandgap and hemocompatibility mechanism of Ti(Ta+5)O2 thin films. Biomaterials. 2002;23(12):2545-52.

91. Sunny MC, Sharma CP. Titanium-Protein Interaction: Changes with Oxide Layer Thickness. Journal of Biomaterials Applications. 1991;6(1):89-98.

92. Maitz MF, Pham M-T, Wieser E, Tsyganov I. Blood Compatibility of Titanium Oxides with Various Crystal Structure and Element Doping. Journal of Biomaterials Applications. 2003;17(4):303-19.

93. Manivasagam VK, Maia Sabino R, Kantam P, Popat K. Surface Modification Strategies to Improve Titanium Hemocompatibility: A Comprehensive Review. Materials Advances. 2021.

94. Zhang F, Liu X, Mao Y, Huang N, Chen Y, Zheng Z, et al. Artificial heart valves:: improved hemocompatibility by titanium oxide coatings prepared by ion beam assisted deposition. Surface and Coatings Technology. 1998;103-104:146-50.

95. Manivasagam VK, Popat KC. In Vitro Investigation of Hemocompatibility of Hydrothermally Treated Titanium and Titanium Alloy Surfaces. ACS Omega. 2020;5(14):8108-20.

96. Zhao A, Wang Z, Zhou S, Xue G, Wang Y, Ye C, et al. Titanium oxide films with vacuum thermal treatment for enhanced hemocompatibility. Surface Engineering. 2015;31(12):898-903.

97. Freitas SC, Barbosa MA, Martins MC. The effect of immobilization of thrombin inhibitors onto self-assembled monolayers on the adsorption and activity of thrombin. Biomaterials. 2010;31(14):3772-80.

98. Maitz MF, Sperling C, Werner C. Immobilization of the irreversible thrombin inhibitor D-Phe-Pro-Arg-chloromethylketone: a concept for hemocompatible surfaces? J Biomed Mater Res A. 2010;94(3):905-12.

99. Yang Z, Tu Q, Maitz MF, Zhou S, Wang J, Huang N. Direct thrombin inhibitor-bivalirudin functionalized plasma polymerized allylamine coating for improved biocompatibility of vascular devices. Biomaterials. 2012;33(32):7959-71.

100. Lu L, Li QL, Maitz MF, Chen JL, Huang N. Immobilization of the direct thrombin inhibitor-bivalirudin on 316L stainless steel via polydopamine and the resulting effects on hemocompatibility in vitro. Journal of Biomedical Materials Research Part A. 2012;100a(9):2421-30.

101. Yang ZL, Zhong S, Yang Y, Maitz MF, Li XY, Tu QF, et al. Polydopamine-mediated long-term elution of the direct thrombin inhibitor bivalirudin from TiO2 nanotubes for improved vascular biocompatibility. Journal of Materials Chemistry B. 2014;2(39):6767-78.

102. Freitas SC, Cereija TB, Figueiredo AC, Osorio H, Pereira PJ, Barbosa MA, et al. Bioengineered surfaces to improve the blood compatibility of biomaterials through direct thrombin inactivation. Acta Biomater. 2012;8(11):4101-10.

103. Dai Y, Dai S, Xie X, Ning J. Immobilizing argatroban and mPEG-NH2 on a polyethersulfone membrane surface to prepare an effective nonthrombogenic biointerface. J Biomater Sci Polym Ed. 2019;30(8):608-28.

104. Major TC, Brisbois EJ, Jones AM, Zanetti ME, Annich GM, Bartlett RH, et al. The effect of a polyurethane coating incorporating both a thrombin inhibitor and nitric oxide on hemocompatibility in extracorporeal circulation. Biomaterials. 2014;35(26):7271-85.

105. Yu J, Brisbois E, Handa H, Annich G, Meyerhoff M, Bartlett R, et al. The immobilization of a direct thrombin inhibitor to a polyurethane as a nonthrombogenic surface coating for extracorporeal circulation. J Mater Chem B. 2016;4(13):2264-72.

106. Weber N, Wendel HP, Ziemer G. Hemocompatibility of heparin-coated surfaces and the role of selective plasma protein adsorption. Biomaterials. 2002;23(2):429-39.

107. Fasl H, Stana J, Stropnik D, Strnad S, Stana-Kleinschek K, Ribitsch V. Improvement of the hemocompatibility of PET surfaces using different sulphated polysaccharides as coating materials. Biomacromolecules. 2010;11(2):377-81.

108. Wulff B, Stahlhoff S, Vonthein R, Schmidt A, Sigler M, Torsello GB, et al. Biomimetic Heparan Sulfate-Like Coated ePTFE Grafts Reduce In-graft Neointimal Hyperplasia in Ovine Carotids. Ann Vasc Surg. 2017;40:274-84.

109. Devine R, Goudie MJ, Singha P, Schmiedt C, Douglass M, Brisbois EJ, et al. Mimicking the Endothelium: Dual Action Heparinized Nitric Oxide Releasing Surface. ACS Appl Mater Interfaces. 2020;12(18):20158-71.

110. Sabino RM, Kauk K, Madruga LYC, Kipper MJ, Martins AF, Popat KC. Enhanced hemocompatibility and antibacterial activity on titania nanotubes with tanfloc/heparin polyelectrolyte multilayers. J Biomed Mater Res A. 2020;108(4):992-1005.

111. Xu F, Flanagan CE, Ruiz A, Crone WC, Masters KS. Polyurethane/dermatan sulfate copolymers as hemocompatible, non-biofouling materials. Macromol Biosci. 2011;11(2):257-66.

112. Dhahri M, Rodriguez-Ruiz V, Aid-Launais R, Ollivier V, Pavon-Djavid G, Journé C, et al. In vitro and in vivo hemocompatibility evaluation of a new dermatan sulfate-modified PET patch for vascular repair surgery. J Biomed Mater Res B Appl Biomater. 2017;105(7):2001-9.

113. Dhahri M, Abed A, Lajimi RH, Mansour MB, Gueguen V, Abdesselem SB, et al. Grafting of dermatan sulfate on polyethylene terephtalate to enhance biointegration. J Biomed Mater Res A. 2011;98(1):114-21.

114. Liberelle B, Merzouki A, De Crescenzo G. Immobilized carboxymethylated dextran coatings for enhanced ELISA. J Immunol Methods. 2013;389(1-2):38-44.

115. McLean KM, Johnson G, Chatelier RC, Beumer GJ, Steele JG, Griesser HJ. Method of immobilization of carboxymethyl-dextran affects resistance to tissue and cell colonization. Colloids Surf B Biointerfaces. 2000;18(3-4):221-34.

116. Michel EC, Montano-Machado V, Chevallier P, Labbe-Barrere A, Letourneur D, Mantovani D. Dextran grafting on PTFE surface for cardiovascular applications. Biomatter. 2014;4:e28805.

117. Monchaux E, Vermette P. Cell adhesion resistance mechanisms using arrays of dextran-derivative layers. J Biomed Mater Res A. 2008;85(4):1052-63.

118. Brisbois EJ, Davis RP, Jones AM, Major TC, Bartlett RH, Meyerhoff ME, et al. Reduction in Thrombosis and Bacterial Adhesion with 7 Day Implantation of S-Nitroso-N-acetylpenicillamine (SNAP)-Doped Elast-eon E2As Catheters in Sheep. J Mater Chem B. 2015;3(8):1639-45.

119. Douglass ME, Goudie MJ, Pant J, Singha P, Hopkins S, Devine R, et al. Catalyzed Nitric Oxide Release via Cu Nanoparticles Leads to an Increase in Antimicrobial Effects and Hemocompatibility for Short-Term Extracorporeal Circulation. ACS Applied Bio Materials. 2019;2(6):2539-48.

120. Wo Y, Brisbois EJ, Wu J, Li Z, Major TC, Mohammed A, et al. Reduction of Thrombosis and Bacterial Infection via Controlled Nitric Oxide (NO) Release from S-Nitroso-N-acetylpenicillamine (SNAP) Impregnated CarboSil Intravascular Catheters. Acs Biomater Sci Eng. 2017;3(3):349-59.

121. Roberts TR, Neufeld MJ, Meledeo MA, Cap AP, Cancio LC, Reynolds MM, et al. A metal organic framework reduces thrombus formation and platelet aggregation ex vivo. J Trauma Acute Care Surg. 2018;85(3):572-9.

122. Majhi S, Mishra A. Exploring potential of glass surface immobilized short antimicrobial peptide (AMP) as antibacterial coatings. Materials Today: Proceedings. 2021.

123. Zhang X-Y, Zhao Y-Q, Zhang Y, Wang A, Ding X, Li Y, et al. Antimicrobial Peptide-Conjugated Hierarchical Antifouling Polymer Brushes for Functionalized Catheter Surfaces. Biomacromolecules. 2019;20(11):4171-9.

124. Costa F, Carvalho IF, Montelaro RC, Gomes P, Martins MCL. Covalent immobilization of antimicrobial peptides (AMPs) onto biomaterial surfaces. Acta Biomaterialia. 2011;7(4):1431-40.

125. Xiao M, Jasensky J, Foster L, Kuroda K, Chen Z. Monitoring Antimicrobial Mechanisms of Surface-Immobilized Peptides in Situ. Langmuir. 2018;34(5):2057-62.

126. Townsend L, Williams RL, Anuforom O, Berwick MR, Halstead F, Hughes E, et al. Antimicrobial peptide coatings for hydroxyapatite: electrostatic and covalent attachment of antimicrobial peptides to surfaces. J R Soc Interface. 2017;14(126).

127. Abbasizadeh N, Rezayan AH, Nourmohammadi J, Kazemzadeh-Narbat M. HHC-36 antimicrobial peptide loading on silk fibroin (SF)/hydroxyapatite (HA) nanofibrous-coated titanium for the enhancement of osteoblast and bactericidal functions. International Journal of Polymeric Materials and Polymeric Biomaterials. 2020;69(10):629-39.

128. Singha P, Locklin J, Handa H. A review of the recent advances in antimicrobial coatings for urinary catheters. Acta Biomaterialia. 2017;50:20-40.

129. Dwyer A. Surface-treated catheters--a review. Semin Dial. 2008;21(6):542-6.

130. Jennings JA, Carpenter DP, Troxel KS, Beenken KE, Smeltzer MS, Courtney HS, et al. Novel Antibiotic-loaded Point-of-care Implant Coating Inhibits Biofilm. Clinical Orthopaedics and Related Research®. 2015;473(7):2270-82.

131. Stevanović M, Djošić M, Janković A, Nešović K, Kojić V, Stojanović J, et al. Assessing the Bioactivity of Gentamicin-Preloaded Hydroxyapatite/Chitosan Composite Coating on Titanium Substrate. ACS Omega. 2020;5(25):15433-45.

132. Douglass M, Hopkins S, Pandey R, Singha P, Norman M, Handa H. S-Nitrosoglutathione-Based Nitric Oxide-Releasing Nanofibers Exhibit Dual Antimicrobial and Antithrombotic Activity for Biomedical Applications. Macromol Biosci. 2020:e2000248.

133. Mondal A, Douglass M, Hopkins SP, Singha P, Tran M, Handa H, et al. Multifunctional S-Nitroso-N-acetylpenicillamine-Incorporated Medical-Grade Polymer with Selenium Interface for Biomedical Applications. ACS Appl Mater Interfaces. 2019;11(38):34652-62.

134. Ghalei S, Li J, Douglass M, Garren M, Handa H. Synergistic Approach to Develop Antibacterial Electrospun Scaffolds Using Honey and S-Nitroso-N-acetyl Penicillamine. Acs Biomater Sci Eng. 2021;7(2):517-26.

135. Choi YJ, Lim JK, Park JJ, Huh H, Kim D-J, Gong C-H, et al. Chlorhexidine and silver sulfadiazine coating on central venous catheters is not sufficient for protection against catheter-related infection: Simulation-based laboratory research with clinical validation. Journal of International Medical Research. 2017;45(3):1042-53.

136. McMahon S, Kennedy R, Duffy P, Vasquez JM, Wall JG, Tai H, et al. Poly(ethylene glycol)-Based Hyperbranched Polymer from RAFT and Its Application as a Silver-Sulfadiazine-Loaded Antibacterial Hydrogel in Wound Care. Acs Appl Mater Inter. 2016;8(40):26648-56.

137. Fischer M, Vahdatzadeh M, Konradi R, Friedrichs J, Maitz MF, Freudenberg U, et al. Multilayer hydrogel coatings to combine hemocompatibility and antimicrobial activity. Biomaterials. 2015;56:198-205.

138. Lorente L, Lecuona M, Jiménez A, Santacreu R, Raja L, Gonzalez O, et al. Chlorhexidine-silver sulfadiazine-impregnated venous catheters save costs. American Journal of Infection Control. 2014;42(3):321-4.

139. Segev G, Bankirer T, Steinberg D, Duvdevani M, Shapur NK, Friedman M, et al. Evaluation of Urinary Catheters Coated with Sustained-Release Varnish of Chlorhexidine in Mitigating Biofilm Formation on Urinary Catheters in Dogs. Journal of Veterinary Internal Medicine. 2013;27(1):39-46.

140. Srisang S, Nasongkla N. Spray coating of foley urinary catheter by chlorhexidine-loadedpoly(ε-caprolactone) nanospheres: effect of lyoprotectants, characteristics, and antibacterial activity evaluation. Pharm Dev Technol. 2019;24(4):402-9.

141. Srisang S, Nasongkla N. Layer-by-layer dip coating of Foley urinary catheters by chlorhexidine-loaded micelles. Journal of Drug Delivery Science and Technology. 2019;49:235-42.

142. Walz JM, Avelar RL, Longtine KJ, Carter KL, Mermel LA, Heard SO, et al. Anti-infective external coating of central venous catheters: A randomized, noninferiority trial comparing 5-fluorouracil with chlorhexidine/silver sulfadiazine in preventing catheter colonization*. Critical Care Medicine. 2010;38(11).

143. Asri LATW, Crismaru M, Roest S, Chen Y, Ivashenko O, Rudolf P, et al. A Shape-Adaptive, Antibacterial-Coating of Immobilized Quaternary-Ammonium Compounds Tethered on Hyperbranched Polyurea and its Mechanism of Action. Advanced Functional Materials. 2014;24(3):346-55.

144. Worley BV, Slomberg DL, Schoenfisch MH. Nitric oxide-releasing quaternary ammonium-modified poly(amidoamine) dendrimers as dual action antibacterial agents. Bioconjug Chem. 2014;25(5):918-27.

145. Harney MB, Pant RR, Fulmer PA, Wynne JH. Surface self-concentrating amphiphilic quaternary ammonium biocides as coating additives. ACS Appl Mater Interfaces. 2009;1(1):39-41.

146. Gottenbos B, van der Mei HC, Klatter F, Nieuwenhuis P, Busscher HJ. In vitro and in vivo antimicrobial activity of covalently coupled quaternary ammonium silane coatings on silicone rubber. Biomaterials. 2002;23(6):1417-23.

147. Li ZS, Yang XX, Liu H, Yang XH, Shan Y, Xu X, et al. Dual-functional antimicrobial coating based on a quaternary ammonium salt from rosin acid with in vitro and in vivo antimicrobial and antifouling properties. Chemical Engineering Journal. 2019;374:564-75.

148. Adlhart C, Verran J, Azevedo NF, Olmez H, Keinanen-Toivola MM, Gouveia I, et al. Surface modifications for antimicrobial effects in the healthcare setting: a critical overview. J Hosp Infect. 2018;99(3):239-49.

149. Milo S, Hathaway H, Nzakizwanayo J, Alves DR, Esteban PP, Jones BV, et al. Prevention of encrustation and blockage of urinary catheters by Proteus mirabilis via pH-triggered release of bacteriophage. Journal of Materials Chemistry B. 2017;5(27):5403-11.

150. Melo LDR, Veiga P, Cerca N, Kropinski AM, Almeida C, Azeredo J, et al. Development of a Phage Cocktail to Control Proteus mirabilis Catheter-associated Urinary Tract Infections. Frontiers in Microbiology. 2016;7(1024).

151. Pavlukhina SV, Kaplan JB, Xu L, Chang W, Yu X, Madhyastha S, et al. Noneluting Enzymatic Antibiofilm Coatings. Acs Appl Mater Inter. 2012;4(9):4708-16.

152. Satishkumar R, Sankar S, Yurko Y, Lincourt A, Shipp J, Heniford BT, et al. Evaluation of the Antimicrobial Activity of Lysostaphin-Coated Hernia Repair Meshes. Antimicrobial Agents and Chemotherapy. 2011;55(9):4379-85.

153. Johnson CT, Wroe JA, Agarwal R, Martin KE, Guldberg RE, Donlan RM, et al. Hydrogel delivery of lysostaphin eliminates orthopedic implant infection by Staphylococcus aureus and supports fracture healing. Proceedings of the National Academy of Sciences. 2018;115(22):E4960-E9.

154. Windolf CD, Lögters T, Scholz M, Windolf J, Flohé S. Lysostaphin-Coated Titan-Implants Preventing Localized Osteitis by Staphylococcus aureus in a Mouse Model. PLOS ONE. 2014;9(12):e115940.

155. Decraene V, Pratten J, Wilson M. Cellulose acetate containing toluidine blue and rose bengal is an effective antimicrobial coating when exposed to white light. Appl Environ Microbiol. 2006;72(6):4436-9.

156. Hwang GB, Allan E, Parkin IP. White Light-Activated Antimicrobial Paint using Crystal Violet. Acs Appl Mater Inter. 2016;8(24):15033-9.

157. Kumaravel V, Nair KM, Mathew S, Bartlett J, Kennedy JE, Manning HG, et al. Antimicrobial TiO2 nanocomposite coatings for surfaces, dental and orthopaedic implants. Chemical Engineering Journal. 2021;416:129071.

158. Noimark S, Allan E, Parkin IP. Light-activated antimicrobial surfaces with enhanced efficacy induced by a dark-activated mechanism. Chemical Science. 2014;5(6):2216-23.

159. Ozkan E, Allan E, Parkin IP. The antibacterial properties of light-activated polydimethylsiloxane containing crystal violet. RSC Advances. 2014;4(93):51711-5.

160. Ahmed I, Boulton AJ, Rizvi S, Carlos W, Dickenson E, Smith NA, et al. The use of triclosan-coated sutures to prevent surgical site infections: a systematic review and meta-analysis of the literature. BMJ open. 2019;9(9):e029727-e.

161. Keskin D, Tromp L, Mergel O, Zu G, Warszawik E, van der Mei HC, et al. Highly Efficient Antimicrobial and Antifouling Surface Coatings with Triclosan-Loaded Nanogels. Acs Appl Mater Inter. 2020;12(52):57721-31.

162. Tran PL, Hamood AN, Reid TW. Antimicrobial Coatings to Prevent Biofilm Formation on Medical Devices. In: Rumbaugh KP, Ahmad I, editors. Antibiofilm Agents: From Diagnosis to Treatment and Prevention. Berlin, Heidelberg: Springer Berlin Heidelberg; 2014. p. 175-204.

163. Bohl KS, West JL. Nitric oxide-generating polymers reduce platelet adhesion and smooth muscle cell proliferation. Biomaterials. 2000;21(22):2273-8.

164. Stamler JS, Vaughan DE, Loscalzo J. Synergistic disaggregation of platelets by tissue-type plasminogen activator, prostaglandin E1, and nitroglycerin. Circulation research. 1989;65(3):796-804.

165. Reichenbach G, Momi S, Gresele P. Nitric oxide and its antithrombotic action in the cardiovascular system. Curr Drug Targets Cardiovasc Haematol Disord. 2005;5(1):65-74.

166. Major TC, Brant DO, Reynolds MM, Bartlett RH, Meyerhoff ME, Handa H, et al. The attenuation of platelet and monocyte activation in a rabbit model of extracorporeal circulation by a nitric oxide releasing polymer. Biomaterials. 2010;31(10):2736-45.

167. Skrzypchak AM, Lafayette NG, Bartlett RH, Zhou Z, Frost MC, Meyerhoff ME, et al. Effect of varying nitric oxide release to prevent platelet consumption and preserve platelet function in an in vivo model of extracorporeal circulation. Perfusion. 2007;22(3):193-200.

168. Tousoulis D, Kampoli AM, Tentolouris C, Papageorgiou N, Stefanadis C. The role of nitric oxide on endothelial function. Curr Vasc Pharmacol. 2012;10(1):4-18.

169. Vaughn MW, Kuo L, Liao JC. Estimation of nitric oxide production and reaction rates in tissue by use of a mathematical model. Am J Physiol-Heart C. 1998;274(6):H2163-H76.

170. Schairer DO, Chouake JS, Nosanchuk JD, Friedman AJ. The potential of nitric oxide releasing therapies as antimicrobial agents. Virulence. 2012;3(3):271-9.

171. Doverspike JC, Mack SJ, Luo A, Stringer B, Reno S, Cornell MS, et al. Nitric Oxide-Releasing Insert for Disinfecting the Hub Region of Tunnel Dialysis Catheters. ACS Appl Mater Interfaces. 2020;12(40):44475-84.

172. Yang L, Jing L, Jiao Y, Wang L, Marchesan JT, Offenbacher S, et al. In Vivo Antibacterial Efficacy of Nitric Oxide-Releasing Hyperbranched Polymers against Porphyromonas gingivalis. Molecular pharmaceutics. 2019;16(9):4017-23.

173. Reynolds MM, Frost MC, Meyerhoff ME. Nitric oxide-releasing hydrophobic polymers: preparation, characterization, and potential biomedical applications. Free Radic Biol Med. 2004;37(7):926-36.

174. Hetrick EM, Schoenfisch MH. Analytical chemistry of nitric oxide. Annu Rev Anal Chem (Palo Alto Calif). 2009;2(1):409-33.

175. Handa H, Brisbois EJ, Major TC, Refahiyat L, Amoako KA, Annich GM, et al. In vitro and in vivo study of sustained nitric oxide release coating using diazeniumdiolate-oped poly(vinyl chloride) matrix with poly(lactide-co-glycolide) additive. J Mater Chem B. 2013;1(29):3578-87.

176. Liang H, Nacharaju P, Friedman A, Friedman JM. Nitric oxide generating/releasing materials. Future Sci OA. 2015;1(1).

177. Engelsman AF, Krom BP, Busscher HJ, van Dam GM, Ploeg RJ, van der Mei HC. Antimicrobial effects of an NO-releasing poly(ethylene vinylacetate) coating on soft-tissue implants in vitro and in a murine model. Acta Biomaterialia. 2009;5(6):1905-10.

178. Jeakle MM, Major TC, Meyerhoff ME, Bartlett RH. Comparison of Diazeniumdiolated Dialkylhexanediamines as Nitric Oxide Release Agents on Nonthrombogenicity in an Extracorporeal Circulation Model. ACS Applied Bio Materials. 2020;3(1):466-76.

179. Zhang Y, Tang K, Chen B, Zhou S, Li N, Liu C, et al. A polyethylenimine-based diazeniumdiolate nitric oxide donor accelerates wound healing. Biomater Sci. 2019;7(4):1607-16.

180. Zhang H, Annich GM, Miskulin J, Osterholzer K, Merz SI, Bartlett RH, et al. Nitric oxide releasing silicone rubbers with improved blood compatibility: preparation, characterization, and in vivo evaluation. Biomaterials. 2002;23(6):1485-94.

181. Yoo J-W, Nurhasni H, Cao J, Choi M, Kim I, Lee BL, et al. Nitric oxide-releasing poly(lactic-co-glycolic acid)-polyethylenimine nanoparticles for prolonged nitric oxide release, antibacterial efficacy, and in vivo wound healing activity. International Journal of Nanomedicine. 2015:3065.

182. Mowery KA, Schoenfisch MH, Saavedra JE, Keefer LK, Meyerhoff ME. Preparation and characterization of hydrophobic polymeric films that are thromboresistant via nitric oxide release. Biomaterials. 2000;21(1):9-21.

183. Yang Y, Qi PK, Yang ZL, Huang N. Nitric oxide based strategies for applications of biomedical devices. Biosurface and Biotribology. 2015;1(3):177-201.

184. Nagababu E, Rifkind JM. Routes for formation of S-nitrosothiols in blood. Cell Biochem Biophys. 2013;67(2):385-98.

185. Grossi L, Montevecchi PC. A Kinetic Study of S-Nitrosothiol Decomposition. Chemistry – A European Journal. 2002;8(2):380-7.

186. Frost MC, Meyerhoff ME. Controlled photoinitiated release of nitric oxide from polymer films containing S-nitroso-N-acetyl-DL-penicillamine derivatized fumed silica filler. J Am Chem Soc. 2004;126(5):1348-9.

187. Broniowska KA, Hogg N. The chemical biology of S-nitrosothiols. Antioxid Redox Signal. 2012;17(7):969-80.

188. Riccio DA, Schoenfisch MH. Nitric oxide release: part I. Macromolecular scaffolds. Chem Soc Rev. 2012;41(10):3731-41.

189. Ketchum AR, Kappler MP, Wu J, Xi C, Meyerhoff ME. The preparation and characterization of nitric oxide releasing silicone rubber materials impregnated with S-nitroso-tert-dodecyl mercaptan. Journal of Materials Chemistry B. 2016;4(3):422-30.

190. Brisbois EJ, Kim M, Wang X, Mohammed A, Major TC, Wu J, et al. Improved Hemocompatibility of Multilumen Catheters via Nitric Oxide (NO) Release from S-Nitroso-N-acetylpenicillamine (SNAP) Composite Filled Lumen. ACS Appl Mater Interfaces. 2016;8(43):29270-9.

191. Brisbois EJ, Major TC, Goudie MJ, Bartlett RH, Meyerhoff ME, Handa H. Improved hemocompatibility of silicone rubber extracorporeal tubing via solvent swelling-impregnation of S-nitroso-N-acetylpenicillamine (SNAP) and evaluation in rabbit thrombogenicity model. Acta Biomater. 2016;37:111-9.

192. Wo Y, Li Z, Brisbois EJ, Colletta A, Wu J, Major TC, et al. Origin of Long-Term Storage Stability and Nitric Oxide Release Behavior of CarboSil Polymer Doped with S-Nitroso-N-acetyl-D-penicillamine. ACS Appl Mater Interfaces. 2015;7(40):22218-27.

193. Pant J, Goudie MJ, Hopkins SP, Brisbois EJ, Handa H. Tunable Nitric Oxide Release from S-Nitroso-N-acetylpenicillamine via Catalytic Copper Nanoparticles for Biomedical Applications. ACS Appl Mater Interfaces. 2017;9(18):15254-64.

194. Douglass ME, Goudie MJ, Pant J, Singha P, Hopkins S, Devine R, et al. Catalyzed Nitric Oxide Release via Cu Nanoparticles Leads to an Increase in Antimicrobial Effects and Hemocompatibility for Short-Term Extracorporeal Circulation. ACS Applied Bio Materials. 2019.

195. Singha P, Workman CD, Pant J, Hopkins SP, Handa H. Zinc-oxide Nanoparticles Act Catalytically and Synergistically with Nitric Oxide Donors to Enhance Antimicrobial Efficacy. Journal of Biomedical Materials Research Part A. 2019;0(ja).

196. Goudie MJ, Brisbois EJ, Pant J, Thompson A, Potkay JA, Handa H. Characterization of an S-nitroso-N-acetylpenicillamine-based nitric oxide releasing polymer from a translational perspective. Int J Polym Mater. 2016;65(15):769-78.

197. Williams DLH. The chemistry of S-nitrosothiols. Accounts of Chemical Research. 1999;32(10):869-76.

198. Hopkins SP, Pant J, Goudie MJ, Schmiedt C, Handa H. Achieving Long-Term Biocompatible Silicone via Covalently Immobilized S-Nitroso- N-acetylpenicillamine (SNAP)

That Exhibits 4 Months of Sustained Nitric Oxide Release. ACS Appl Mater Interfaces. 2018;10(32):27316-25.

199. Devine R, Goudie MJ, Singha P, Schmiedt C, Douglass M, Brisbois EJ, et al. Mimicking the Endothelium: Dual Action Heparinized Nitric Oxide Releasing Surface. ACS Applied Materials & Interfaces. 2020;12(18):20158-71.

200. Singh RJ, Hogg N, Joseph J, Kalyanaraman B. Mechanism of Nitric Oxide Release from S-Nitrosothiols. Journal of Biological Chemistry. 1996;271(31):18596-603.

201. Cha W, Meyerhoff ME. Catalytic generation of nitric oxide from S-nitrosothiols using immobilized organoselenium species. Biomaterials. 2007;28(1):19-27.

202. Lutzke A, Melvin AC, Neufeld MJ, Allison CL, Reynolds MM. Nitric oxide generation from S-nitrosoglutathione: New activity of indium and a survey of metal ion effects. Nitric Oxide. 2019;84:16-21.

203. Harding JL, Reynolds MM. Metal organic frameworks as nitric oxide catalysts. J Am Chem Soc. 2012;134(7):3330-3.

204. Harding JL, Metz JM, Reynolds MM. A Tunable, Stable, and Bioactive MOF Catalyst for Generating a Localized Therapeutic from Endogenous Sources. Adv Funct Mater. 2014;24(47):7503-9.

205. Rubin HN, Neufeld BH, Reynolds MM. Surface-Anchored Metal–Organic Framework–Cotton Material for Tunable Antibacterial Copper Delivery. ACS Applied Materials & Interfaces. 2018;10(17):15189-99.

206. Duncan MJ, Wheatley PS, Coghill EM, Vornholt SM, Warrender SJ, Megson IL, et al. Antibacterial efficacy from NO-releasing MOF–polymer films. Materials Advances. 2020;1(7):2509-19.

207. Yu H, Yu S, Qiu H, Gao P, Chen Y, Zhao X, et al. Nitric oxide-generating compound and bio-clickable peptide mimic for synergistically tailoring surface anti-thrombogenic and anti-microbial dual-functions. Bioact Mater. 2021;6(6):1618-27.

208. Homeyer KH, Goudie MJ, Singha P, Handa H. Liquid-Infused Nitric-Oxide-Releasing Silicone Foley Urinary Catheters for Prevention of Catheter-Associated Urinary Tract Infections. Acs Biomater Sci Eng. 2019;5(4):2021-9.

209. Noh H, Vogler EA. Volumetric interpretation of protein adsorption: competition from mixtures and the Vroman effect. Biomaterials. 2007;28(3):405-22.

210. Kang GD, Cao YM. Development of antifouling reverse osmosis membranes for water treatment: A review. Water Res. 2012;46(3):584-600.

211. Tsibouklis J, Stone M, Thorpe AA, Graham P, Peters V, Heerlien R, et al. Preventing bacterial adhesion onto surfaces: the low-surface-energy approach. Biomaterials. 1999;20(13):1229-35.

212. Singha P, Pant J, Goudie MJ, Workman CD, Handa H. Enhanced antibacterial efficacy of nitric oxide releasing thermoplastic polyurethanes with antifouling hydrophilic topcoats. Biomater Sci. 2017;5(7):1246-55.

213. Liu Q, Singha P, Handa H, Locklin J. Covalent Grafting of Antifouling Phosphorylcholine-Based Copolymers with Antimicrobial Nitric Oxide Releasing Polymers to Enhance Infection-Resistant Properties of Medical Device Coatings. Langmuir. 2017;33(45):13105-13.

214. Singha P, Goudie MJ, Liu Q, Hopkins S, Brown N, Schmiedt CW, et al. Multipronged Approach to Combat Catheter-Associated Infections and Thrombosis by Combining Nitric Oxide and a Polyzwitterion: a 7 Day In Vivo Study in a Rabbit Model. ACS Appl Mater Interfaces. 2020;12(8):9070-9.

215. Devine R, Goudie MJ, Singha P, Schmiedt C, Douglass M, Brisbois EJ, et al. Mimicking the Endothelium: Dual Action Heparinized Nitric Oxide Releasing Surface. Acs Appl Mater Inter. 2020.

216. Wong T-S, Kang SH, Tang SKY, Smythe EJ, Hatton BD, Grinthal A, et al. Bioinspired self-repairing slippery surfaces with pressure-stable omniphobicity. Nature. 2011;477:443.

217. Kim P, Kreder MJ, Alvarenga J, Aizenberg J. Hierarchical or Not? Effect of the Length Scale and Hierarchy of the Surface Roughness on Omniphobicity of Lubricant-Infused Substrates. Nano Letters. 2013;13(4):1793-9.

218. Leslie DC, Waterhouse A, Berthet JB, Valentin TM, Watters AL, Jain A, et al. A bioinspired omniphobic surface coating on medical devices prevents thrombosis and biofouling. Nat Biotechnol. 2014;32(11):1134-40.

219. Yuan S, Luan S, Yan S, Shi H, Yin J. Facile Fabrication of Lubricant-Infused Wrinkling Surface for Preventing Thrombus Formation and Infection. ACS Applied Materials & Interfaces. 2015;7(34):19466-73.

220. Yao X, Dunn SS, Kim P, Duffy M, Alvarenga J, Aizenberg J. Fluorogel elastomers with tunable transparency, elasticity, shape-memory, and antifouling properties. Angew Chem Int Ed Engl. 2014;53(17):4418-22.

221. Epstein AK, Wong TS, Belisle RA, Boggs EM, Aizenberg J. Liquid-infused structured surfaces with exceptional anti-biofouling performance. Proc Natl Acad Sci U S A. 2012;109(33):13182-7.

222. Kratochvil MJ, Welsh MA, Manna U, Ortiz BJ, Blackwell HE, Lynn DM. Slippery Liquid-Infused Porous Surfaces that Prevent Bacterial Surface Fouling and Inhibit Virulence Phenotypes in Surrounding Planktonic Cells. ACS Infect Dis. 2016;2(7):509-17.

223. Manna U, Raman N, Welsh MA, Zayas-Gonzalez YM, Blackwell HE, Palecek SP, et al. Slippery Liquid-Infused Porous Surfaces that Prevent Microbial Surface Fouling and Kill Non-Adherent Pathogens in Surrounding Media: A Controlled Release Approach. Adv Funct Mater. 2016;26(21):3599-611.

224. Wallin RF, Arscott EF. A practical guide to ISO 10993-5: Cytotoxicity. Medical Device and Diagnostic Industry. 1998;20:96-8.

225. Nalezinkova M. In vitro hemocompatibility testing of medical devices. Thromb Res. 2020;195:146-50.

226. Haycox CL, Ratner BD. In vitro platelet interactions in whole human blood exposed to biomaterial surfaces: Insights on blood compatibility. Journal of Biomedical Materials Research. 1993;27(9):1181-93.

227. Verheye S, Markou CP, Salame MY, Wan B, King SB, 3rd, Robinson KA, et al. Reduced thrombus formation by hyaluronic acid coating of endovascular devices. Arterioscler Thromb Vasc Biol. 2000;20(4):1168-72.

228. Smith RS, Zhang Z, Bouchard M, Li J, Lapp HS, Brotske GR, et al. Vascular catheters with a nonleaching poly-sulfobetaine surface modification reduce thrombus formation and microbial attachment. Sci Transl Med. 2012;4(153):153ra32.

229. Snyder TA, Tsukui H, Kihara S, Akimoto T, Litwak KN, Kameneva MV, et al. Preclinical biocompatibility assessment of the EVAHEART ventricular assist device: coating comparison and platelet activation. J Biomed Mater Res A. 2007;81(1):85-92.

230. Goudie MJ, Brainard BM, Schmiedt CW, Handa H. Characterization and in vivo performance of nitric oxide-releasing extracorporeal circuits in a feline model of thrombogenicity. J Biomed Mater Res A. 2017;105(2):539-46.

231. Brancato L, Decrop D, Lammertyn J, Puers R. Surface Nanostructuring of Parylene-C Coatings for Blood Contacting Implants. Materials (Basel). 2018;11(7).

232. Escudero ML, Llorente I, Pérez-Maceda BT, José-Pinilla SS, Sánchez-López L, Lozano RM, et al. Electrochemically reduced graphene oxide on CoCr biomedical alloy: Characterization, macrophage biocompatibility and hemocompatibility in rats with graphene and graphene oxide. Materials Science and Engineering: C. 2020;109:110522.

233. Roberts TR, Choi JH, Wendorff DS, Harea GT, Beely BM, Sieck KN, et al. Tethered Liquid Perfluorocarbon Coating for 72 Hour Heparin-Free Extracorporeal Life Support. ASAIO J. 2021.

234. Douglass ME, Goudie MJ, Pant J, Singha P, Hopkins S, Devine R, et al. Catalyzed Nitric Oxide Release Via Cu Nanoparticles Leads to an Increase in Antimicrobial Effects and Hemocompatibility for Short Term Extracorporeal Circulation. ACS Appl Bio Mater. 2019;2(6):2539-48.

235. Roberts TR, Choi JH, Wendorff DS, Harea GT, Beely BM, Sieck KN, et al. Tethered Liquid Perfluorocarbon Coating for 72 Hour Heparin-Free Extracorporeal Life Support. ASAIO J. 2021;67(7):798-808.

236. Sjollema J, Zaat SAJ, Fontaine V, Ramstedt M, Luginbuehl R, Thevissen K, et al. In vitro methods for the evaluation of antimicrobial surface designs. Acta Biomater. 2018;70:12-24.

237. Brisbois EJ, Major TC, Goudie MJ, Meyerhoff ME, Bartlett RH, Handa H. Attenuation of thrombosis and bacterial infection using dual function nitric oxide releasing central venous catheters in a 9day rabbit model. Acta Biomater. 2016;44:304-12.

238. Hsu SH, Tseng HJ, Lin YC. The biocompatibility and antibacterial properties of waterborne polyurethane-silver nanocomposites. Biomaterials. 2010;31(26):6796-808.

239. Yu K, Lo JCY, Yan M, Yang X, Brooks DE, Hancock REW, et al. Anti-adhesive antimicrobial peptide coating prevents catheter associated infection in a mouse urinary infection model. Biomaterials. 2017;116:69-81.

240. Park DS, Bae I-H, Jeong MH, Lim K-S, Hong YJ, Shim JW, et al. Anti-restenotic and anti-thrombotic effect of polymer-free N-TiO2 film-based tacrolimus-eluting stent in a porcine model. Materials Today Communications. 2020;22:100777.

241. The Evolution of Animal Models in Wound Healing Research: 1993–2017. Advances in Wound Care. 2019;8(12):692-702.

242. Hetrick EM, Prichard HL, Klitzman B, Schoenfisch MH. Reduced foreign body response at nitric oxide-releasing subcutaneous implants. Biomaterials. 2007;28(31):4571-80.

243. Chandorkar Y, K R, Basu B. The Foreign Body Response Demystified. Acs Biomater Sci Eng. 2019;5(1):19-44.

244. Douglass M, Hopkins S, Chug MK, Kim G, Garren MR, Ashcraft M, et al. Reduction in Foreign Body Response and Improved Antimicrobial Efficacy via Silicone-Oil-Infused Nitric-Oxide-Releasing Medical-Grade Cannulas. ACS Applied Materials & Interfaces. 2021.

CHAPTER 2:

MULTIFUNCTIONAL *S*-NITROSO-*N*-ACETYLPENICILLAMINE-INCORPORATED MEDICAL-GRADE POLYMER WITH SELENIUM INTERFACE FOR BIOMEDICAL APPLICATIONS[2]

[2] Douglass M*, Mondal A*, Hopkins S, Singha P, Tran M, Handa H, and Brisbois B. Multifunctional S-Nitroso-N-acetylpenicillamine-Incorporated Medical-Grade Polymer with Selenium Interface for Biomedical Applications. 2019. *ACS Applied Materials & Interfaces*. 11, 38, 34652-34662. Reprinted here with permission of the publisher. (* indicates that these authors contributed equally).

2.1 Abstract

Modern crisis in implantable or indwelling blood-contacting medical devices are mainly due to the dual problems of infection and thrombogenicity. There is a paucity of biomaterials that can address both the problems simultaneously through a singular platform. Taking cues from the body's own defense mechanism against infection and blood clotting (thrombosis) via the endogenous gasotransmitter nitric oxide (NO), both of these issues are addressed through the development of a layered *S*-nitroso-*N*-acetylpenicillamine (SNAP) doped polymer with a blended selenium (Se) - polymer interface. The unique capability of the SNAP-Se-1 polymer composites to explicitly release NO from the SNAP reservoir as well as generate NO via the incorporated Se is reported for the first time. The NO release from the SNAP doped polymer increased substantially in the presence of the Se interface. The Se interface is also able to generate NO in the presence of *S*-nitrosoglutathione (GSNO) and glutathione (GSH), demonstrating the capability of generating NO from endogenous *S*-nitrosothiols (RSNO). Scanning electron microscopy-energy dispersive spectroscopy (SEM-EDS) traces distribution of elemental Se nanoparticles on the interface and the surface properties were evaluated by surface wettability and roughness. The SNAP-Se-1 efficiently inhibits the growth of bacteria and reduces platelet adhesion while showing minimal cytotoxicity, thus potentially eliminating the risks of systemic antibiotic and blood coagulation therapy. The SNAP-Se-1 exhibits antibacterial activity of ~2.39 and ~2.25 log reductions in the growth of clinically challenging adhered Gram-positive *Staphylococcus aureus* and Gram-negative *Escherichia coli*. SNAP-Se-1 also significantly reduces platelet adhesion by 85.5% compared to corresponding controls. WST-8 based cell viability test performed on NIH 3T3 mouse fibroblast cells provide supporting evidence for the potential biocompatibility of the material *in*

vitro. These results highlight the prospective utility of SNAP-Se-1 as a blood-contacting infection-resistant biomaterial *in vitro* which can be further tuned by application specificity.

2.2 Introduction

Indwelling or implantable medical devices such as stents, orthopedic implants, catheters, heart valves, and vascular grafts have revolutionized the way patients are treated for various diseases. However, increasing incidences of medical device failure have posed a serious problem, leading to increased rates of patient mortality and morbidity. Despite advancements in the materials and design of implantable medical devices, two persistent problems that contribute to device failure and limit successful therapeutics are bacterial infection and thrombus formation(1, 2).

Medical device-associated infections account for 47.4% of hospital acquired infections (HAIs) in critically ill patients(3). At least 700,000 patients are affected annually by HAIs, leading to a staggering financial burden of approximately $45 billion in US alone(4, 5). The rapid emergence of antibiotic resistance has aggravated nosocomial infections and is one of the major driving forces behind reducing efficacy of antibiotic therapy in treating such infections(6). Attachment of planktonic bacteria on biomaterial surface marks the onset of bacterial colonization. Pathogenic bacteria physically aggregate on the surface and eventually forms a clustered ecosystem surrounded by a polymer matrix called biofilms(7). Biofilms play a pivotal role in the infection of implantable medical devices by drastically reducing the susceptibility of antimicrobial agents through intrinsic or acquired (e.g. plasmid exchange etc.) mechanisms(8). Most clinically relevant bacteria such as *Staphylococcus aureus (S. aureus)*, *Escherichia coli (E. coli)*, *Pseudomonas aeruginosa (P. aeruginosa)*, *Enterococcus faecalis*, and *Staphylococcus epidermidis (S. epidermis)* are associated with biofilm formation on medical devices. Diffusion of

antimicrobial agents through the extracellular polysaccharides of a biofilm is significantly reduced by limiting their rate of transport(8). Due to increased tolerance to antibiotics and resistance towards phagocytosis and other components of the body's defense system, bacterial biofilms can result in chronic infections(9, 10).

For blood-contacting devices, exposure to blood can activate complex, intermingled processes leading to protein adsorption and platelet adhesion, ultimately resulting in device occlusion and clot formation(11, 12). Medical device-induced thrombosis severely limits the success of some of the most widely utilized life-saving cardiovascular and renal treatments. In fact, device-induced clotting has been reported to occur in 22% of extracorporeal life support treatments(13). Consequently, blood-contacting devices require the use of systemic anti-platelet or anti-coagulant therapy; however, the administration of anti-platelet drugs, such as clopidogrel, or anticoagulants, such as unfractionated heparin, can often lead to increased or uncontrolled bleeding and heparin-induced thrombocytopenia(14, 15). Moreover, thrombus formation arising from interaction between blood-contacting device interfaces and platelets may increase the likelihood of biofilm formation, as the adhered plasma proteins aid in bacterial adhesion(16). Platelets adhering to surfaces can play a role in pathogenesis of bacteria like *S. aureus* in causing bloodstream infections(17).

Despite extensive research, an ideal non-thrombogenic and infection-resistant biomaterial remains an open challenge in the field of medical devices. The biosynthesis of NO within endothelial cells, macrophages, and endogenous RSNOs in blood play an important role in inhibiting platelet adhesion and aggregation to the blood vessels and providing innate immunity against bacterial infections(18, 19). The short half-life (on the order of seconds), rapid diffusion and reactivity of NO can help reduce a broad range of microbial burden(20). Exogenous delivery

of NO via NO donor molecules have been previously shown to be effective against HAI-relevant strains of bacteria such as *S. aureus, E. coli, S. epidermis,* and *P. aeruginosa*, making it an attractive candidate for improving antimicrobial activity(21). To improve antibacterial and antiplatelet activity of biomaterials, both exogenous and endogenous NO donors such as RSNOs, *N*-diazeniumdiolates, organic nitrates and nitrites, and metal nitrosyl complexes have been utilized to provide localized NO release to surrounding tissue(21, 22). RSNOs, among others, have emerged as exceptionally beneficial due to their steady release and innate biocompatibility(23).

However, exogenous mechanisms of NO delivery in blood contacting devices have been limited to either NO-release (NOrel) through donor molecules or NO-generation (NOgen) catalytically generating NO at the device interface via interaction with endogenous RSNOs in the blood circulation(24, 25). NOrel materials rely on a finite reservoir of donor molecules which release NO at favorable physiological conditions. In contrast, NOgen materials catalytically generate NO at local material interfaces, often involving natural enzymes or catalysts such as metal ions (Cu^{2+}, Fe^{2+}, Co^{2+}, Ni^{2+}, Zn^{2+})(26). Either approach by itself has some shortcomings. NOrel strategy which relies on a finite source of NO suffer from donor exhaustion over time, which in turn impairs longevity of NOrel materials. While NOgen polymers involving catalytic NO generation via circulating RSNO has the potential to solve those issues, the initial NO flux of NOgen materials may not be adequate in preventing early onslaught of infection or platelet activation. In a 4 h experiment on rabbit thrombogenicity model by Major *et al.*, although extracorporeal loops coated with 10 wt% Cu combined with a saline infusion improved platelet counts, loops coated with 10 wt% Cu with a systemic SNAP infusion best preserved platelet counts(27). However, systemic SNAP infusion can cause hypotension(28), hyperglycemia(29) and/or decrease in cell viability(30). The current deficits can be solved through a robust

combination which integrates properties of NOrel and NOgen in a single polymer composite, simultaneously addressing the issues of infection and thrombosis, as well as preventing suppressive antibiotic or antiplatelet therapies.

In the physiological production of NO, Se-based enzymes or organoselenium species facilitate endogenous generation of NO by catalytically decomposing RSNO(31-33). Selenium, an essential trace element, plays a crucial function as the active site of numerous Se-dependent enzymes such as peroxidase, iodothyronine deiodinase, glutathione peroxidase (GPx)(34). It has been established that diselenides catalyze the decomposition of RSNOs in the presence of thiols to produce NO, and GPx alone can catalyze the same without the need for thiols or hydrogen peroxide (H_2O_2)(35). Se nanoparticles have also been noted to have innate antimicrobial and platelet-modulating capabilities when doped with other polymers or inorganic compounds(36, 37).

In this study, the unique combination of NOrel and NOgen chemistries within a medical grade polymer has been assessed. The combination can elevate the initial NO release from SNAP reservoir as well as sustain long-term release from endogenous RSNOs which can be instrumental in averting challenges of infection and thrombosis associated with device implants. After confirming the distribution and surface morphology via SEM-EDS and contact angle studies, the antibacterial efficacy, anti-platelet adhesion, and cytotoxic properties of polymer composites were studied *in vitro*.

2.3 Materials & Methods

2.3.1 Materials

N-Acetyl-*D*-penicillamine (NAP), tetrahydrofuran (THF), sodium nitrite ($NaNO_2$), ethylenediaminetetraacetic acid (EDTA), hydrochloric acid, and selenium powder (-100 mesh) were purchased from Sigma Aldrich (St. Louis, MO 63103). CarboSil-2080A™ (CarboSil) was

purchased from DSM (Berkeley, CA). Phosphate-buffered saline (PBS), pH 7.4, used for *in vitro* experiments contained 138 mM NaCl, 2.7 mM KCl, and 10 mM sodium phosphate. Dulbecco's modified Eagle's medium (DMEM) and trypsin-EDTA were purchased from Corning (Manassas, VA 20109). The Cell Counting Kit-8 (CCK-8) was purchased from Sigma Aldrich (St. Louis, MO 63103). Penicillin-Streptomycin (Pen-Strep) and fetal bovine serum (FBS) was obtained from Gibco-Life Technologies (Grand Island, NY 14072). The bacterial strains *S. aureus* (ATCC 6538) and *E. coli* (ATCC 11303) were purchased from American Type Culture Collection (ATCC). LB broth was obtained from Fisher Bioreagents (Fair Lawn, NJ). LB Agar was purchased from Difco Laboratories Inc (Detroit, MI). Reagents used for NO generation. The lactic dehydrogenase (LDH) kit was purchased from Roche Life Sciences (Indianapolis, IN). Glutathione reduced was purchased from Goldbio (St. Louis, MO).

2.3.2 Synthesis of SNAP

SNAP was synthesized from NAP by modification of a previously established protocol(38). Equimolar ratio of $NaNO_2$ and NAP were added to a mixture of de-ionized water and methanol containing 1 M HCl and 1 M H_2SO_4. The mixture was stirred in a reaction vessel in the absence of light (to avoid activation of NO release with light as a stimulant) for 15 minutes and then cooled in an ice bath for 4 h to obtain precipitated SNAP crystals. The SNAP crystals appear green in color. After precipitation of the SNAP crystals, the precipitate was collected, and vacuum dried overnight in the dark to remove any trace solvent present with the crystals.

2.3.3 Fabrication of Polymer Composites

SNAP-Se polymer composites were prepared by dissolving 70 mg/mL CarboSil in THF at room temperature for 2 h in the dark. After completely dissolving, 10 wt% SNAP was added to the solution and stirred for an additional 10 min. The solution was then cast into a 2.5 cm (diameter)

Teflon mold and was allowed to dry overnight in the dark to prevent any premature light-induced NO release. Carbosil control samples were made similarly, but without the addition of SNAP. Each sample was then cut into 1 cm^2 circular samples and dip coated into a 50 mg/mL solution of CarboSil followed by a second coat of 50 mg/mL CarboSil solution containing different concentrations of Se (1, 5, 10 wt% Se). Control samples were fabricated by coating twice with 50 mg/mL CarboSil without Se. The dip-coated polymer composites were dried overnight.

The following polymer composites were fabricated for the study:

1. 70 mg/mL CarboSil dip coated twice with 50 mg/mL CarboSil (hereon as CarboSil)
2. 10 wt% SNAP-incorporated 70 mg/mL CarboSil dip coated twice with 50 mg/mL CarboSil (hereon as C-SNAP)
3. 10 wt% SNAP-incorporated 70 mg/mL CarboSil dip coated with 50 mg/mL CarboSil and again dip coated with 1 wt% Se-incorporated 50 mg/mL CarboSil (hereon as SNAP-Se-1)
4. 10 wt% SNAP-incorporated 70 mg/mL CarboSil dip coated with 50 mg/mL CarboSil and again dip coated with 5 wt% Se-incorporated 50 mg/mL CarboSil (hereon as SNAP-Se-5)
5. 10 wt% SNAP-incorporated 70 mg/mL CarboSil dip coated with 50 mg/mL CarboSil and again dip coated with 10 wt% Se-incorporated 50 mg/mL CarboSil (hereon as SNAP-Se-10)
6. 70 mg/mL CarboSil dip coated with 50 mg/mL CarboSil and again dip coated with 1 wt% Se-incorporated 50 mg/mL CarboSil (hereon as C-Se)

2.3.4 Nitric Oxide Kinetics

NO release: Nitric oxide release from the samples was measured using Sievers 280i Nitric Oxide Analyzers (NOAs, GE Analytical, Boulder, Colorado, US). The composites were added to reaction vessels containing 3 mL of PBS. The sample holder was partially immersed into a water

bath at 37°C to maintain a physiologically relevant temperature. A Pasteur pipet connected to N_2 supply tank was used to seal off the open end of the sample holder as well as carry N_2 gas into the PBS containing the sample. Reaction vessels were kept away from light at all times to avoid unnecessary activation of NO release in the presence of light. Nitric oxide released by the composites (n = 3) were simultaneously swept and purged by high purity N_2 gas at a constant flow rate of 200 mL min^{-1}. The NO purged from the chamber flows into the chemiluminescence reaction chamber. In the reaction chamber, NO reacts with ozone supplied from a separate oxygen tank to produce nitrogen dioxide at an excited state (NO^{2*}). When the nitrogen dioxide decays, it emits a photon which is used to detect the original concentration of NO. Real time measurement of NO was measured in the form of ppb, which was converted to NO flux units by incorporating NOA constants (mol ppb^{-1} s^{-1}). Prior to measuring the flux, a baseline measurement was first conducted for 1-2 minutes. Samples were incubated at 37°C in the dark in between measurements. The flow rate was set to 200 mL/min with a chamber pressure of 5.4 Torr and an oxygen pressure of 6.0 psi.

NO generation: NO generated from the Se composites were measured via Sievers 280i NOAs. GSNO, used as the substrate for NO generation was prepared by the reaction of equimolar GSH and $NaNO_2$ in 0.06 M H_2SO_4. The prepared solution had GSNO (1 µM) and 30 µM GSH in an amber reaction vessel containing PBS at 37 ºC. An addition of 0.5 mM EDTA chelated and stabilized the GSNO in the solution to prevent spontaneous generation of NO due to heat(39). After a baseline of release was obtained, a 1 cm^2 C-Se polymer composite sample was placed in the reaction vessel. For the study involving NO generation measurement after exposure to fibrinogen (Fg), the C-Se samples were pre-adsorbed in Fg from human plasma (prepared at a concentration of 2 mg mL^{-1} in phosphate buffer) for 60 min. After 60 mins, the samples were washed with phosphate buffer thrice to get rid of non-bound proteins and then placed in the

reaction vessel. NO was continuously swept from the headspace of the sample vessel and purged from the solution with a nitrogen sweep gas and bubbler into the chemiluminescence detection chamber.

2.3.5 Scanning Electron Microscopy and Energy-Dispersive X-ray Spectroscopy

Scanning Electron Microscopy (SEM, FEI Teneo, FEI Co.) is a technique utilizing a focused electron beam to examine surface morphology. The SEM instrument was accompanied with an Energy-Dispersive X-ray spectroscopy system (EDS, Oxford Instruments) in order to determine the concentration and dispersion of SNAP and Se nanoparticles in the samples using elemental analysis. The presence of SNAP was measured by the detection of sulfur located in the *S*-NO bond. An accelerating voltage of 5.00 kV and 20.00 kV was employed to examine samples with SEM and EDS, respectively. Samples were coated with 10 nm of gold-palladium using a Leica sputter coater prior to inspection (Leica Microsystems).

2.3.6 Surface Wettability

Surface wettability provides information on the hydrophobicity or hydrophilicity of the surface. The static contact angle was measured for the purpose using Krüss DSA 100 drop shape analyzer. Contact angle was measured for CarboSil, C-SNAP, C-Se and SNAP-Se-1. A 1 μL droplet of water was placed on the samples that were kept on glass slides. The average of left and right contact angles of the water drop on the composite surface were measured via the Krüss software.

2.3.7 Quantification of SNAP and Se Leaching

Measurement of SNAP leaching: SNAP leaching was measured under physiological conditions for over the course of 24 h. C-SNAP and SNAP-Se-1 polymer composites were soaked 2 mL in PBS at an adjusted pH of 7.4 and incubated before measuring with a Thermo Scientific

Genysis 10S UV-Vis Spectrophotometer (UV-Vis). Absorbance was recorded at 340 nm for each sample throughout several timepoints in the ~24 h timespan, which corresponds to the presence of the *S*-nitroso group of the SNAP molecule(40). PBS was used as a blank control. The concentration of SNAP leaching was calculated from a calibration curve based on known SNAP concentrations dissolved in a PBS solution.

Measurement of Se leaching: Inductively coupled plasma mass spectroscopy (ICP-MS) is a technique used to detect trace elements of interest. During this study, a VG ICP-MS Plasma Quad 3 instrument was used to analyze the samples for Se leaching from the fabricated composites. Samples containing Se interface were soaked in DMEM for 24 h under physiological conditions (37° C, 5% CO_2). The polymer composites were then removed and the leachate solutions were tested for ^{82}Se isotopes by adapting a previously established protocol(41).

2.3.8 In vitro Bacterial Adhesion Study

To evaluate the reduction in viability of bacteria adhered to the polymer composites, they were taken from the 24 well plate after 24 h of exposure and rinsed in PBS to remove any loosely attached bacteria. Adhered bacteria were detached by sonication (Omni-TH sonicator) for 60 s at 25000 rpm and vortexed for an additional 60 s. The resulting solution consisting of the detached bacteria were then serially diluted (10^{-1} to 10^{-5}) and plated on LB agar plates for 24 h at 37° C. Colony-forming units (CFU) were counted to determine the number of viable bacteria per cm^2 of both the control and test samples. The percentage of reduction in bacterial viability was determined by the following equation:

$$\%\ Reduction\ in\ bacterial\ viability = \frac{C_{control} - C_{test}}{C_{control}}\ x\ 100$$

$$\text{where } C = \frac{CFU}{cm^2}$$

Protocols regarding the use of bacteria strains were used in a BSL-2 facility approved by the University of Georgia.

2.3.9 In vitro Platelet Adhesion

All protocols involving the use of whole blood, plasma, and platelets were approved by the Institutional Animal Care and Use Committee at the University of Georgia prior to experimentation. Fresh porcine blood was drawn through a blind draw with 3.8% sodium citrate (9:1 blood/citrate ratio). After collection, the blood was centrifuged at 300 RCF for 13 minutes and again at 4000 RCF for 20 min using an Allegra X-30 Centrifuge (Beckman-Coulter, Brea, CA) to separate out the platelet rich plasma (PRP) and platelet poor plasma (PPP), respectively. Next, the total platelet count was determined using a hemocytometer (Fisher), and the PRP and PPP were combined to achieve a final concentration of 2×10^8 platelets/mL. $CaCl_2$ was added at a concentration of 5 mM to reverse the effect of sodium citrate. Samples were added to culture tubes containing 3 mL of the final platelet concentration and incubated at 37°C on a rocker at 25 rpm for 2 h. The samples were then removed and infinitely washed in PBS to remove any loosely attached platelets. Next, an LDH assay was prepared to determine the number of adhered platelets. Samples were stored in Eppendorf tubes containing 500 µL of 2 v/v% Triton-PBS solution for 30 min at room temperature, which lyses the platelets adhered to the surface of the samples. Solutions were plated in a 96-well plate, and Roche Cytotoxicity Detection Kit was utilized to quantify platelet adherence using a BioTek Cytation5 plate reader (BioTek, Winooski, VT) at 492 nm. A calibration curve composed of known platelet counts was generated. The % reduction in platelet adhesion in comparison to control polymer composites were calculated by the following formula:

$$\% \, Reduction = \frac{P_{control} - P_{test}}{P_{control}} \, x \, 100$$

where $P = \frac{\#\, of\ platelets}{cm^2}$

2.3.10 In vitro Cytotoxicity

Interactions between host tissues and any biomaterial requires an evaluation of its biocompatibility during development phase. Due to the reaction of host body in response to a foreign substance in contact, the cellular tolerance level becomes an important factor while maintaining safe levels of biochemical stability and morphology. For this purpose, the biological evaluation of the cells *in vitro* had been conducted to test if the extracts from our material show any toxicity towards the cells.

Cell culture: 3T3 Mouse fibroblast cells (ATCC 1658) were cultured in 75 cm^2 T-flask containing DMEM with 4.5 g/L glucose and L-glutamine, 10% FBS, and 1% Pen-Strep, and incubated at 37 °C in a humidified atmosphere with 5% CO_2. The fibroblast cells were trypsinized (0.18% trypsin and 5 mM EDTA) post confluency of ~ 90%. The cells were then seeded into a 96-well plate at a concentration of 5000 cells/mL.

In vitro cytotoxicity assay: The cytotoxicity assay was conducted in accordance with the ISO 10993 standard using a CCK-8 assay kit. The manufacturer's (Sigma Aldrich) protocol was followed. The CCK-8 kit utilizes the highly water-soluble tetrazolium salt, WST-8 [2-(2-methoxy-4-nitrophenyl)-3-(4-nitrophenyl)-5-(2,4-disulfophenyl)-2H-tetrazolium monosodium salt], which is reduced by dehydrogenases in live cells to form formazan (an orange-colored product). Formazan can be spectroscopically detected at 450 nm wavelength. Thus, the number of living cells is directly proportional to the amount of formazan dye generated by the dehydrogenases in

the cells. All protocols pertaining to the use of mammalian cells were approved by the University of Georgia.

Extract preparation: Extract was obtained by soaking the polymer composites in DMEM by following the ISO standards (ISO 10993-5:2009 Test for *in vitro* cytotoxicity). Control and test samples were soaked (after UV sterilization) in DMEM in amber vials (to prevent NO release by light stimulation) and incubated for 24 h at 37 °C. After 24 h, the samples were removed, and the extracts used for the study.

Cell viability: A 96-well plate containing suspension of 100 μL of cultured cells (5000 cells/mL) in each well was prepared and pre-incubated in a humidified incubator at 37 °C, 5% CO_2 for 24 h. After 24 h, the cells were exposed to 10 μL of the different extracts (n = 7) and incubated for another 24 h to allow the extracts to act on the cells. To each of the wells, 10 μL of the CCK-8 solution was added and incubated for 3 h. The absorbance was measured at 450 nm. Results have been reported as percentage relative cell viability (with respect to positive control) using the following equation.

$$\%\ Cell\ viability = \frac{Absorbance\ of\ the\ test\ samples - Blank}{Absorbance\ of\ the\ control\ samples - Blank} \times 100$$

2.3.11 Statistical Analysis

All data are expressed as mean ± standard deviation. The results between the control and test samples were analyzed by a comparison of means using a student's t-test assuming unequal variances. Values of $p < 0.05$ were considered statistically significant.

2.4 Results & Discussion

2.4.1 Fabrication of Combined NOrel/NOgen Polymer Composites

The objective in design and fabrication of our biomaterial was to integrate NOrel and NOgen chemistries within a single platform in order to promote antibacterial and antiplatelet activity. By doing so, the material will have NO donor reservoir (SNAP) which will provide acute NO release that will prevent the initial onslaught of bacteria and blood clots, as well as have the capability of NOgen materials to generate NO in a highly localized manner from the RSNO present in circulating blood. At the same time, the aim of the study was to minimize complexity in design and fabrication as well as improve functionality. In principle, the design framework with blended Se interface has multiple utility. Apart from being a NOrel material due to the presence of SNAP, the Se interface imparts NOgen capability to the biomaterial which, in practice, can potentially solve the dual problems of infection and thrombogenicity without the limitations of time as a factor.

X-ray diffraction studies in the past have shown that when the concentration of SNAP exceeds its CarboSil solubility (> 4 wt%), the remaining SNAP crystallizes, resulting in longer shelf life and NO release(42, 43). Therefore, based on the previously conducted studies, 10 wt% SNAP was used in all the polymer composites. The interfacial layers had 1, 5, and 10 wt% of Se blended with 50 mg/mL CarboSil. The middle layer consisted only of 50 mg/mL CarboSil for all samples in order to prevent any leaching of SNAP from the base polymer composite. The C-SNAP polymer composite had a thickness of 276.8 ± 3.1 μm while the ones with Se interface, the thickness was 436.0 ± 16.8 μm. The following sections discuss in detail physical and biological characterizations exploring the functionalities stated above.

In vitro NO-releasing kinetics: The initial evaluation of NO release was the basis of selection of Se weight percentage for the Se interface. Therefore, the polymer composites under consideration were C-SNAP, SNAP-Se-1, SNAP-Se-5 and SNAP-Se-10. It is pertinent to note that the endothelium generates NO at a rate ranging between 0.5 – 4.0 x 10^{-10} mol cm^{-2} min^{-1}, which plays key roles in physiological processes such as vasodilation, angiogenesis, and platelet aggregation and activation(44). Hence, to mimic the native endothelium careful modulation of flux from NO-releasing polymer composites is desired. The addition of the Se interface significantly increased the release of NO from the polymer composites on the first day (**Figure 2.1**). On Day 1 the C-SNAP had a flux of 2.24 ± 0.3 x 10^{-10} mol cm^{-2} min^{-1}, similar to release rates reported in previous literature(45, 46). The SNAP-Se-1, SNAP-Se-5 and SNAP-Se-10 polymer composites showed release rates of 5.89 ± 1.18 x 10^{-10} mol cm^{-2} min^{-1}, 15.70 ± 3.91 x 10^{-10} mol cm^{-2} min^{-1}, and 12.18 ± 3.19 x 10^{-10} mol cm^{-2} min^{-1}, respectively, which were found to be significantly higher than the initial NO release from the C-SNAP polymer composites ($P < 0.05$). While SNAP-Se-5 and SNAP-Se-10 significantly increased the initial release from the polymer composites compared to C-SNAP and SNAP-Se-1, this trend did not continue during the entire 7-d period. In fact, on Day 7, SNAP-Se-5 and SNAP-Se-10 release rates were 0.23 ± 0.04 x 10^{-10} mol cm^{-2} $min^{-1}$and 0.07 ± 0.003 x 10^{-10} mol cm^{-2} min^{-1}, respectively which was similar to the C-SNAP flux of 0.07 ± 0.05 x 10^{-10} mol cm^{-2} min^{-1}. SNAP-Se-1, however, maintained a physiologically relevant flux of 0.8 ± 0.5 x 10^{-10} mol cm^{-2} min^{-1} by Day 7. Also, interestingly, no significant difference in initial release was found from increasing the concentration of Se beyond 5% ($P > 0.05$). NO release on Day 1 provides circumstantial evidence suggesting the presence of the Se interface can potentially play a catalytic role. Although the exact mechanism of Se based catalysis is yet to be identified, previous researchers have found other Se-based catalysts to have similar effects on the NO release(32, 33,

35). High concentrations of NO can alter cellular functions, which can result in cytotoxicity towards mammalian cells(47). Moreover, modifiable catalytic surface technologies which successfully increase the NO release for an extended period of time can increase the antimicrobial and thromboresistant activity of NO devices while simultaneously avoiding cytotoxicity towards mammalian cells. Therefore, due to the initial higher release and higher concentrations of Se in SNAP-Se-5 and SNAP-Se-10, we proceeded with SNAP-Se-1 to maximize antimicrobial and antiplatelet activity while minimizing the risk of cytotoxicity. For the duration of the study, SNAP-Se-1 polymer composites have been subjected to further evaluation due to its ability to maximize NO flux and longevity while minimizing Se required.

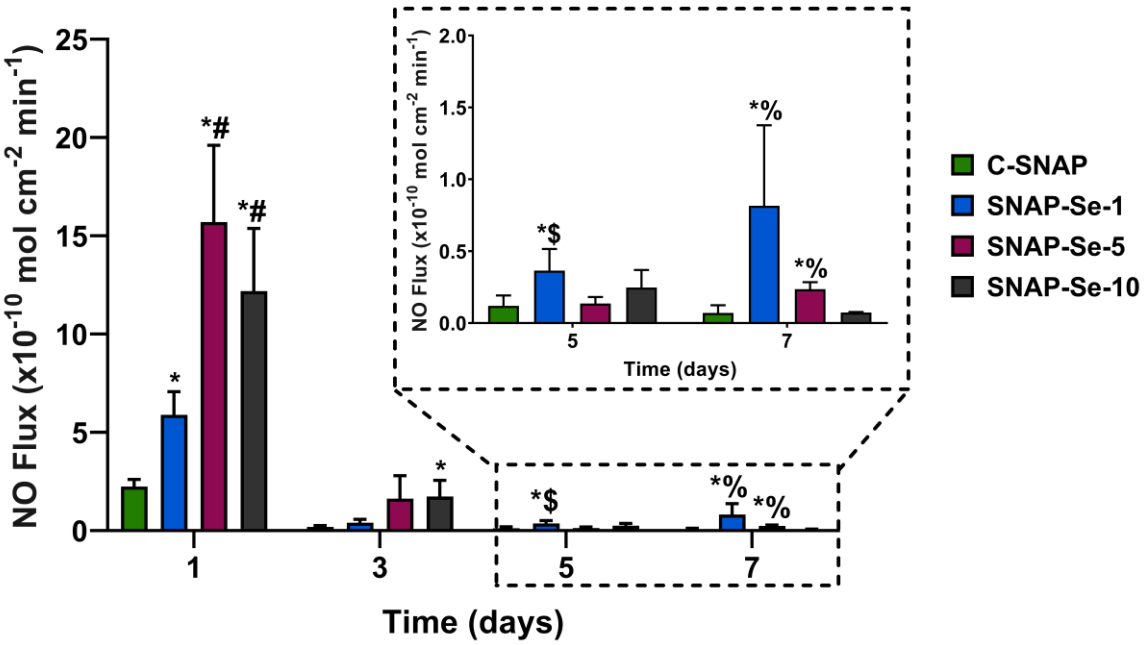

Figure 2.1 - Graph reporting the NO flux analysis of SNAP, SNAP-Se-1, SNAP-Se-5 and SNAP-Se-10 polymer composites. Error bars represent standard deviation (n=3). Standard two-tailed student t-test was performed to determine the significance groups at the same time points. '*'= $p < 0.05$ vs. control; '#' = $p < 0.05$ vs. SNAP-Se-1; '$' = $p < 0.05$ vs. SNAP-Se-5; '%' = $p < 0.05$ vs. SNAP-Se-10.

In vitro NO generation: The primary limitation for NOrel biomaterials that incorporate NO donating molecules is that this reservoir eventually becomes exhausted over a period of time. This has led to the investigation of NO generating materials that are able to catalytically react with

endogenous RSNOs, such as GSNO, that are present within the blood to locally release NO at the material interface. The catalytic release of RSNOs has been demonstrated in the past using this mechanism from polymers containing certain metals such as copper or metal organic framework (MOF) molecules(48, 49). Polymer films containing organoselenium moieties have also been proven to catalyze RSNO decomposition to generate NO(33). However, catalytic generation of NO from polymer composites with embedded Se placed in solutions with low concentrations (1 μM) of RSNOs have not been investigated. This concentration corresponds to the approximate range of GSNO present in blood (0.5 – 2 μM)(50) that has the potential to be catalytically influenced from the Se containing materials. Passive NO generation was tested by submerging the fabricated C-Se polymer composites into a PBS solution containing 1 μM GSNO and 30 μM GSH to simulate the RSNO environment seen in the blood. Additionally, 500 μM EDTA was incorporated into the solution to chelate any possible trace metals and to ensure the NO generation was solely from the immersed C-Se. The C-Se interfaces are capable of generating NO from endogenous RSNOs (**Figure 2.2**). The polymer composites were able to generate a flux (> 0.5 x 10^{-10} mol cm^{-2} min^{-1}) capable of mimicking the protective effects seen in native endothelium. To simulate better physiological condition, the C-Se polymer composites were also pre-adsorbed with Fg (2 mg mL^{-1} in phosphate buffer for 1 h. As expected, the NO generation levels were lower (~0.3 x 10^{-10} mol cm^{-2} min^{-1}) but the polymer composites were still able to generate a physiologically relevant amount of NO. While the polymer composites that contain both SNAP and Se exhibit high initial releases of NO for the few first days, which is necessary for eliminating bacteria and preventing biofilm formation, this subsequent prolonged passive NO generation still exhibits levels of NO that is capable of preventing platelet activation. This unique combination of NOrel and NOgen chemistries within medical devices polymers can be immensely advantageous in terms

of overcoming challenges with device implants by providing potent antimicrobial activity both acutely (at the time of surgical placement) as well as continued NO generation to protect from chronic or late device infections.

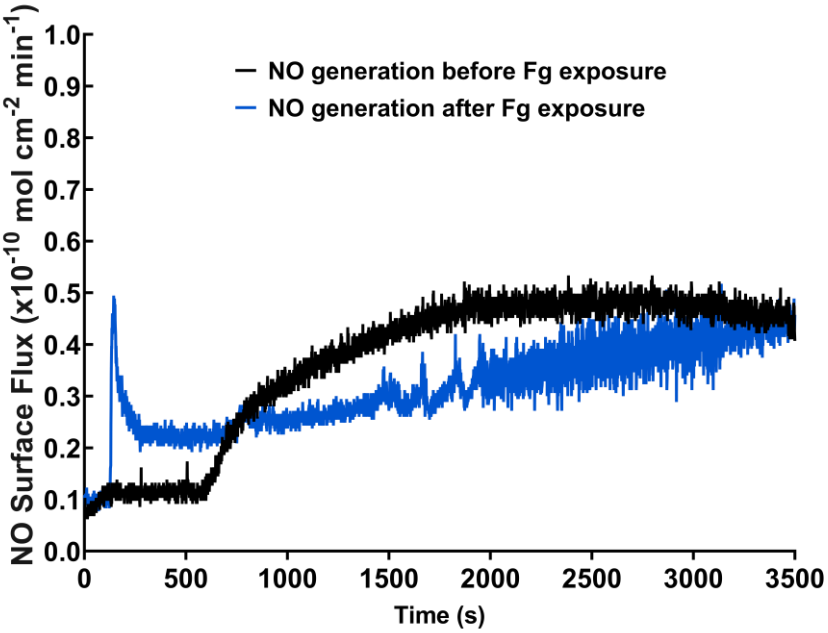

Figure 2.2: Graph demonstrating representative real-time NO generation from C-Se (containing 1% Se) in the presence of GSNO (1 µM) before and after exposure to fibrinogen under physiological conditions (37 ^{o}C, pH 7.4)

2.4.2 Analysis of Surface Composition and Morphology with SEM-EDS

SEM was deployed to investigate the surface morphology of the SNAP-Se-1 polymer composite. Prior to adding a Se interfacial layer, the SNAP incorporated CarboSil was imaged (**Figure 2.3A**). The addition of a Se interface (**Figure 2.3C**) did not significantly alter the surface morphology of the original composite. To confirm the presence of SNAP incorporated into the CarboSil composites and Se incorporated Carbo1Sil on the surface, elemental maps were constructed using EDS. In order to detect SNAP, the presence of sulfur (S) located in the *S*-NO bond of SNAP was determined (**Figure 2.3B**). After coating, the SNAP-Se-1 polymer composite was scanned to determine the presence of Se in the outer layer (**Figure 2.3D**). Both S and Se maps indicated the presence and even distribution of SNAP and Se in their respective layers.

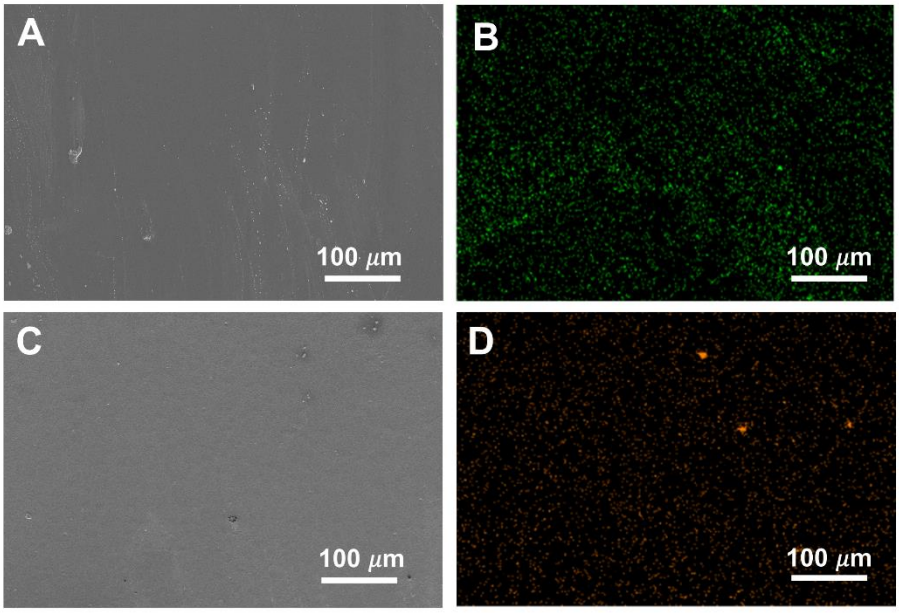

Figure 2.3 – SEM and EDS analysis of SNAP-Se-1 polymer composites. (A) – SEM image of SNAP composite prior to being coated with Se layer and (C) - after coating with 1% Se interface. (B) - Prior to coating, the detection of sulfur was used to analyze the presence of SNAP in the SNAP composite. (D) - After coating, the detection of Se was used to analyze the presence of Se in the SNAP-Se-1 polymer composite.

2.4.3 Leaching of SNAP and Se

Leaching of SNAP: The initial leaching of NO donors can affect the lifetime of NO-releasing medical devices by significantly reducing the time duration of NO release from devices. Additionally, devices can exhibit a "burst release" effect, resulting in an elevated NO flux during the first few hours after beginning its use. Controlling excessive leaching is crucial as the amount of NO released into the bloodstream can cause adverse side effects such as vasodilation, resulting in lowered blood pressure(40). In order to avert this, hydrophobic coatings have previously been applied to control the amount of NO donor leached, especially in the first few hours of use(51). Additional layers of CarboSil have in the past been optimized to result in less SNAP leaching when samples are initially immersed(46). Therefore, to reduce SNAP leaching, each sample was coated with two hydrophobic polymer layers (CarboSil and/or Carbosil-Se). Because Se species have shown to have antimicrobial effects by directly interacting with bacteria, the outer most layer from

SNAP-Se-1 and C-Se polymer composites were composed of 1 wt% (w/w) of Se incorporated CarboSil acting as the interface, while the middle coat consisted of only CarboSil(52-54). To determine the amount of SNAP leaching from the polymer composites, samples were soaked in PBS and measured at different time points over a 24 h time period with UV-Vis spectrophotometer. Both the C-SNAP and SNAP-Se-1 polymer composites exhibited similar leaching patterns, only leaching a total of 0.1990 mg/cm^2 and 0.1469 mg/cm^2 of SNAP per cm^2 of polymer composite after over 24 h of incubation in PBS, respectively **(Figure 2.4A).** This suggests that the addition of Se to the polymer composites did not significantly affect SNAP leaching. Less than 5% of the total NO donor stored in each of the samples were leached after 24 h of incubation in an aqueous environment, suggesting that the amount of SNAP leached will not significantly affect the lifetime of NO release from the composites (**Figure 2.4B**).

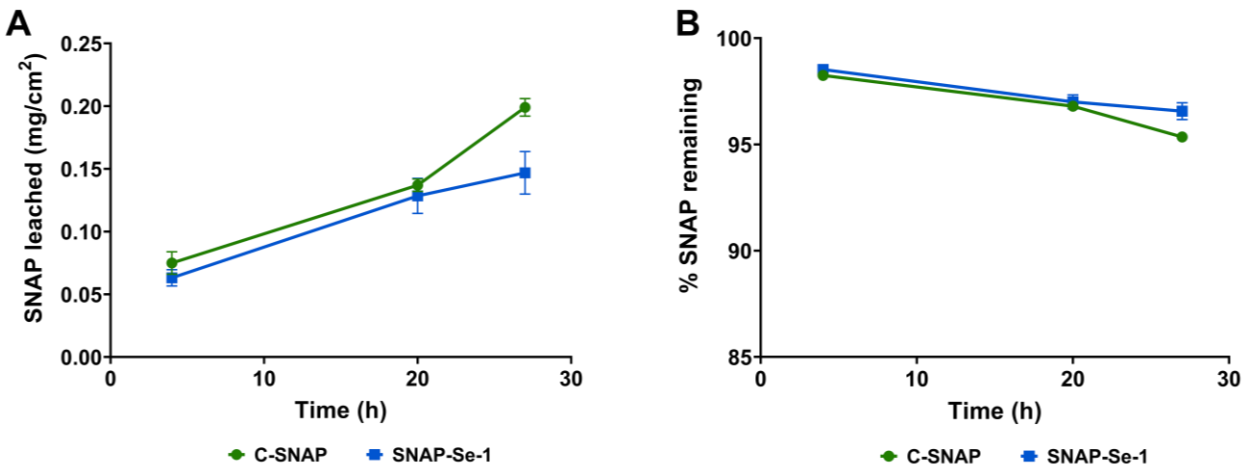

Figure 2.4 – SNAP leaching (A) and % of SNAP remaining (B) in the polymer composites after 24 h. Both C-SNAP and SNAP-Se-1 showed less than 5% of SNAP leaching from the composites. No significant difference was found between either sample. The data is reported in means ± SD.

Leaching of Se: Although Se is essential for survival, excess Se could lead to cytotoxic effects. Previous research has suggested that an intake level of 400 µg/d of Se is the upper tolerable limit for an individual(55). Therefore, when considering the possible side effects of cytotoxicity, it is important to ensure that the level of Se leaching is below the tolerable threshold. However,

low levels of Se leaching can be promising. Se in the past have demonstrated superior bactericidal capabilities(37). In order to determine the level of Se leaching from the composites, a VG ICP-MS Plasma Quad 3 instrument was used to measure 24 h leachate samples in complete DMEM cell culture media. Both C-Se and SNAP-Se-1 polymer composites leached less than 6 µg/L Se into the media, which equates to roughly 0.01% of total Se originally incorporated into the polymer composites. This is significantly less than the suggested daily Se concentration intake. There was no significant difference found between the leaching of SNAP-Se-1 and C-Se (**Table 2.1**).

Table 2.1 – Se leaching measurements of C-Se and SNAP-Se-1 polymer composites. No statistical difference of Se leaching was found between the SNAP-Se-1 and C-Se polymer composites. Data is reported in means ± SD (n=3).

Polymer composite	Se leaching (µg/L)	% Se leaching
C-Se	5.2 ± 1.2	0.014 ± .003
SNAP-Se-1	4.4 ± 1.3	0.012 ± .003

2.4.4 Surface Wettability

Surface wettability provides information about the surface-liquid interfacial tension by establishing the angle of a liquid drop on the solid surface. The surface property of polymer composites can dictate the interaction of bacteria and blood proteins with the polymer composites(56, 57). A surface contact angle higher than 90º is generally considered to be hydrophobic(58). As shown in **Table 2.2**, the polymer composites containing the Se interface had a slightly lower hydrophobicity. The result is also in agreement with reduction in water contact angle observed on a Se coated titanium substrate which was mainly ascribed to contribution of the roughness factor and presence of air pockets(55).

Table 2.2 - Water contact angle measurements of the polymer composites using Krüss DSA100 Drop Shape Analyzer. Data represents mean ± SD (n=3)

Polymer composite	Contact Angle (º)
CarboSil	100.12 ± 0.57
C-Se	88.98 ± 1.30
C-SNAP	100.00 ± 1.44
SNAP-Se-1	80.28 ± 0.94

2.4.5 Reduction in Adhered Bacteria

Infection is problematic for the use of medical devices, limiting success and rates of mortality. Unlike antibiotics, which have specific mechanisms to kill bacteria, NO has a broad range of bactericidal mechanisms and therefore has encountered less resistance than antibiotics(20). The first few hours after device implementation are crucial in preventing infection, as medical device-related infection due to biofilm formation has been previously reported to occur rapidly after insertion (less than 24 h)(2, 59). In order to avert the risk of infection, NO-incorporated devices have been devised to reduce the number of viable bacteria adhered to the surface of devices(21, 60). In addition, Se has been shown to have antimicrobial behavior(61, 62). In this study, we set out to explore the antibacterial effect of incorporating Se with the NO donor SNAP in the hydrophobic polymer CarboSil. In order to do so, the polymer composites were exposed to two strains of bacteria commonly associated with HAIs, *S. aureus* (Gram-positive) and *E. coli* (Gram-negative) for 24 h to assess the reduction in the viability of bacteria adhered to the surface of the polymer composites. The combination of Se and SNAP best reduces the number of bacteria adhered to the surface of the polymer composites for both strains of bacteria (**Figure 2.5**).

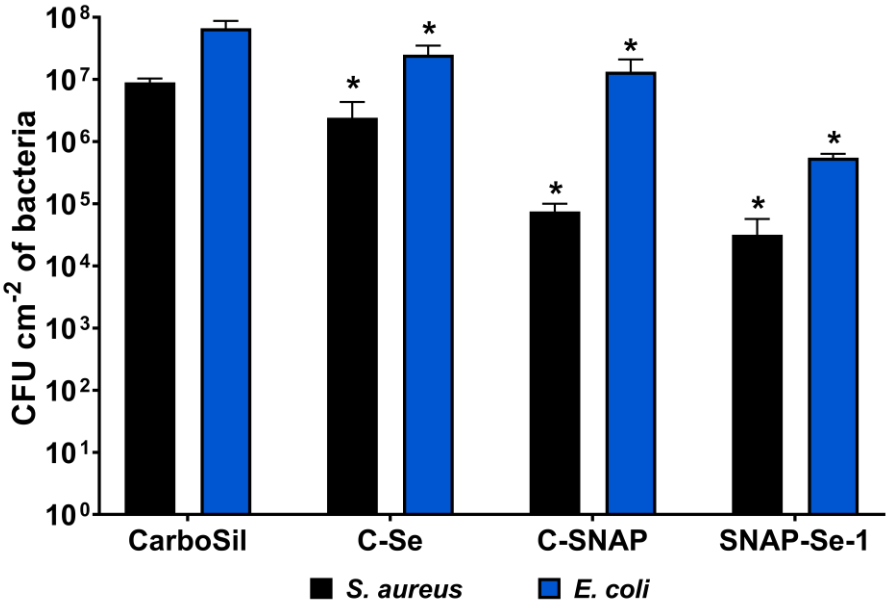

Figure 2.5- Graph demonstrating the reduction in the viability of adhered Gram-negative *E. coli* and Gram-positive *S. aureus* after 24 h. Error bars represent standard deviation (n=5). '*'= $p < 0.05$ vs. CarboSil controls.

The combination of Se interface with NO release was able to reduce the number of adhered *E. coli* and *S. aureus* by 99.18 ± 0.13% and 99.65 ± 0.28% respectively **(Table 2.3)**. The reduction efficiency of SNAP-Se-1 towards viability of adhered bacteria can be attributed to the compounded antimicrobial activity of both agents as well as the increase in NO flux in 24 h. The bactericidal effect of NO includes multiple mechanism routes including DNA cleavage, nitrosative and oxidative action, and formation of peroxynitrite or superoxide(20, 22) In addition, Se had been shown to inhibit growth of bacteria by impairing DNA structures or by reactive oxygen species (ROS) generation in several studies(54, 63). The exact mechanism, however, is yet to be established. Due to the ability of Se interface to generate physiologically relevant NO catalytically in the presence of RSNOs which circulate in blood, it would, in principle, prove to be effective in resisting chronic infections locally. The current study can form the basis of further assessments into mechanism and surface-associated catalytic NO generation and its ability to prevent bloodstream infections *in vivo*.

Table 2.3- Comparative analysis of bacterial CFU/cm^2 adhering to CarboSil, C-Se, C-SNAP and SNAP-Se-1 polymer composites.

Bacterial strain		CarboSil	C-Se	C-SNAP	SNAP-Se-1
S. aureus	Average CFU	9×10^6	2.43×10^6	7.5×10^4	3.17×10^4
	Reduction efficiency (%)	-	73.01 ± 21.3	99.16 ± 0.27	99.65 ± 0.28
	p-value vs. CarboSil control	-	0.008	0.003	0.003
E. coli	Average CFU	6.6×10^7	2.5×10^7	1.33×10^7	5.5×10^5
	Reduction efficiency (%)	-	62.50 ± 15	80.00 ± 11.4	99.18 ± 0.13
	p-value vs. CarboSil control	-	0.03	0.01	0.005

2.4.6 Reduction in Platelet Adhesion

The clinical standard to prevent blood clot formation on indwelling blood-contacting medical devices is systemic anti-platelet and anticoagulation therapies. Unfortunately, systemic anti-platelet and anticoagulation therapies can lead to a number of undesired side effects such as undesired or uncontrolled bleeding. Therefore, a device that can exhibit inherent antiplatelet activity to reduce the occurrence of thrombosis is of significant interest. In this study, the ability of the polymer composites to prevent platelet adhesion was assessed using an LDH assay after exposure to a porcine platelet concentration of 2 x 10^8 platelets/mL. The combination of Se interface and SNAP best inhibited platelets from adhering, showing an 85.5% reduction as compared to CarboSil controls (**Figure 2.6**).

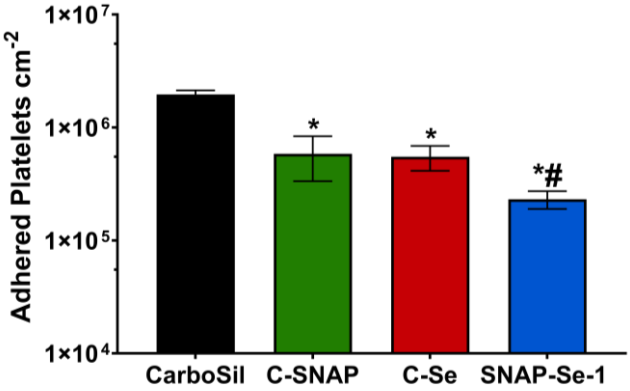

Figure 2.6- Graphical representation of the LDH assay demonstrating reduction in platelet adhesion after exposure to porcine PRP in a 2 h study. The SNAP-Se-1 polymer composite provided the largest decrease in platelet adhesion, showing 85.5 % reduction when compared to that of the controls. Error bars represent standard deviation. '*'= $p < 0.05$ vs. CarboSil control; '#'= $p < 0.05$ vs. C-SNAP.

From the NO release profiles, it is evident that the SNAP-Se-1 polymer composites exhibited greater NO release compared to C-SNAP. The elevated NO at the upper physiological ranges can significantly inhibit platelet adhesion as observed in previous studies *in vitro* and *in vivo*(46, 64). It is also interesting to observe a 72.8% reduction in platelet adhesion by C-Se as compared to CarboSil polymer composites. Although the mechanism of inhibition of platelet adhesion or resistance to platelet aggregation by Se is poorly understood, various forms of Se have been shown to reduce or inhibit platelet aggregation(65, 66). Similar reduction in platelet adhesion was observed via SEM study conducted on Se blended polyurethanes(36). The low levels of NO generated from RSNOs as seen from NO generation studies also holds the potential for SNAP-Se-1 polymer composite to be ideal for blood contacting applications (e.g., vascular grafts, stents). In fact, Major et al. demonstrated that in a 4 h rabbit model, extracorporeal loops coated with only 10 wt% Cu infused with saline solution showed improved platelet counts compared to control loops with intravenous infusion of an RSNO(27). Moreover, in a study on electrochemically modulated NO generation via a Cu(II)-tri(2- pyridylmethyl)amine (Cu(II)TPMA) catalyst, researchers showed that NOGen materials were capable of reducing thrombus formation in catheters(67). In the current scope of this study, further tunability of Se interfacial layer and its interaction with RSNOs embedded in the polymer as well as circulating in blood has not been focused due to limited knowledge of the mechanism through which it reduces platelet adhesion. However, the present result demonstrates that a Se interface on a NO releasing polymer composite can significantly reduce platelet adhesion. This capability can further be extended in combination with other antiplatelet therapies to improve overall hemocompatibility of blood-contacting devices.

2.4.7 In vitro Cytotoxicity

In order to demonstrate the effect of toxicity elicited by extracts from CarboSil, C-SNAP, C-Se and SNAP-Se-1 polymer composites, cytotoxicity testing was conducted in accordance with ISO 10993 standards. NIH 3T3 mouse fibroblast cell line (ATCC 1658) was used for this study. All the polymer composites were soaked in DMEM at 37ºC for 24 h to allow sample extracts to diffuse into the medium. After 24 h, the extracts were exposed to mouse fibroblast cells cultured simultaneously with extract preparation. After 24 h of incubation post addition of the extracts, CCK-8 dye was added to each well and incubated for 3 h. The change in color intensity due to formation of formazan was measured at 450 nm using a multiplate reader. The control had no extracts. It consisted of only cells growing on the 96-wells. With respect to the control, the mouse fibroblast cells demonstrated no significant difference in the presence of the extracts from all the samples (n=7, **Figure 2.7**). Previous studies conducted by the Handa lab and other labs have shown the non-cytotoxicity and potential biocompatibility of NO releasing polymers via SNAP donor(46, 51, 68). In the recent past, cytotoxicity studies conducted with increasing amount of Se in a Se blended polyurethane has shown slight decrease in viability of mouse fibroblast cells. Toxicity elicited by Se or Se species has mostly been ascribed to oxidative damage(69). At 1 wt% Se concentration and negligible leaching of Se from the interfacial layer, the viability of mouse fibroblast cells were 91.3 ± 5.4 %. SNAP-Se-1, however, had improved viability at 97.37 ± 4.94 %. The results from this study provides supporting evidence towards the potential biocompatibility of the SNAP-Se-1 polymer composite. Even though, antibacterial and anti-platelet adhesion characteristic of SNAP-Se-1 is of utmost importance, it should not compromise the biocompatibility of mammalian cells. Further *in vivo* testing in animal models would help establish the biocompatibility of SNAP-Se-1.

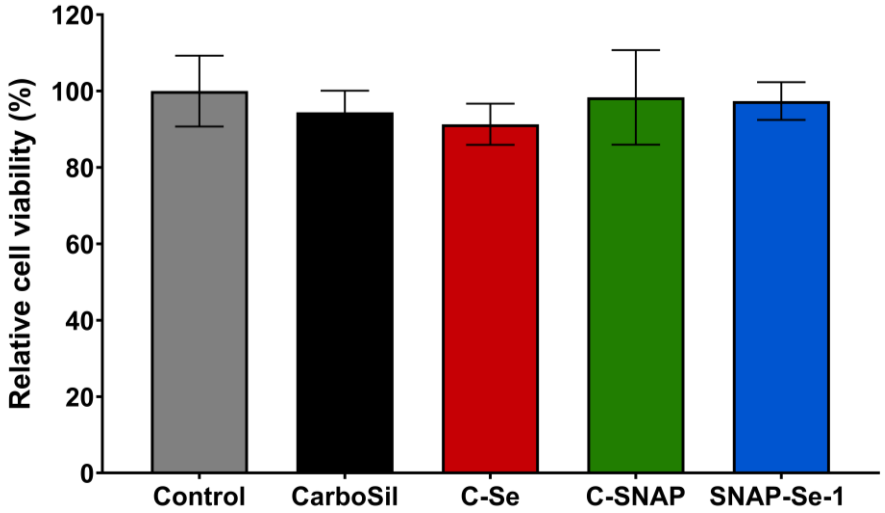

Figure 2.7- Graph demonstrating 24 h cell viability of NIH 3T3 mouse fibroblast cells using WST dye based CCK-8 assay. The error bar represents standard deviation (n=7). The results were not statistically significant ($p > 0.05$).

2.5 Conclusion

The current premise of these findings presents a promising biomaterial specifically designed to integrate properties of both NOrel and NOgen materials in order to achieve localized NO at polymer interfaces. The findings demonstrate that a Se interface containing 1 wt % Se blended with CarboSil on a NO releasing polymer composite elevates the NO release to 5.89 ± 1.18 x 10^{-10} mol cm^{-2} min^{-1} compared to 2.24 ± 0.36 x 10^{-10} mol cm^{-2} min^{-1}. In addition to that, NO (> 0.5 x 10^{-10} mol cm^{-2} min^{-1}) was also generated by C-Se polymer composites in the presence of 1 µM GSNO thus exhibiting NO generating capabilities. As an extension, in principle, not only does SNAP-Se-1 polymer composites have the much-needed elevated release in the beginning required to prevent infection and platelet adhesion, these surfaces can sustainably generate NO by reacting with RSNOs circulating within the blood. The SNAP-Se-1 significantly reduced the adhesion of *E. coli* and *S. aureus* by greater than 2 log reduction which are among prominent pathogens causing nosocomial infections. The LDH assay-based platelet adhesion studies reveal that SNAP-Se-1 can effectively reduce platelet adhesion. Leaching of SNAP and Se was measured through a spectrophotometric method and ICP-MS, respectively. Leaching from either species did

not elicit cytotoxicity in mouse fibroblast cells. Both the leaching and cytotoxicity studies provide important supporting evidence towards the biocompatibility of SNAP-Se-1. The results from this work provides proof of principle for further design and development of polymeric biomaterials incorporating both NOrel and NOgen capabilities in a single platform. This unique approach of combining NOrel and NOgen polymer chemistries can provide localized NO at the polymer interface in order to overcome both acute and chronic biocompatibility and microbial challenges associated with indwelling medical devices. However, further testing in pre-clinical settings will be critical to establish antibacterial and anti-platelet adhesion efficacies as well as determine the safety towards clinical use.

2.6 References

1. Gorbet MB, Sefton MV. Biomaterial-associated thrombosis: roles of coagulation factors, complement, platelets and leukocytes. Biomaterials. 2004;25(26):5681-703.

2. Donlan RM. Biofilms and device-associated infections. Emerg Infect Dis. 2001;7(2):277-81.

3. Magill SS, Edwards JR, Bamberg W, Beldavs ZG, Dumyati G, Kainer MA, et al. Multistate point-prevalence survey of health care-associated infections. The New England journal of medicine. 2014;370(13):1198-208.

4. Scott RD. The Direct medical costs of healthcare-associated infections in U.S. hospitals and the benefits of prevention. 2009.

5. Glied S, Cohen B, Liu J, Neidell M, Larson E. Trends in mortality, length of stay, and hospital charges associated with health care-associated infections, 2006-2012. Am J Infect Control. 2016;44(9):983-9.

6. Stewart PS, Costerton JW. Antibiotic resistance of bacteria in biofilms. Lancet. 2001;358(9276):135-8.

7. Bjarnsholt T, Alhede M, Alhede M, Eickhardt-Sorensen SR, Moser C, Kuhl M, et al. The in vivo biofilm. Trends Microbiol. 2013;21(9):466-74.

8. Donlan RM. Biofilm formation: a clinically relevant microbiological process. Clin Infect Dis. 2001;33(8):1387-92.

9. Hoiby N, Bjarnsholt T, Givskov M, Molin S, Ciofu O. Antibiotic resistance of bacterial biofilms. Int J Antimicrob Ag. 2010;35(4):322-32.

10. Wolcott RD, Ehrlich GD. Biofilms and chronic infections. JAMA. 2008;299(22):2682-4.

11. Fernandez-Ruiz I. Milestone 12: In search of better therapies to prevent device-induced thrombosis. Nat Rev Cardiol. 2017.

12. Jaffer IH, Fredenburgh JC, Hirsh J, Weitz JI. Medical device-induced thrombosis: what causes it and how can we prevent it? J Thromb Haemost. 2015;13 Suppl 1:S72-81.

13. Extracorporeal Life Support Organization (ELSO) Extracorporeal Life Support (ECLS) registry report international summary [Internet]. 2017.

14. Bick RL, Frenkel EP. Clinical aspects of heparin-induced thrombocytopenia and thrombosis and other side effects of heparin therapy. Clin Appl Thromb Hemost. 1999;5 Suppl 1:S7-15.

15. Angiolillo DJ, Guzman LA, Bass TA. Current antiplatelet therapies: benefits and limitations. Am Heart J. 2008;156(2 Suppl):S3-9.

16. Carballo J, Ferreiros CM, Criado MT. Influence of blood proteins in the in vitro adhesion of Staphylococcus epidermidis to teflon, polycarbonate, polyethylene and bovine pericardium. Rev Esp Fisiol. 1991;47(4):201-8.

17. Herrmann M, Lai QJ, Albrecht RM, Mosher DF, Proctor RA. Adhesion of Staphylococcus aureus to surface-bound platelets: role of fibrinogen/fibrin and platelet integrins. J Infect Dis. 1993;167(2):312-22.

18. Foley E, O'Farrell PH. Nitric oxide contributes to induction of innate immune responses to gram-negative bacteria in Drosophila. Genes Dev. 2003;17(1):115-25.

19. Radomski MW, Moncada S. The biological and pharmacological role of nitric oxide in platelet function. Adv Exp Med Biol. 1993;344:251-64.

20. Fang FC. Perspectives series: host/pathogen interactions. Mechanisms of nitric oxide-related antimicrobial activity. J Clin Invest. 1997;99(12):2818-25.

21. Yang T, Zelikin AN, Chandrawati R. Progress and Promise of Nitric Oxide-Releasing Platforms. Adv Sci (Weinh). 2018;5(6):1701043.

22. Carpenter AW, Schoenfisch MH. Nitric oxide release: part II. Therapeutic applications. Chem Soc Rev. 2012;41(10):3742-52.

23. Kim J, Saravanakumar G, Choi HW, Park D, Kim WJ. A platform for nitric oxide delivery. Journal of Materials Chemistry B. 2014;2(4):341-56.

24. Frost MC, Reynolds MM, Meyerhoff ME. Polymers incorporating nitric oxide releasing/generating substances for improved biocompatibility of blood-contacting medical devices. Biomaterials. 2005;26(14):1685-93.

25. Seabra AB, Durán N. Nitric oxide-releasing vehicles for biomedical applications. Journal of Materials Chemistry. 2010;20(9):1624-37.

26. McCarthy CW, Guillory RJ, 2nd, Goldman J, Frost MC. Transition-Metal-Mediated Release of Nitric Oxide (NO) from S-Nitroso-N-acetyl-d-penicillamine (SNAP): Potential Applications for Endogenous Release of NO at the Surface of Stents Via Corrosion Products. ACS Appl Mater Interfaces. 2016;8(16):10128-35.

27. Major TC, Brant DO, Burney CP, Amoako KA, Annich GM, Meyerhoff ME, et al. The hemocompatibility of a nitric oxide generating polymer that catalyzes S-nitrosothiol decomposition in an extracorporeal circulation model. Biomaterials. 2011;32(26):5957-69.

28. Rassaf T, Kleinbongard P, Preik M, Dejam A, Gharini P, Lauer T, et al. Plasma nitrosothiols contribute to the systemic vasodilator effects of intravenously applied NO: experimental and clinical study on the fate of NO in human blood. Circulation research. 2002;91(6):470-7.

29. McGrowder D, Ragoobirsingh D, Dasgupta T. Effects of S-nitroso-N-acetyl-penicillamine administration on glucose tolerance and plasma levels of insulin and glucagon in the dog. Nitric Oxide. 2001;5(4):402-12.

30. Fatokun AA, Stone TW, Smith RA. Prolonged exposures of cerebellar granule neurons to S-nitroso-N-acetylpenicillamine (SNAP) induce neuronal damage independently of peroxynitrite. Brain Res. 2008;1230:265-72.

31. Cai W, Wu J, Xi C, Ashe AJ, 3rd, Meyerhoff ME. Carboxyl-ebselen-based layer-by-layer films as potential antithrombotic and antimicrobial coatings. Biomaterials. 2011;32(31):7774-84.

32. Cha W, Meyerhoff ME. Catalytic generation of nitric oxide from S-nitrosothiols using immobilized organoselenium species. Biomaterials. 2007;28(1):19-27.

33. Yang J, Welby JL, Meyerhoff ME. Generic nitric oxide (NO) generating surface by immobilizing organoselenium species via layer-by-layer assembly. Langmuir. 2008;24(18):10265-72.

34. Rayman MP. The importance of selenium to human health. Lancet. 2000;356(9225):233-41.

35. Hou Y, Guo Z, Li J, Wang PG. Seleno compounds and glutathione peroxidase catalyzed decomposition of S-nitrosothiols. Biochem Biophys Res Commun. 1996;228(1):88-93.

36. Qu BL, Yuan LG, Li JG, Wang J, Lv HY, Yang XN. Selenium-containing polyurethane with elevated catalytic stability for sustained nitric oxide release. Journal of Materials Chemistry B. 2019;7(1):150-6.

37. Cremonini E, Zonaro E, Donini M, Lampis S, Boaretti M, Dusi S, et al. Biogenic selenium nanoparticles: characterization, antimicrobial activity and effects on human dendritic cells and fibroblasts. Microb Biotechnol. 2016;9(6):758-71.

38. Chipinda I, Simoyi RH. Formation and stability of a nitric oxide donor: S-nitroso-N-acetylpenicillamine. J Phys Chem B. 2006;110(10):5052-61.

39. Liu K, Meyerhoff ME. Preparation and characterization of an improved Cu(2+)-cyclen polyurethane material that catalyzes generation of nitric oxide from S-nitrosothiols. J Mater Chem. 2012;22(36):18784-7.

40. Brisbois EJ, Handa H, Major TC, Bartlett RH, Meyerhoff ME. Long-term nitric oxide release and elevated temperature stability with S-nitroso-N-acetylpenicillamine (SNAP)-doped Elast-eon E2As polymer. Biomaterials. 2013;34(28):6957-66.

41. Vanhoe H, Vandecasteele C, Versieck J, Dams R. Determination of iron, cobalt, copper, zinc, rubidium, molybdenum, and cesium in human serum by inductively coupled plasma mass spectrometry. Anal Chem. 1989;61(17):1851-7.

42. Wo Y, Li Z, Brisbois EJ, Colletta A, Wu J, Major TC, et al. Origin of Long-Term Storage Stability and Nitric Oxide Release Behavior of CarboSil Polymer Doped with S-Nitroso-N-acetyl-D-penicillamine. ACS Appl Mater Interfaces. 2015;7(40):22218-27.

43. Wo Y, Li Z, Colletta A, Wu J, Xi C, Matzger AJ, et al. Study of Crystal Formation and Nitric Oxide (NO) Release Mechanism from S-Nitroso-N-acetylpenicillamine (SNAP)-Doped CarboSil Polymer Composites for Potential Antimicrobial Applications. Compos B Eng. 2017;121:23-33.

44. Vaughn MW, Kuo L, Liao JC. Estimation of nitric oxide production and reaction rates in tissue by use of a mathematical model. Am J Physiol. 1998;274(6):H2163-76.

45. Brisbois EJ, Kim M, Wang X, Mohammed A, Major TC, Wu J, et al. Improved Hemocompatibility of Multilumen Catheters via Nitric Oxide (NO) Release from S-Nitroso-N-acetylpenicillamine (SNAP) Composite Filled Lumen. ACS Appl Mater Interfaces. 2016;8(43):29270-9.

46. Pant J, Goudie MJ, Hopkins SP, Brisbois EJ, Handa H. Tunable Nitric Oxide Release from S-Nitroso-N-acetylpenicillamine via Catalytic Copper Nanoparticles for Biomedical Applications. ACS Appl Mater Interfaces. 2017;9(18):15254-64.

47. Kroncke KD, Fehsel K, Kolb-Bachofen V. Nitric oxide: cytotoxicity versus cytoprotection--how, why, when, and where? Nitric Oxide. 1997;1(2):107-20.

48. Oh BK, Meyerhoff ME. Spontaneous catalytic generation of nitric oxide from S-nitrosothiols at the surface of polymer films doped with lipophilic copperII complex. J Am Chem Soc. 2003;125(32):9552-3.

49. Harding JL, Metz JM, Reynolds MM. A Tunable, Stable, and Bioactive MOF Catalyst for Generating a Localized Therapeutic from Endogenous Sources. Adv Funct Mater. 2014;24(47):7503-9.

50. Stamler JS. S-nitrosothiols in the blood: roles, amounts, and methods of analysis. Circulation research. 2004;94(4):414-7.

51. Goudie MJ, Pant J, Handa H. Liquid-infused nitric oxide-releasing (LINORel) silicone for decreased fouling, thrombosis, and infection of medical devices. Sci Rep. 2017;7(1):13623.

52. Khiralla GM, El-Deeb BA. Antimicrobial and antibiofilm effects of selenium nanoparticles on some foodborne pathogens. Lwt-Food Sci Technol. 2015;63(2):1001-7.

53. Nguyen THD, Vardhanabhuti B, Lin MS, Mustapha A. Antibacterial properties of selenium nanoparticles and their toxicity to Caco-2 cells. Food Control. 2017;77:17-24.

54. Tran PA, Webster TJ. Selenium nanoparticles inhibit Staphylococcus aureus growth. Int J Nanomedicine. 2011;6:1553-8.

55. Ramos JF, Webster TJ. Cytotoxicity of selenium nanoparticles in rat dermal fibroblasts. Int J Nanomedicine. 2012;7:3907-14.

56. Vijayanand K, Pattanayak DK, Mohan T, Banerjee R. Interpreting blood-biomaterial interactions from surface free energy and work of adhesion. Trends Biomater Artif Organs. 2005;18(2):73-83.

57. Dexter SC. Influence of Substratum Critical Surface-Tension on Bacterial Adhesion - Insitu Studies. J Colloid Interf Sci. 1979;70(2):346-54.

58. Förch R, Schönherr H, Schonherr H, Jenkins ATA. Surface design: applications in bioscience and nanotechnology: John Wiley & Sons; 2009.

59. Trautner BW, Darouiche RO. Catheter-associated infections: pathogenesis affects prevention. Arch Intern Med. 2004;164(8):842-50.

60. Douglass ME, Goudie MJ, Pant J, Singha P, Hopkins S, Devine R, et al. Catalyzed Nitric Oxide Release via Cu Nanoparticles Leads to an Increase in Antimicrobial Effects and Hemocompatibility for Short-Term Extracorporeal Circulation. ACS Applied Bio Materials. 2019;2(6):2539-48.

61. Kheradmand E, Rafii F, Yazdi MH, Sepahi AA, Shahverdi AR, Oveisi MR. The antimicrobial effects of selenium nanoparticle-enriched probiotics and their fermented broth against Candida albicans. Daru. 2014;22.

62. Yip J, Liu LW, Wong KH, Leung PHM, Yuen CWM, Cheung MC. Investigation of Antifungal and Antibacterial Effects of Fabric Padded with Highly Stable Selenium Nanoparticles. J Appl Polym Sci. 2014;131(17).

63. Chudobova D, Cihalova K, Dostalova S, Ruttkay-Nedecky B, Rodrigo MA, Tmejova K, et al. Comparison of the effects of silver phosphate and selenium nanoparticles on Staphylococcus aureus growth reveals potential for selenium particles to prevent infection. FEMS Microbiol Lett. 2014;351(2):195-201.

64. Brisbois EJ, Major TC, Goudie MJ, Meyerhoff ME, Bartlett RH, Handa H. Attenuation of thrombosis and bacterial infection using dual function nitric oxide releasing central venous catheters in a 9day rabbit model. Acta Biomater. 2016;44:304-12.

65. Douillet C, Bost M, Accominotti M, BorsonChazot F, Ciavatti M. In vitro and in vivo effects of selenium and selenium with vitamin E on platelet functions in diabetic rats relationship to platelet sorbitol and fatty acid distribution. Biol Trace Elem Res. 1996;55(3):263-77.

66. Zbikowska HM, Wachowicz B, Krajewski T. Selenium compounds inhibit the biological activity of blood platelets. Platelets. 1999;10(2-3):185-90.

67. Ren H, Wu JF, Xi CW, Lehnert N, Major T, Barlett RH, et al. Electrochemically Modulated Nitric Oxide (NO) Releasing Biomedical Devices via Copper(II)-Tri(2-pyridylmethyl)amine Mediated Reduction of Nitrite. Acs Appl Mater Inter. 2014;6(6):3779-83.

68. Hopkins SP, Pant J, Goudie MJ, Schmiedt C, Handa H. Achieving Long-Term Biocompatible Silicone via Covalently Immobilized S-Nitroso- N-acetylpenicillamine (SNAP) That Exhibits 4 Months of Sustained Nitric Oxide Release. ACS Appl Mater Interfaces. 2018.

69. Spallholz JE. On the nature of selenium toxicity and carcinostatic activity. Free Radical Biology and Medicine. 1994;17(1):45-64.

CHAPTER 3:

CATALYZED NITRIC OXIDE RELEASE VIA CU NANOPARTICLES LEADS TO AN INCREASE IN ANTIMICROBIAL EFFECTS AND HEMOCOMPATIBILITY FOR SHORT-TERM EXTRACORPOREAL CIRCULATION[3]

[3] Douglass M*, Goudie M*, Pant J, Singha P, Hopkins S, Devine R, Schmiedt C, and Handa H. Catalyzed Nitric Oxide Release via Cu Nanoparticles Leads to an Increase in Antimicrobial Effects and Hemocompatibility for Short-Term Extracorporeal Circulation. 2019. *ACS Applied Bio Materials*. 2, 6, 2539-2548. Reprinted here with permission of the publisher. (* indicates that these authors contributed equally).

3.1 Abstract

Devices used for extracorporeal circulation are met with two major medical concerns: thrombosis and infection. A device that allows for anticoagulant-free circulation while reducing risk of infection has yet to be developed. We report the use of a copper nanoparticle (Cu NP) catalyst for the release of nitric oxide (NO) from the endogenous donor S-nitrosoglutathione (GSNO) in a coating applied to commercial Tygon S3^{TM} E-3603 poly(vinyl chloride) tubing in order to reduce adhered bacterial viability and the occurrence thrombosis for the first time in an animal model. Cu GSNO coated material demonstrated a nitric oxide (NO) release flux ranging from an initial flux of $6.3 \pm 0.9 \times 10^{-10}$ mol cm^{-2} min^{-1} to $7.1 \pm 0.4 \times 10^{-10}$ mol cm^{-2} min^{-1} after 4 h of release, while GSNO loops without Cu NPs only ranged from an initial flux of $1.1 \pm 0.2 \times 10^{-10}$ mol cm^{-2} min^{-1} to $2.3 \pm 0.2 \times 10^{-10}$ mol cm^{-2} min^{-1} after 4 h of release, indicating that the addition of Cu NPs can increase NO flux up to five times in the same 4 h period. Additionally, a 3-log reduction in *S. aureus* and 1-log reduction in *P. aeruginosa* was observed in viable bacterial adhesion over a 24 h period compared to control loops. A Cell Counting Kit-8 (CCK-8) assay was used to validate no overall cytotoxicity towards 3T3 mouse fibroblasts. Finally, extracorporeal circuits were coated and exposed to 4 h of blood flow under an *in vivo* rabbit model. The Cu GSNO combination was successful in maintaining 89.3% of baseline platelet counts, while the control loops were able to maintain 67.6% of the baseline. These results suggest that the combination of Cu NPs with GSNO increases hemocompatibility and antimicrobial properties of ECC loops without any cytotoxic effects towards mammalian cells.

3.2 Introduction

Blood contacting devices used for extracorporeal circulation (ECC) are instrumental during medical procedures such as open-heart surgery, tissue oxygenation, and hemodialysis. However, despite the extensive use of these medical devices, thrombosis and infection still remain two major limitations(1, 2). When blood is introduced to a foreign surface, platelets can adhere, leading to thrombus formation. All current ECC strategies require systemic anticoagulation in order to maintain patency(3). However, administration of anticoagulants such as heparin requires a careful balance between under- and over-dosage in order to reduce thrombus formation while preventing excessive or uncontrolled bleeding(3). According to previous reports, bleeding and thrombosis occur at a rate of 38% and 31%, respectively, in extracorporeal life support patients(4). Moreover, despite systemic anticoagulation, platelet counts can still reduce to less than 40% of the normal count within the first few hours(5).

Additionally, hospital acquired infections (HAIs) are the leading cause of complications for hospitalized patients(6). Of those obtained, approximately 15% of HAIs are primary bloodstream infections alone(7). Though antibiotics are currently being used to control infection, the Center for Disease Control and Prevention estimates that approximately 2 million people are infected with antibiotic-resistant bacteria yearly, and 23,000 die as a result(8). Frequent exposure to foreign devices and line movement result in life-threatening localized and bloodstream infection(9). Previous reports have indicated that biofilms can begin to form within a few hours, showing visible development within 5 h after inoculation(10, 11). Moreover, extracorporeal membrane oxygenation (ECMO) devices have been reported to have a colonization rate of 32%, which was attributed to the artificial surfaces that comprise of the circuit allowing pathogen adhesion and colonization(12). These adverse effects can complicate medical procedures relying

on ECC, increasing hospital stay and risk of death. An anti-thrombogenic and antimicrobial ECC apparatus that allows for anticoagulant-free circulation with reduced rates of infection has yet to be developed.

Due to the essential role of the key signaling molecule nitric oxide (NO) in the nervous, immune, and cardiovascular systems, researchers have recently looked into incorporating synthetic NO donors into medical devices in order to alleviate side effects that commonly occur with implantation(13, 14). Mimicking NO release from endothelial cells can assist in achieving a truly hemocompatible surface. Nitric oxide is particularly useful for two specific areas of interest related directly to blood-contacting medical device applications: platelet activation regulation and immune response(15). Specifically, NO has shown to reduce platelet activity and is produced by macrophages to target both Gram-positive and Gram-negative bacterial pathogens(16-19). To improve the hemocompatibility and antimicrobial behavior of these devices, both exogenous and endogenous NO donors such as S-nitrosothiols (RSNOs), N-diazeniumdiolates, organic nitrates and nitrites, and metal nitrosyl complexes have been incorporated into natural and synthetic polymers to provide an source of localized nitric oxide from device surface to surrounding tissue(20, 21). While many NO donors have been developed, RSNOs have been of particular interest due to their straightforward synthesis and steady release, simulating physiological conditions(22). Amongst the RSNOs, S-nitrosoglutathione (GSNO) is one of the most prevalent naturally occurring S-nitrosothiols found physiologically, responsible for modulating vasodilation and inhibiting platelet aggregation(13, 23, 24). Compared to their NO-releasing counterparts, endogenous RSNOs such as GSNO are superior due to their innate biocompatibility(24). In the body, the endogenous NO donor GSNO behaves as a bioavailable reservoir for NO in the bloodstream and within cells(13, 24, 25). In addition to its superior biocompatibility, GSNO has

also been found to be very stable in comparison to other RSNOs(26). This increased stability also gives a more consistent NO release profile over the tested time period, leading to less variation in flux as typically observed in SNAP coatings(27). When devices are under flow conditions, the need for a stable donor only increases. For these reasons, there has been growing interest in utilizing GSNO as a therapeutic agent(26). Therefore, incorporating GSNO into polymers used for blood-contacting applications to act as a stable, biocompatible NO reservoir is of significant interest.

The release of NO from GSNO is mediated through the cleavage of the S-NO bond present in all RSNO species, and can occur through several different mechanisms: light decomposition, thermal decomposition, and metal ion particle catalysis(13, 28). First, the S-NO bond can be cleaved photolytically by the irradiation of GSNO absorbance bands at 336 and 545 nm(13, 23). However, photocatalysis requires significant exposure to light, which limits medical applications. Secondly, although RSNOs can be stimulated at higher temperatures, extracorporeal devices are used at ambient temperatures. Therefore, the addition of a catalyst to the polymer to increase the nitric oxide flux from the polymer over the pertinent application period is of substantial interest. In addition to photolytic catalysis, the presence of transition metal ion particles have shown to have a strong catalytic effect on RSNOs(29). In the body, copper mediates GSNO decomposition through Cu^{+} interaction with the nitrosothiol, ultimately releasing NO(23). Copper nanoparticles (Cu NPs), in addition to their potential catalytic effect on GSNO, can also interact with endogenous RSNOs found in the blood(30). Cu NPs also possess an innate antimicrobial effect and are less cytotoxic than previously explored silver nanoparticles(31, 32).

We report a unique multi-layer Cu GSNO coating applied to commercial Tygon S3^{TM} E-3603 poly(vinyl chloride) (PVC) tubing, a medical grade polymer commonly used in blood

circulation applications, in order to reduce the occurrence of thrombosis and infection. The effect of the addition of Cu NP on GSNO in CarboSil, a medical grade polymer, is measured by the NO release over a 4 h period. *In vitro* viability of adhered bacteria was measured by counting the colony forming units (CFU) per cm^2 of polymer loops exposed to the Gram-positive strain *Staphylococcus aureus* (*S. aureus*) and the Gram-negative strain *Pseudomonas aeruginosa* (*P. aeruginosa*) for 24 h at 37° C. Cytotoxicity towards 3T3 mouse fibroblasts were assessed with a Cell Counting Kit-8 (CCK-8) after 24 h of leachate exposure. An *in vivo* 4 h ECC rabbit model was then used to measure hemocompatibility.

3.3 Materials & Methods

3.3.1 Materials

Sodium nitrite, tetrahydrofuran (THF), ethylenediaminetetraacetic acid (EDTA), and the CCK-8 kit were purchased from Sigma Aldrich (St. Louis, MO 63103). Tygon S3^{TM} E-3603 poly(vinyl chloride) tubing was purchased from Fisher Healthcare (Houston, TX). Acetone was purchased from VWR (Radnor, PA). Carbosil-2080A (CarboSil) was purchased from DSM (Berkeley, CA). Cu NPs (99%, 40−60 nm) were obtained from SkySpring Nanomaterials, Inc. (Houston, TX). Phosphate-buffered saline (PBS), pH 7.4, was used for all *in vitro* experiments, which contained 138 mM NaCl, 2.7 mM KCl, and 10 mM sodium phosphate. Glutathione, Dulbecco's modified Eagle's medium (DMEM), and trypsin-EDTA were purchased from Corning (Manassas, VA 20109). The antibiotic Penicillin-Streptomycin (Pen-Strep) and fetal bovine serum (FBS) were purchased from Gibco-Life Technologies (Grand Island, NY 14072). The bacterial strains *P. aeruginosa* (ATCC 27853) and *S. aureus* (ATCC 5538), and mouse 3T3 fibroblast cells (ATCC 1658) were purchased from American Type Culture Collection (ATCC). LB broth was obtained from Fisher Bioreagents (Fair Lawn, NJ). LB Agar was obtained from Difco

Laboratories Inc (Detroit, MI). Both the 16-gauge and 14-gauge IV polytetrafluroethylene (PTFE) angiocatheters were purchased from Exel International Co. (Redondo Beach, CA).

3.3.2 Synthesis of GSNO

GSNO was synthesized by dissolving 900 mg of glutathione in a solution containing 12 M of HCl and DI water and chilled in an ice bath for 10 min. $NaNO_2$ was then added to the solution and was chilled for 40 min. Acetone was stirred into the solution for 10 min. The precipitate was collected via filtration and dried in a desiccator in the dark overnight.

3.3.3 Fabrication of Cu GSNO Polymeric Coated ECC Loops

Preparation of ECC loops used for animal testing was done following a previously describe protocol(33-35). Briefly, the fully constructed loop configuration consisted of two 16 cm length pieces of PVC loops (1/4 inch ID) connected on either side of one 8 cm length piece of PVC loop (3/8 inch ID), which creates the thrombogenicity chamber that creates a disturbed flow and recirculation within the loop based on previous design(1). 16-gauge and 14-gauge IV PTFE angiocatheters (Exel International, Co., Redondo Beach, CA) were then placed on either end of the assembled loop using 2 luer-lock PVC connectors. The 3/8 inch and 1/4 inch loop pieces were solvent welded together using a diluted solution of Carbosil in THF (25 mg/mL).

A multilayered coating system was employed for all ECC loops where designated solutions are filled through the tubing lumen and drained according to **Figure 3.1**.

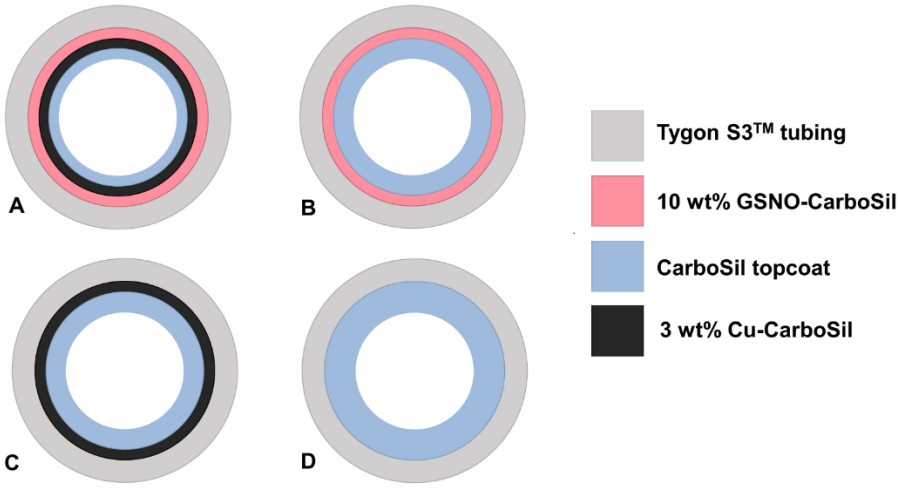

Figure 3.1 - Schematic of the fabrication of ECC loops. Cross-sections shows the layer-by-layer composition of each ECC tubing. Cu GSNO ECC loops (A) were compared to GSNO (B), Cu (C), and CarboSil control (D) loops.

Solutions of CarboSil in THF at a concentration of 50 mg/mL were first prepared. A 10 wt% suspension of GSNO or a 3 wt% suspension of Cu NPs with respect to the CarboSil solution were then added to the CarboSil solutions. A 3 wt% Cu NP solution was used based on a previous report that optimized the concentration of Cu NPs incorporated with the RSNO *S*-nitroso-N-acetylpenicillamine (SNAP)(36). For Cu GSNO loops, two coats of the GSNO solution were first employed, followed by two coats of Cu NP solution, and a final topcoat of CarboSil solution. Each coat was allowed to dry for 1 h at room temperature in the dark to avoid any undesired light catalysis with GSNO prior to any subsequent layer being added. After the final layer was added, loops were allowed to dry for 48 h at room temperature before being kept in a desiccator for 24 h to ensure there was no THF remaining. Loops consisting of either only GSNO (GSNO), copper nanoparticles (Cu), or Carbosil (CarboSil control) were also prepared. GSNO loops contained two coats of GSNO solution, followed by three coats of CarboSil solution. Cu loops contained two coats of Cu NP solution and three coats of CarboSil solution. CarboSil control loops were prepared with five coats of CarboSil solution. Each loop was coated with an equal number of total coats (5

total coats) to ensure that the thickness of the final multi-layered loop remained the same, and scanning electron microscopy (SEM) was later deployed to ensure that the thicknesses remained the same. Based on drying times used in previous studies, the assembled and coated loops were allowed to dry under ambient conditions for 48 h followed by vacuum drying for 24 h(1, 36-38). Previous studies have indicated that layers ~50 microns in thickness are adequate to prevent leaching from ECC loops(39). Prior to each rabbit experiment, loops were presoaked with saline for 1 h and drained.

3.3.4 Scanning Electron Microscopy (SEM) and Energy-Dispersive X-ray Spectroscopy (EDS)

Scanning electron microscopy (SEM, FEI Teneo, FEI Co.) was employed at an accelerating voltage of 10.00 kV to examine the morphology of the fabricated materials along with the dispersion of Cu NPs and GSNO particles throughout the sample surfaces. The SEM was equipped with a large detector energy dispersive X-ray spectroscopy (EDS, Oxford Instruments) system used for elemental analysis and mapping of the elements. All materials were coated with gold-palladium to a thickness of 10 nm using a Leica sputter coater.

3.3.5 Detection of Cu NP and GSNO Leaching from ECC Loops

Inductively coupled plasma mass spectrometry (ICP-MS) is a highly sensitive technique that can measure the presence of trace elements of interest. Detection of copper leaching from polymer coatings was done using a VG ICP-MS Plasma Quad 3 instrument. Cu GSNO polymer films were weighed, measured, and then soaked in DMEM for 24 h. Afterwards, the films were removed and the solution containing potential copper leachate was tested for ^{65}Cu isotopes following a previously established protocol(40).

GSNO leaching was measured during a 4 h incubation period under standard conditions. GSNO loops and Cu GSNO loops were soaked in 1 mL PBS (pH 7.4) and measured with a Thermo

Scientific Genysis 10S UV-Vis Spectrophotometer (UV-vis). Known GSNO concentrations were dissolved in 1 mL of PBS to determine a standard curve. Absorbance was recorded at 340 nm for each sample throughout several timepoints in the 4 h timespan, which corresponds to the absorbance maxima of the S-NO bond found in RSNOs(41). Pure PBS was used as a blank control.

3.3.6 NO-Releasing Kinetics

NO release was recorded using a Sievers Chemiluminescence NOA 280i (Boulder, CO). Samples were submerged in 4 mL of PBS buffer solution (pH = 7.4) maintained at 37 °C in a dark reaction vessel to prevent any light catalysis. With GSNO samples, 100 μm of EDTA was added to the PBS buffer solution to prohibit any metal ion activity in the buffer from interacting with the samples. In the PBS solution containing samples with Cu NPs, however, no EDTA was added so that the catalytic activity of the Cu NPs would not be interfered with. To measure the NO levels released from each sample, nitric oxide was constantly swept from the headspace of the chamber and purged from the buffer solution by a bubbler and nitrogen sweep gas at 200 mL min^{-1} into the chemiluminescence detection chamber. In the chamber, NO reacts with ozone (O_3) to produce a nitrogen dioxide (NO^2*) at an excited state. The excited nitrogen dioxide decays and emits a photon used to detect the original concentration of NO released measured in ppb. After taking in consideration the NOA constant (mol ppb^{-1} s^{-1}) and the surface area of the sample, the data was converted to surface flux ($x10^{-10}$ mol cm^{-2} min^{-1}). Each sample was measured for 4 h.

To calculate the cumulative release, loops were measured prior to and after coating with the GSNO layer. The weight of the GSNO layer was then used to calculate the mg of GSNO incorporated. The initial amount of GSNO was compared to the amount of NO released during the 4 h period, which was calculated through the flux measured to compute the % cumulative release according to **Equation 3.1:**

$$\%\ Cumulative\ Release = \frac{mg\ GSNO\ used}{mg\ initial\ GSNO}$$

3.3.7 Colony-Forming Units Quantification on Coating Surface

Viable bacterial adhesion was measured using a modified version of a previously established protocol(42, 43). First, isolated colonies of bacteria (*S. aureus* and *P. aeruginosa*) were cultured in LB broth at 37 °C until reaching a concentration of ~10^6 CFU per mL verified by optical density measured by UV-vis. The culture was then centrifuged at 2500 revolutions per minute (RPM) for 7 min. The broth was removed, and the culture was resuspended in PBS. In a 24-well plate, 1 mL of the PBS-bacteria suspension was transferred to each well, each containing a different sample type and then incubated for 24 h. Each sample was then immersed in 1 mL of PBS contained in a 15 mL centrifuge tube and homogenized for 60 s at 25000 rpm using an Omni-TH homogenizer (Omni, Kennesaw, GA) and subsequently vortexed for 60 s to ensure any bacteria attached to the surface of the sample was transferred to the PBS solution. Serial dilutions made from the resulting PBS solution were then transferred to LB agar plates and cultured in an incubator at 37 °C. The CFUs per cm^2 of tested loops were hand-counted from each sample type to determine bacterial inhibition effectiveness.

3.3.8 In vitro 24 h 3T3 Mouse Fibroblast Cytotoxicity

To establish that the Cu GSNO synthesized polymer does not have any cytotoxic effects towards mammalian cells, cytotoxicity assessment was measured according to ISO 10993 standards.

3.3.9 Cell Culture Preparation

Before performing the toxicity assays, 3T3 mouse fibroblast cells were grown in a 75 cm^2 T-flask containing DMEM with supplements. The cells were kept in culture at 37°C in a

humidified atmosphere with 5% CO_2. The medium was replaced every 2-3 d until a confluency of 80-90% was reached after which cells were sub-cultured with trypsin-EDTA (0.18% trypsin and 5 mM EDTA) and incubated for 5 minutes. The cell suspension was then collected and counted using a hemocytometer using trypan blue dye exclusion method. After cell counting, 100 µL cells were transferred to a 96 well plate with each of the well containing 5000 cells per mL with n=7 of each sample type. This was followed by a 24 h incubation.

3.3.10 Cytotoxicity Measurements using WST-8 Dye

The leachates from the samples were collected from DMEM medium that contains 1 mg/mL of sample (10 mg dry weight in 10 mL medium) incubated for 24 h at 37°C. Thereafter, 10 µL of leachate solution was added to each of the wells and incubated for a period of 24 h in a 96 well plate. After 24 h, 10 µL dye solution from WST-8 based CCK-8 kit was used. The manufacturer's (Sigma-Aldrich) protocol was followed while using the CCK-8 kit which utilizes highly water-soluble tetrazolium salt. WST-8 [2-(2-methoxy-4-nitrophenyl)-3-(4-nitrophenyl)-5-(2,4-disulfophenyl)-2H-tetrazolium monosodium salt] is reduced by dehydrogenases in live cells to give formazan (an orange color product) detected at 450 nm. Thus, the number of living cells is directly proportional to the amount of the formazan dye generated by dehydrogenases in cells. Results were reported as percentage cell viability (percentage of control) after subtracting the average absorbance of the medium (without cells) as follows according to **Equation 3.2**:

$$\%\ Cell\ Viability = \frac{Absorbance\ of\ the\ test\ samples}{Absorbance\ of\ the\ control\ samples}\ x100$$

3.3.11 In vivo Assessment of Hemocompatibility of NO-Releasing Extracorporeal Circuits

The rabbit model to evaluate hemocompatibility of the ECC loops was used as previously reported(1, 37, 39, 41). The animal handling and surgical procedures were approved by the

University Committee on the Use and Care of Animals in accordance with university and federal regulations. A total of 12 New Zealand white rabbits (Charles River) were used in this study. Initially, all rabbits (2.5–3.5 kg) were anesthetized with intramuscular injections of 5 mg kg^{-1} xylazine injectable (AnaSed® Lloyd Laboratories Shenandoah, Iowa) and 30 mg kg^{-1} ketamine hydrochloride (Hospira, Inc. Lake Forest, IL).

Isoflurane gas (maintenance anesthesia) was administered via inhalation at a rate of 1.5–3% via mechanical ventilation which was done via a tracheotomy and using an A.D.S. 2000 Ventilator (Engler Engineering Corp.Hialeah, FL). Peek inspiratory pressure was set to 15 cm of H_2O and the ventilator flow rate set to 8 L min^{-1}. In order to aid in maintenance of blood pressure stability, IV fluids of Lactated Ringer's were given at a rate of 10 mL kg^{-1} h^{-1}. For monitoring blood pressure and collecting blood samples, the rabbits' right femoral artery was cannulated using a 16-gauge IV angiocatheter (Jelco®, Johnson & Johnson, Cincinnati, OH). Blood pressure and derived heart rate were monitored with a Series 7000 Monitor (Marquette Electronics Milwaukee, WI). Body temperature was monitored with a rectal probe and maintained at 37 °C using a water-jacketed heating blanket.

Prior to placement of the arteriovenous (A-V) custom-built ECC loops, the rabbit left carotid artery and right external jugular vein were isolated and baseline cell counts were drawn from the femoral catheter. Baseline blood samples were collected for platelet and total white blood cell (WBC) counts which were measured on a Heska Element HT5 Hemotology Analyzer. After baseline blood measurements, the custom-built ECC device was placed into position by cannulating the left carotid artery for ECC in flow and the right external jugular vein for ECC out flow. The flow through the ECC device was initiated by unclamping the arterial and venous sides of ECC loops and blood flow in the ECC loop was monitored with an ultrasonic flow probe and

flow meter (Transonic HT207 Ithaca, NY). Occlusions of the ECC tubing was considered to be 100% if the flow through the circuit was observed to be ≤ 5 mL min^{-1}. Animals were not systemically anticoagulated during the experiments.

Following the initiation of ECC blood flow, whole blood samples were collected in 3.2% sodium citrate vacutainers (Becton, Dickinson. Franklin Lakes, NJ) in 3 mL volumes for cell counts each hour during the 4 h experiment.

After 4 h of blood flow or once the ECC circuit was fully occluded, the ECC loops were clamped, removed from the rabbit, and rinsed with 30 mL of saline and drained. Due to the opacity of the ECC loops, the thrombogenicity chamber was longitudinally cut open to observe the extent of thrombus formation. The thrombogenicity chamber was photographed and the thrombus was gently transferred to a formalin container to be preserved until massed for quantification. The rabbits were euthanized using a dose of Fatal Plus (130 mg kg^{-1} sodium pentobarbital). Prior to euthanasia, all rabbits were given a dose of 400 U/kg sodium heparin to prevent post-mortem thrombosis.

3.3.12 Statistical Analysis

All measured data is reported as a mean ± standard deviation. A standard two-tailed t-test was performed to determine significance ($p < 0.05$).

3.4 Results & Discussion

3.4.1 Surface Morphology and Leaching Characterization

SEM imaging and Elemental Mapping. Images of the surface were investigated for uniform deposition of GSNO and copper particles in the different layers of the polymer coating. First, both PVC loops and CarboSil-coated loops were imaged (**Figure 3.2A and B**) prior to adding the Cu NP and GSNO layers. Neither of these materials exhibited sulfur or copper elements as expected,

therefore only SEM images are presented (elements detected were C, O, Cl from the polymers Au and Pd from sputter coating). As shown in Figure **3.2C** and **3.2E**, the addition of Cu NPs and GSNO did not significantly alter the topography of the coating. As seen in **Figure 3.2D,** Cu NPs were present and evenly dispersed throughout the coating. For the detection of GSNO, sulfur was mapped on the surface as GSNO was the only sulfur-containing compound in the polymer coating. As observed in **Figure 3.2F**, the surface had an evenly dispersed coating of GSNO. It can be noted that each layer was mapped in the absence of CarboSil topcoats as the presence of a topcoat reduces the ability to detect the elements of interest. However, because the loops were assembled layer-by-layer, these results accurately demonstrate the distribution of GSNO and Cu NPs within their respective layers that overall compose the entire ECC device coating.

After the entire coating process was complete, to ensure uniform coating thickness, cross-sections of each multi-layered tubing were imaged using SEM (**Figure 3.3**). The thickness of the resulting layers were measured and averaged to confirm uniform coating (n=10). Measurements showed that the thicknesses between each sample type were similar, indicating that the addition of GSNO and Cu had no significant effect on the coating process (CarboSil – 56.6 ± 1.9 µm, Cu – 56.8 ± 3.9 µm, GSNO – 57.6 ± 1.5 µm, Cu GSNO – 57.1 ± 4.2 µm).

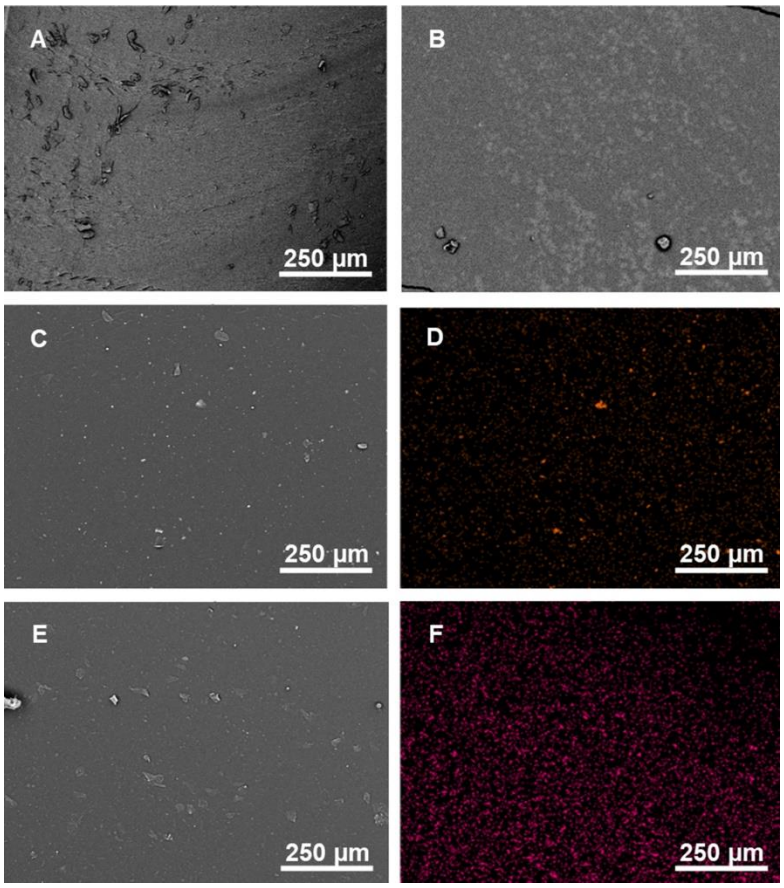

Figure 3.2 - SEM (A, B, C, and E) and EDS (D and F) analysis of the inner surface of the ECC loops. Both PVC (A) and CarboSil (B) tubing were imaged as control for test samples. The copper layer (C) and GSNO layer (E) did not significantly alter the morphology of the Tygon tubing. EDS mapping of copper (D) and sulfur (F) demonstrate the presence and even distribution of Cu NPs (orange) and GSNO (pink) within their respective layers.

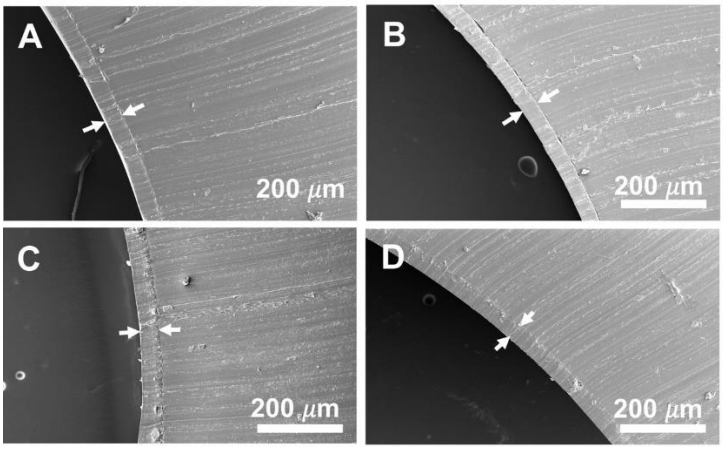

Figure 3.3 - SEM analysis of the cross section of the final multi-layered ECC loops. The white arrows indicate the coating on the inner surface of the tubing. Measurements indicate uniform coating thickness between each sample (A – CarboSil coating, B – Cu coating, C – GSNO coating, D – Cu GSNO coating).

Copper and GSNO Leaching. Controlling the amount of copper leaching from polymers is crucial due to the inherent cytotoxic effects it has when at high enough concentrations. In the presence of an aqueous environment, metallic Cu can oxidize, resulting in Cu ions leaching into the surrounding environment. Each ECC loop was top coated with a layer of 50 mg/mL concentration of CarboSil to prevent excessive copper and GSNO leaching. After 24 h of soaking 1 mg sections of both Cu and Cu GSNO loops in DMEM at 37º C, ICP-MS was performed to detect exact amounts of copper ions leached into the media **(Table 3.1)**. Both types of loops saw less than 11 x 10^{-6} mg of copper ions leached per mg of tubing, which equates to less than 0.1% of the total copper stored within the films. Moreover, like Ag NPs, Cu NPs possess innate antimicrobial effects, but are less cytotoxic than Ag NPs(31, 32). Previously reported copper leaching at similar levels showed beneficial antimicrobial activity while maintaining high mammalian cell viability(36).

Table 3.1 – Total amount of Cu leached after 24 h of soaking in DMEM at 37º C. No significant difference was found between Cu and Cu GSNO samples ($p > 0.05$). The data are means ± SD.

Sample	Cu leaching (mg Cu/mg tubing)
Cu	$9.9 \pm 0.5 \times 10^{-6}$
Cu + GSNO	$10.7 \pm 0.5 \times 10^{-6}$

GSNO leaching studies were performed to determine the amount of NO leached into PBS during a 4 h incubation period. Initial leaching can severely limit the total time duration and consistency of the NO release from polymeric surfaces(44). Although the use of hydrophobic polymers minimize water uptake, and therefore minimize leaching, even when RSNOs are incorporated into a hydrophobic polymer and/or are top-coated with a hydrophobic polymer, low levels of leaching can still occur due to the water uptake into the film. Previous studies have shown that the majority of leaching occurs within the first few hours(38, 41, 45, 46). Moreover, this initial

leaching is most likely due to trace amounts of diffusion that occurs when the final top coat is applied. Since it is a THF based solution, it will partially dissolve the underlying GSNO-CarboSil layer and allow some of the GSNO to be mixed in with this top coat. Therefore, in this study, we examined GSNO leaching over the first 4 h of soaking in a PBS solution. GSNO leaching was measured with UV-vis. During the first hour, less than 0.3 mg of total GSNO coated had leached from both the GSNO loops and Cu GSNO loops per mL of PBS, which equates to less than 2% of total GSNO originally incorporated into the loops, indicating that the samples did not experience a "burst effect" that corresponds to a high amount of GSNO being leached when initially immersed in PBS **(Table 3.2).** After 4 h of incubation, ~ 1.0 mg of total GSNO, which corresponds to less than 7% of total GSNO initially coated, per mL of PBS had leached from the surface.

Table 3.*2* - Concentration of GSNO leaching over 4 h of soaking in PBS at 37º C. No significant difference was found between GSNO and Cu GSNO samples ($p > 0.05$). The data are means ± SD

Time	GSNO (mg/mL)	Cu + GSNO (mg/ml)
1 h	0.1 ± 0.2	0.2 ± 0.2
2 h	0.7 ± 0.3	0.4 ± 0.5
4 h	0.8 ± 0.2	1.0 ± 0.3

3.4.2 NO Release from Cu GSNO ECC Loops

In the past, NO-releasing materials have been proven effective in reducing viability of adhered bacteria and platelet activation(47, 48). Although light catalysis is a known method to increase the release of NO from NO donors, this method has its limitations in biomedical device applications. Moreover, increasing the concentration of the NO donor within the polymer does not simply increase the release rate of NO, and also can have negative effects on the mechanical integrity of the materials(38, 49). Therefore, other methods need to be explored in order to control the NO release to fit desired applications. In this study, Cu NPs were incorporated into the polymer to increase the nitric oxide flux from the polymer. GSNO loops were compared to the Cu GSNO

loops to measure the catalytic effect of Cu on the NO release **(Figure 3.4A)**. Over a 4 h period, the GSNO loops were found to release an average flux between 1.1 ± 0.2 x10^{-10} mol cm^{-2} min^{-1} (after 1 h of release) to 2.3 ± 0.2 x10^{-10} mol cm^{-2} min^{-1} (after 4 h PBS incubation) **(Figure 3.4A)**. However, when 3 wt.% Cu was incorporated into the polymer coatings, the average flux increased to 6.3 ± 0.9 x10^{-10} mol cm^{-2} min^{-1} (after 1 h of release) to 7.1 ± 0.4 x10^{-10} mol cm^{-2} min^{-1} (after 4 h of PBS incubation) over the same 4 h period **(Figure 3.4A)**. The Cu GSNO loops had a maximum flux of 10.3 ± 0.8 x10^{-10} mol cm^{-2} min^{-1}, while the GSNO loops only showed a maximum flux of 2.3 ± 0.2 x10^{-10} mol cm^{-2} min^{-1} towards the end of the incubation period. Based on this data, it can be concluded that the presence of Cu NPs in an adjacent layer has a catalytic effect on the NO release without creating a burst effect that results in all of the NO being released at once. The cumulative release profile indicates that the Cu GSNO loops used ~5% more of the nitric oxide stored in the polymer when compared to the GSNO loops over the same 4 h period **(Figure 3.4B)**. As can be observed, the presence of Cu NPs elevates the total amount NO being released over the 4 h application period, but the % of NO released over time remains consistent. No burst effect that quickly extinguishes the NO supply is observed.

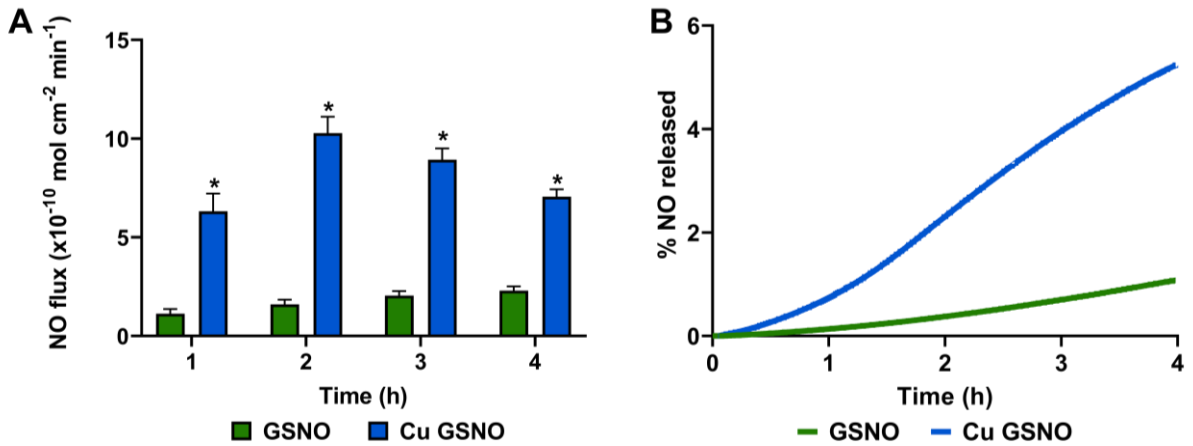

Figure 3.4 – Hourly average (A) and cumulative (B) NO release analysis of control GSNO tubing compared to Cu GSNO tubing over a 4 h period. P-values < 0.05 were used to determine statistical significance indicated by *. For the real-time flux measurements, the data are presented as means ± SD. Cumulative release is reported as means of cumulative NO release for each sample. NO release increases when Cu NPs are present in the sample. N=3 per sample.

The NO flux behavior over the 4 h period of the two sample types can be explained by two phenomena. First, CarboSil is a hydrophobic polymer, exhibiting a contact angle greater than 100° and a water uptake of 0.7 ± 0.2 wt.% in previous literature(38, 50). Therefore, when the samples are initially immersed in PBS, the water uptake time is extremely gradual, corresponding to the gradual increase of NO release in both the control and the Cu GSNO samples in the first two hours. Although the control continues to increase gradually after the first two hours, the Cu GSNO samples experience a slight decrease in NO release. This can be explained by the ability of Cu^{2+} to be reduced to Cu^{+}. Only Cu^{+} contributes to the catalytic effect of NO release(51). According to literature, unlike other NO donors, the release of NO from RSNOs is governed by heat, moisture, light, and/or metal ion catalysis. Initially, RSNOs present can decompose with the assistance of heat, moisture, and/or light, resulting in the release of NO and a byproduct of a reactive RS^{-} species. The RS^{-} species produced from the passive decomposition of GSNO readily reduces Cu^{2+}, which is present of Cu NP corrosion, resulting in Cu^{+} and RSSR. This mechanism has been previously detailed by Burg et al and further discussed by Pant et al(36, 52). Increasing the levels of Cu NPs in the samples has previously been established to increase the levels of NO from other NO donors, which suggests that if more Cu^{2+} is initially available to diffuse through the film, more Cu^{2+} can be reduced to Cu^{+}(36). However, for this study, we limited our scope to Cu NP levels that have previously been described to give maximum levels of NO release before reaching a range that is beyond the physiological range(36).

3.4.3 In vitro Analysis of Bacteria Eradication on ECC Surface

Bacterial adhesion to a polymer surface is problematic for biomaterials, limiting the efficacy of a material and increasing the risk of infection and mortality for patients(53). NO donors can avert risk of infection associated with medical devices, showing a reduction in viable bacteria

adhered both *in vitro* and *in vivo*(16, 45, 54, 55). In addition, heavy metals have been reported to have an innate oligodynamic effect, resulting in the reduction of viable bacteria(56, 57). To measure the antibacterial impact of a Cu GSNO combination, 24 h *in vitro* bacterial adhesion was measured by exposing a Gram-positive and Gram-negative bacterial strain commonly associated with hospital-acquired infections, *S. aureus* and *P. aeruginosa*, to prepared loops of each material type. **Figure 3.5** shows a comparison of bacterial colony-forming units per cm^2 present on the bacteria in relation to the CarboSil control. Cu GSNO was found to have the most significant reduction, resulting in a 3-log reduction with *S. aureus* and a 1-log reduction with *P. aeruginosa* when compared to the CarboSil control.

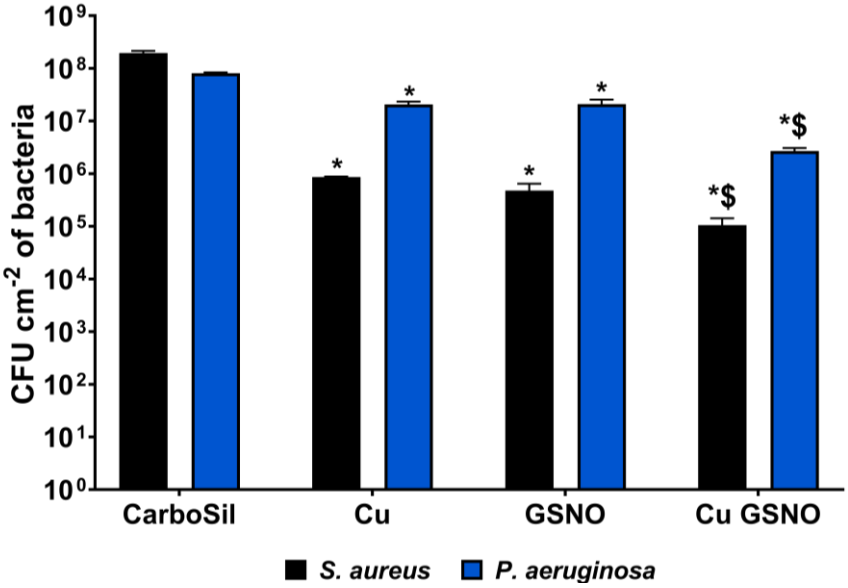

Figure 3.5 - CFU/cm^2 quantification of viable gram-positive (*S. aureus*) and gram-negative (*P. aeruginosa*) bacteria adhered to control and test surfaces after 24 h. The Cu GSNO combination showed the greatest reduction in viable bacteria of both strains, which can be explained by the catalytic increase in NO flux and oligodynamic role of the Cu nanoparticles. P <0.05 were considered significantly different. Note: *, $, % indicate significant difference in CFU/cm^2 of that sample to the CarboSil, 3% Cu, and GSNO controls, respectively. The data are means ± SD.

When isolating each material type, Cu- as well as GSNO-coated loops both demonstrated bacterial adhesion inhibition on both strains **(Table 3.3).** The Cu loop showed a 99.6% ± 0.1% and 74.1% ± 5.5% reduction in viable adhered *S. aureus* and *P. aeruginosa*, respectively. The

antimicrobial effects of Cu NPs is well-documented and explains why the Cu loops showed increased antibacterial activity(31, 32). The GSNO loops showed a 99.74% ± 0.04% and 74.58% ± 12.3% reduction in viable adhered *S. aureus* and *P. aeruginosa*, respectively. However, when combining the two, the catalytic effect of copper on the nitric oxide release increased the nitric oxide flux from the surface, which corresponded with a decrease in viable bacterial adhesion to 99.94% ± 0.03% and 96.7% ± 0.5% for *S. aureus* and *P. aeruginosa*, respectively. These findings show that the NO flux from the surface of the loops is inversely proportional to the number of viable bacteria found on the surface, indicating that increasing the surface flux during the application period increases the likelihood that infection can be averted. Moreover, NO donors can be combined with other therapeutic materials such as quaternary ammonium ions, diatomaceous earth particle, and silicone oil in order to improve antimicrobial performance(44, 48, 58, 59). Therefore, the combined bactericidal effects of the low concentration of copper with the nitric oxide donor GSNO provides an innovative way to amplify the reduction of bacterial adhesion to a polymeric surface for biomedical applications, a method that can in the future be combined with other antimicrobial materials.

Table 3.3 - % of bacterial adhesion reduction in GSNO, Cu, and Cu GSNO samples compared to a CarboSil control. The data are means ± SD.

Sample	*S. aureus*	*P. aeruginosa*
GSNO	99.74% ± 0.04%	74.6% ± 12.3%
Cu	99.6% ± 0.1%	74.1% ± 5.5%
Cu GSNO	99.94% ± 0.03%	96.7% ± 0.5%

3.4.4 Cytotoxicity of Cu GSNO ECC Loops

Antibacterial and antithrombic potential are important attributes to validate the success of a material for biomedical application, but not at the cost of any undesirable side effects like

cytotoxicity towards healthy cells. Therefore, in order to establish that the antibacterial and antithrombic Cu GSNO coatings are not toxic towards mammalian cells, mouse fibroblast cells were exposed to 24 h leachate collected from the sample. In the current study, the result showed that the material is completely safe as the viability of the mammalian cells exposed to Cu GSNO leachate was similar to that of Carbosil control as shown in **Figure 3.6.**

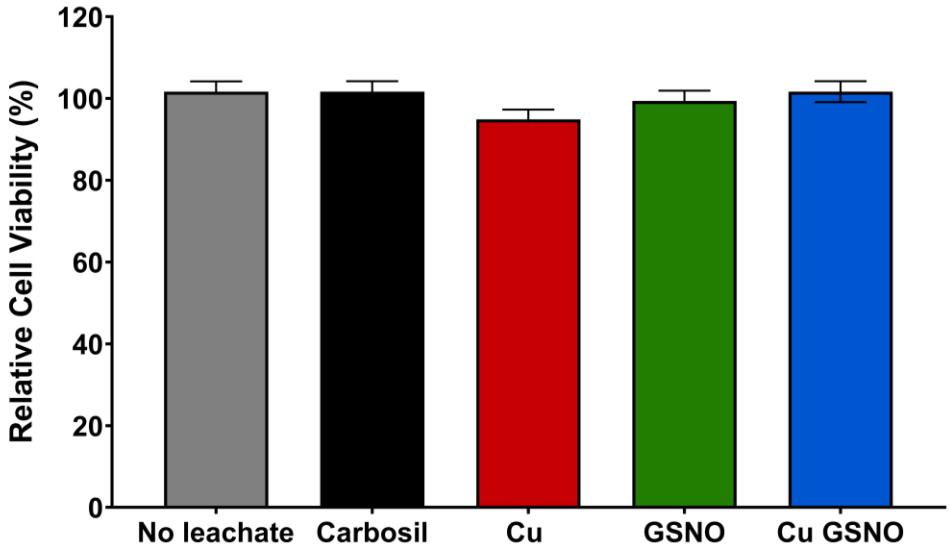

Figure 3.6 - Cytotoxicity measurements of each sample type against 3T3 mouse fibroblast cells (n=7). The samples were soaked for 24 h in DMEM, and the resulting leachates were then added to the cells to measure for cytotoxicity. All samples showed >95% cell viability, indicating that none of the samples had cytotoxic effect. The data are means ± SD. P-values < 0.05 were used to compare.

This is in agreement with the previous report where copper nanoparticles assisted NO release from another NO donor, SNAP, was non-cytotoxic to mammalian cells while maintaining its antibacterial and antithrombotic effect(36). Other studies have also tested NO donors on the mammalian system and found them to be innocuous at the tested dose(59). In conclusion, Cu GSNO composite is not toxic to mouse fibroblast cells, providing strong evidence about its biocompatible nature. This combined with the antibacterial and antithrombic effects makes the material highly translational and supports its testing in clinical models in future.

3.4.5 In Vivo 4 h Extracorporeal Hemocompatibility in Rabbit Model

The ability for materials to prevent thrombus formation and platelet consumption is critical for blood contacting medical devices. Evaluation of novel materials *in vivo* is critical as *in vitro* assays are commonly required to include various anticoagulants to decrease the thrombotic nature of the blood. Similarly, the activity and viability of cells in the blood decrease as it is removed from the body, where high variability can be seen between freshly drawn and stored blood. Therefore, the ECC model is valuable in its ability to maintain fresh blood *in vivo* without the use of anticoagulants. Both platelet concentration (% of baseline) and overall thrombus formation were used as metrics to determine the overall hemocompatibility of the various polymer coatings.

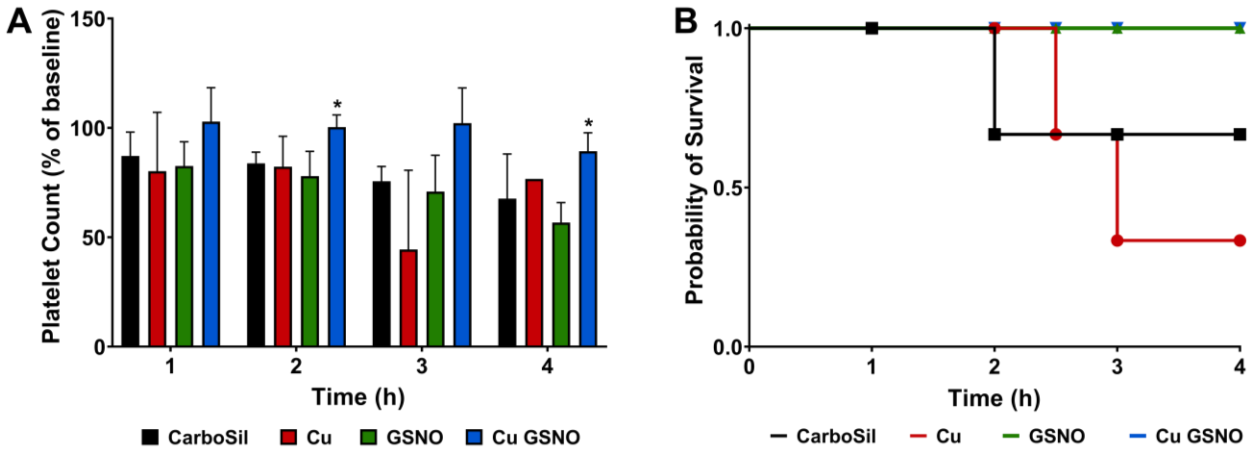

Figure 3.7 – Analysis of the platelet count (A) based of the baseline count and rabbit survival (B) (n=3). Cu GSNO loops maintained the highest platelet count throughout the 4 h application period. Both NO-releasing groups showed 100% survival. The data are means ± SD. Statistical significance (*) was found using a standard two-tailed student t-test between the Cu GSNO and GSNO groups at 2 h and 4 h ($P < 0.05$). Because some CarboSil and Cu loops did not survive, t-tests could not be performed for these groups beyond 2 h and 3 h, respectively.

Platelet counts were monitored over the 4 h ECC experiments, corrected for hemodilution from the IV fluids, and are summarized in **Figure 3.7A**. During the entire 4 h procedure, Cu GSNO loops maintained higher platelet counts compared to other test loops. At the end of 4 h duration, Cu GSNO loops maintained 89.3% ± 8.5% of the baseline platelet count, while GSNO, Cu, and CarboSil loops dropped to 56.71% ± 9.09%, 76.7%, and 67.6 ± 20.4%, respectively, indicating

that the higher NO release exhibited by the Cu GSNO loops assisted in maintaining the platelet counts. While the platelet counts for the Cu and CarboSil loops appear to be higher than the GSNO loop, both non-NO-releasing material combinations had loops that showed complete occlusion of the ECC circuit (< 5 mL min^{-1}) prior to the 4 h end point. CarboSil control loops showed N=1 loop occluding at 2 h after loop placement, while Cu loops showed N=2 occluding at 2.5 h and 3 h (**Figure 3.7B**). Average platelet count for non-surviving loops could not be accounted for beyond point of occlusion. Because one of the CarboSil and two of the Cu loops clotted prior to the end of the experiment, no statistical significance could be calculated with these two groups. On the other hand, for both NO-releasing loops (GSNO and Cu GSNO), all 3 rabbits survived the 4 h procedure. However, though all GSNO loops survived the 4 h duration, GSNO loops showed a lower platelet count compared to Cu GSNO loops. The higher NO release from the Cu GSNO combination showed significantly higher platelet counts compared to the GSNO loops alone (p = 0.02). This indicates that the higher levels of NO released during the 4 h period significantly increases the hemocompatibility of the device. As established in previous literature, higher levels of NO release from the surface are needed to prevent platelet activation and clot formation(34). Similar elevated NO flux from ECC loops has showed to preserve >80% of the platelet count compared to control loops(35). Moreover, Cu NPs combined with SNAP have shown to preserve >90% of the platelet count compared to control loops, while ECC loops with only Cu NPs or with only SNAP did not preserve platelet counts as well (~25% platelet consumption)(37). This can further be observed in the images of the thrombo-chambers post-procedure (**Figure 3.8)**. These serve as a visual representation of the clot formation that occurred in the control loops in comparison to the lack of occlusion in the Cu GSNO samples, which can be attributed to the higher-level nitric oxide release present in the Cu GSNO loops. The CarboSil control, Cu, and

GSNO loops all showed thrombus formation, while only one Cu GSNO loop showed any clot formation at the end of the 4 h procedure. The lack of thrombus formation found only with Cu GSNO samples suggests that higher levels of nitric oxide release are necessary to create a surface environment that reduces thrombus formation and continues to preserve platelet count. Similar findings have been made with on NO donors at similar higher levels of NO release are better able to reduce clot formation and prevent platelet count reduction, which improves the hemocompatibility of the device(37, 41). Overall, Cu GSNO loops showed the greatest percentage of platelet count and least amount of thrombus formation, indicating this combination creates the greatest hemocompatibility of the tested devices.

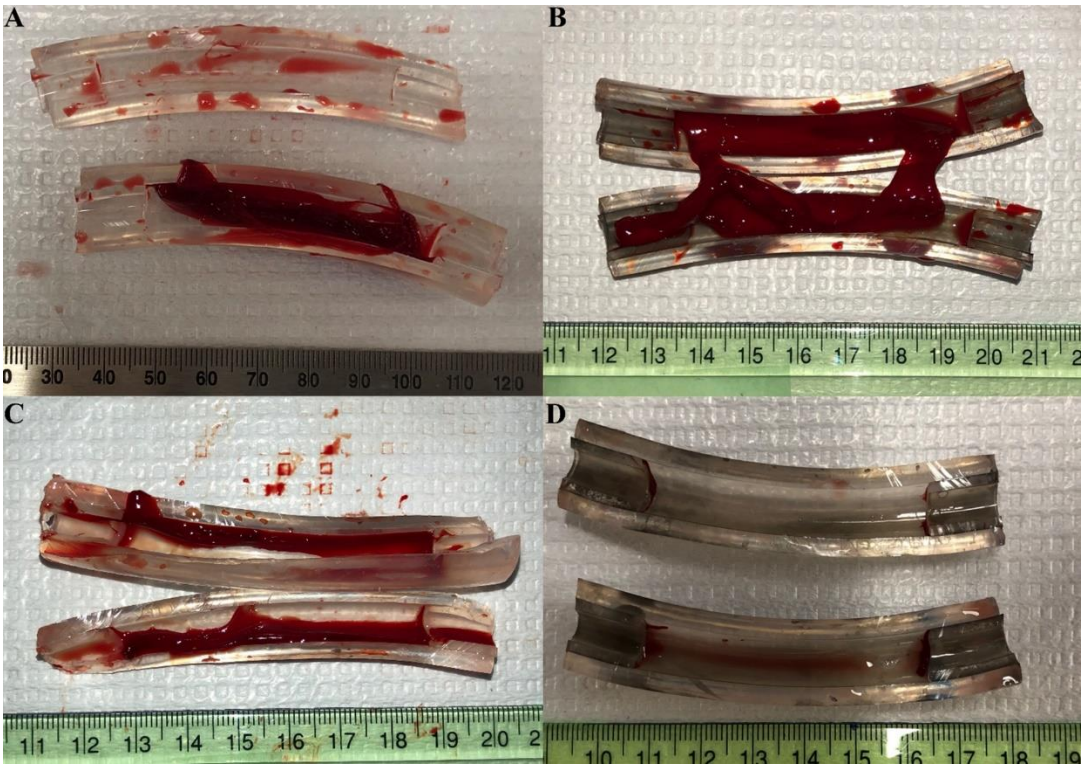

Figure 3.8 – Representative photos of thrombogenicity chambers after 4 h ECC. (A) CarboSil control, (B) Cu, and (C) GSNO showed more clot formation when compared to (D) Cu GSNO.

3.5 Conclusion

In this work, Cu NPs were layered with the NO donor GSNO to create a catalyzed NO-releasing medical grade polymer to improve the hemocompatibility and reduce chances of infection of medical devices. The addition of Cu NPs and GSNO had no significantly negative effect on the surface morphology of the coated ECC loops in comparison to the bare PVC and CarboSil controls. Both the GSNO (indicated by the sulfur present in the GSNO molecule) and Cu NPs were deposited evenly throughout their respective layers and the weight percentage of Cu NPs found (~2.5 wt. %) was close to the actual amount of Cu NPs originally used (3 wt. %). The incorporation of Cu NPs increased the NO release from a maximum of $2.3 \pm 0.2 \times 10^{-10}$ mol cm^{-2} min^{-1} to a maximum of $10.3 \pm 0.8 \times 10^{-10}$ mol cm^{-2} min^{-1} during the 4 h application period, demonstrating a NO flux that is approximately five times higher than the GSNO loop. After exposing each sample type to a Gram-positive (*S. aureus*) and Gram-negative (*P. aeruginosa*) bacterial strain, the Cu GSNO showed the greatest reduction in viable bacterial adhesion, reducing the count of viable bacteria on the polymer surface by 99.94% ± 0.03% and 96.7% ± 0.5% for *S. aureus* and *P. aeruginosa*, respectively (up to 3-log reduction). The both the individual controls as well as the combination of Cu NPs and GSNO were found to be noncytotoxic towards mammalian cells as demonstrated by the CCK-8 assay performed on 3T3 mouse fibroblast. The Cu GSNO combination was able to significantly reduce overall thrombus mass and decrease platelet consumption (10.7 ± 8.5% of baseline) after 4 h exposure to blood in a rabbit ECC model. Overall, we found that the Cu GSNO combination can increase the nitric oxide released from a polymer for relevant window of time for extracorporeal blood circulation periods, resulting in a reduction in viable adhered bacteria and platelet adhesion, which suggests that this combination can improve biocompatibility while preventing infection for medical applications.

3.6 References

1. Brisbois EJ, Major TC, Goudie MJ, Bartlett RH, Meyerhoff ME, Handa H. Improved hemocompatibility of silicone rubber extracorporeal tubing via solvent swelling-impregnation of S-nitroso-N-acetylpenicillamine (SNAP) and evaluation in rabbit thrombogenicity model. Acta Biomater. 2016;37:111-9.

2. Major TC, Brisbois EJ, Jones AM, Zanetti ME, Annich GM, Bartlett RH, et al. The effect of a polyurethane coating incorporating both a thrombin inhibitor and nitric oxide on hemocompatibility in extracorporeal circulation. Biomaterials. 2014;35(26):7271-85.

3. Kessler M, Moureau F, Nguyen P. Anticoagulation in Chronic Hemodialysis: Progress Toward an Optimal Approach. Semin Dial. 2015;28(5):474-89.

4. Dalton HJ, Garcia-Filion P, Holubkov R, Moler FW, Shanley T, Heidemann S, et al. Association of bleeding and thrombosis with outcome in extracorporeal life support. Pediatr Crit Care Med. 2015;16(2):167-74.

5. Annich GM. Extracorporeal life support: the precarious balance of hemostasis. J Thromb Haemost. 2015;13 Suppl 1:S336-42.

6. Guggenbichler JP, Assadian O, Boeswald M, Kramer A. Incidence and clinical implication of nosocomial infections associated with implantable biomaterials - catheters, ventilator-associated pneumonia, urinary tract infections. GMS Krankenhhyg Interdiszip. 2011;6(1):Doc18.

7. Hugonnet S, Sax H, Eggimann P, Chevrolet JC, Pittet D. Nosocomial bloodstream infection and clinical sepsis. Emerg Infect Dis. 2004;10(1):76-81.

8. Barriere SL. Clinical, economic and societal impact of antibiotic resistance. Expert Opinion on Pharmacotherapy. 2015;16(2):151-3.

9. Bull T, Corley A, Smyth DJ, McMillan DJ, Dunster KR, Fraser JF. Extracorporeal membrane oxygenation line-associated complications: in vitro testing of cyanoacrylate tissue adhesive and securement devices to prevent infection and dislodgement. Intens Care Med Exp. 2018;6(1):6.

10. Harrison-Balestra C, Cazzaniga AL, Davis SC, Mertz PM. A wound-isolated Pseudomonas aeruginosa grows a biofilm in vitro within 10 hours and is visualized by light microscopy. Dermatol Surg. 2003;29(6):631-5.

11. Shanks RM, Donegan NP, Graber ML, Buckingham SE, Zegans ME, Cheung AL, et al. Heparin stimulates Staphylococcus aureus biofilm formation. Infect Immun. 2005;73(8):4596-606.

12. Thomas G, Hraiech S, Cassir N, Lehingue S, Rambaud R, Wiramus S, et al. Venovenous extracorporeal membrane oxygenation devices-related colonisations and infections. Ann Intensive Care. 2017;7(1):111.

13. Seabra AB, De Oliveira MG. Poly(vinyl alcohol) and poly(vinyl pyrrolidone) blended films for local nitric oxide release. Biomaterials. 2004;25(17):3773-82.

14. Zhao Y, Vanhoutte PM, Leung SW. Vascular nitric oxide: Beyond eNOS. J Pharmacol Sci. 2015;129(2):83-94.

15. Hou YC, Janczuk A, Wang PG. Current trends in the development of nitric oxide donors. Curr Pharm Des. 1999;5(6):417-41.

16. Brisbois EJ, Davis RP, Jones AM, Major TC, Bartlett RH, Meyerhoff ME, et al. Reduction in Thrombosis and Bacterial Adhesion with 7 Day Implantation of S-Nitroso-N-acetylpenicillamine (SNAP)-Doped Elast-eon E2As Catheters in Sheep. J Mater Chem B. 2015;3(8):1639-45.

17. Charville GW, Hetrick EM, Geer CB, Schoenfisch MH. Reduced bacterial adhesion to fibrinogen-coated substrates via nitric oxide release. Biomaterials. 2008;29(30):4039-44.

18. Friedman A, Blecher K, Sanchez D, Tuckman-Vernon C, Gialanella P, Friedman JM, et al. Susceptibility of Gram-positive and -negative bacteria to novel nitric oxide-releasing nanoparticle technology. Virulence. 2011;2(3):217-21.

19. Hibbs JB, Jr., Taintor RR, Vavrin Z, Rachlin EM. Nitric oxide: a cytotoxic activated macrophage effector molecule. Biochem Biophys Res Commun. 1988;157(1):87-94.

20. Roveda Júnior AC, Franco DW. Nitric oxide releasing-dendrimers: an overview. Brazilian Journal of Pharmaceutical Sciences. 2013;49:1-14.

21. Jones A, Pant J, Lee E, Goudie MJ, Gruzd A, Mansfield J, et al. Nitric oxide-releasing antibacterial albumin plastic for biomedical applications. J Biomed Mater Res A. 2018;106(6):1535-42.

22. Seabra AB, Fitzpatrick A, Paul J, De Oliveira MG, Weller R. Topically applied S-nitrosothiol-containing hydrogels as experimental and pharmacological nitric oxide donors in human skin. Br J Dermatol. 2004;151(5):977-83.

23. Frost MC, Reynolds MM, Meyerhoff ME. Polymers incorporating nitric oxide releasing/generating substances for improved biocompatibility of blood-contacting medical devices. Biomaterials. 2005;26(14):1685-93.

24. Kim J, Saravanakumar G, Choi HW, Park D, Kim WJ. A platform for nitric oxide delivery. Journal of Materials Chemistry B. 2014;2(4):341-56.

25. de Oliveira MG, Shishido SM, Seabra AB, Morgon NH. Thermal Stability of Primary S-Nitrosothiols: Roles of Autocatalysis and Structural Effects on the Rate of Nitric Oxide Release. The Journal of Physical Chemistry A. 2002;106(38):8963-70.

26. Broniowska KA, Diers AR, Hogg N. S-nitrosoglutathione. Biochim Biophys Acta. 2013;1830(5):3173-81.

27. Williams DLH. The chemistry of S-nitrosothiols. Accounts Chem Res. 1999;32(10):869-76.

28. Heikal L, Martin GP, Dailey LA. Characterisation of the decomposition behaviour of S-nitrosoglutathione and a new class of analogues: S-Nitrosophytochelatins. Nitric Oxide. 2009;20(3):157-65.

29. Mcaninly J, Williams DLH, Askew SC, Butler AR, Russell C. Metal-Ion Catalysis in Nitrosothiol (Rsno) Decomposition. J Chem Soc Chem Comm. 1993(23):1758-9.

30. McCarthy CW, Guillory RJ, 2nd, Goldman J, Frost MC. Transition-Metal-Mediated Release of Nitric Oxide (NO) from S-Nitroso-N-acetyl-d-penicillamine (SNAP): Potential Applications for Endogenous Release of NO at the Surface of Stents Via Corrosion Products. ACS Appl Mater Interfaces. 2016;8(16):10128-35.

31. AshaRani PV, Mun GLK, Hande MP, Valiyaveettil S. Cytotoxicity and Genotoxicity of Silver Nanoparticles in Human Cells. Acs Nano. 2009;3(2):279-90.

32. Ostaszewska T, Sliwinski J, Kamaszewski M, Sysa P, Chojnacki M. Cytotoxicity of silver and copper nanoparticles on rainbow trout (Oncorhynchus mykiss) hepatocytes. Environ Sci Pollut Res Int. 2018;25(1):908-15.

33. Brisbois EJ, Handa H, Major TC, Bartlett RH, Meyerhoff ME. Long-term nitric oxide release and elevated temperature stability with S-nitroso-N-acetylpenicillamine (SNAP)-doped Elast-eon E2As polymer. Biomaterials. 2013;34(28):6957-66.

34. Handa H, Major TC, Brisbois EJ, Amoako KA, Meyerhoff ME, Bartlett RH. Hemocompatibility Comparison of Biomedical Grade Polymers Using Rabbit Thrombogenicity Model for Preparing Nonthrombogenic Nitric Oxide Releasing Surfaces. J Mater Chem B. 2014;2(8):1059-67.

35. Major TC, Brant DO, Reynolds MM, Bartlett RH, Meyerhoff ME, Handa H, et al. The attenuation of platelet and monocyte activation in a rabbit model of extracorporeal circulation by a nitric oxide releasing polymer. Biomaterials. 2010;31(10):2736-45.

36. Pant J, Goudie MJ, Hopkins SP, Brisbois EJ, Handa H. Tunable Nitric Oxide Release from S-Nitroso-N-acetylpenicillamine via Catalytic Copper Nanoparticles for Biomedical Applications. ACS Appl Mater Interfaces. 2017;9(18):15254-64.

37. Major TC, Brant DO, Burney CP, Amoako KA, Annich GM, Meyerhoff ME, et al. The hemocompatibility of a nitric oxide generating polymer that catalyzes S-nitrosothiol decomposition in an extracorporeal circulation model. Biomaterials. 2011;32(26):5957-69.

38. Wo Y, Li Z, Brisbois EJ, Colletta A, Wu J, Major TC, et al. Origin of Long-Term Storage Stability and Nitric Oxide Release Behavior of CarboSil Polymer Doped with S-Nitroso-N-acetyl-D-penicillamine. ACS Appl Mater Interfaces. 2015;7(40):22218-27.

39. Goudie MJ, Brainard BM, Schmiedt CW, Handa H. Characterization and in vivo performance of nitric oxide-releasing extracorporeal circuits in a feline model of thrombogenicity. J Biomed Mater Res A. 2017;105(2):539-46.

40. Vanhoe H, Vandecasteele C, Versieck J, Dams R. Determination of iron, cobalt, copper, zinc, rubidium, molybdenum, and cesium in human serum by inductively coupled plasma mass spectrometry. Anal Chem. 1989;61(17):1851-7.

41. Hopkins SP, Pant J, Goudie MJ, Schmiedt C, Handa H. Achieving Long-Term Biocompatible Silicone via Covalently Immobilized S-Nitroso- N-acetylpenicillamine (SNAP) That Exhibits 4 Months of Sustained Nitric Oxide Release. ACS Appl Mater Interfaces. 2018;10(32):27316-25.

42. Goudie MJ, Singha P, Hopkins SP, Brisbois EJ, Handa H. Active release of an antimicrobial and antiplatelet agent from a non-fouling surface modification. ACS Appl Mater Interfaces. 2019;11(4):4523-30.

43. Torres N, Oh S, Appleford M, Dean DD, Jorgensen JH, Ong JL, et al. Stability of antibacterial self-assembled monolayers on hydroxyapatite. Acta Biomater. 2010;6(8):3242-55.

44. Goudie MJ, Pant J, Handa H. Liquid-infused nitric oxide-releasing (LINORel) silicone for decreased fouling, thrombosis, and infection of medical devices. Sci Rep. 2017;7(1):13623.

45. Singha P, Pant J, Goudie MJ, Workman CD, Handa H. Enhanced antibacterial efficacy of nitric oxide releasing thermoplastic polyurethanes with antifouling hydrophilic topcoats. Biomater Sci. 2017;5(7):1246-55.

46. Wo Y, Brisbois EJ, Wu J, Li Z, Major TC, Mohammed A, et al. Reduction of Thrombosis and Bacterial Infection via Controlled Nitric Oxide (NO) Release from S-Nitroso-N-acetylpenicillamine (SNAP) Impregnated CarboSil Intravascular Catheters. ACS Biomater Sci Eng. 2017;3(3):349-59.

47. Gierke GE, Nielsen M, Frost MC. S-Nitroso-N-acetyl-D-penicillamine covalently linked to polydimethylsiloxane (SNAP-PDMS) for use as a controlled photoinitiated nitric oxide release polymer. Sci Technol Adv Mater. 2011;12(5):055007.

48. Pant J, Gao J, Goudie MJ, Hopkins SP, Locklin J, Handa H. A multi-defense strategy: Enhancing bactericidal activity of a medical grade polymer with a nitric oxide donor and surface-immobilized quaternary ammonium compound. Acta Biomater. 2017;58:421-31.

49. Goudie MJ, Brisbois EJ, Pant J, Thompson A, Potkay JA, Handa H. Characterization of an S-nitroso-N-acetylpenicillamine-based nitric oxide releasing polymer from a translational perspective. Int J Polym Mater. 2016;65(15):769-78.

50. Liu Q, Singha P, Handa H, Locklin J. Covalent Grafting of Antifouling Phosphorylcholine-Based Copolymers with Antimicrobial Nitric Oxide Releasing Polymers to Enhance Infection-Resistant Properties of Medical Device Coatings. Langmuir. 2017;33(45):13105-13.

51. Harding JL, Reynolds MM. Metal organic frameworks as nitric oxide catalysts. J Am Chem Soc. 2012;134(7):3330-3.

52. Burg A, Cohen H, Meyerstein D. The reaction mechanism of nitrosothiols with copper(I). Journal of Biological Inorganic Chemistry. 2000;5(2):213-7.

53. Yuan Y, Hays MP, Hardwidge PR, Kim J. Surface characteristics influencing bacterial adhesion to polymeric substrates. Rsc Advances. 2017;7(23):14254-61.

54. Brisbois EJ, Major TC, Goudie MJ, Meyerhoff ME, Bartlett RH, Handa H. Attenuation of thrombosis and bacterial infection using dual function nitric oxide releasing central venous catheters in a 9day rabbit model. Acta Biomater. 2016;44:304-12.

55. Xu LC, Wo Y, Meyerhoff ME, Siedlecki CA. Inhibition of bacterial adhesion and biofilm formation by dual functional textured and nitric oxide releasing surfaces. Acta Biomater. 2017;51:53-65.

56. Rtimi S, Giannakis S, Pulgarin C. Self-Sterilizing Sputtered Films for Applications in Hospital Facilities. Molecules. 2017;22(7):1074.

57. Wakshlak RB, Pedahzur R, Avnir D. Antibacterial activity of silver-killed bacteria: the "zombies" effect. Sci Rep. 2015;5:9555.

58. Grommersch BM, Pant J, Hopkins SP, Goudie MJ, Handa H. Biotemplated Synthesis and Characterization of Mesoporous Nitric Oxide-Releasing Diatomaceous Earth Silica Particles. ACS Appl Mater Interfaces. 2018;10(3):2291-301.

59. Pant J, Goudie MJ, Chaji SM, Johnson BW, Handa H. Nitric oxide releasing vascular catheters for eradicating bacterial infection. J Biomed Mater Res B Appl Biomater. 2017;106(8):2849-57.

CHAPTER 4:

STABLE ANTIFOULING NITRIC OXIDE-RELEASING PLATFORM DESIGNED FOR LONG-TERM INDWELLING MEDICAL DEVICE APPLICATIONS[4]

[4] Douglass M*, Hopkins S*, Devine R, Garren M, and Handa H. Stable Liquid-Infused Nitric Oxide-Releasing Platform Designed for Long-Term Indwelling Medical Device Applications. To be submitted to *ACS Applied Materials & Interfaces*. (* indicates that these authors contributed equally).

4.1. Abstract

Currently available indwelling medical devices frequently fail due to infection, biofouling, and device-induced thrombosis, leading to catastrophic side effects including loss of device function, additional surgery, and increased morbidity and mortality. To prevent these events from occurring, we developed a multifunctional antimicrobial and antithrombotic polymeric platform using sustained nitric oxide (NO)-releasing chemistry via the covalent attachment of a common synthetic NO donor, S-nitroso-N-acetylpenicillamine (SNAP), onto medical-grade polydimethylsiloxane (PDMS) with an antifouling liquid-infused interface. As a result, optimized surfaces exhibited consistent, elevated NO release profiles (> 0.5 x 10^{-10} mol cm^{-2} min^{-1}) for 30 d with virtually no NO donor leaching. Immersed materials also maintained low sliding angle measurements (~20°) for 7 d. The synthesized materials maintained potent antimicrobial efficacies after 24 h, 7 d, 14 d, and 28 d against both Gram-positive methicillin-resistant *Staphylococcus aureus* (MRSA) (92.6 ± 1.8% reduction after 28 d) and Gram-negative *Pseudomonas aeruginosa* (*P. aeruginosa*) (98.2 ± 0.3% reduction after 28 d) compared to control materials. The resulting material also exhibited improved *in vitro* hemocompatibility, reducing fibrinogen adsorption by 30.3 ± 10.2% and platelet adhesion by 66.5 ± 11.2% compared to control materials. Finally, *in vitro* cytotoxicity measured against human umbilical vein endothelial cells (HUVEC) and human fibroblasts showed that the synthesized materials did not result in any cytotoxic activity (> 90% viability). In all, the modified medical-grade PDMS exhibiting sustained NO-releasing properties with a liquid-infused interface provides a promising solution for medical device-associated infection and thrombosis.

Key Words: Antimicrobial, medical device, antifouling, nitric oxide

4.2. Introduction

Long-term, indwelling medical devices such as vascular catheters, chest ports, stents, and pacemakers are vital for the diagnosis, mitigation, and treatment of a substantial number of diseases and ailments. However, currently available devices frequently fail due to catastrophic events commonly associated with medical device use including infection, biofouling, and device-induced thrombosis. Medical device-related infections represent a substantial number of nosocomial infections – in critically ill patients, vascular catheter use accounts for 87% of bloodstream infections, urinary catheter use accounts for 95% of urinary tract infections, and mechanical ventilation accounts for 86% of pneumonia infections(1). Vascular access used for the administration of intravenous therapies, antibiotic treatments, and blood transfusions constitutes a breach in the barrier between the outside environment and the bloodstream, further increasing the risk of local and systemic infections including catheter-related bloodstream infections (CRBSIs), septic thrombophlebitis, endocarditis, and other metastatic infections(2). The current standard for controlling infection is antibiotic treatment, but due to the emergence of antibiotic resistance coupled with the persistent presence of microbial biofilms, which readily form on foreign surfaces and exhibit defensive mechanisms including poor antibiotic penetration, limited nutrient uptake, and adaptive stress responses,(3) alternative means to prevent and combat infection are needed.

Beyond the issues of infection, when medical devices are exposed to blood, proteins rapidly adsorb and a complex sequence of biochemical reactions is triggered, ultimately resulting in thrombus formation. Clots formed on the surface can totally occlude the device, obstruct device function, and can break off and move further downstream, potentially causing pulmonary embolism or myocardial infarction(4). Venous thromboembolism is one of the most prevalent complications associated with indwelling vascular access devices, reportedly occurring in 11-25%

of critically ill patients with central venous catheters(5). Such complications can result in increased medical costs, extended hospitalization, or increased morbidity(6). To maintain device patency, clinicians currently administer anticoagulation therapies to prevent thrombosis, but systemic anticoagulation requires a careful balance between over- and under-administration to prevent clotting while avoiding hemorrhaging(7). For indwelling vascular access devices, heparin-based lock solutions therapies are regularly used to prevent device occlusion but can lead to complications such as low platelet counts, internal bleeding, and thrombocytopenia(8, 9). Systemic anticoagulation also fails to prevent the adsorption of plasma proteins such as fibrinogen, a central player in the formation of dense fibrin networks and an anchor exploited by bacteria to increase adhesion and biofilm development(10-12).

To reduce the frequency of medical device-associated infections, researchers have begun to develop different antimicrobial surface modifications (eg., antibiotic-releasing surfaces, silver-based coatings) to counteract bacterial colonization(13, 14). However, the development of antibiotic resistance remains a significant limiting factor of antibiotic-eluting surfaces(14). Moreover, commercial catheters impregnated with antibiotics and antiseptic agents (eg., silver-coated) have shown mixed clinical efficacy against infection(15-19). In fact, silver nanoparticle-impregnated central venous catheters demonstrated no change in the rate of acquired CRBSIs when compared to controls(20). In addition, silver-eluting central venous catheters invoke a pro-thrombotic response as a result of rapid thrombin generation, restricting its applications for blood-contacting medical devices(21).

To prevent surface-induced thrombosis, hemocompatible surface modifications aim to disrupt the coagulation cascade by preventing protein adsorption, impeding platelet adhesion and activation, or inhibiting thrombin-mediated reactions. Antithrombotic surface modifications can

be broken down into two categories based on the method of increasing hemocompatibility: (1) passive surface strategies, which minimize contact with blood components, and (2) active surface strategies, which store and release antithrombotic or fibrinolytic agents that directly interrupt coagulation(22). However, due to the complexity of the physiological components and mechanisms that lead to medical device-induced thrombosis, a long-term antithrombotic solution for medical devices will likely require a combination of strategies(23). Routine failure of blood-contacting devices can be attributed to the material's inability to replicate the multifunctional antithrombotic functionality of the surrounding vasculature(24). Despite tremendous efforts that have been made, a single platform that exhibits comprehensive hemocompatibility has yet to be fabricated(25).

To reduce the threat of infection and thrombosis related to medical device surfaces, more recent efforts have been focused on directly mimicking antimicrobial, antifouling, or antithrombotic materials found in nature(26-28). In response, nitric oxide (NO)-releasing surfaces have been fabricated to improve both the hemocompatible and antimicrobial capabilities of medical device surfaces(27, 29-35). In the body, NO is a gaseous free radical molecule responsible for numerous biological functions including regulating platelet adhesion and aggregation, immune response, inflammation, cell proliferation, and neurotransmission(36, 37). Activated immune cells produce potent, high doses of NO able to diffuse across bacterial cell membranes and induce nitrosative and oxidative damage, resulting in DNA alteration, enzyme inhibition, and lipid peroxidation(38). Moreover, NO is continuously produced by the endothelium, inhibiting platelet aggregation and adhesion(39). Different NO donor molecules including *S*-nitrosothiols (RSNOs)(31, 32, 40) and *N*-diazeniumdiolates(41, 42) have been incorporated into polymeric materials to improve its antibacterial efficacy, biocompatibility, and blood compatibility. RSNOs

including *S*-nitroso-*N*-acetyl penicillamine (SNAP) (33, 43), *S*-nitrosoglutathione (32, 44), and *S*-nitrosocysteine (45, 46) have been extensively utilized for the fabrication of NO-releasing materials due to their excellent biocompatibility and highly tunable NO release achieved through the cleavage of the S-NO bond mediated via thermal degradation, light catalysis, or metal ion catalysis(47). However, to date, the majority of NO-releasing materials exhibit a high initial burst release of NO, quickly draining the NO reservoir stored in the material and limiting the long-term duration of NO release. To extend the stability and duration of NO release, the NO donor SNAP has previously been covalently attached to poly(dimethylsiloxane) (PDMS), resulting in > 4 months of NO release with virtually no SNAP leaching(48). Therefore, this NO-releasing platform that exhibits durable NO release characteristics can be advantageous for preventing thrombosis and infection for long-term, indwelling medical devices including vascular catheters, chest ports, stents, and pacemakers.

Despite their promising antithrombotic and antibacterial effects, previous NO-releasing platforms have been challenged with increased protein adsorption(49). Inspired by the protective mucus layer in the gastrointestinal tract and low friction surface of the *Nepenthes* pitcher plants, researchers have recently designed a slippery, liquid-infused modification that uses an immobilized liquid layer to minimize biofouling(50, 51). Unlike superhydrophobic surfaces prone to physical damage and instability under dynamic conditions, liquid-infused surfaces exhibit an antifouling compressible, self-repairing liquid interface(52). A recently popularized method of achieving an antifouling interface is through the infusion of silicone oil into silicone-based polymer matrices, providing a simple, nontoxic means of achieving a stable liquid-infused omniphobic surface(27, 51). NO-releasing platforms have been combined with liquid-infused modifications to render the surface antifouling, bactericidal, and antithrombotic(27, 53, 54).

In this study, a multifunctional antifouling, antimicrobial, and antithrombotic platform was developed for long-term, indwelling medical device applications by combining sustained NO-releasing chemistry via covalent SNAP attachment with an antifouling, slippery interface (LI-NO-PDMS). The novel platform was thoroughly characterized through sliding angle measurements, swelling ratio analysis, NO release kinetics, and NO donor leaching measurements. Moreover, the antimicrobial efficacy of the synthesized material was extensively examined after 24 h, 7 d, 14 d, and 28 d against both Gram-positive methicillin-resistant *Staphylococcus aureus* (MRSA) and Gram-negative *Pseudomonas aeruginosa* (*P. aeruginosa*). *In vitro* platelet adhesion and protein adsorption measurements were conducted to determine improvements in hemocompatibility. Finally, *in vitro* cytotoxicity was measured against human umbilical vein endothelial cells (HUVEC) and human fibroblasts using a CCK-8 assay. The combination of covalently immobilized SNAP with a liquid-infused, slippery interface on a medical-grade PDMS substrate results in robust antimicrobial and hemocompatible characteristics capable of reducing the rate of infection and thrombosis for long-term indwelling medical device applications.

4.3. Materials & Methods

4.3.1. Materials

N-Acetyl-D-penicillamine (NAP), hydroxy-terminated PDMS (2550-3570 cSt), toluene, dibutyltin dilaurate, *tert*-butyl nitrite, pyridine, acetic anhydride, chloroform, anhydrous magnesium sulfate, (3-amino-propyl) trimethoxysilane, 1,4,8,11-tetraazacyclotetradecane (cyclam), hexanes, dodecylbenzene sulfonic acid, ethylenediaminetetraacetic acid (EDTA), and hydrochloric acid were purchased from Sigma-Aldrich. Silicone oil (50 cSt) was purchased from Fisher Scientific. Phosphate-buffered saline (PBS), pH 7.4, was used for *in vitro* experiments contained 138 mM NaCl, 2.7 mM KCl, and 10 mM sodium phosphate. MRSA (ATCC BA 41), *P.*

aeruginosa (ATCC 9027), and human fibroblasts (CRL 2522) were purchased from American Type Culture Collection. HUVEC were purchased from ThermoFisher Scientific (C0035C). LB broth was obtained from Fisher Bioreagents. LB Agar was purchased from Difco Laboratories. EGM-2 Endothelial Cell Growth Medium-2 BulletKit was purchased from Lonza. Trypsin-EDTA were purchased from Corning (Manassas, VA20109). The Cell Counting Kit-8 (CCK-8) was purchased from Sigma-Aldrich (St. Louis, MO 63103). Eagle's Minimum Essential Medium (EMEM) was purchased from American Type Culture Collection (USA). Fetal bovine serum was procured from VWR (USA). All other cell culture related supplies were purchased from Thermo Fisher Scientific.

4.3.2. Synthesis of LI-NO-PDMS and NO-PDMS Materials

4.3.2.1. Synthesis of NAP-Thiolactone

The synthesis of NAP-thiolactone was performed according to previously optimized procedures(48, 55). Briefly, 5 g of NAP was dissolved in 10 mL of pyridine in a round-bottom flask and chilled on ice for 1 h. Separately, acetic anhydride (10 mL) was combined with pyridine (10 mL) and also chilled on ice for 1 h. The solutions were then stirred together for 24 h under argon before being rotary evaporated at 60 °C until all of the pyridine and a majority of the acetic anhydride was evaporated. Chloroform (20 mL) was subsequently added to remaining solution and washed with 1 M HCl. The resulting organic layer was dried over anhydrous magnesium sulfate, and the chloroform was evaporated using a desiccator maintained at room temperature. The resulting precipitate was reconstituted in hexanes and kept covered at -20°C overnight before being filtered, washed with additional hexanes, and left to dry under vacuum.

4.3.2.2. Fabrication of NO-PDMS

The fabrication of NO-PDMS was performed according to slightly modified, previously established procedures(48, 56). Briefly, hydroxy-terminated PDMS (1.6 g) was dissolved in toluene (8 mL) at room temperature. Separately, (3-aminopropyl)-trimethoxysilane (0.3 g, 1.67 mmol) and dibutyltin dilaurate (2.4 mg) were added to toluene (2 mL). The solutions were then stirred together for 24 h, and then NAP-thiolactone (300 mg, 1.73 mmol) was stirred into the solution for 48 h. *Tert*-butyl nitrite (500 µL), first chelated by vortexing with a 20 mM cyclam solution three times, was added to nitrosate the NAP-PDMS solution (3 mL), forming a green solution. Additionally, to increase nitrosation and crosslinking efficiency, dodecylbenzene sulfonic acid (0.5 wt% of polymer mass in solution) was added. To fabricate films, the NO-PDMS solution was added to rectangular Teflon molds and dried overnight in the dark at room temperature.

4.3.2.3. Liquid-Infusion of NO-PDMS (LI-NO-PDMS) Materials

Liquid-infusion of the fabricated NO-PDMS was achieved based on a previously established procedure(27). Briefly, NO-PDMS samples were immersed and swelled in silicone oil (50 cSt) kept in dark conditions at room temperature. To measure the swelling ratio of the silicone oil-swelled samples (LI-NO-PDMS) over time, the samples were massed before (M_0) and after infusion (M_1), and the following equation was used (**Equation 4.1**):

$$Swelling\ Ratio = \frac{M_1}{M_0}$$

Equation 4.1. Equation used to determine swelling ratio over time of NO-PDMS samples after immersion in silicone oil

4.3.3. Material Characterization

4.3.3.1. Sliding Angle Characterization

Prior to measurement, each sample was washed in DI water and dried with a nitrogen stream to ensure the surface was contaminant-free. Sliding angle measurements of 10 µL water droplets were quantified by slowly increasing the angle of LI-NO-PDMS and NO-PDMS samples mounted on a glass slide until water droplets on the surface of the samples slid off. Fifteen measurements on three different coated glass slides at separate positions for each sample type were taken. The sliding angles were determined with a digital protractor. The samples were stored at 37 °C in PBS in an incubator between measurements over 7 d.

4.3.3.2. SNAP Leaching Measurements

Cumulative SNAP leaching was measured at 37 °C in 4 mL of PBS. Leachates were collected from both LI-NO-PDMS and NO-PDMS samples over 48 h. Periodically, the optical density of the PBS was measured using a Thermo Scientific Genysis 10 S UV-Vis Spectrophotometer at 340 nm (absorbance maxima of the S-NO bond present in the SNAP molecule) to determine the concentration of SNAP that leached from the samples(44). Samples were stored in an incubator maintained at 37 °C between measurements. Blank PBS was used as a control, and a standard curve generated from known concentrations of SNAP-PBS solutions was used to determine the amount of SNAP present in the collected leachates.

4.3.4. NO Release Measurements

NO release kinetics of LI-NO-PDMS and NO-PDMS samples were measured using a Sievers Chemiluminescence NOA 280i over 30 d. Samples were submerged in PBS in an amber reaction vessel kept at 37 °C using a heated water bath. The PBS was supplemented with 100 mM of EDTA to prevent any unwanted NO catalysis from metallic ions present in the PBS. NO released from

the samples was purged from the PBS solution into a chemiluminescent detection chamber using a bubbler and nitrogen sweep gas (200 mL min^{-1}). The purged NO then reacts with ozone present in the chamber, resulting in an excited form of nitrogen dioxide NO^{2*}, which quickly emits a photon used to detect the amount of NO that was originally released from the sample. The average NO flux ($x10^{-10}$ mol cm^{-2} min^{-1}) of each sample type was determined using the NOA constant (mol ppb^{-1} s^{-1}) and surface area of the sample.

4.3.5. In vitro Antimicrobial Efficacy Measurements over 28 Days

The antimicrobial efficacies of the fabricated materials against Gram-positive and Gram-negative bacterial strains were analyzed after 24 h, 7 d, 14 d, and 28 d of exposure. To determine the initial antimicrobial effects (eg., immediately after insertion of a medical device), a 24 h bacterial adhesion assay was conducted. Isolated strains of MRSA and *P. aeruginosa* were separately inoculated in 15 mL of LB broth at 37 °C in an incubator shaker at 120 rpm for 15 h. After the inoculation period, the culture was centrifuged at 2500 rpm for 7.5 min, washed with sterile PBS, and centrifuged again at 2500 rpm. After centrifugation, the samples were resuspended in PBS and diluted to achieve a final concentration of ~10^8 CFU/mL. The samples (Control PDMS, NO-PDMS, LI-PDMS, and LI-NO-PDMS) were placed in the wells of a 24-well plate (n=4) and incubated with 1 mL of bacterial solution each for 24 h at 37 °C and 120 rpm.

After incubation, the viability of adhered bacterial was assessed by sonicating each sample post-incubation in 1 mL of sterile PBS at 25000 rpm for 60 s followed by vortexing for an additional 30 s. Prior to sonicating, each sample was gently washed with sterile PBS to remove any loosely adhered bacteria. The resulting bacteria-PBS solution was serially diluted, plated on LB agar plates, and kept at 37 °C for 24 h. Colony-forming units (CFUs) were measured to determine the number of viable adhered bacteria normalized to the surface area of each material.

The reduction in viability of adhered bacteria was calculated according to the following equation, Where C = CFU cm^{-2} (**Equation 4.2**):

$$\%\ \text{Reduction in adhered bacterial viability} = \frac{C_{control} - C_{test}}{C_{control}} \times 100$$

Equation 4.2. Formula used to determine the % reduction in adhered bacterial viability after 24 h, 7 d, 14 d, and 28 d of bacterial exposure

To determine the antimicrobial efficacy of the materials after extended periods of time (7, 14, and 28 d), CDC biofilm bioreactors (**Figure 4.1**) were used to model biofilm formation. To do so, MRSA and *P. aeruginosa* were inoculated in LB broth for 15 h broth at 37 °C in an incubator shaker at 120 rpm. The optical density was measured after, and the bacterial culture was diluted to achieve a final concentration of ~10^8 CFU/mL and used for incubation with the samples in the bioreactor. The samples were incubated for 1 h and stirred at 200 rpm. After 1 h, the samples were stirred at 120 rpm and supplied with additional nutrient medium (2 g L^{-1} LB broth) at a rate of ~1.6 mL min^{-1}. All bioreactors were equipped with an outlet that led to a waste container. The flow was maintained throughout the study until reaching pre-determined endpoints. At termination, the samples were removed and gently washed with sterile PBS. Each sample was sonicated in 1 mL of sterile PBS at 25000 rpm for 60 s followed by vortexing for an additional 30 s. The resulting solution was serially diluted, plated on LB agar plates, and kept at 37 °C for 24 h. Colony-forming units (CFUs) were measured to determine the viability of adhered bacteria normalized to the surface area of each material. The reduction in viability of adhered bacteria was calculated according to the equation above (**Equation 4.2**).

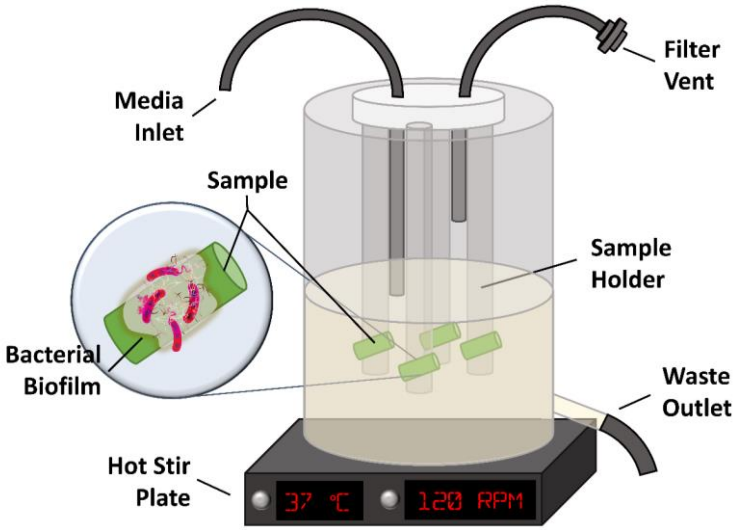

Figure 4.1. Schematic of the CDC bioreactor setup used to evaluate the antimicrobial activity of the materials over 28 d.

4.3.6. In vitro Fibrinogen Adsorption Assay

Levels of fibrinogen adsorption were quantified using FITC-labeled human fibrinogen. The labeled fibrinogen was diluted with unlabeled fibrinogen in PBS (pH 7.4) at a 1:10 ratio at a total fibrinogen concentration of 4 mg mL^{-1}. Samples were incubated in PBS at 37 °C for 30 minutes to allow surface equilibrium. The labeled-unlabeled fibrinogen solution was then added to the solution, resulting in a physiological concentration of 2 mg mL^{-1}. The samples were exposed to fibrinogen for 90 minutes at 37 °C. After 90 minutes, the samples were gently washed with PBS to remove any non-bound fibrinogen. Fibrinogen adsorbed onto the surface was then quantified in a plate reader (Biotek, Winooski, Vermont) by measuring the excitation/emission at 495 and 519 nm, and collected data was interpolated using a standard curve. Additionally, a microscope (AMG, Mill Creek, Washington) with a green fluorescence filter was used to image the labeled fibrinogen that adsorbed on the sample surfaces.

4.3.7. In Vitro Platelet Adhesion Assay

To determine the antiplatelet activity of the samples, an *in vitro* platelet adhesion assay was executed based on previous studies(32, 47). Briefly, whole porcine blood (3.8% sodium citrate) was centrifuged at 300 RCF for 13 min to separate and collect platelet-rich plasma (PRP), and again was centrifuged at 4000 RCF for 20 min to separate and collect platelet-poor plasma (PPP). The PRP was diluted with PPP to achieve a final platelet concentration of 2 x 10^8 platelets per mL. A $CaCl_2$ solution was added prior to material exposure at a final concentration of 2 mM. Samples were immersed in 3 mL of the final platelet solution and kept on a rocker for 2 h at 37 °C. The samples were then removed and washed with a buffered saline solution. Samples were then kept in 2 v/v% Triton-PBS (500 µL) for 30 min to lyse the adhered platelets. The resulting solutions were dispensed in a 96-well plate, and a Roche Cytotoxicity Detection Kit was prepared to determine the number of adhered platelets. The absorbance was measured at 492 nm using a BioTek Cytation 5 plate reader. Reductions in platelet adhesion were determined using the following formula (**Equation 4.3**), where P_c is the number of adhered platelets per cm^2 on control samples and P_t is the number of adhered platelets per cm^2 on test samples:

$$\%\ \text{Reduction in adhered platelets} = \frac{P_c - P_t}{P_c} \times 100$$

Equation 4.3. Formula used to measure the % reduction in adhered platelets per cm^2 compared to unmodified control samples.

4.3.8. In Vitro Whole Blood Exposure

Samples were exposed to porcine whole blood for 60 s and were subsequently gently rinsed with PBS and fixed for scanning electron microscopy (SEM, FEI Teneo). An accelerating voltage of 10.00 kV was used to analyze samples. Prior to SEM imaging, samples were sputter-coated with 10 nm thickness of gold-palladium.

4.3.9. In Vitro Cytotoxicity Measurements

4.3.9.1. Culture Method

Both HUVEC and human fibroblasts were revived from cryo stocks stored in liquid nitrogen vapor phase. Fibroblasts were cultured in EMEM supplemented with 10% FBS. HUVEC cells were cultured in EGM-2 supplemented with the following components from the EGM-2 BulletKit: FBS, hydrocortisone, hFGF-B, VEGF, R3-IGF-1, ascorbic acid, hEGF, GA-1000, and heparin. Both cell lines were incubated under 5% CO_2 humid atmosphere at 37 ºC. Cells were grown to 70-80% confluency then detached via 0.05% trypsin with 5 mM EDTA. Cell counting was done using an EVE^{TM} Cell Counter (NanoEnTek, Waltham, MA USA) with trypan blue cell staining. After cell counting, cells were resuspended and seeded into 96-well, tissue culture-treated polystyrene plates to achieve an initial seeding density of 5,000 cells/well. For each experiment, cells were grown for 24 h before exposure to film leachates.

4.3.9.2. Cytotoxicity Evaluation of Film Leachates

Circular coupons of 3/8” in diameter from each film type were prepared with normalization of surface area across each sample type. Coupons were sterilized via UV exposure for 15 min on each side. Each coupon was then individual submerged in 2 mL of culture media for the respective cell line in a sealed glass vial and incubated for 24 h at 37 ºC. A separate sample of control media without any film was also incubated at these conditions. After the 24 h incubation, media on seeded plates was aspirated off and replaced with an equal volume of media with leachates from the film samples. For each film coupon, a total of five wells were treated with film leachate. For each experimental run, a total of three coupons per film type were tested. Each plate included experimental controls including unseeded wells with media and seeded wells treated with incubated media without leachate.

Following 24 h incubation under media with film leachates, 10 µL of Cell Counting Kit-8 (CCK-8, Enzo Life Sciences) reagent was added to individual wells. The CCK-8 treated plate was then incubated for an additional 1 h. The CCK-8 assay kit contains WST-8, a tetrazolium salt that is readily reduced by cellular dehydrogenase activity to form a soluble yellow salt detectable at 450 nm. Reference readings at 650 nm were used to correct for noise. Relative viability of leachate-treated cells normalized against untreated cells was then calculated as follows (**Equation 4.4**):

$$\%\ Cell\ viability = \frac{Absorbance\ of\ the\ test\ samples - Blank}{Absorbance\ of\ the\ control\ samples - Blank} \times 100$$

Equation 4.4. Formula used to measure the relative viability of cells exposed to leachates collected from samples compared to cells without leachate exposure.

4.3.10. Statistical Analysis

All data is reported in mean ± SD. A Student's t-test was used to compare the significance between material types during material characterization, and p values < 0.05 were considered significant. For *in vitro* antimicrobial efficacies, cytotoxicity, protein adsorption, and platelet adhesion studies, which all compared the means of four groups, an ANOVA test with post-hoc Tukey was used to determine significance, and p values < 0.05 were considered significant.

4.4. Results & Discussion

4.4.1. Material Optimization & Characterization

4.4.1.1. Optimization of Silicone Oil Infusion of NO-PDMS

Antifouling liquid-infused surfaces have shown tremendous potential in reducing protein and bacterial fouling(27, 57, 58). In this work, a stable NO-releasing platform previously optimized(48) to exhibit potent antimicrobial and antiplatelet activity was modified to achieve a liquid-infused, antifouling interface via silicone oil infusion (**Figure 4.2**). To optimize the silicone oil infusion process of fabricated NO-PDMS, swelling ratios were measured over time to

maximize slippery surface characteristics (**Figure 4.3A**). Liquid infused silicone-based surfaces with a swelling ratio of approximately 2.0 have previously been shown to retain slippery surface characteristics capable of reducing bacterial adhesion and protein adsorption for an extended period of time (> 7 d)(27). Therefore, in this study, the swelling time of NO-PDMS materials to

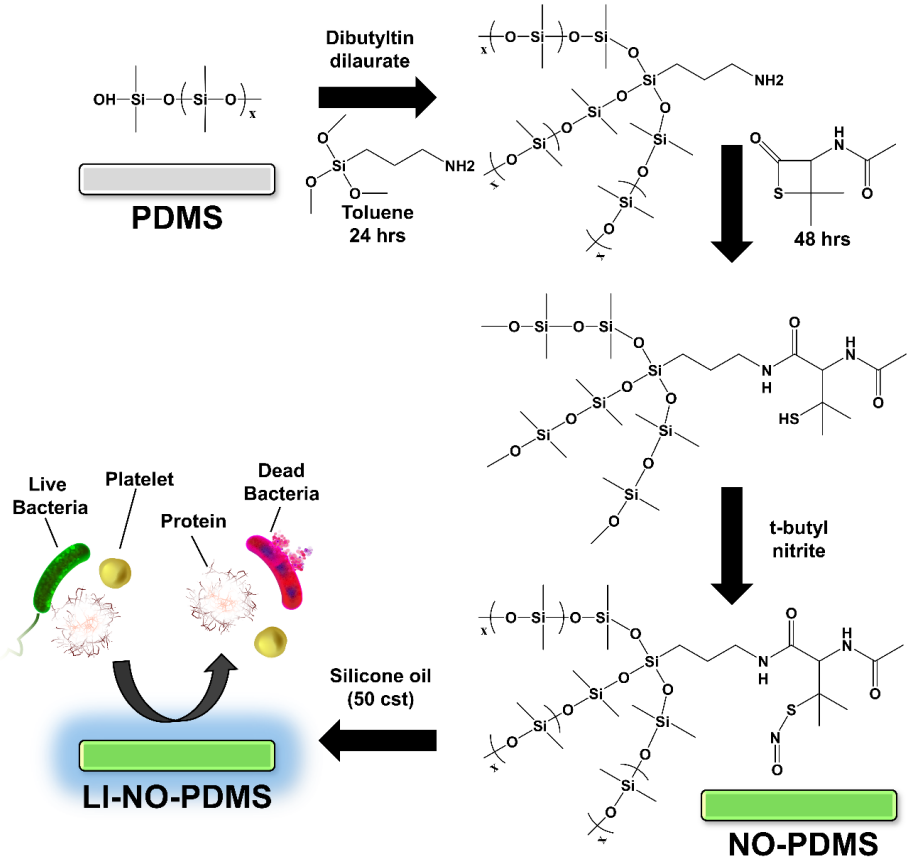

Figure 4.2. Fabrication of SNAP-immobilized, silicone oil-infused PDMS (LI-NO-PDMS). The NO donor SNAP was covalently bound to hydroxy-terminated PDMS prior to infusion of silicone oil (50 cst).

achieve a swelling ratio of 2.0 was determined. As shown in **Figure 4.3A**, after 8 h of swelling in a silicone oil solution, the materials had a swelling ratio of 2.0 ± 0.1. To ensure that the achieved slippery interface could be maintained under physiological conditions for an extended period, the sliding angles of LI-NO-PDMS and NO-PDMS incubated at 37 °C in PBS were compared over 7 d (**Figure 4.3B**). Over the 7-d period, LI-NO-PDMS maintained a sliding angle of 19-25. In comparison, NO-PDMS surfaces exhibited sliding angles > 90° throughout the same 7-d period. This demonstrates LI-NO's capability to retain a slippery interface even when stored in an aqueous

environment at a physiologically relevant temperature. It can be noted that there was a slight increase in sliding angle between the LI-NO surfaces prior to storage (7.1 ± 3.3°) and after 24 h of storage (19.1 ± 1.9°) ($p < 0.05$). This can be attributed to excess surface oil initially present at the interface that was not completely infused within the polymer. However, after 24 h of incubation, the sliding angle of LI-NO surfaces remained constant, and therefore shows great promise in retaining antifouling functionality desired to enhance hemocompatibility and antimicrobial properties for long-term medical device applications.

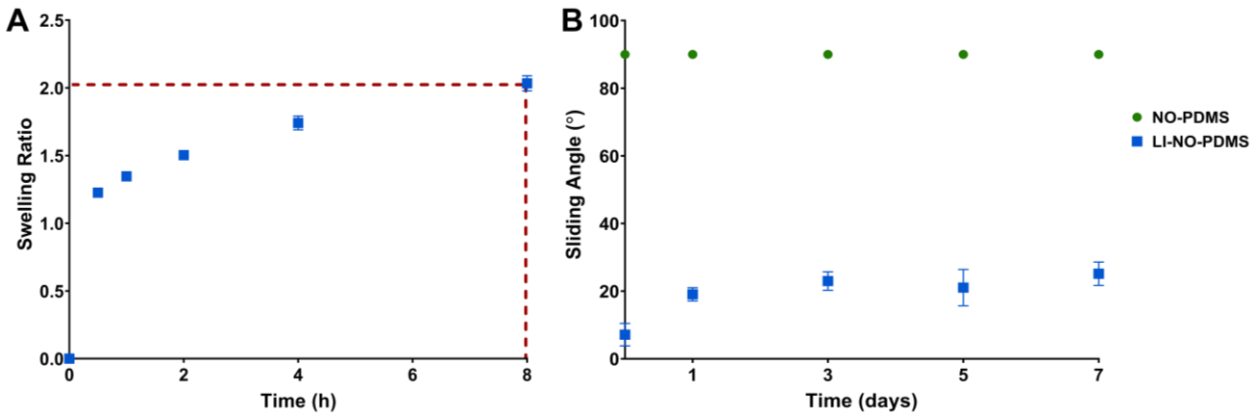

Figure 4.3. Liquid infusion optimization of NO-PDMS materials**.** (A) Swelling ratio of NO-PDMS materials within silicone oil. The optimized swelling time was found to be 8 h, which gave a swelling ratio of 2.0. (B) Sliding angle of NO-PDMS and LI-NO-PDMS surfaces when being kept in PBS at 37 °C over 7 d. LI-NO-PDMS shows significantly lower sliding angle measurements compared to NO-PDMS during the entire incubation period ($p < 0.001$).

4.4.1.2. NO Release Measurements & SNAP Leaching Measurements

NO is a key endogenous gaseous free radical that is well-documented to mediate cardiovascular hemostasis, immune response, and wound healing(37, 59-61). However, the concentration, rate, and longevity of NO release is key in determining the physiological effects NO will have on platelet function, bacterial viability, and surrounding tissue. Healthy endothelium produces NO at an estimated flux of 0.5-4 x 10^{-10} mol cm^{-2} min^{-1}(60). Therefore, in this work, developed NO-releasing materials were evaluated based on their ability to sustain long-term NO flux > 0.5 x 10^{-10} mol cm^{-2} min^{-1} to minimize potential thrombus formation and combat infection

for long-term, indwelling medical device interfaces. **Figure 4.4A** shows the NO release of both NO-PDMS and LI-NO-PDMS over the course of a 30-d period. The measured NO flux for both the LI-NO-PDMS and NO-PDMS remained > 0.5 x 10^{-10} mol cm^{-2} min^{-1} flux throughout the 30 d, demonstrating the stability of the material even after extended periods of time under physiological conditions. Previous reports indicate similar NO release kinetics for other SNAP-immobilized polymers(48, 62). Interestingly, the LI-NO-PDMS materials had a significantly ($p < 0.001$) higher NO release profile at initially (8.7 ± 0.2 x 10^{-10} mol cm^{-2} min^{-1}) and after 24 h (5.7 ± 0.2 x 10^{-10} mol cm^{-2} min^{-1}) compared to NO-PDMS materials both initially (5.5 ± 0.2 x 10^{-10} mol cm^{-2} min^{-1}) and after 24 h (4.1 ± 0.2 x 10^{-10} mol cm^{-2} min^{-1}). Because silicone oil acts as a spacer between polymer chains, increased ion interaction with the SNAP groups in the material could result in increased NO release. However, after 3 d, the differences between the samples were minimal. By the end of the study at 30 d, both LI-NO-PDMS and NO-PDMS materials exhibited an NO flux of approximately 0.5 x 10^{-10} mol cm^{-2} min^{-1} with no statistical significance between the two sample types (LI-NO-PDMS - 0.589 ± 0.002 x 10^{-10} mol cm^{-2} min^{-1}; NO-PDMS - 0.55 ± 0.08 x 10^{-10} mol cm^{-2} min^{-1}). Therefore, infusing NO-PDMS samples with silicone oil did not affect the long-term NO release characteristics.

The lifetime of materials incorporated with active agents can be severely impacted by leaching when submerged in an aqueous environment. Although some coating technologies have utilized antimicrobial (e.g. antibiotics, chlorine, silver ions) leaching as a means to combat bacterial infection, this method is significantly hindered by the longevity of antimicrobial release, quickly exhausting the available supply and rendering the material vulnerable to infection(63). For NO-releasing materials, uncontrolled high doses of NO as a result of NO donor leaching can lead to potential cytotoxicity towards mammalian cells(64, 65). Therefore, the SNAP leaching

kinetics of LI-NO-PDMS and NO-PDMS materials submerged in PBS (pH 7.4) at 37 °C were measured over 48 h to simulate physiological conditions, which historically has been when most leaching has occurred with NO donor-incorporated materials(47, 66). As shown in **Figure 4.4B**, both NO-PDMS and LI-NO-PDMS showed minimal leaching after 48 h and were not significantly different from each other ($P > 0.05$). After 48 h, NO-PDMS and LI-NO-PDMS only leached 0.0351 ± 0.0001 and 0.0339 ± 0.0009 mg of SNAP per mg of substrate, respectively, which is < 1% of the total SNAP originally attached. This can be attributed to the fact that the NO donor group is covalently attached to the backbone of the PDMS, virtually eliminating risk of SNAP leaching loss. Therefore, the lack of leachates confirms that the covalent attachment of SNAP results in a stable NO-releasing platform which minimizes potential cytotoxic events and delocalized NO release downstream from the material surface that can occur with significant NO donor leaching.

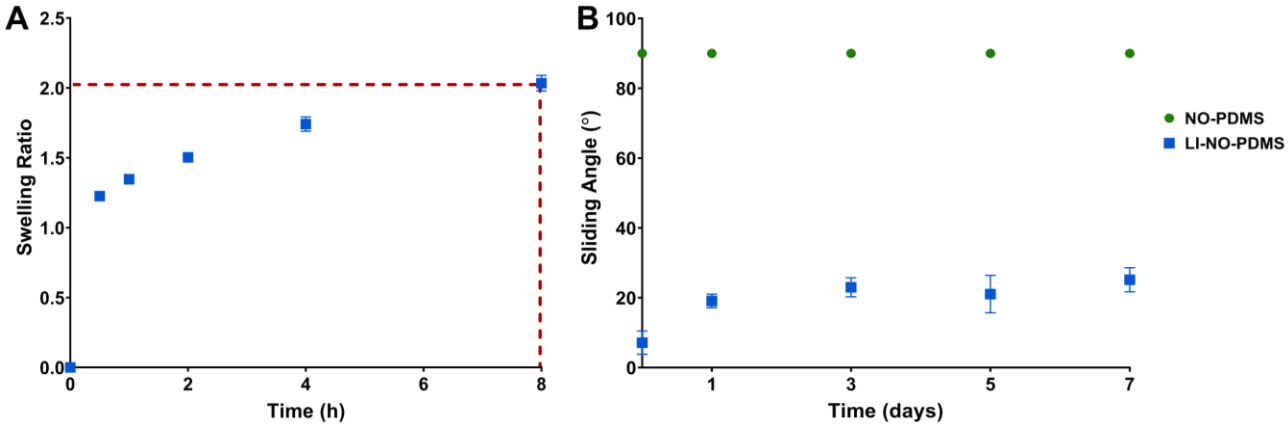

Figure 4.4. (A) NO release characteristics of LI-NO-PDMS and NO-PDMS materials when placed within PBS containing 0.01M EDTA at 37 °C over the course of 30 d. (B) SNAP leaching (mg of SNAP per mg of polymer) from both NO-PDMS and LI-NO-PDMS polymers in PBS at 37°C for 48 h. (*** = $p < 0.001$).

4.4.2. In Vitro Short-Term (24 h) and Long-Term (7-28 Days) Antimicrobial Efficacy

With the goal of reducing medical device-associated infections in mind, researchers have developed both active (bactericidal) and passive (antifouling) antimicrobial surface modifications

to combat bacterial adhesion and colonization(67). However, both passive and active surface strategies have major shortcomings that prevent successful antimicrobial behavior for long-term applications. While able to largely reduce the adhesion of microbes to surfaces, passive surface strategies fail to affect the viability of invading pathogens. Moreover, active surfaces store and release antimicrobial agents that dynamically attack invading bacterial pathogens but have little effect on surface fouling and commonly contain a limited reservoir of antimicrobial agents. However, a platform which contains dual passive-active antimicrobial surface strategies that exhibits both bactericidal and antiadhesive qualities can improve the long-term antimicrobial efficacy of the material. In this work, the NO donor SNAP was covalently attached to medically relevant PDMS to achieve stable NO-releasing properties (active strategy) followed by the liquid infusion of biocompatible silicone oil (passive strategy). The short-term (24 h) and long-term (7-28 d) antimicrobial efficacies were evaluated against Gram-positive MRSA (**Figure 4.5**) and Gram-negative *P. aeruginosa* (**Figure 4.6**).

To understand the initial antimicrobial activity of the fabricated materials, samples were exposed to common nosocomial infection-causing pathogens, MRSA and *P. aeruginosa*, for 24 h under physiological conditions (**Figure 4.5A and 4.6A**). Alone, LI-PDMS moderately reduced the number of viable MRSA and *P. aeruginosa* by 67.8 ± 13.7 and 56.9 ± 3.2%, suggesting that the liquid infusion resulted in decreased bacterial adhesion which has been shown previously by other groups(51, 68). Similarly, NO-PDMS also significantly reduced the number of viable adhered MRSA and *P. aeruginosa* by 98.3 ± 1.2 % and 85.1 ± 2.5%. This is expected as NO-releasing materials have historically demonstrated potent antimicrobial and biofilm-dispersing properties with limited resistance(69, 70). However, LI-NO-PDMS best reduced the viability of both adhered MRSA by 99.3 ± 0.3 % and *P. aeruginosa* by 94.8 ± 0.3% compared to control PDMS after 24 h

of exposure. This is in agreement with previous reports assessing the short-term (24 h) antimicrobial efficacy of liquid-infused, NO-releasing platforms, which also found that the combination of liquid-infused (passive) and NO-releasing (active) antimicrobial surface modifications best results in decreased adhered bacterial viability(54).

To date, two major shortcomings of NO-releasing materials has been high initial burst release coupled with NO donor leaching, quickly depleting the NO reservoir stored in the material and limiting the extent to which the material is able to combat infection for long-term applications. Similarly, superhydrophobic surfaces have been a popular means of achieving antifouling activity for biomedical applications, but due limitations in durability and instability of the trapped air pockets, have failed to improve the hemocompatibility of devices for long-term indwelling medical device applications(52, 71). In this work, to extend the antimicrobial surface properties for long-term applications, steady NO-release and robust antifouling technologies achieved through the covalent attachment of SNAP and liquid infusion of silicone oil were deployed. To determine the long-term antimicrobial efficacy, LI-NO-PDMS and control materials were challenged against MRSA and *P. aeruginosa* in CDC bioreactors for 7, 14, and 28 d. The CDC bioreactor allows for vigorous antimicrobial testing by mimicking shear environments seen within the vasculature, best illustrating the effectiveness of NO-releasing, liquid-infused surfaces in preventing bacterial colonization and biofilm formation. As shown in **Figure 4.5 and 4.6**, LI-NO-PDMS was significantly effective in reducing the number of viable adhered MRSA and *P. aeruginosa* at every measured timepoint for up to 28 d compared to untreated materials and exhibited greater reductions in the number of adhered, viable bacteria compared to LI-PDMS and NO-PDMS materials at every timepoint. **Table 4.1** lists the exact % reduction in viable adhered bacteria compared to control PDMS for LI, NO, and LI-NO-PDMS samples. Liquid-infused surfaces have previously resulted

in reduction in biofilm formation through decreased bacterial adhesive forces, decreasing bacterial colonization over time(72). However, liquid-infused surfaces do not affect bacterial viability, failing to provide potent antimicrobial efficacy against the initial onslaught of bacteria that can be introduced immediately. As stated previously, NO-releasing materials have previously demonstrated antimicrobial and biofilm-dispersing capabilities with limited development of resistance through multiple antimicrobial mechanisms including lipid oxidation, enzyme denaturation, and DNA deamination(38, 69, 70). However, in this study, the effectiveness of the NO-releasing surfaces slightly decreases over time. This can be attributed to a decrease in the NO release at later time points. Therefore, these results strongly suggest that the stable NO-releasing platform combined with a liquid-infused, slippery interface results in synergistic antimicrobial activity for not only short-term, but also long-term applications.

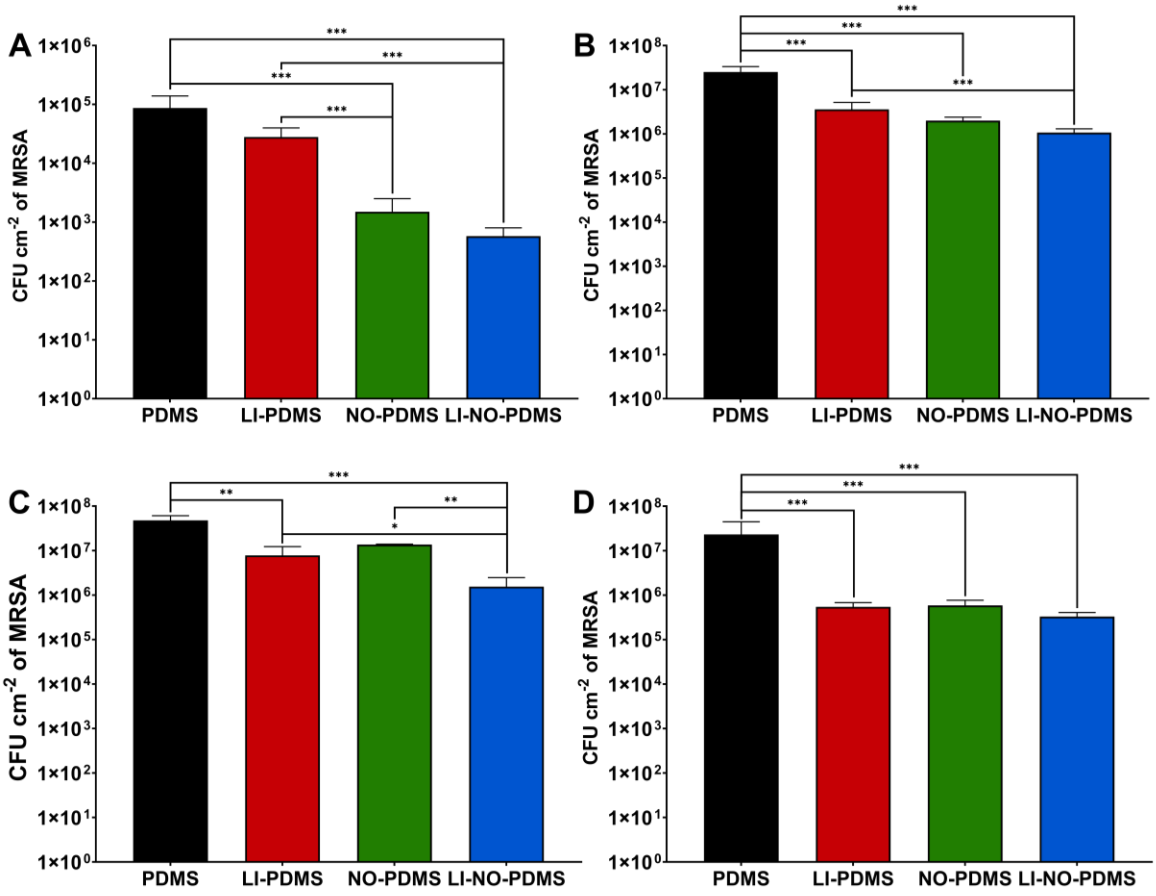

Figure 4.5. Antimicrobial results of LI-NO-PDMS surfaces against MRSA after 24 h (A), 7 d (B), 14 d (C), and 28 d (D) using a 24 h adhesion assay and CDC biofilm reactors (for studies >24 h). Significance in bacterial reduction between groups were indicated according to ANOVA statistical analysis (* = $p < 0.05$, ** = $p < 0.01$, *** = $p < 0.001$).

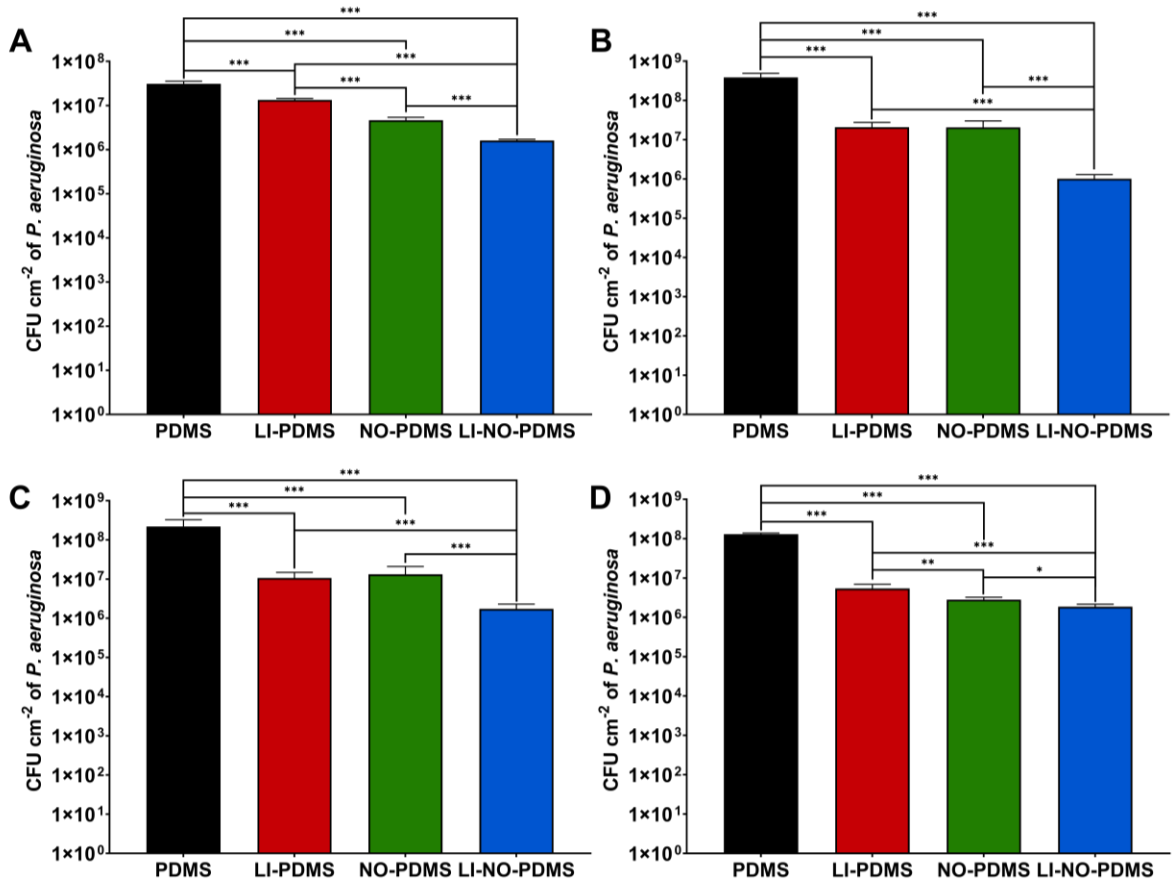

Figure 4.6. Antimicrobial results of LI-NO-PDMS surfaces against *P. aeruginosa* after 24 h (A), 7 d (B), 14 d (C), and 28 d (D) using a 24 h adhesion assay and CDC biofilm reactors (for studies >24 h). Significance in bacterial reduction between groups were indicated according to ANOVA statistical analysis (* = $p < 0.05$, ** = $p < 0.01$, *** = $p < 0.001$).

Table 4.1. Percent reductions in viability of adhered bacteria when comparing LI-PDMS, NO-PDMS, and LI-NO-PDMS materials to control PDMS materials.

	LI-PDMS	**NO-PDMS**	**LI-NO-PDMS**
24 h MRSA (%)	67.8 ± 13.7	98.3 ± 1.2	99.3 ± 0.3
7 d MRSA (%)	85.8 ± 6.1	92.1 ± 1.5	95.8 ± 0.9
14 d MRSA (%)	78.2 ± 2.0	71.3 ± 0.6	96.7 ± 1.9
28 d MRSA (%)	87.6 ± 3.0	86.7 ± 4.1	92.6 ± 1.8
	LI-PDMS	**NO-PDMS**	**LI-NO-PDMS**
24 h P. aeruginosa (%)	56.9 ± 3.2	85.1 ± 2.5	94.8 ± 0.3
7 d P. aeruginosa (%)	95.6 ± 2.8	94.7 ± 2.4	99.7 ± 0.1
14 d P. aeruginosa (%)	95.1 ± 1.9	94.0 ± 3.5	99.2 ± 0.3
28 d P. aeruginosa (%)	94.7 ± 1.5	97.2 ± 0.4	98.2 ± 0.3

4.4.3. Antifouling and Hemocompatible Evaluations

4.4.3.1. In Vitro Fibrinogen Adsorption

Previous studies have indicated that fibrinogen adsorption onto medical device surfaces propagates undesired platelet adhesion and provides an anchor for bacterial attachment, necessitating antifouling surfaces for medical device applications(10-12). To determine if the liquid-infused surfaces (LI-PDMS and LI-NO-PDMS) demonstrate improved antifouling properties, samples were incubated with fibrinogen at physiological concentrations (2 mg/mL) for 90 minutes. As shown in **Figure 4.7A**, the liquid infusion of silicone oil resulted in a significant decrease of fibrinogen adsorption ($p < .05$, $n=3$). Adsorption of fibrinogen in LI-PDMS (**Figure 4.7D**) and LI-NO-PDMS (**Figure 4.7F**) samples was reduced by 46.5 ± 8.4% and 30.3 ± 10.2% when compared to control PDMS (**Figure 4.7C**), respectively. Previous reports have similarly shown that liquid infused silicone reduces the attachment of foulants including bacteria and proteins through the creation of a low-adhesion surface(27, 51). On the other hand, SNAP samples (**Figure 4.7E**) exhibited a significant increase in fibrinogen adsorption by 107.9 ± 71.6% when compared to PDMS. The phenomena of increased protein adsorption on NO-releasing surfaces has been observed in the past(73). However, it has been shown that the adsorbed fibrinogen on NO-releasing surfaces is less thrombotic compared to adsorbed fibrinogen on non-NO-releasing surfaces, which suggests that the presence of NO alters the structure of fibrinogen and may lead to enhanced adsorption(49). Further study needs to be conducted to confirm exactly how NO release affects the conformation of fibrinogen.

4.4.3.2. In Vitro Platelet Adhesion Measurements

Despite material improvements and systemic anticoagulation intervention, device-induced thrombosis remains one of the leading adverse events with indwelling blood-contacting medical

devices that often results in consequential side effects including device failure, embolism, extended hospitalization, and increased morbidity and mortality(74). Therefore, in order to improve the hemocompatibility of these devices, researchers have begun to develop passive and active surface modifications inspired by nature(22). NO-releasing surfaces, an active strategy that results in a localized production of nitric oxide at the surface, has gained tremendous popularity for improving the antithrombotic characteristics of different materials as a result of NO's role in platelet quiescence(29, 30, 75, 76). Moreover, antifouling strategies including liquid-infused super slippery surfaces that minimize biofouling of platelets and plasma proteins have shown promising improvements in hemocompatibility(27, 57, 77). Therefore, in this study, the NO donor SNAP was covalently attached to PDMS, a medically-relevant polymer commonly utilized for long-term indwelling medical device applications, followed by liquid infusion of silicone oil, resulting in a sustained NO-releasing platform with an antifouling interface. To assess the antithrombotic characteristics of the resulting material, platelet-rich porcine plasma was exposed for 2 h and the number of adhered platelets was quantified. As shown in **Figure 4.7B**, LI-NO-PDMS significantly reduced the number of platelets adhered to the surface by 66.5 ± 11.2%. Individually, LI-PDMS and NO-PDMS samples reduced the number of adhered platelets by 46.7 ± 27.9% and 45.2 ± 11.2%. Therefore, together the resulting localized NO release and silicone oil infusion resulted in a combined improvement of hemocompatibility. Similar trends of reduced platelet adhesion from NO-releasing surfaces and/or liquid-infused surfaces have been previously characterized(27, 50, 58, 78-80). In support of these findings, SEM images of materials exposed to porcine whole blood showed that plasma proteins and platelets rapidly adsorbed and adhered to the surface of untreated PDMS surfaces (**Figure 4.7G, H**). However, LI-PDMS (**Figure 4.7I, J**), NO-PDMS (**Figure 4.7K, L**), and LI-NO-PDMS (**Figure 4.7M, N**) samples showed a noticeable reduction in platelets

present on the surface. Moreover, while LI-PDMS samples failed to minimize the activation of platelets that did adhere to the surface, both NO-PDMS and LI-NO-PDMS samples showed reduced platelet activation. This is characteristic of NO, which has previously been established to reduce platelet aggregation and activation by inhibiting GPIIb/IIIa expression, increasing cGMP activation of protein kinase G, and modulated Ca^{2+} influx(32, 81).

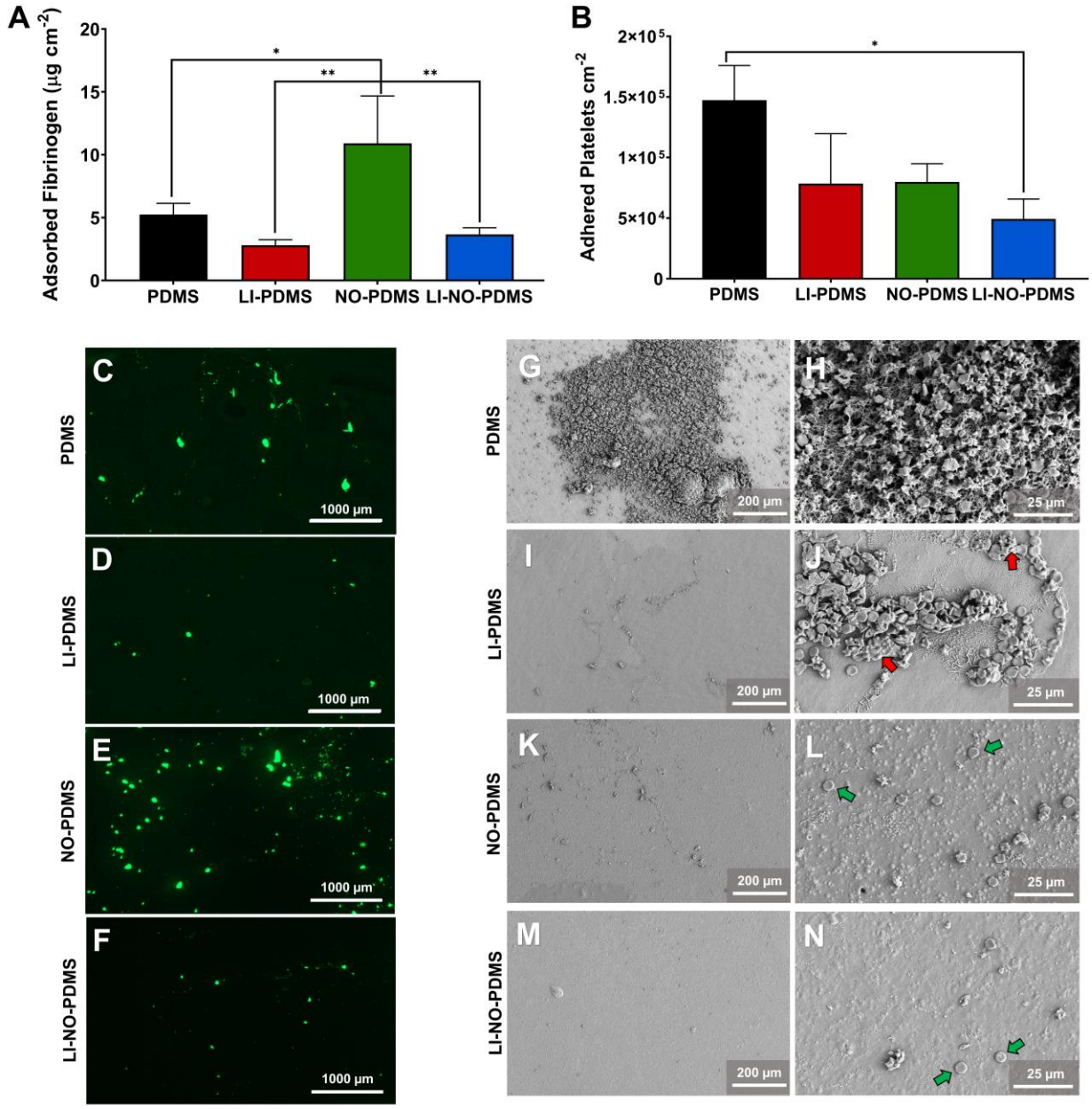

Figure 4.7. (A) Quantification of adsorbed fibrinogen to PDMS and LI-NO-PDMS polymer surfaces. (B) Platelet adhesion measurements after 2 h of *in vitro* porcine platelet rich plasma exposure. Images of fluorescently labeled fibrinogen (C-F) show that while NO-PDMS samples show an increased level of

protein adsorption, LI-PDMS and LI-NO-PDMS surfaces showed reduced levels of protein adsorption. (G-N) SEM images were also taken after porcine whole blood exposure for 60 s, showing a noticeable reduction in activated platelets and fibrin formation on LI-NO-PDMS surfaces compared to control PDMS surfaces. Red arrows indicate activated platelets, and green arrows indicate inactivated platelets.

4.4.4. Cytocompatibility of LI-NO Materials

In addition to evaluating efficacy, materials used for medical device applications should be cytocompatible with mammalian cells to ensure safety. In this study, CCK-8 assays were carried out to determine any toxic response towards leachates developed from covalent NO-PDMS and liquid-infused films in human primary cells. To this end, both human BJ fibroblasts and HUVECs were cultured against leachates acquired from films following 24 h incubation in culture media under physiological conditions. These conditions follow the International Organization for Standardization (ISO) 10993-5 for the biological evaluation of medical devices through *in vitro* tests for cytotoxicity(82). Prior work has individually considered NO-releasing PDMS, liquid-infused, and combination substrates with SNAP and liquid infusion for antimicrobial applications(27, 54). In these previous studies, covalent SNAP-PDMS showed over a 80% reduction in total leached SNAP compared to blended SNAP substrates with over 97% viability of 3T3 mouse fibroblast cells when exposed to leachates from covalent SNAP-PDMS films(48). Similarly, prior work with liquid-infused NO-releasing materials containing blended NO donors showed nearly 100% viability of 3T3 cells exposed to liquid-infused silicone and greater than 120% viability with liquid-infused, SNAP-impregnated films(27). Enhanced viability of fibroblast cells after exposure to NO donor compounds such as SNAP is expected as NO is a key mediator of fibroblast proliferation and migration in wound healing(83, 84). Similarly, vascular endothelial cells are the key producers of NO for regulation of vascular homeostasis, making it a key component of contemporary approaches to developing artificial endothelium(85).

In the case of LI-NO substrates, no appreciable cytotoxic effect was observed over 24 h of leaching and subsequent incubation of BJ fibroblasts and HUVECs (**Figure 4.8**). BJ fibroblasts and HUVECs exhibited an enhanced 105 ± 9.2% and 104 ± 6.1% viability after exposure to PDMS control leachates. These results concur with prior results and may result from trace amounts of primary amine-containing APTMS leachates from the control films(48). Introduction of immobilized SNAP to these films showed no statistically significant difference in cellular viability ($P > 0.05$). Although liquid infusion led to a minor decline in viability in BJ fibroblast cells (92.6 ± 3.5%), these results were not significant with respect to the PDMS control ($P > 0.05$). Non-volatile medical grade silicone oils have been extensively evaluated in literature with no expected cytotoxicity in indwelling applications provided careful moderation by adjusting infused amounts(86). Finally, both NO-PDMS and LI-NO-PDMS exhibited no appreciable effect on cellular viability with respect to PDMS controls in both cell lines ($P > 0.05$). These results are expected, as NAP, the precursor to SNAP, is approved by the FDA for treatment of heavy metal poisoning and cystinuria(87, 88). Taken all together, cytocompatibility of covalent-SNAP and liquid-infused substrates motivates interest in their application to indwelling medical devices, especially to combat bacterial infection with the potential for reduced incidence of failure from device occlusion via clot formation.

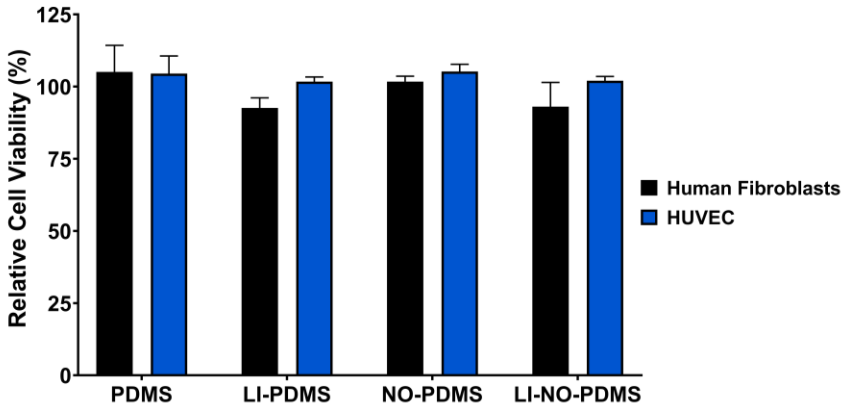

Figure 4.8. Relative cell viability of BJ fibroblasts and HUVECs treated with leachates gathered from prepared films following 24 h in physiological conditions. Data represented as mean ± SD.

4.5. Conclusion

In this work, a stable NO-releasing, liquid-infused PDMS (LI-NO-PDMS) platform was fabricated via covalent SNAP immobilization and silicone oil infusion to improve the antimicrobial and antifouling properties for long-term, indwelling medical device applications. The fabrication and optimization of the liquid-infusion protocol resulted in super slippery properties capable of reducing thrombosis and infection. LI-NO-PDMS surfaces maintained a stable, physiologically relevant NO flux ($> 0.5 \times 10^{-10}$ mol cm^{-2} min^{-1}) for 30 d with < 1% of SNAP leaching. As a result, LI-NO-PDMS materials robustly challenged in a series of CDC biofilm reactor studies for 7, 14, and 28 d demonstrated synergistic antimicrobial effects, resulting in up to 99.9% reduction in both adhered MRSA and *P. aeruginosa* viability and > 92% reduction in adhered bacterial viability at any time point and. Herein, one of the most exhaustive study has been performed to date determining *in vitro* antimicrobial efficacy of NO-releasing materials using CDC biofilm bioreactors over 28 d. Improved antifouling properties were demonstrated through a substantial reduction in fibrinogen adsorption (30.3 ± 10.2% reduction) and platelet adhesion (66.5 ± 11.2% reduction) to the surface compared to unmodified controls. Finally, leachates extracted from the materials did not exhibit any cytotoxic response towards human fibroblast and endothelial cell lines. In conclusion, these results are substantially promising for the prevention of medical device-induced clotting and biofilm formation. Currently, no study combining a stable NO-releasing platform ($> 0.5 \times 10^{-10}$ mol cm^{-2} min^{-1} for 30+ d) with slippery surface properties, leaving this technology to be in a unique position to address the widespread problems associated with medical device-related complications.

4.6 References

1. Darouiche RO. Device-associated infections: a macroproblem that starts with microadherence. Clin Infect Dis. 2001;33(9):1567-72.

2. Mermel LA, Allon M, Bouza E, Craven DE, Flynn P, O'Grady NP, et al. Clinical practice guidelines for the diagnosis and management of intravascular catheter-related infection: 2009 Update by the Infectious Diseases Society of America. Clin Infect Dis. 2009;49(1):1-45.

3. Stewart PS. Mechanisms of antibiotic resistance in bacterial biofilms. Int J Med Microbiol. 2002;292(2):107-13.

4. Burns KEA, McLaren A. Catheter-related right atrial thrombus and pulmonary embolism: A case report and systematic review of the literature. Can Respir J. 2009;16(5):163-5.

5. White D, Woller SC, Stevens SM, Collingridge DS, Chopra V, Fontaine GV. Comparative thrombosis risk of vascular access devices among critically ill medical patients. Thrombosis Research. 2018;172:54-60.

6. Dillon PA, Foglia RP. Complications associated with an implantable vascular access device. J Pediatr Surg. 2006;41(9):1582-7.

7. Roberts TR, Harea GT, Singha P, Sieck KN, Beely BM, Wendorff DS, et al. Heparin-Free Extracorporeal Life Support Using Tethered Liquid Perfluorocarbon: A Feasibility and Efficacy Study. ASAIO J. 2020;66(7):809-17.

8. Warkentin TE. Heparin-induced thrombocytopenia. Critical Decisions in Thrombosis and Haemostasis BC Decker Inc Hamilton, Pagg. 1998:100-8.

9. Fidlar E, Jaques L. The effect of commercial heparin on the platelet count. The Journal of laboratory and clinical medicine. 1948;33(11):1410-23.

10. Charville GW, Hetrick EM, Geer CB, Schoenfisch MH. Reduced bacterial adhesion to fibrinogen-coated substrates via nitric oxide release. Biomaterials. 2008;29(30):4039-44.

11. Horbett TA. Fibrinogen adsorption to biomaterials. J Biomed Mater Res A. 2018;106(10):2777-88.

12. Mohammad SF, Topham NS, Burns GL, Olsen DB. Enhanced bacterial adhesion on surfaces pretreated with fibrinogen and fibronectin. ASAIO Trans. 1988;34(3):573-7.

13. Liu L, Shi H, Yu H, Yan S, Luan S. The recent advances in surface antibacterial strategies for biomedical catheters. Biomater Sci. 2020;8(15):4095-108.

14. Singha P, Locklin J, Handa H. A review of the recent advances in antimicrobial coatings for urinary catheters. Acta Biomater. 2017;50:20-40.

15. Johnson JR, Johnston B, Kuskowski MA. In vitro comparison of nitrofurazone- and silver alloy-coated foley catheters for contact-dependent and diffusible inhibition of urinary tract infection-associated microorganisms. Antimicrob Agents Chemother. 2012;56(9):4969-72.

16. Johnson JR, Kuskowski MA, Wilt TJ. Systematic review: antimicrobial urinary catheters to prevent catheter-associated urinary tract infection in hospitalized patients. Ann Intern Med. 2006;144(2):116-26.

17. Kowalczuk D, Ginalska G, Piersiak T, Miazga-Karska M. Prevention of biofilm formation on urinary catheters: comparison of the sparfloxacin-treated long-term antimicrobial catheters with silver-coated ones. J Biomed Mater Res B Appl Biomater. 2012;100(7):1874-82.

18. Morris NS, Stickler DJ. Encrustation of indwelling urethral catheters by Proteus mirabilis biofilms growing in human urine. J Hosp Infect. 1998;39(3):227-34.

19. Riley DK, Classen DC, Stevens LE, Burke JP. A large randomized clinical trial of a silver-impregnated urinary catheter: lack of efficacy and staphylococcal superinfection. Am J Med. 1995;98(4):349-56.

20. Antonelli M, De Pascale G, Ranieri V, Pelaia P, Tufano R, Piazza O, et al. Comparison of triple-lumen central venous catheters impregnated with silver nanoparticles (AgTive®) vs conventional catheters in intensive care unit patients. J Hosp Infect. 2012;82(2):101-7.

21. Stevens KN, Crespo-Biel O, van den Bosch EE, Dias AA, Knetsch ML, Aldenhoff YB, et al. The relationship between the antimicrobial effect of catheter coatings containing silver nanoparticles and the coagulation of contacting blood. Biomaterials. 2009;30(22):3682-90.

22. Maitz MF, Martins MCL, Grabow N, Matschegewski C, Huang N, Chaikof EL, et al. The blood compatibility challenge. Part 4: Surface modification for hemocompatible materials: Passive and active approaches to guide blood-material interactions. Acta Biomater. 2019;94:33-43.

23. Lavery KS, Rhodes C, McGraw A, Eppihimer MJ. Anti-thrombotic technologies for medical devices. Adv Drug Deliv Rev. 2017;112:2-11.

24. Harding JL, Metz JM, Reynolds MM. A Tunable, Stable, and Bioactive MOF Catalyst for Generating a Localized Therapeutic from Endogenous Sources. Advanced Functional Materials. 2014;24(47):7503-9.

25. Ashcraft M, Douglass M, Chen Y, Handa H. Combination strategies for antithrombotic biomaterials: an emerging trend towards hemocompatibility. Biomater Sci. 2021;9(7):2413-23.

26. Ergene C, Yasuhara K, Palermo EF. Biomimetic antimicrobial polymers: recent advances in molecular design. Polym Chem-Uk. 2018;9(18):2407-27.

27. Goudie MJ, Pant J, Handa H. Liquid-infused nitric oxide-releasing (LINORel) silicone for decreased fouling, thrombosis, and infection of medical devices. Sci Rep. 2017;7(1):13623.

28. May RM, Magin CM, Mann EE, Drinker MC, Fraser JC, Siedlecki CA, et al. An engineered micropattern to reduce bacterial colonization, platelet adhesion and fibrin sheath formation for improved biocompatibility of central venous catheters. Clin Transl Med. 2015;4.

29. Brisbois EJ, Kim M, Wang X, Mohammed A, Major TC, Wu J, et al. Improved Hemocompatibility of Multilumen Catheters via Nitric Oxide (NO) Release from S-Nitroso-N-acetylpenicillamine (SNAP) Composite Filled Lumen. ACS Appl Mater Interfaces. 2016;8(43):29270-9.

30. Brisbois EJ, Major TC, Goudie MJ, Bartlett RH, Meyerhoff ME, Handa H. Improved hemocompatibility of silicone rubber extracorporeal tubing via solvent swelling-impregnation of S-nitroso-N-acetylpenicillamine (SNAP) and evaluation in rabbit thrombogenicity model. Acta Biomater. 2016;37:111-9.

31. Devine R, Goudie MJ, Singha P, Schmiedt C, Douglass M, Brisbois EJ, et al. Mimicking the Endothelium: Dual Action Heparinized Nitric Oxide Releasing Surface. ACS Appl Mater Interfaces. 2020;12(18):20158-71.

32. Douglass M, Hopkins S, Pandey R, Singha P, Norman M, Handa H. S-Nitrosoglutathione-Based Nitric Oxide-Releasing Nanofibers Exhibit Dual Antimicrobial and Antithrombotic Activity for Biomedical Applications. Macromol Biosci. 2020:e2000248.

33. Estes LM, Singha P, Singh S, Sakthivel TS, Garren M, Devine R, et al. Characterization of a nitric oxide (NO) donor molecule and cerium oxide nanoparticle (CNP) interactions and their synergistic antimicrobial potential for biomedical applications. J Colloid Interface Sci. 2020.

34. Hibbard HAJ, Reynolds MM. Synthesis of novel nitroreductase enzyme-activated nitric oxide prodrugs to site-specifically kill bacteria. Bioorg Chem. 2019;93:103318.

35. Maloney SE, McGrath KV, Ahonen MJR, Soliman DS, Feura ES, Hall HR, et al. Nitric Oxide-Releasing Hyaluronic Acid as an Antibacterial Agent for Wound Therapy. Biomacromolecules. 2020.

36. Tuteja N, Chandra M, Tuteja R, Misra MK. Nitric Oxide as a Unique Bioactive Signaling Messenger in Physiology and Pathophysiology. J Biomed Biotechnol. 2004;2004(4):227-37.

37. Garren MR, Ashcraft M, Qian Y, Douglass M, Brisbois EJ, Handa H. Nitric oxide and viral infection: Recent developments in antiviral therapies and platforms. Appl Mater Today. 2021;22.

38. Schairer DO, Chouake JS, Nosanchuk JD, Friedman AJ. The potential of nitric oxide releasing therapies as antimicrobial agents. Virulence. 2012;3(3):271-9.

39. Wang GR, Zhu Y, Halushka PV, Lincoln TM, Mendelsohn ME. Mechanism of platelet inhibition by nitric oxide: in vivo phosphorylation of thromboxane receptor by cyclic GMP-dependent protein kinase. Proc Natl Acad Sci U S A. 1998;95(9):4888-93.

40. Ghalei S, Mondal A, Hopkins S, Singha P, Devine R, Handa H. Silk Nanoparticles: A Natural Polymeric Platform for Nitric Oxide Delivery in Biomedical Applications. ACS Appl Mater Interfaces. 2020.

41. Feura ES, Yang L, Schoenfisch MH. Antibacterial activity of nitric oxide-releasing carboxymethylcellulose against periodontal pathogens. J Biomed Mater Res A. 2020.

42. Suchyta DJ, Schoenfisch MH. Encapsulation of N-Diazeniumdiolates within Liposomes for Enhanced Nitric Oxide Donor Stability and Delivery. Mol Pharm. 2015;12(10):3569-74.

43. Mondal A, Devine R, Estes L, Manuel J, Singha P, Mancha J, et al. Highly hydrophobic polytetrafluoroethylene particle immobilization via polydopamine anchor layer on nitric oxide releasing polymer for biomedical applications. J Colloid Interface Sci. 2020.

44. Douglass ME, Goudie MJ, Pant J, Singha P, Hopkins S, Devine R, et al. Catalyzed Nitric Oxide Release via Cu Nanoparticles Leads to an Increase in Antimicrobial Effects and Hemocompatibility for Short-Term Extracorporeal Circulation. ACS Applied Bio Materials. 2019;2(6):2539-48.

45. Frost MC, Meyerhoff ME. Synthesis, characterization, and controlled nitric oxide release from S-nitrosothiol-derivatized fumed silica polymer filler particles. J Biomed Mater Res A. 2005;72(4):409-19.

46. Ratanatawanate C, Chyao A, Balkus KJ, Jr. S-nitrosocysteine-decorated PbS QDs/TiO2 nanotubes for enhanced production of singlet oxygen. J Am Chem Soc. 2011;133(10):3492-7.

47. Mondal A, Douglass M, Hopkins SP, Singha P, Tran M, Handa H, et al. Multifunctional S-Nitroso-N-acetylpenicillamine-Incorporated Medical-Grade Polymer with Selenium Interface for Biomedical Applications. ACS Appl Mater Interfaces. 2019;11(38):34652-62.

48. Hopkins SP, Pant J, Goudie MJ, Schmiedt C, Handa H. Achieving Long-Term Biocompatible Silicone via Covalently Immobilized S-Nitroso- N-acetylpenicillamine (SNAP) That Exhibits 4 Months of Sustained Nitric Oxide Release. ACS Appl Mater Interfaces. 2018;10(32):27316-25.

49. Lantvit SM, Barrett BJ, Reynolds MM. Nitric oxide releasing material adsorbs more fibrinogen. Journal of Biomedical Materials Research Part A. 2013;101(11):3201-10.

50. Leslie DC, Waterhouse A, Berthet JB, Valentin TM, Watters AL, Jain A, et al. A bioinspired omniphobic surface coating on medical devices prevents thrombosis and biofouling. Nat Biotechnol. 2014;32(11):1134-40.

51. MacCallum N, Howell C, Kim P, Sun D, Friedlander R, Ranisau J, et al. Liquid-Infused Silicone As a Biofouling-Free Medical Material. Acs Biomater Sci Eng. 2015;1(1):43-51.

52. Wang CH, Guo ZG. A comparison between superhydrophobic surfaces (SHS) and slippery liquid-infused porous surfaces (SLIPS) in application. Nanoscale. 2020;12(44):22398-424.

53. Chug MK, Feit C, Brisbois EJ. Increasing the Lifetime of Insulin Cannula with Antifouling and Nitric Oxide Releasing Properties. ACS Applied Bio Materials. 2019;2(12):5965-75.

54. Homeyer KH, Goudie MJ, Singha P, Handa H. Liquid-Infused Nitric-Oxide-Releasing Silicone Foley Urinary Catheters for Prevention of Catheter-Associated Urinary Tract Infections. ACS Biomaterials Science & Engineering. 2019;5(4):2021-9.

55. Moynihan HA, Roberts SM. Preparation of Some Novel S-Nitroso Compounds as Potential Slow-Release - Agents of Nitric-Oxide in-Vivo. J Chem Soc Perk T 1. 1994(7):797-805.

56. Gierke GE, Nielsen M, Frost MC. S-Nitroso-N-acetyl-D-penicillamine covalently linked to polydimethylsiloxane (SNAP-PDMS) for use as a controlled photoinitiated nitric oxide release polymer. Sci Technol Adv Mater. 2011;12(5):055007.

57. Sotiri I, Overton JC, Waterhouse A, Howell C. Immobilized liquid layers: A new approach to anti-adhesion surfaces for medical applications. Exp Biol Med (Maywood). 2016;241(9):909-18.

58. Yuan S, Li Z, Song L, Shi H, Luan S, Yin J. Liquid-Infused Poly(styrene-b-isobutylene-b-styrene) Microfiber Coating Prevents Bacterial Attachment and Thrombosis. ACS Appl Mater Interfaces. 2016;8(33):21214-20.

59. Tripathi MK, Kartawy M, Amal H. The role of nitric oxide in brain disorders: Autism spectrum disorder and other psychiatric, neurological, and neurodegenerative disorders. Redox Biol. 2020;34:101567.

60. Vaughn MW, Kuo L, Liao JC. Estimation of nitric oxide production and reaction rates in tissue by use of a mathematical model. Am J Physiol. 1998;274(6):H2163-76.

61. Yang Y, Qi PK, Yang ZL, Huang N. Nitric oxide based strategies for applications of biomedical devices. Biosurface and Biotribology. 2015;1(3):177-201.

62. Hopkins SP, Frost MC. Synthesis and Characterization of Controlled Nitric Oxide Release from S-Nitroso-N-Acetyl-d-Penicillamine Covalently Linked to Polyvinyl Chloride (SNAP-PVC). Bioengineering (Basel). 2018;5(3).

63. Yatvin J, Gao J, Locklin J. Durable defense: robust and varied attachment of non-leaching poly"-onium" bactericidal coatings to reactive and inert surfaces. Chem Commun (Camb). 2014;50(67):9433-42.

64. Kolb H, Kolb-Bachofen V. Nitric oxide in autoimmune disease: cytotoxic or regulatory mediator? Immunol Today. 1998;19(12):556-61.

65. Singha P, Workman CD, Pant J, Hopkins SP, Handa H. Zinc-oxide nanoparticles act catalytically and synergistically with nitric oxide donors to enhance antimicrobial efficacy. J Biomed Mater Res A. 2019;107(7):1425-33.

66. Brisbois EJ, Handa H, Major TC, Bartlett RH, Meyerhoff ME. Long-term nitric oxide release and elevated temperature stability with S-nitroso-N-acetylpenicillamine (SNAP)-doped Elast-eon E2As polymer. Biomaterials. 2013;34(28):6957-66.

67. Rigo S, Cai C, Gunkel-Grabole G, Maurizi L, Zhang X, Xu J, et al. Nanoscience-Based Strategies to Engineer Antimicrobial Surfaces. Adv Sci (Weinh). 2018;5(5):1700892.

68. Wei C, Zhang G, Zhang Q, Zhan X, Chen F. Silicone Oil-Infused Slippery Surfaces Based on Sol-Gel Process-Induced Nanocomposite Coatings: A Facile Approach to Highly Stable Bioinspired Surface for Biofouling Resistance. ACS Appl Mater Interfaces. 2016;8(50):34810-9.

69. Barraud N, Hassett DJ, Hwang SH, Rice SA, Kjelleberg S, Webb JS. Involvement of nitric oxide in biofilm dispersal of Pseudomonas aeruginosa. J Bacteriol. 2006;188(21):7344-53.

70. Singha P, Goudie MJ, Liu Q, Hopkins S, Brown N, Schmiedt CW, et al. Multipronged Approach to Combat Catheter-Associated Infections and Thrombosis by Combining Nitric Oxide and a Polyzwitterion: a 7 Day In Vivo Study in a Rabbit Model. ACS Appl Mater Interfaces. 2020;12(8):9070-9.

71. Toes GJ, van Muiswinkel KW, van Oeveren W, Suurmeijer AJ, Timens W, Stokroos I, et al. Superhydrophobic modification fails to improve the performance of small diameter expanded polytetrafluoroethylene vascular grafts. Biomaterials. 2002;23(1):255-62.

72. Doll K, Yang I, Fadeeva E, Kommerein N, Szafranski SP, Bei der Wieden G, et al. Liquid-Infused Structured Titanium Surfaces: Antiadhesive Mechanism to Repel Streptococcus oralis Biofilms. ACS Appl Mater Interfaces. 2019;11(26):23026-38.

73. Devine R, Singha P, Handa H. Versatile biomimetic medical device surface: hydrophobin coated, nitric oxide-releasing polymer for antimicrobial and hemocompatible applications. Biomaterials science. 2019.

74. Jaffer IH, Weitz JI. The blood compatibility challenge. Part 1: Blood-contacting medical devices: The scope of the problem. Acta Biomater. 2019;94:2-10.

75. Major TC, Handa H, Brisbois EJ, Reynolds MM, Annich GM, Meyerhoff ME, et al. The mediation of platelet quiescence by NO-releasing polymers via cGMP-induced serine 239 phosphorylation of vasodilator-stimulated phosphoprotein. Biomaterials. 2013;34(33):8086-96.

76. Zhang H, Annich GM, Miskulin J, Osterholzer K, Merz SI, Bartlett RH, et al. Nitric oxide releasing silicone rubbers with improved blood compatibility: preparation, characterization, and in vivo evaluation. Biomaterials. 2002;23(6):1485-94.

77. Epstein AK, Wong TS, Belisle RA, Boggs EM, Aizenberg J. Liquid-infused structured surfaces with exceptional anti-biofouling performance. Proc Natl Acad Sci U S A. 2012;109(33):13182-7.

78. Goudie MJ, Singha P, Hopkins SP, Brisbois EJ, Handa H. Active Release of an Antimicrobial and Antiplatelet Agent from a Nonfouling Surface Modification. ACS Appl Mater Interfaces. 2019;11(4):4523-30.

79. Wong TS, Kang SH, Tang SK, Smythe EJ, Hatton BD, Grinthal A, et al. Bioinspired self-repairing slippery surfaces with pressure-stable omniphobicity. Nature. 2011;477(7365):443-7.

80. Yuan S, Luan S, Yan S, Shi H, Yin J. Facile Fabrication of Lubricant-Infused Wrinkling Surface for Preventing Thrombus Formation and Infection. ACS Appl Mater Interfaces. 2015;7(34):19466-73.

81. Simon-Walker R, Romero R, Staver JM, Zang Y, Reynolds MM, Popat KC, et al. Glycocalyx-Inspired Nitric Oxide-Releasing Surfaces Reduce Platelet Adhesion and Activation on Titanium. Acs Biomater Sci Eng. 2017;3(1):68-77.

82. Wallin RF, Arscott EF. A practical guide to ISO 10993-5: Cytotoxicity. Medical Device and Diagnostic Industry. 1998;20:96-8.

83. Han G, Nguyen LN, Macherla C, Chi Y, Friedman JM, Nosanchuk JD, et al. Nitric Oxide–Releasing Nanoparticles Accelerate Wound Healing by Promoting Fibroblast Migration and Collagen Deposition. The American Journal of Pathology. 2012;180(4):1465-73.

84. Ghalei S, Li J, Douglass M, Garren M, Handa H. Synergistic Approach to Develop Antibacterial Electrospun Scaffolds Using Honey and S-Nitroso-N-acetyl Penicillamine. Acs Biomater Sci Eng. 2021.

85. Roberts TR, Garren M, Handa H, Batchinsky AI. Toward an Artificial Endothelium: Development of Blood-Compatible Surfaces for Extracorporeal Life Support. J Trauma Acute Care Surg. 2020.

86. Howell C, Grinthal A, Sunny S, Aizenberg M, Aizenberg J. Designing Liquid-Infused Surfaces for Medical Applications: A Review. Adv Mater. 2018;30(50):e1802724.

87. Kark RA, Poskanzer DC, Bullock JD, Boylen G. Mercury poisoning and its treatment with N-acetyl-D,L-penicillamine. N Engl J Med. 1971;285(1):10-6.

88. Stephens AD, Watts RW. The treatment of cystinuria with N-acetyl-D-penicillamine, a comparison with the results of D-penicillamine treatment. Q J Med. 1971;40(159):355-70.

CHAPTER 5:

REDUCTION IN FOREIGN BODY RESPONSE AND IMPROVED ANTIMICROBIAL EFFICACY VIA SILICONE OIL-INFUSED NITRIC OXIDE-RELEASING MEDICAL GRADE CANNULAS[5]

[5] Douglass M, Hopkins S, Chug MK, Kim G, Garren M, Ashcraft M, Nguyen DT, Tayag N, Handa H, and Brisbois EJ. Reduction in Foreign Body Response and Improved Antimicrobial Efficacy via Liquid-Infused Nitric Oxide-Releasing Medical Grade Cannulas. 2021. *ACS Applied Materials & Interfaces*. Reprinted here with permission of the publisher.

5.1 Abstract

Foreign body response and infection are two universal complications that occur with indwelling medical devices. In response, researchers have developed different antimicrobial and antifouling surface strategies to minimize bacterial colonization and fibrous encapsulation. In this study, the nitric oxide donor *S*-nitroso-*N*-acetylpenicillamine (SNAP) and silicone oil were impregnated into silicone rubber cannulas (SR-SNAP-Si) using a solvent swelling method to improve the antimicrobial properties and decrease the foreign body response. The fabricated SR-SNAP-Si cannulas demonstrated a stable, prolonged NO release, exhibited minimal SNAP leaching, and maintained sliding angles < 15 ° for 21 d. SR-SNAP-Si cannulas displayed enhanced antimicrobial efficacy against *Staphylococcus aureus* in a 7-d biofilm bioreactor study, reducing the viability of adhered bacteria by 99.2 ± 0.2% compared to unmodified cannulas while remaining non-cytotoxic towards human fibroblast cells. Finally, SR-SNAP-Si cannulas were evaluated for the first time in a 14- and 21-d subcutaneous mouse model, showing significantly enhanced biocompatibility compared to control cannulas by reducing the thickness of fibrous encapsulation by 60.9 ± 6.1% and had a 60.8 ± 10.5% reduction in cell density around the implant site after 3 weeks. Thus, this work demonstrates that antifouling, NO-releasing surfaces can improve the lifetime and safety of indwelling medical devices.

5.2 Introduction

Subcutaneously implanted medical devices including insulin infusion cannulas, port catheters, and sensors have revolutionized healthcare, allowing wearable, easy access for medication and self-monitoring health. However, chronic inflammation, granulation tissue development, fibrous encapsulation, and infection greatly impact implanted device functionality and lifetime(1). Within the first few hours of implantation, neutrophils are recruited to the implant site, initiating an immune response and inflammation through generating reactive oxygen species, releasing antimicrobial granules, and producing extracellular traps(2). As time progresses, further recruited macrophages form foreign body giant cells, demonstrate increase levels of phagocytosis, and promote inflammatory cytokine secretion(3). The subsequent migration and adhesion of macrophages can damage biomaterials through the secretion of degradative species (reactive oxygen intermediates, enzymes, and acids), rendering device failure(1). Fibroblast cells migrate to the device interface to form a dense fibrous matrix that encapsulates the implant, walling off the device and, in the case of medication delivery, decreasing the efficiency of absorption(4, 5). For example, fibrous encapsulation of insulin infusion cannulas results in increased variability of insulin absorption and subsequent uncontrolled blood glucose levels; as a result, catheters are commonly required to be relocated every 2-3 days(4).

Moreover, despite improvements in prevention and interventional strategies, infection remains one of the leading complications associated with indwelling medical devices. In fact, over half of healthcare-associated infections can be attributed to complications associated with indwelling medical devices, and as medical device use continues to expand, the number of infections is expected to increase further(6). Invading pathogens readily adhere to foreign surfaces and form highly impenetrable, drug-resistant biofilm networks, rendering treatment using conventional antibiotic therapies largely ineffective. Therefore, an interface that exhibits

consistent, localized antimicrobial activity is needed to prevent and combat medical device-related infections.

To mitigate foreign body response and infection, researchers have begun developing and combining active and passive surface strategies for medical device applications(7). One promising class of materials that can reduce chronic inflammation and bacterial viability is nitric oxide (NO)-releasing surfaces(8, 9). These platforms locally deliver NO, a versatile endogenous free radical that plays a key role in modulating inflammation, immune response, and wound healing(10). In the body, NO is produced by endothelial cells to inhibit leukocyte and platelet adhesion and control vasodilation(10). Moreover, immune cells such as macrophages release NO at high concentrations, exacting multiple antimicrobial mechanisms against invading pathogens including DNA alterations, enzyme inhibition, and lipid peroxidation, making the development of resistance against NO difficult(11). Therefore, surfaces that release NO at physiological levels can enhance the anti-inflammatory, antimicrobial, and biocompatible properties of the medical device(12). Stable and biocompatible NO-releasing silicone-based materials have been achieved previously through a simple one-step NO donor impregnation solvent swelling method, showing great translational potential(13).

One limitation of NO-releasing materials, however, is that they do not prevent surface fouling. Inspired by the gastrointestinal tract, which contains a thick mucus liquid coating that protects against bacterial colonization,(14, 15) and the micro/nanostructure of the carnivorous *Nepenthes* pitcher plant that binds a liquid layer to the interface,(16) several research groups have developed biomimetic slippery liquid-infused (LI) surfaces which contain a thin liquid surface layer that results in a passive non-fouling, low-adhesion interface(14, 15, 17). The infusion of silicone oil (Si) into silicone-based materials has been previously demonstrated as a

straightforward, non-toxic, and effective modification that reduces protein adsorption, bacterial adhesion, and platelet adhesion(14). To capitalize on both the active antimicrobial and anti-inflammatory mechanisms of NO and the passive antifouling capabilities of liquid infused surfaces, previous studies have combined these two surface strategies, presenting a promising platform for preventing medical device-associated infection and surface fouling(14, 18, 19). However, the foreign body response of these materials is yet to be investigated.

For this study, the fabrication, *in vitro* analysis, and *in vivo* evaluation of NO-releasing, silicone oil-infused silicone rubber (SR-SNAP-Si) cannula tubing is described. The SR-SNAP-Si cannulas were constructed using a two-step solvent swelling process with the NO donor *S*-nitroso-*N*-acetylpenicillamine (SNAP) and silicone oil. The long-term NO release profiles, SNAP leaching, and sliding angles were investigated for 21 d. The antimicrobial efficacy of the fabricated cannulas against *Staphylococcus aureus* (*S. aureus*) was investigated using a 7-d CDC biofilm bioreactor study, and the cytotoxicity towards human fibroblasts cells was determined. Finally, the foreign body response to modified cannulas was compared in an *in vivo* 14- and 21-d subcutaneous mouse model. These findings provide a promising anti-inflammatory, antimicrobial, and biocompatible platform for long-term implanted medical device applications.

5.3 Materials & Methods

5.3.1 Materials

N-Acetyl-D-penicillamine (NAP), sodium chloride, copper (II) chloride dihydrate, L-cysteine, potassium chloride, sodium phosphate dibasic, potassium phosphate monobasic, ethylenediaminetetraacetic acid (EDTA), tetrahydrofuran (THF), sodium nitrite, sulfuric acid, and Cell Counting Kit-8 (CCK-8) were purchased from Sigma-Aldrich (St. Louis, MO). Methanol, hydrochloric acid, formalin, and 10 cSt silicone oil were obtained from Fisher Scientific

(Pittsburgh, PA). HelixMark® silastic silicone cannula tubing (60-011-05), ethanol, and fetal bovine serum (FBS) were obtained from VWR (Radnor, PA). Trypsin-EDTA (0.25%) was obtained from Corning (Manassas, VA). The bacterial strain of *S. aureus* (ATCC 6538), the human BJ fibroblast cell line (ATCC CRL 2522), and Eagle's Minimum Essential Medium (EMEM) were obtained from American Type Culture Collection. Phosphate buffered saline (PBS, pH 7.4) containing 138 mM NaCl, 2.7 mM KCl, 1.8 mM KH_2PO_4, 8.2 mM Na_2HPO_4, and 100 μM EDTA were used in all *in vitro* experiments. Gill's Hematoxylin #3 was purchased from Polysciences, Inc (Warrington, PA), and Eosin Y solution was purchased from Sigma-Aldrich (St. Louis, MO). A Trichrome Stain Kit (ab150686) was purchased from Abcam (Cambridge, UK).

5.3.2 Fabrication of SR-SNAP-Si Cannulas

SNAP Synthesis. The NO donor molecule SNAP was synthesized according to a previously established method(20). In short, 12 M HCl and 18 M H_2SO_4 were combined with NAP in a solution of methanol and DI water. A solution of 1M $NaNO_2$. was added. The solution was stirred in the dark and kept in an ice bath for 8 h to allow for SNAP crystal precipitation. After precipitation, the SNAP was collected through vacuum filtration, thoroughly washed with DI water, and dried overnight under vacuum to remove any trace solvent. SNAP purity was verified to be >90% for each batch(21).

SNAP Impregnation. SNAP-impregnated (SR-SNAP) cannulas were fabricated using a previously reported protocol via a SNAP swelling method(14, 22, 23). Briefly, HelixMark® silastic silicone cannula tubing (60-011-05) with an approximate length of 2 cm, an inner diameter of 2.16 mm, and an outer diameter of 1.02 mm was soaked in a SNAP-THF solution (125 mg mL^{-1}) for 24 h at room temperature. The tubing was subsequently removed and allowed to dry under ambient, dark

conditions for 24 h to remove any trace solvent. After drying, the samples were sonicated in DI water for 10 min to remove any SNAP crystals formed on the surface.

Silicone Oil Infusion. To generate an antifouling interface, SR-SNAP cannulas were immersed in 10 cSt silicone oil for 24 h following previous methods, resulting in SR-SNAP-Si cannulas(14). Unmodified cannulas (SR) were also immersed in silicone oil for 24 h to form SR-Si cannulas. After swelling, the samples were removed and gently cleaned with a kim wipe to remove any excess oil from the surface. SNAP-loaded samples were protected from light during the swelling process.

5.3.3 Silicone Oil Swelling/Deswelling Ratio Measurements

Silicone oil swelling was determined by measuring the mass change of the cannulas before swelling and throughout the swelling process (M_0 = initial mass; M_i = mass at timepoint) (**Equation 5.1**). Samples were kept at room temperature during the swelling process. Care was taken to wipe excess silicone oil off the cannulas before measurement. Deswelling of silicone oil was subsequently measured by measuring the mass change of samples after wrapped in moist Covidien 9024 Curity 4" X 4" and 3M™ Tegaderm™ dressing at 37°C to mimic a subcutaneous environment. Deswelling was measured throughout a 21-d incubation period.

Equation 5.1. $$Swelling\ Ratio = \frac{M_i}{M_0}$$

5.3.4 Sliding Angle Measurements

Improved, long-term antifouling surface properties after silicone oil swelling were confirmed via sliding angle measurements. 1 µL droplets of DI water were placed on SR-SNAP-Si and SR-SNAP cannulas. The samples were then slowly tilted whilst video recorded. Frame-by-frame analysis in ImageJ allowed for determination of the angle at which the droplets began to

slide. Sliding angles were measured every 7 d throughout a 21-d incubation period. Samples were incubated in moist conditions at 37°C in between measurements.

5.3.5 NO Release Analysis

The real-time NO release measurements from SR-SNAP-Si and SR-SNAP cannulas were quantified by a gold standard chemiluminescence method using a Zysense chemiluminescence Nitric Oxide Analyzer (NOA) 280i (Frederick, CO). A 2 cm segment of an SR-SNAP-Si cannula was wrapped in moist Covidien 9024 Curity 4" X 4" and 3M™ Tegaderm™ dressing prior to testing the NO release to mimic the subcutaneous setting. NO released from the sample at 37 °C was detected in the chemiluminescence detector generating the subsequent ppm/ppb of NO released, which was standardized by the surface area of samples to obtain the final flux levels in units of mol cm^{-2} min^{-1}. Samples were incubated in moist conditions at 37°C with protection from light and the NO release was computed at various time points during the 21 d of the experiment.

5.3.6 SNAP Leaching Measurements

SNAP leaching was measured over the course of 24 h under physiological conditions. The absorbance of leachates collected from SR-SNAP and SR-SNAP-Si cannulas incubated in PBS for varying amounts of time were measured using a Thermo Scientific Genysis 10S UV−vis Spectrophotometer (UV−vis). A calibration curve was generated using known concentrations of SNAP dissolved in PBS. The absorbance values were recorded for each sample at 336 nm after 30 min, 1 h, 4 h, 8 h, and 24 h of incubation in PBS. Between each absorbance recording, the PBS solution was replaced. To calculate the % of SNAP leached from the material, the concentrations of SNAP leached were divided by the total amount of SNAP loaded into the tubing originally (0.030 ± 0.002 mg SNAP mg^{-1} tubing).

5.3.7 Antimicrobial Efficacy in 7-d CDC Biofilm Bioreactor

The antimicrobial activity of SR-SNAP-Si cannulas was assessed in a 7-d *in vitro* CDC biofilm bioreactor against *S. aureus*. The CDC bioreactor is a highly favorable environment for modeling biofilm formation by providing a continuous flow of nutrients over a prolonged period. In this study, the antimicrobial efficacies of SR-SNAP-Si, SR-SNAP, SR-Si, and SR were compared in a 7-d model. First, an isolated colony of *S. aureus* was inoculated in LB broth for 16 h at 37°C. The optical density of the resulting solution was measured at 600 nm to determine the concentration of bacteria. LB medium (350 mL, 2 g L^{-1}) was combined with the bacterial solution to reach a concentration of ~10^6 colony-forming units (CFU) per mL. The bioreactor was kept at 37°C and a continuous flow of sterile media (2 g L^{-1}) at a rate of 1 L per d was maintained. An outlet to a sealed container was available for waste. After 7 d of exposure, the samples were removed and gently rinsed with PBS to remove any loosely attached bacteria. The samples were subsequently homogenized in sterile PBS for 60 s and vortexed at 30 s to transfer bound bacteria into the solution. Serial dilutions (10^{-1} to 10^{-5}) were plated on LB agar plates. The % bacterial inhibition was calculated using **Equation 5.2,** where C = $\frac{CFU}{cm^2}$:

Equation 5.2. $$\%\ Bacterial\ inhibition = \frac{(C_{control} - C_{test})}{C_{control}}\ x\ 100$$

5.3.8 *In vitro* Cytotoxicity Assessment

In vitro cytotoxicity against human fibroblasts (ATCC CRL-2522) was measured using a CCK-8 assay by ISO 10993 standards. Fibroblasts were cultured in a humified incubator (5% CO_2, 37°C) using a 75 cm^2 T-flask and EMEM medium supplemented with 10% FBS until reaching 80% confluency. Cells were removed from the flask using 0.05% trypsin with 5 mM of EDTA and counted using an EVE cell counter (NanoEntek, Waltham, MA USA). Cells were then seeded in tissue-culture treated 96-well plates (100 µL per well, 5000 cells $well^{-1}$). Simultaneously, leachates

from each material type were prepared by incubating 10 mg of samples in 10 mL of EMEM for 24 h. After incubation, the media in each well was replaced with 100 µL of corresponding leachate-containing media (n=6 per material sample) and incubated for an additional 24 h. The next day, 10 µL of the CCK-8 kit dye was added to each well and incubated for 1 h prior to absorbance measurements. The dye consists of a tetrazolium salt (WST-8 [2-(2-methoxy-4-nitrophenyl)-3-(4-nitrophenyl)-5-(2,4-disulfophenyl)-2H-tetrazolium monosodium salt), which dehydrogenases present in live cells reduce to orange-colored formazan detectable at 450 nm. Negative controls (cells without any leachates) were also measured for relative cell viability calculations. Absorbance was measured at 450 nm with reference measurement at wavelength of 650 nm. Percent relative cell viability with respect to negative controls was measured according to **Equation 5.3**, where A is the adjusted absorbance reading:

Equation 5.3. $$\%\ Cell\ Viability = \frac{A_{test}}{A_{control}}\ x\ 100$$

5.3.9 *In vivo* 14- and 21-d Subcutaneous Mouse Model

Mouse Model. All surgical procedures and animal handling were approved prior to experimentation by the University Committee on the Use and Care of Animals at the University of Georgia. In this study, SR-SNAP-Si and control cannulas (SR-SNAP, SR-Si, and SR) were subcutaneously implanted in a 14 and 21 d mouse model (n=4). Sixteen C57BL/6 mice (8-12 weeks old) were purchased from Jackson Laboratory. Prior to surgery, the animals were acclimated to the housing (single housing, 70-72° F ± 4° F, 30-70% humidity, and a 12 h light/dark cycle) for at least one week. Two days before and three days after surgery, the animals were fed MediGel CPF carprofen (ClearH_2O) as a sole nutrition source for pain management. Otherwise, the mice were fed Irradiated Pico Lab Rodent Diet 20 #5053 for the duration of the study.

In preparation for surgery, scrubbing was performed from the tip of the fingers to the elbows and sterile gloves were then placed with assistance to maintain sterility during the procedure. A surgical cap, facemask, and surgical scrubs were worn throughout the procedure. Topical 2.5% lidocaine/2.5% prilocaine cream (Hi-Tech Pharmaceuticals) was applied to the animals 10 minutes prior to aseptic prep. Mice were anesthetized using isoflurane inhalation (3-5% induction; 1.5-2% maintenance in 100% oxygen). During the surgery, a single ~1.5 cm incision was made in the interscapular region (midline dorsum), and subcutaneous pockets were prepared by blunt dissection ~1 cm from the site of incision. For each mouse, two cannulas (1.5 cm length, hydrogen peroxide gas-sterilized) were subcutaneously implanted (one on the left side of the incision, one on the right side) and tacked down with a single interrupted suture (Ethicon PDS II Suture #Z422, Size 4/0, FS-2 Needle). The incision was then closed using sterile wound clips (AutoClip 12020-00, Fine Science Tools) and tissue glue. After being taken off anesthesia, 1 mL of sterile saline was administered subcutaneously to maintain hydration, and the animal was placed on a towel over a covered heating pad to keep warm until recovered from anesthesia.

After the surgery, the animals were monitored for erythema, discharge, swelling, and retention of wound clips, and the animal's behavior was also monitored for any abnormal activity (overgrooming, itching, or painful behavior). The weight of each animal was measured prior to surgery and continuously monitored during the daily post-surgery inspections (daily for the first 4 d after surgery, then every 2-3 d thereafter). Wound clips were removed 7-10 d post-procedure. Cages were changed weekly until pre-determined endpoints (14 or 21 d).

Histological Analysis. At the pre-determined endpoints, the mice were euthanized using gradual CO_2 displacement followed by cervical dislocation. The cannula and the surrounding site were excised and fixed using formalin, embedded in paraffin wax, sectioned, and stained for histological

measurements. Hematoxylin and eosin (H&E) staining was performed to observe cell density and migration. Briefly, samples were deparaffinized and rehydrated in consecutive xylene, 100% ethanol, 95% ethanol, 80% ethanol, and deionized (DI) water baths for 3 minutes each. The samples were then stained with hematoxylin by exposing to the following solutions consecutively: hematoxylin (3 min), DI water (rinse), tap water (5 min), acid ethanol (dip 10x), tap water (2 x 1 min), and DI water (2 min). To perform eosin staining and dehydration, the slides were immersed in eosin (30 s), 95% ethanol (3 x 5 min), 100% ethanol (3 x 5 min), and xylene (3 x 15 min). Mounting media was then applied before coverslips were placed on top of the slides after the staining process was completed.

Trichrome staining was performed to measure fibrous encapsulation around the implant site. Briefly, samples were deparaffinized and rehydrated by immersing slides in consecutive 3 min xylene, 100% ethanol, 95% ethanol, 80% ethanol, and DI water baths. Next, slides were kept in Bouin's solution overnight at room temperature. The samples were then rinsed in running water for 5 min prior to staining. To stain, the slides were exposed to the following solutions consecutively: Gills Hematoxylin (3 min), DI water, tap water (5 min), acid ethanol (dipped quickly 10x), tap water (2 x 1 min), and DI water (2 min). Next, the samples were exposed to Biebrich Scarlet-Acid Fuchsin (5 min), rinsed with DI water, phosphotungstic/phosphomolybdic acid solution (1:1 ratio, 10 min), aniline blue solution (5 min), DI water (rinse), and 1% acetic acid solution (3 min). The samples were then dehydrated using 95% and 100% ethanol baths, followed by clearing slides in xylene (3 x 10 min). Mounting media was then applied before coverslips were placed on top of the slides after the staining process was completed.

5.3.10 Statistical Analysis

SNAP leaching, swelling ratio, *in vitro,* and *in vivo* data is reported in terms of mean ± standard deviation. NO release data is reported in terms of mean ± SEM. A student's *t*-test was performed to determine the statistical significance for NO release characterization, leaching studies, and silicone oil swelling/deswelling ratio measurements. A one-way ANOVA (Tukey's post hoc) was used when more than two sample types were tested (antimicrobial testing, cytotoxicity, and *in vivo* studies) to determine significance between control and test samples, where values of $p < 0.05$ were considered significant.

5.4 Results & Discussion

5.4.1 21-d NO release Analysis and SNAP Leaching of SR-SNAP-Si Cannulas

Long-term implanted medical devices frequently fail due to inflammation, fibrous encapsulation, and infection(24). To improve the antifouling and antimicrobial efficacies of cannula tubing, HelixMark® silastic silicone tubing was impregnated with the NO donor SNAP via a solvent-swelling method followed by the liquid infusion of silicone oil (10 cSt) based on previously established methods (**Figure 1A**)(13, 14, 18, 19).

NO-releasing materials have shown significant progress in reducing foreign body response,(8, 25) minimizing bacterial colonization,(11, 26) improving hemocompatibility,(13, 27, 28) and accelerating wound healing(29, 30). However, the long-term efficacy of these surfaces is directly dependent on the material's ability to provide a stable, sustained NO release. In this study, the long-term NO release from SNAP-loaded cannulas (SR-SNAP-Si and SR-SNAP) was characterized in real time under moist conditions *in vitro* via chemiluminescence using NO analyzers with a response time of < 1 sec (**Figure 1B**). The results suggest a prolonged release rate of NO at physiologically relevant levels in the range $0.5 - 4 \times 10^{-10}$ mol cm^{-2} min^{-1} similar to that of endothelial cells under normal conditions(31). The NO release was monitored over 21 d. During the duration of the 21-d study, no significant difference in the NO release levels were found

between SR-SNAP-Si and SR-SNAP cannulas ($p > 0.05$). For both sample types, the levels of NO flux were seen to be slightly higher in the initial days, which can be attributed to the existence of crystallized SNAP in the outer water-rich regions of the polymer that can relatively diffuse out faster. After the depletion of the SNAP reservoir in these layers, the levels of NO from the cannula gradually fall. Interestingly, while the SR-SNAP samples showed a decline in NO release below the physiological levels after 12 d, SR-SNAP-Si samples continued to release NO > 0.5×10^{-10} mol cm^{-2} min^{-1} for at least 19 d likely due to the silicone oil layer reducing hydration of the cannula and interaction of salt ions with the impregnated SNAP. Overall, SR-SNAP-Si cannulas exhibited a stable NO release profile for greater than 2 weeks, demonstrating the synthesized cannula's potential for long-term applications. Our prior work examining these liquid-infused, NO-releasing cannulas with similar NO-release profiles showed remarkable resistance to both protein adsorption and bacterial adhesion(18).

Although NO-releasing materials are well-documented to provide beneficial antimicrobial and cytocompatible characteristics for different biomaterials, significantly high levels of NO as a result of NO donor leaching can lead to cytotoxic events(32). Moreover, significant amounts of NO donor leaching will deplete the amount of NO stored in the material, decreasing the lifetime of the NO-releasing platform(33). To quantify the SNAP leaching behavior of the SR-SNAP-Si and SR-SNAP cannulas, samples were immersed in PBS at 37°C, and SNAP present in the PBS as a result of leaching was periodically measured with UV-Vis absorbance (**Figure 1C**). No significant difference in the cumulative amount of SNAP leached was found between SR-SNAP and SR-SNAP-Si samples at each time point over the course of the 24 h study ($p > 0.05$). After 24 h, only 2.2 ± 0.5% and 2.5 ± 0.3% of SNAP originally stored in the materials had leached from SR-SNAP and SR-SNAP-Si samples, respectively. Previous reports of SNAP-impregnated

materials have shown similar SNAP leaching characteristics(14, 18). In total, SNAP-impregnated samples showed promising long-term NO release characteristics with minimal SNAP leaching.

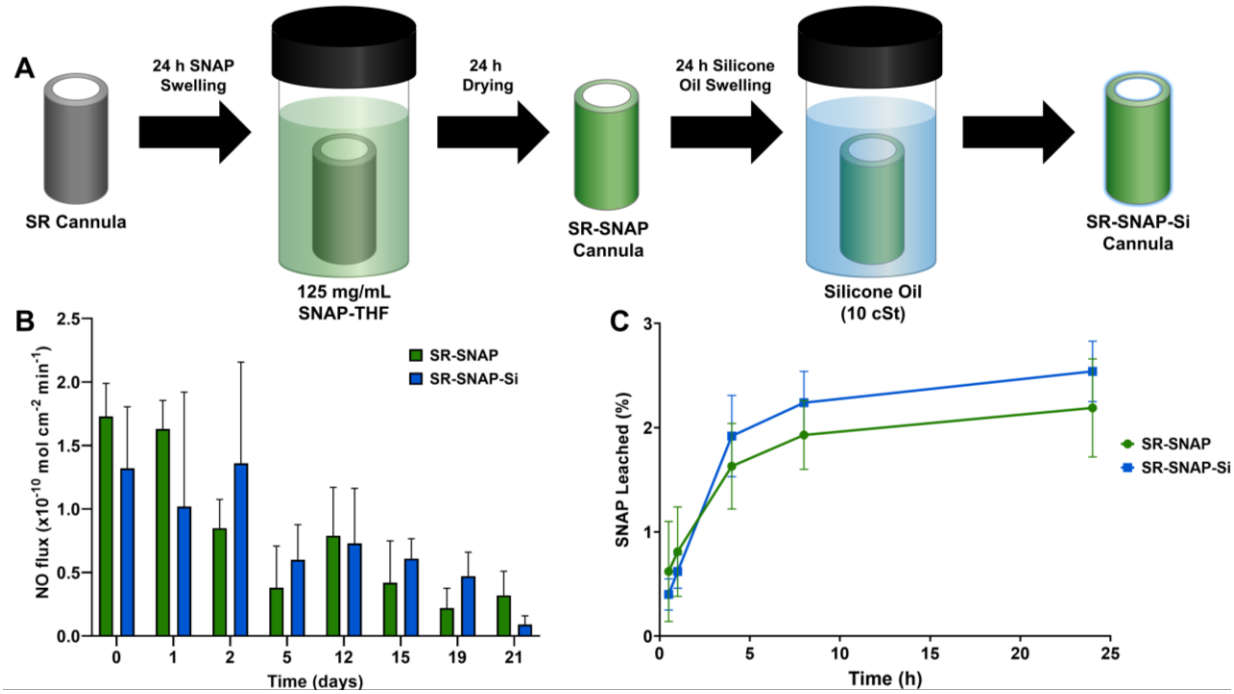

Figure 5.1. (A) Fabrication process of NO-releasing, liquid-infused SR-SNAP-Si cannulas. (B) *In vitro* real-time NO release from SR-SNAP-Si and SR-SNAP cannulas (n=3) measured using a chemiluminescence NO analyzer. The NO flux levels were measured at 37°C in moist conditions for 21 d. (C) Cumulative SNAP leaching measurements (n=4) in PBS at 37°C.

5.4.2 Silicone Oil Infusion Characterization and Sliding Angle Measurements

After the SNAP solvent swelling process, samples were swelled with silicone oil (10 cSt) according to a previously established method to achieve an antifouling interface(18, 34). The swelling ratio of silicone oil-swelled materials was characterized by measuring the change in mass over swelling time (**Figure 2A**). As reflected by the swelling ratio measurements, after 24 h of silicone oil immersion, the silicone oil uptake for both SR-Si and SR-SNAP-Si samples leveled off. No significant difference in swelling ratios were found between SR-SNAP-Si (2.18 ± 0.05 after 24 h) and SR-Si cannulas (2.10 ± 0.04 after 24 h) ($p > 0.05$). The deswelling behavior was also monitored for 21 d in moist conditions at 37°C to simulate a subcutaneous environment. As shown, both SR-SNAP-Si and SR-Si cannulas maintained virtually the same swelling ratio after

21 d of incubation (SR-SNAP-Si: 2.16 ± 0.04; SR-Si: 2.06 ± 0.03), indicating that there was no significant silicone oil loss during the incubation period ($p > 0.05$). Previous work has shown that an insignificant amount of SNAP leaching occurs during silicone oil infusion due to the low solubility of SNAP in silicone oil (0.4 μg mL^{-1}), so no significant changes in SNAP loading is expected to occur(14).

The retention of silicone oil was confirmed by sliding angle measurements over 21 d with incubation under moist conditions (**Figure 2B**). SR-SNAP cannulas maintained sliding angles > 90° whereas SR-SNAP-Si cannulas maintained < 15° throughout the 21-d study. Previous work by MacCallum et al. demonstrated that under continuous flow conditions, silicone oil-infused PDMS retains its antifouling properties(34). This supports that the SR-SNAP-Si cannulas have prolonged antifouling properties, continuing to be effective even after 21 d of exposure to physiologically relevant environments. A visual representation of the slippery interface can be seen in **Figure 2C-2J**. While droplets of DI water with methylene blue adhered to the surface of unmodified SR cannulas (**Figure 2C, 2D**) and SR-SNAP cannulas (**Figure 2G, 2H)**, droplets from the same solution easily glided off SR-Si cannulas (**Figure 2E, 2F**) and SR-SNAP-Si cannulas (**Figure 2I, 2J)**, demonstrating the antifouling potentials of these surfaces.

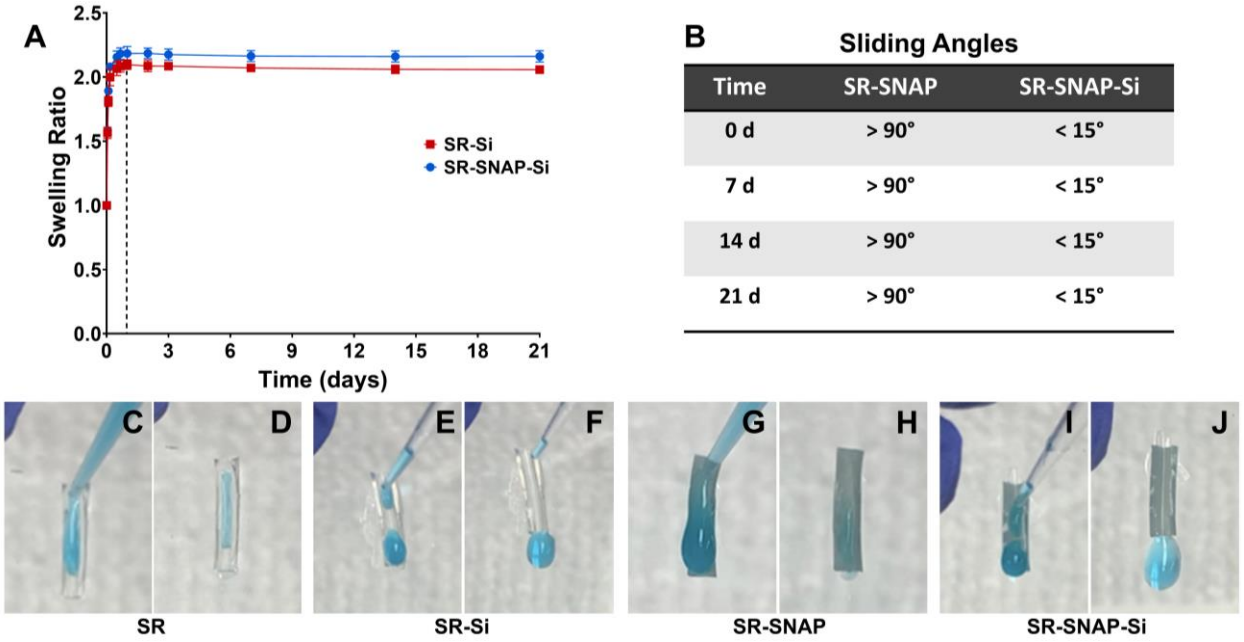

Figure 5.2. (A) Silicone oil swelling (0-24 h) and deswelling behavior (24 h – 21 d) of SR-Si and SR-SNAP-Si cannulas kept in moist conditions at 37°C. (B) Sliding angle measurements of SR-SNAP and SR-SNAP-Si cannulas stored in moist conditions (37°C) over a 21-d period. (C-J) Qualitative demonstration of slippery, antifouling behavior of silicone oil-infused cannulas (E-F, I-J) repelling DI water droplets compared to samples without silicone oil infusion, which did not repel water droplets as effectively (C-D, G-H).

5.4.2 *In vitro* antimicrobial activity of SR-SNAP-Si cannulas in a continuous flow CDC bioreactor

In attempt of reducing rates of infection, both active and passive surface strategies have been employed to improve the antimicrobial properties of medical devices(7). NO-releasing surfaces have gained tremendous popularity in rendering a surface antimicrobial by releasing potent concentrations of NO, which actively exerts broad-spectrum antimicrobial activity through lipid oxidation, denaturation of enzymes, and DNA deamination(11, 14). However, NO-releasing surfaces fail to prevent bacterial adhesion. In contrast, liquid-infused surfaces exhibit passive antifouling, “slippery” properties that prevent bacterial adhesion and subsequent biofilm formation, but do not directly inhibit bacterial viability(35). In this work, a NO-releasing platform (active) containing a liquid-infused interface (passive) was combined to reduce bacterial colonization even after extended exposure. To determine the effectiveness of our fabricated

materials, we examined the antimicrobial properties in a 7-d CDC bioreactor setup against *S. aureus*, one of the most prevalent causes of hospital-acquired infections and cannula site infections(36). As shown in **Figure 3A,** SR-SNAP-Si cannulas exhibited the greatest reduction in viable adhered bacteria compared to control SR cannulas (99.2 ± 0.2% reduction, $p < 0.001$). Alone, SR-Si and SR-SNAP cannulas reduced the number of viable adhered bacteria by 91.1 ± 5.0% ($p < 0.001$) and 95.9 ± 2.0% ($p < 0.001$) compared to control SR cannulas, respectively. Interestingly, SR-SNAP-Si cannulas also significantly reduced the viability of adhered *S. aureus* compared to SR-Si and SR-SNAP cannulas by 91.0 ± 2.5% ($p < 0.01$) and 80.3 ± 5.5% ($p < 0.05$). This finding exemplifies that combination surface strategies enhance the antimicrobial properties of SR through the bactericidal nature of NO and antifouling properties of liquid-infused surfaces. Slippery surfaces have been previously combined with other biocidal and anti-biofilm compounds to improve antimicrobial surface properties including quorum sensing inhibitor-releasing surfaces(37) and triclosan-releasing surfaces(35). However, due to NO's multiple antimicrobial actions, bacteria have historically developed little resistance, making NO-releasing surfaces an attractive alternative to both traditional antibiotic and biocidal therapies(38, 39). Outside of its antimicrobial properties, NO also exhibits wound-healing, anti-inflammatory, antiviral, and antithrombotic characteristics, making NO-releasing materials a unique multifunctional solution for problems commonly associated with indwelling medical devices(8, 40). The results from this study demonstrate the need for the combination of controlled release of bactericidal agents and antifouling surface properties to best reduce bacterial colonization over an extended period of time.

5.4.3 *In vitro* cytotoxicity measurement against human fibroblasts

Leachates from different antimicrobial agents added to medical device surfaces can negatively impact the health of surrounding tissues, potentially resulting in severe levels of

cytotoxicity and tissue necrosis. Therefore, an *in vitro* cytotoxicity assessment is a necessary first step in ensuring safe and effective clinical use(41). In this study, the cytotoxicity of each fabricated material towards human fibroblasts was evaluated using a CCK-8 kit(42). To collect leachates, each sample type (SR-SNAP-Si, SR-SNAP, SNAP-Si, and SR) was incubated in EMEM media for 24 h at 37°C. Human fibroblasts were simultaneously grown in a 96-well plate for 24 h at 37°C prior to leachate exposure. As shown in **Figure 3B**, none of the samples showed any cytotoxic effects against human fibroblasts (> 95% relative cell viability). Moreover, no statistically significant difference was found between any treated and untreated SR cannula ($p > 0.05$). These results are expected as NO-releasing materials have been previously found to be non-cytotoxic, and in some cases even showed increased cell viability in mammalian cells due to NO's role in cell proliferation and protection(14, 43). In addition, silicone oils have been extensively characterized as biocompatible(14, 44, 45). In total, the results from this study indicate that all aspects of the fabricated cannulas were non-cytotoxic and suitable for more extensive *in vivo* evaluation.

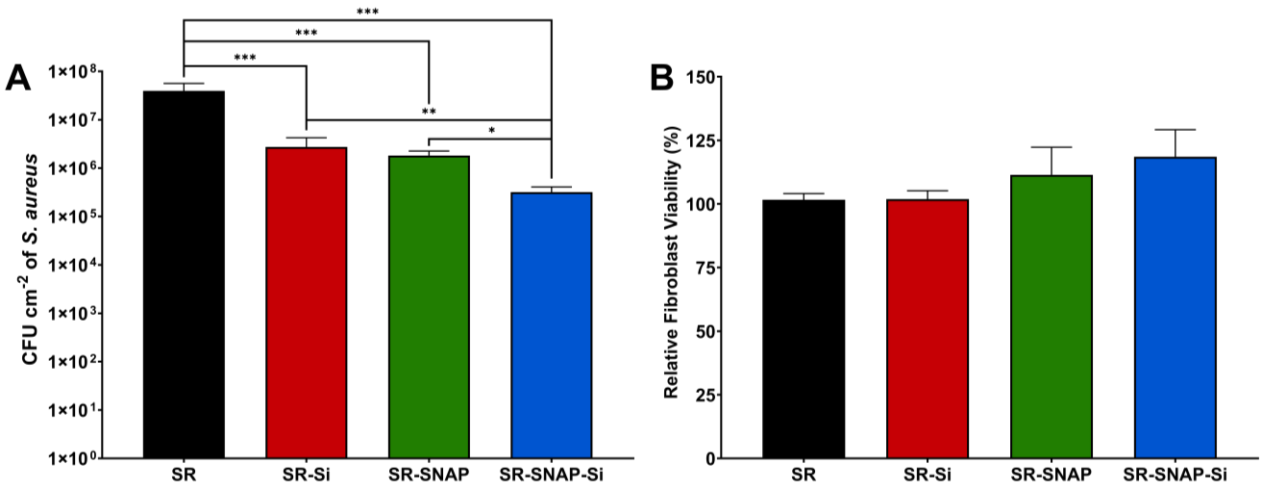

Figure 5.3. (A) Viable bacterial adhesion measurements of *S. aureus* after an *in vitro* 7-d CDC biofilm bioreactor study. SR-SNAP-Si surfaces best reduced the number of viable adhered bacteria compared to untreated SR control, SR-Si, and SR-SNAP cannulas. (B) *In vitro* cytotoxicity against human fibroblasts using a CCK-8 assay showed that there was no significant cytotoxicity ($p > 0.05$). (* = $p < 0.05$, ** = $p < 0.01$, *** = $p < 0.001$).

5.4.4 *In vivo* Evaluation of SR-SNAP-Si Cannulas in a 14- & 21-d Subcutaneous Mouse Model

When medical devices are implanted, the presence of a foreign body coupled with the injury incurred during implantation triggers a host immune response. The foreign body response results in acute and chronic inflammation along with fibrous encapsulation that walls off the implant from the surrounding tissue, compromising device functionality and lifetime(1, 46). In an effort to reduce the impact of the inflammatory response and promote wound-healing processes, NO-releasing platforms have been evaluated *in vivo*, which have resulted in decreased fibrous encapsulation and increased tissue integration(8, 47). Moreover, researchers have observed that liquid-infused surfaces reduce the foreign body response, decreasing leukocyte migration, inflammatory response, protein adhesion, and fibrous encapsulation(48-50). Therefore, in this work, the efficacy of a combined NO-releasing, liquid-infused surface was evaluated in an *in vivo* subcutaneous mouse model. Modified (SR-Si, SR-SNAP, SR-SNAP-Si) and untreated (SR) cannulas were implanted subcutaneously for 14 and 21 d under the dorsal skin on the lower back areas of the mice. After 14 and 21 d, tissue was excised from the sight of implantation and stained using H&E and trichrome staining kits (**Figure 4A-P**). As shown in **Figure 4Q**, SR-SNAP-Si cannulas had significantly reduced the thickness of the fibrous encapsulation surrounding the implant after 21 d by 60.9 ± 6.1% compared to unmodified cannulas. This can be attributed to several factors. First, both NO-releasing platforms and treatment of wound sites with exogenous NO donor molecules have resulted in decreased inflammatory cell recruitment,(51, 52) promotion of re-endothelialization,(51) and modulated collagen synthesis, which can reduce fibrous encapsulation(8). Similar to the findings in this study, Hetrick et al. demonstrated that NO-releasing xerogel-coated silicone elastomer implants resulted in decreased thickness of fibrous encapsulation by >50%(8). In addition to the benefits provided by NO-releasing characteristics,

antifouling, liquid-infused surfaces have shown excellent capabilities in reduce protein adsorption and fibroblast attachment, which play a major role in the production of a fibrous capsule around foreign implants(49, 53, 54).

Similar to the trend found with the fibrous encapsulation, SR-SNAP-Si cannulas reduced the density of inflammatory cells and migrated fibroblasts within 100 μm of the implant site by 60.8 ± 10.5% compared to unmodified cannulas after 21 d (**Figure 4R**). Reduction in cell density in proximity to a foreign body in parallel with decreased fibrous encapsulation is an indication of improved resolution in inflammation(55). Previous reports evaluating the anti-inflammatory effects of NO-releasing platforms implanted subcutaneously similarly showed a marked decrease in inflammatory cells around the implant(8, 25, 56). Under normal conditions, NO produced by the endothelium inhibits leukocyte and platelet adhesion, increases vasodilation, and inhibits smooth muscle proliferation(10). In addition, liquid-infused surfaces are well-established to repel protein adsorption ordinarily that plays a role in initiating foreign body response(1, 48, 49). The results indicate that the combination of an NO-releasing platform with a slippery, antifouling interface is capable of reducing the foreign body response after 21 d of implantation, and which can improve the longevity of long-term medical device implants including insulin pumps, port catheters, and sensors. Given the promising results, future studies better understanding the initial inflammatory response of NO-releasing, slippery surfaces can be conducted.

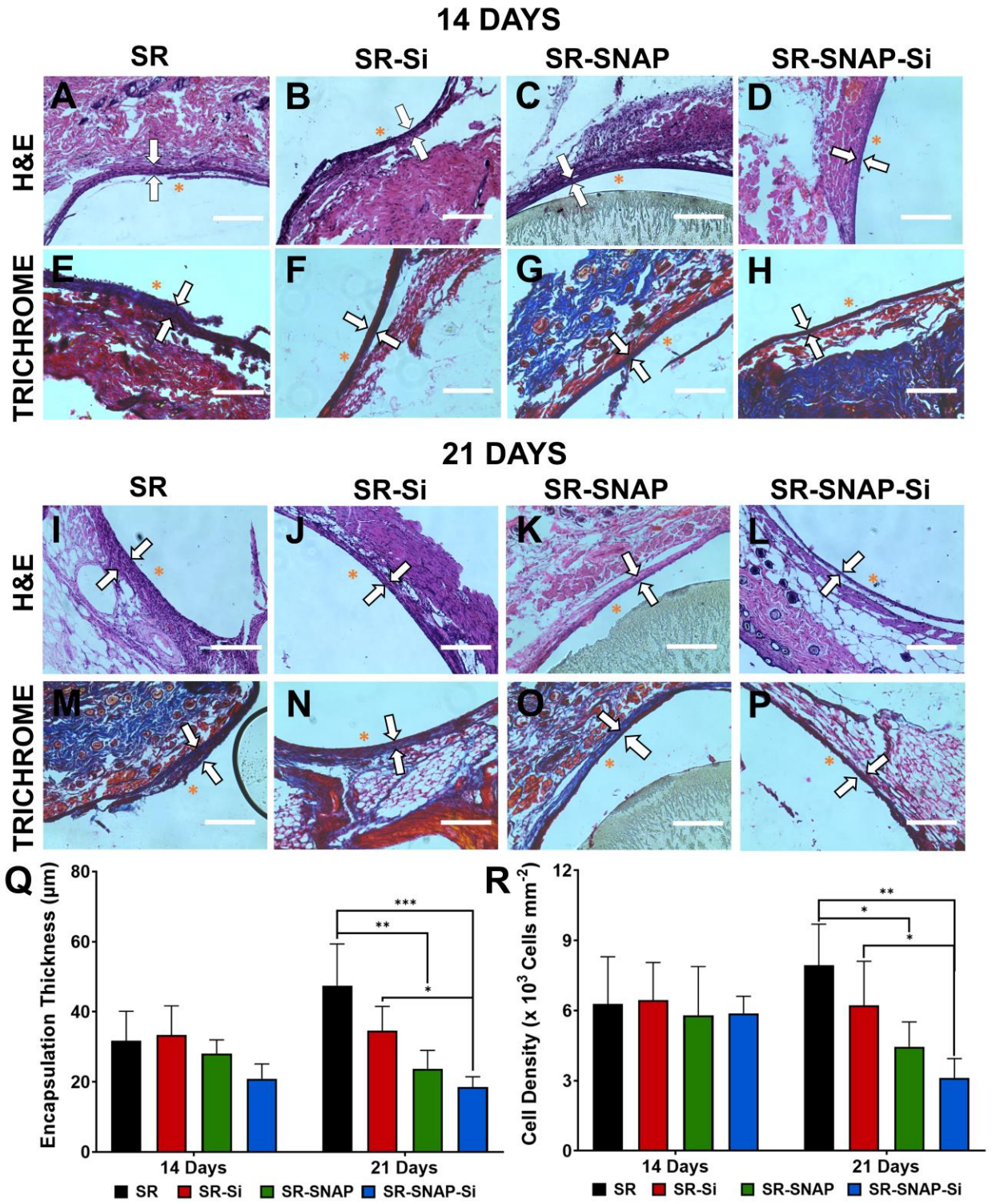

Figure 5.4. Hematoxylin & eosin (H&E)- and trichrome-stained tissue after 14 and 21 d at the cannula implant site (A-P). Thickness of the fibrous encapsulation (white arrows) formed around the implants were measured at each time points for all samples (Q). The nuclei of migrated fibroblasts and inflammatory cells stained purple, and cell density mm^{-2} within 100 µm of the implant site was quantified using ImageJ (R). (* = $p < 0.05$, ** = $p < 0.01$, *** = $p < 0.001$). White bar = 200 µm; orange asterisk = implant site.

5.5 Conclusion

Traditionally, the functionality and lifetime of implanted medical devices are significantly impacted by fibrous encapsulation, chronic inflammation, and infection. In this work, the nitric oxide donor SNAP and silicone oil were combined into a single platform using a simple solvent swelling method to increase the antimicrobial properties and decrease the foreign body response of the material. The SR-SNAP-Si cannulas resulted in a stable, prolonged NO release similar to that of the native endothelium (0.5 - 4 × 10^{-10} mol cm^{-2} min^{-1}), exhibited minimal SNAP and silicone oil leaching, and maintained sliding angles < 15° for 3 weeks. As a result, SR-SNAP-Si optimally decreased the viability of adhered *S. aureus* by 99.2 ± 0.2% compared to control cannulas after exposure in a 7-d CDC biofilm bioreactor. Moreover, the combination of a NO-releasing, liquid-infused platform was evaluated for the first time in a 21-d subcutaneous mouse model, reducing the fibrous encapsulation thickness by 60.9 ± 6.1% and decreasing cell density within 100 μm of the implant site by 60.8 ± 10.5%. In conclusion, this work demonstrates the potential of the combined NO-releasing, liquid-infused interface for deterring foreign body response, chronic inflammation, and infection, which is paramount for improving the long-term usability of medical devices including insulin pumps, sensors and monitors, and port catheters.

5.6 References

1. Anderson JM, Rodriguez A, Chang DT. Foreign body reaction to biomaterials. Semin Immunol. 2008;20(2):86-100.

2. Selders GS, Fetz AE, Radic MZ, Bowlin GL. An overview of the role of neutrophils in innate immunity, inflammation and host-biomaterial integration. Regen Biomater. 2017;4(1):55-68.

3. Bridges AW, Garcia AJ. Anti-inflammatory polymeric coatings for implantable biomaterials and devices. J Diabetes Sci Technol. 2008;2(6):984-94.

4. Hauzenberger JR, Hipszer BR, Loeum C, McCue PA, DeStefano M, Torjman MC, et al. Detailed Analysis of Insulin Absorption Variability and the Tissue Response to Continuous Subcutaneous Insulin Infusion Catheter Implantation in Swine. Diabetes Technol Ther. 2017;19(11):641-50.

5. Witherel CE, Abebayehu D, Barker TH, Spiller KL. Macrophage and Fibroblast Interactions in Biomaterial-Mediated Fibrosis. Adv Healthc Mater. 2019;8(4):e1801451.

6. VanEpps JS, Younger JG. Implantable Device-Related Infection. Shock. 2016;46(6):597-608.

7. Rigo S, Cai C, Gunkel-Grabole G, Maurizi L, Zhang X, Xu J, et al. Nanoscience-Based Strategies to Engineer Antimicrobial Surfaces. Adv Sci (Weinh). 2018;5(5):1700892.

8. Hetrick EM, Prichard HL, Klitzman B, Schoenfisch MH. Reduced foreign body response at nitric oxide-releasing subcutaneous implants. Biomaterials. 2007;28(31):4571-80.

9. Hou Z, Wu Y, Xu C, Reghu S, Shang Z, Chen J, et al. Precisely Structured Nitric-Oxide-Releasing Copolymer Brush Defeats Broad-Spectrum Catheter-Associated Biofilm Infections In Vivo. ACS Cent Sci. 2020;6(11):2031-45.

10. Sharma JN, Al-Omran A, Parvathy SS. Role of nitric oxide in inflammatory diseases. Inflammopharmacology. 2007;15(6):252-9.

11. Schairer DO, Chouake JS, Nosanchuk JD, Friedman AJ. The potential of nitric oxide releasing therapies as antimicrobial agents. Virulence. 2012;3(3):271-9.

12. Wang X, Jolliffe A, Carr B, Zhang Q, Bilger M, Cui Y, et al. Nitric oxide-releasing semi-crystalline thermoplastic polymers: preparation, characterization and application to devise anti-inflammatory and bactericidal implants. Biomater Sci. 2018;6(12):3189-201.

13. Brisbois EJ, Major TC, Goudie MJ, Bartlett RH, Meyerhoff ME, Handa H. Improved hemocompatibility of silicone rubber extracorporeal tubing via solvent swelling-impregnation of S-nitroso-N-acetylpenicillamine (SNAP) and evaluation in rabbit thrombogenicity model. Acta Biomaterialia. 2016;37:111-9.

14. Goudie MJ, Pant J, Handa H. Liquid-infused nitric oxide-releasing (LINORel) silicone for decreased fouling, thrombosis, and infection of medical devices. Sci Rep. 2017;7(1):13623.

15. Sotiri I, Tajik A, Lai Y, Zhang CT, Kovalenko Y, Nemr CR, et al. Tunability of liquid-infused silicone materials for biointerfaces. Biointerphases. 2018;13(6):06D401.

16. Moerman F, Partington E. Chapter 30 - Novel Materials of Construction in the Food Industry. In: Lelieveld H, Holah J, Gabrić D, editors. Handbook of Hygiene Control in the Food Industry (Second Edition). San Diego: Woodhead Publishing; 2016. p. 395-444.

17. Wei C, Zhang G, Zhang Q, Zhan X, Chen F. Silicone Oil-Infused Slippery Surfaces Based on Sol-Gel Process-Induced Nanocomposite Coatings: A Facile Approach to Highly Stable Bioinspired Surface for Biofouling Resistance. ACS Appl Mater Interfaces. 2016;8(50):34810-9.

18. Chug MK, Feit C, Brisbois EJ. Increasing the Lifetime of Insulin Cannula with Antifouling and Nitric Oxide Releasing Properties. ACS Applied Bio Materials. 2019;2(12):5965-75.

19. Homeyer KH, Goudie MJ, Singha P, Handa H. Liquid-Infused Nitric-Oxide-Releasing Silicone Foley Urinary Catheters for Prevention of Catheter-Associated Urinary Tract Infections. Acs Biomater Sci Eng. 2019;5(4):2021-9.

20. Singha P, Goudie MJ, Liu Q, Hopkins S, Brown N, Schmiedt CW, et al. Multipronged Approach to Combat Catheter-Associated Infections and Thrombosis by Combining Nitric Oxide and a Polyzwitterion: a 7 Day In Vivo Study in a Rabbit Model. ACS Appl Mater Interfaces. 2020;12(8):9070-9.

21. Goudie MJ, Brisbois EJ, Pant J, Thompson A, Potkay JA, Handa H. Characterization of an S-nitroso-N-acetylpenicillamine-based nitric oxide releasing polymer from a translational perspective. Int J Polym Mater. 2016;65(15):769-78.

22. Chug MK, Feit C, Brisbois EJ. Increasing the Lifetime of Insulin Cannula with Antifouling and Nitric Oxide Releasing Properties. ACS Applied Bio Materials. 2019.

23. Brisbois EJ, Major TC, Goudie MJ, Bartlett RH, Meyerhoff ME, Handa H. Improved hemocompatibility of silicone rubber extracorporeal tubing via solvent swelling-impregnation of S-nitroso-N-acetylpenicillamine (SNAP) and evaluation in rabbit thrombogenicity model. Acta Biomater. 2016;37:111-9.

24. Patel PJ, Benasi K, Ferrari G, Evans MG, Shanmugham S, Wilson DM, et al. Randomized trial of infusion set function: steel versus teflon. Diabetes Technol Ther. 2014;16(1):15-9.

25. Malone-Povolny MJ, Bradshaw TM, Merricks EP, Long CT, Nichols TC, Schoenfisch MH. Combination of Nitric Oxide Release and Surface Texture for Mitigating the Foreign Body Response. Acs Biomater Sci Eng. 2021;7(6):2444-52.

26. Wo Y, Xu LC, Li Z, Matzger AJ, Meyerhoff ME, Siedlecki CA. Antimicrobial nitric oxide releasing surfaces based on S-nitroso-N-acetylpenicillamine impregnated polymers combined with submicron-textured surface topography. Biomater Sci. 2017;5(7):1265-78.

27. Brisbois EJ, Kim M, Wang XW, Mohammed A, Major TC, Wu JF, et al. Improved Hemocompatibility of Multilumen Catheters via Nitric Oxide (NO) Release from S-Nitroso-N-acetylpenicillamine (SNAP) Composite Filled Lumen. Acs Appl Mater Inter. 2016;8(43):29270-9.

28. Major TC, Handa H, Annich GM, Bartlett RH. Development and hemocompatibility testing of nitric oxide releasing polymers using a rabbit model of thrombogenicity. J Biomater Appl. 2014;29(4):479-501.

29. Lowe A, Bills J, Verma R, Lavery L, Davis K, Balkus KJ, Jr. Electrospun nitric oxide releasing bandage with enhanced wound healing. Acta Biomater. 2015;13:121-30.

30. Povoa VCO, Dos Santos G, Picheth GF, Jara CP, da Silva LCE, de Araujo EP, et al. Wound healing action of nitric oxide-releasing self-expandable collagen sponge. J Tissue Eng Regen Med. 2020;14(6):807-18.

31. Vaughn MW, Kuo L, Liao JC. Estimation of Nitric Oxide Production and Reactionrates in Tissue by Use of a Mathematical Model. Am J Physiol Heart Circ Physiol. 1998;274(6):H2163-H76.

32. Rong F, Tang Y, Wang T, Feng T, Song J, Li P, et al. Nitric Oxide-Releasing Polymeric Materials for Antimicrobial Applications: A Review. Antioxidants (Basel, Switzerland). 2019;8(11):556.

33. Pant J, Goudie MJ, Hopkins SP, Brisbois EJ, Handa H. Tunable Nitric Oxide Release from S-Nitroso-N-acetylpenicillamine via Catalytic Copper Nanoparticles for Biomedical Applications. ACS Appl Mater Interfaces. 2017;9(18):15254-64.

34. MacCallum N, Howell C, Kim P, Sun D, Friedlander R, Ranisau J, et al. Liquid-Infused Silicone As a Biofouling-Free Medical Material. Acs Biomater Sci Eng. 2015;1(1):43-51.

35. Manna U, Raman N, Welsh MA, Zayas-Gonzalez YM, Blackwell HE, Palecek SP, et al. Slippery Liquid-Infused Porous Surfaces that Prevent Microbial Surface Fouling and Kill Non-Adherent Pathogens in Surrounding Media: A Controlled Release Approach. Adv Funct Mater. 2016;26(21):3599-611.

36. Nowakowska M, Jarosz-Chobot P, Polanska J, Machnica L. Bacterial strains colonizing subcutaneous catheters of personal insulin pumps. Pol J Microbiol. 2007;56(4):239-43.

37. Kratochvil MJ, Welsh MA, Manna U, Ortiz BJ, Blackwell HE, Lynn DM. Slippery Liquid-Infused Porous Surfaces that Prevent Bacterial Surface Fouling and Inhibit Virulence Phenotypes in Surrounding Planktonic Cells. ACS Infect Dis. 2016;2(7):509-17.

38. Friedman A, Blecher K, Sanchez D, Tuckman-Vernon C, Gialanella P, Friedman JM, et al. Susceptibility of Gram-positive and -negative bacteria to novel nitric oxide-releasing nanoparticle technology. Virulence. 2011;2(3):217-21.

39. Hetrick EM, Shin JH, Paul HS, Schoenfisch MH. Anti-biofilm efficacy of nitric oxide-releasing silica nanoparticles. Biomaterials. 2009;30(14):2782-9.

40. Garren MR, Ashcraft M, Qian Y, Douglass M, Brisbois EJ, Handa H. Nitric oxide and viral infection: Recent developments in antiviral therapies and platforms. Appl Mater Today. 2021;22:100887-.

41. Li W, Zhou J, Xu Y. Study of the in vitro cytotoxicity testing of medical devices. Biomed Rep. 2015;3(5):617-20.

42. Hopkins SP, Pant J, Goudie MJ, Schmiedt C, Handa H. Achieving Long-Term Biocompatible Silicone via Covalently Immobilized S-Nitroso- N-acetylpenicillamine (SNAP)

That Exhibits 4 Months of Sustained Nitric Oxide Release. ACS Appl Mater Interfaces. 2018;10(32):27316-25.

43. Champeau M, Povoa V, Militao L, Cabrini FM, Picheth GF, Meneau F, et al. Supramolecular poly(acrylic acid)/F127 hydrogel with hydration-controlled nitric oxide release for enhancing wound healing. Acta Biomater. 2018;74:312-25.

44. Colthurst MJ, Williams RL, Hiscott PS, Grierson I. Biomaterials used in the posterior segment of the eye. Biomaterials. 2000;21(7):649-65.

45. Romano MR, Ferrara M, Gatto C, Giurgola L, Zanoni M, Angi M, et al. Safety of silicone oils as intraocular medical device: An in vitro cytotoxicity study. Exp Eye Res. 2020;194:108018.

46. Su JT, Simpson SM, Sung S, Tfaily EB, Veazey R, Marzinke M, et al. A Subcutaneous Implant of Tenofovir Alafenamide Fumarate Causes Local Inflammation and Tissue Necrosis in Rabbits and Macaques. Antimicrobial Agents and Chemotherapy. 2020;64(3):e01893-19.

47. Kim JO, Noh JK, Thapa RK, Hasan N, Choi M, Kim JH, et al. Nitric oxide-releasing chitosan film for enhanced antibacterial and in vivo wound-healing efficacy. Int J Biol Macromol. 2015;79:217-25.

48. Chen J, Howell C, Haller CA, Patel MS, Ayala P, Moravec KA, et al. An immobilized liquid interface prevents device associated bacterial infection in vivo. Biomaterials. 2017;113:80-92.

49. Howell C, Grinthal A, Sunny S, Aizenberg M, Aizenberg J. Designing Liquid-Infused Surfaces for Medical Applications: A Review. Adv Mater. 2018;30(50):e1802724.

50. Sutherland DW, Jr., Zhang X, Charest JL. Water Infused Surface Protection as an Active Mechanism for Fibrin Sheath Prevention in Central Venous Catheters. Artif Organs. 2017;41(10):E155-E65.

51. Amadeu TP, Seabra AB, de Oliveira MG, Costa AM. S-nitrosoglutathione-containing hydrogel accelerates rat cutaneous wound repair. J Eur Acad Dermatol Venereol. 2007;21(5):629-37.

52. Gifford R, Batchelor MM, Lee Y, Gokulrangan G, Meyerhoff ME, Wilson GS. Mediation of in vivo glucose sensor inflammatory response via nitric oxide release. J Biomed Mater Res A. 2005;75(4):755-66.

53. Doll K, Fadeeva E, Schaeske J, Ehmke T, Winkel A, Heisterkamp A, et al. Development of Laser-Structured Liquid-Infused Titanium with Strong Biofilm-Repellent Properties. ACS Appl Mater Interfaces. 2017;9(11):9359-68.

54. Yao X, Dunn SS, Kim P, Duffy M, Alvarenga J, Aizenberg J. Fluorogel elastomers with tunable transparency, elasticity, shape-memory, and antifouling properties. Angew Chem Int Ed Engl. 2014;53(17):4418-22.

55. Bridges AW, Whitmire RE, Singh N, Templeman KL, Babensee JE, Lyon LA, et al. Chronic inflammatory responses to microgel-based implant coatings. J Biomed Mater Res A. 2010;94(1):252-8.

56. Nichols SP, Koh A, Brown NL, Rose MB, Sun B, Slomberg DL, et al. The effect of nitric oxide surface flux on the foreign body response to subcutaneous implants. Biomaterials. 2012;33(27):6305-12.

CHAPTER 6:

CONCLUSIONS AND FUTURE DIRECTIONS

6.1 Conclusions

Due to multifunctional antimicrobial and hemocompatible surface properties, NO-releasing materials have been well-documented to reduce device-induced thrombosis and infection both *in vitro* and *in vivo*. However, despite decades of development, NO-releasing materials 1) have a limited NO reservoir, 2) lack of NO release tunability, and 3) do not prevent biofouling, potentially affecting clinical efficacy. Therefore, this dissertation focused on combining NO-releasing platforms with different surface modifications that can mitigate these limitations (i.e., metal nanoparticles, liquid infusion), and the antimicrobial and hemocompatible efficacies of the joint surface strategies were thoroughly evaluated. In addition, these studies were the first to evaluate tunable NO release and antifouling, NO-releasing surfaces in *in vivo* models, highlighting the importance of combining different surface strategies to improve the biocompatibility of medical devices.

In Chapter 2, a layered SNAP-doped polymer with a blended Se-polymer interface was fabricated to combine both NO-releasing properties (from the polymer) and NO-generating capabilities (from Se interactions with GSNO in the surrounding environment). After 24 h of *in vitro* exposure, the SNAP-Se-1 platform reduced the viability of both adhered Gram-positive *S. aureus* (~2.39 log reduction) and Gram-negative *E. coli* (~2.25 log reduction) compared to unmodified materials. SNAP-Se-1 materials also significantly reduced *in vitro* platelet adhesion

by 85.5% compared to corresponding controls and did not cause any significant cytotoxic effect towards NIH 3T3 mouse fibroblasts. This study was the first to combine NO-generating and NO-releasing technologies into a single platform, and these results highlight the prospective utility of SNAP-Se-1 as a multifunctional hemocompatible and antimicrobial platform capable of both NO-releasing and NO-generating properties to improve the safety and longevity of blood-contacting materials. This work has been published in *ACS Applied Materials & Interfaces*(1).

In Chapter 3, a copper nanoparticle (Cu NP) catalyst coating for the tunable, catalyzed release of NO was combined with a polymeric GSNO coating applied to commercial Tygon S3^{TM} E-3603 poly(vinyl chloride) tubing. Cu-GSNO samples exhibited higher levels of NO release over the same incubation period, with an NO flux ranging from $6.3 \pm 0.9 \times 10^{-10}$ mol cm^{-2} min^{-1} to $7.1 \pm 0.4 \times 10^{-10}$ mol cm^{-2} min^{-1} after 4 h of release, while GSNO loops without Cu NPs only ranged from an initial flux of $1.1 \pm 0.2 \times 10^{-10}$ mol cm^{-2} min^{-1} to $2.3 \pm 0.2 \times 10^{-10}$ mol cm^{-2} min^{-1} after 4 h of release. As a result, Cu GSNO samples exhibited more potent antimicrobial effects against *S. aureus* (~3 log reduction) and *P. aeruginosa* (~1 log reduction) *in vitro*. Moreover, this study was the first to evaluate the combination of NO-releasing surfaces with a copper catalyst for improved hemocompatibility *in vivo*. Cu GSNO samples best maintained platelet counts (89.3% of baseline platelet count) in a 4 h *in vivo* rabbit ECC study, while control loops only maintained 67.6% of the baseline count. These results highlight the importance of tunable NO-releasing surfaces to improve the hemocompatibility and antimicrobial properties of materials used for blood-contacting applications. This work has been published in *ACS Applied Bio Materials*(2).

In Chapters 4 & 5, SNAP-incorporated materials were combined with an antifouling, liquid-infused interface achieved via silicone oil infusion, and the antibacterial, biocompatible, and antifouling efficacies of the combined surface strategies were monitored *in vitro* and *in vivo*. In

Chapter 4, SNAP was covalently attached to PDMS, which was subsequently infused with silicone oil to achieve both sustained NO-releasing chemistry and antifouling surface properties. Optimized surfaces exhibited consistent, elevated NO release profiles (> 0.5 x 10^{-10} mol cm^{-2} min^{-1}) for 30 d, virtually no SNAP leaching, and low sliding angle measurements (~20°). The synthesized materials exhibited potent antimicrobial efficacies (>90% reduction) against Gram-positive MRSA and Gram-negative *P. aeruginosa* after 24 h, 7 d, 14 d, and 28 d of bacterial exposure. Moreover, the combined material reduced *in vitro* fibrinogen adsorption by 30.3 ± 10.2% and platelet adhesion by 66.5 ± 11.2%, demonstrating great potential for blood-contacting applications.

In Chapter 5, SNAP-impregnated silicone rubber cannulas were similarly infused with silicone oil to achieve an antifouling interface, and the material's efficacy in reducing bacterial colonization and minimizing foreign body response was evaluated *in vitro* and *in vivo*, respectively. Similar to the findings in Chapter 4, this material demonstrated a stable, prolonged NO release (0.5 - 4 × 10^{-10} mol cm^{-2} min^{-1}) during a 3-week incubation period, exhibited minimal SNAP leaching, and maintained sliding angles < 15 ° for 21 d. In a 7-d CDC biofilm reactor, SR-SNAP-Si substrates reduced adhered *S. aureus* viability by >99% compared to unmodified SR controls and did not exhibit any cytotoxic effects towards 3T3 mouse fibroblasts *in vitro*. Finally, SR-SNAP-Si cannulas were evaluated for the first time in 14- and 21-d subcutaneous mouse models, reducing the thickness of the fibrous encapsulation around the implant by 60.9 ± 6.1% and resulting in a 60.8 ± 10.5% reduction in cell density around the implant site after 3 weeks. This study was the first to evaluate combined bioactive NO-releasing surfaces with an antifouling liquid-infused interface in an *in vivo* mouse model, and validates that antifouling, NO-releasing surfaces provide both antimicrobial properties while mitigating fibrous encapsulation, which can improve the

lifetime and safety of indwelling materials. This work has been published in *ACS Applied Materials & Interfaces*(3).

In summary, this dissertation work focuses on the combination of NO-releasing materials with other surface strategies to improve the lifetime of NO production at the material interface (NO-releasing + NO-generating surfaces), improve the NO release tunability to achieve more potent antimicrobial and hemocompatible effects (NO-releasing surface + metal NP catalyst), and reduce biofouling from protein, bacteria, and platelets (NO-releasing surface + antifouling interface). All materials demonstrated improved antimicrobial and antithrombotic properties *in vitro* and/or *in vivo* without resulting in any cytotoxicity. However, future studies that further elucidate NO release levels needed for specific applications still need to be conducted (discussed in Section 6.2).

6.2 Future Directions

In this dissertation, the hemocompatibility and antimicrobial efficacy of material surfaces were improved through heightened NO release via catalytic nanoparticles. The results from this work demonstrated a straightforward, simple method of tuning NO flux from NO-releasing materials. However, the extent to which increasing the NO surface flux positively affects biocompatibility has yet to be fully explored. Although NO-releasing surfaces have routinely improved the antimicrobial and hemocompatible surface properties of different biomaterials and medical devices *in vitro* and *in vivo*, the impact on specific NO release profiles on bacterial viability, platelet activity, protein adsorption and conformation, and mammalian cell viability is not well understood. Moreover, high doses of NO may be cytotoxic towards mammalian cells. Defining a target NO release profile for specific application requirements is needed for optimizing clinical efficacy while minimizing potential costs (**Figure 6.1**).

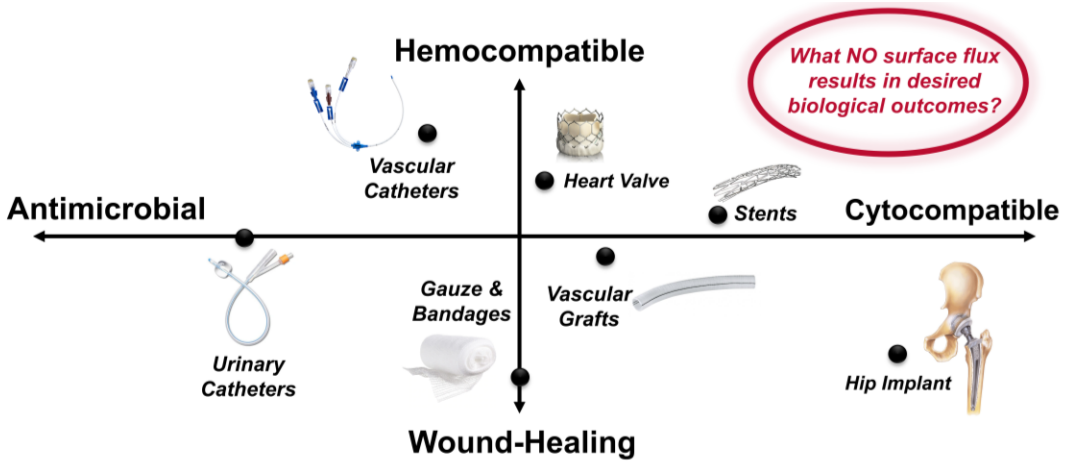

Figure 6.1. Desired surface properties for different medical devices are often at the expense of other surface properties. Therefore, NO release profiles required to achieve device-specific needs is vital for optimizing clinical efficacy.

Although NO's effect on bacterial pathogens has been demonstrated both *in vitro* and *in vivo*, the exact range of NO release needed to achieve antimicrobial efficacy has yet to be determined. In the body, high concentrations of NO (> 1 µM) are released by immune cells to directly combat invading pathogens through the generation of reactive nitrogen and oxygen intermediates that can alter DNA, inhibit enzyme functions, and lead to lipid peroxidation(4). Moreover, bacteria within biofilms treated with low doses of NO have been shown to transition back to a planktonic state, increasing bacterial susceptibility to antibiotics(5). In fact, co-treating bacteria with NO and antibiotics can slow the development of antibiotic resistance(6). Interestingly, surfaces with NO release levels as low as ~0.1 x 10^{-10} mol cm^{-2} min^{-1} have still been able to reduce the viability of adhered *S. aureus* by ~60%(7). Understanding the NO release levels required to achieve bactericidal properties, anti-biofilm characteristics, and deterred antibiotic resistance development is essential while improving interfaces intended to resist infection.

In addition to affecting bacterial viability, different NO levels can potentially modulate protein adsorption, platelet activation and adhesion, and hemolysis. NO inhibits platelet activation

through increasing cGMP, modulating Ca^{2+} influx, and inhibiting GPIIb/IIIa expression(8, 9). Interestingly, however, previous studies have found the NO-releasing materials can actually slightly increase fibrinogen adsorption yet remain non-thrombogenic(10). The effect of NO release on protein conformation is not well understood. In addition to alterations in platelet and protein activity, although some NO-releasing substrates have shown to be non-hemolytic, the threshold of NO release compatible with RBCs has yet to be determined(11). Therefore, a better understanding of NO release on vital blood components is needed to determine the safety and antithrombotic efficacy of NO-releasing materials for blood-contacting applications.

Finally, depending on the concentration and cell line, NO can promote cell proliferation and wound healing or can be cytotoxic towards mammalian cells. In the body, NO has been linked to the promotion of angiogenesis, cell proliferation and differentiation, and collagen deposition(12). However, high concentrations of NO can result in mammalian cell death due to oxidative stress, DNA damage, and disruption in cytosolic calcium(13). Therefore, the NO release exhibited by indwelling medical devices should be tightly regulated to ensure the safety of NO-releasing materials while promoting wound healing and mitigating foreign body response and inflammation.

To analyze the effect of different NO release profiles on pathogens, mammalian cells, and blood components, several different design aspects must be considered. First, significant amounts of NO donor leaching into the surrounding environment can lead to physiological effects (eg., increased cytotoxicity and delocalized NO release) otherwise not observed. Therefore, minimizing leaching is crucial to truly correlate the effect of different NO release profiles on material-environment interactions. One method that can resolve this issue is through the use of materials that have NO donors covalently bound to the surface, which exhibit virtually no leaching(14).

Another design consideration is the ability to easily and predictably control NO release to achieve different test NO release profiles. Previous studies have found that increasing NO donor storage in a material does not directly correlate to higher stabilized NO fluxes and can alter material's mechanical properties (15, 16). However, NO release from RSNOs can be modulated through the utilization of a catalyst (light, heat, metal NPs). Although this dissertation highlighted the tunability of NO release using metal NPs, the leaching of metal NPs can itself impact bacterial and mammalian cell viability(2). Moreover, most *in vitro* studies predicting clinical efficacy are performed at a maintained temperature of 37 °C, eliminating heat as a tool to modulate NO release. Therefore, light catalysis remains the only viable option to modulate NO release in real-time without contributing additional variables. Previous studies have demonstrated that RSNOs can be easily tuned by visible light(17). However, the method of light exposure and dosage must remain consistent between NO release measurements and *in vitro* analysis in order to accurately correlate the impact of NO release on pathogens, blood components, and mammalian cells. **Figure 6.2** shows a schematic of a potential light setup to ensure that the light treatments remain the same regardless of the study, so that the level of NO release can be accurately predicted.

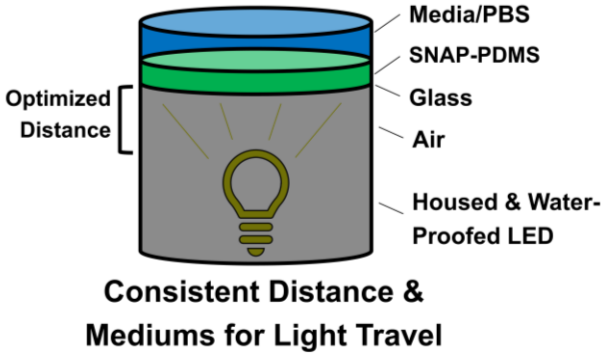

Figure 6.2. Schematic of light setup to modulate NO release from an NO-releasing SNAP-PDMS surface, ensuring that the distance and mediums that the light travels through remains consistent.

In summary, this dissertation work demonstrated that by modulating the NO release through the inclusion of catalytic nanoparticles, the hemocompatibility and antimicrobial efficacy

of biomaterials can be improved. However, an in-depth study understanding the implications of NO release profiles on the body has yet to be conducted. Although NO-releasing materials have shown promising *in vitro* and *in vivo* antimicrobial and hemocompatible surface properties, an NO-releasing medical device has yet to reach market. Understanding the relationship between NO release profiles and pathogen viability, platelet adhesion, protein adsorption and conformation, and mammalian cell proliferation is essential in better designing and predicting the clinical efficacy of NO-releasing materials for specific applications.

6.3 References

1. Mondal A, Douglass M, Hopkins SP, Singha P, Tran M, Handa H, et al. Multifunctional S-Nitroso-N-acetylpenicillamine-Incorporated Medical-Grade Polymer with Selenium Interface for Biomedical Applications. ACS Appl Mater Interfaces. 2019;11(38):34652-62.

2. Douglass ME, Goudie MJ, Pant J, Singha P, Hopkins S, Devine R, et al. Catalyzed Nitric Oxide Release via Cu Nanoparticles Leads to an Increase in Antimicrobial Effects and Hemocompatibility for Short-Term Extracorporeal Circulation. ACS Applied Bio Materials. 2019;2(6):2539-48.

3. Douglass M, Hopkins S, Chug MK, Kim G, Garren MR, Ashcraft M, et al. Reduction in Foreign Body Response and Improved Antimicrobial Efficacy via Silicone-Oil-Infused Nitric-Oxide-Releasing Medical-Grade Cannulas. ACS Applied Materials & Interfaces. 2021.

4. Schairer DO, Chouake JS, Nosanchuk JD, Friedman AJ. The potential of nitric oxide releasing therapies as antimicrobial agents. Virulence. 2012;3(3):271-9.

5. Barraud N, Storey MV, Moore ZP, Webb JS, Rice SA, Kjelleberg S. Nitric oxide-mediated dispersal in single- and multi-species biofilms of clinically and industrially relevant microorganisms. Microbial Biotechnology. 2009;2(3):370-8.

6. Rouillard KR, Novak OP, Pistiolis AM, Yang L, Ahonen MJR, McDonald RA, et al. Exogenous Nitric Oxide Improves Antibiotic Susceptibility in Resistant Bacteria. ACS Infectious Diseases. 2021;7(1):23-33.

7. Hopkins SP, Pant J, Goudie MJ, Schmiedt C, Handa H. Achieving Long-Term Biocompatible Silicone via Covalently Immobilized S-Nitroso- N-acetylpenicillamine (SNAP) That Exhibits 4 Months of Sustained Nitric Oxide Release. ACS Appl Mater Interfaces. 2018;10(32):27316-25.

8. Douglass M, Hopkins S, Pandey R, Singha P, Norman M, Handa H. S-Nitrosoglutathione-Based Nitric Oxide-Releasing Nanofibers Exhibit Dual Antimicrobial and Antithrombotic Activity for Biomedical Applications. Macromol Biosci. 2020:e2000248.

9. Simon-Walker R, Romero R, Staver JM, Zang Y, Reynolds MM, Popat KC, et al. Glycocalyx-Inspired Nitric Oxide-Releasing Surfaces Reduce Platelet Adhesion and Activation on Titanium. Acs Biomater Sci Eng. 2017;3(1):68-77.

10. Zang Y, Popat KC, Reynolds MM. Nitric oxide-mediated fibrinogen deposition prevents platelet adhesion and activation. Biointerphases. 2018;13(6):06e403.

11. Brisbois EJ, Major TC, Goudie MJ, Meyerhoff ME, Bartlett RH, Handa H. Attenuation of thrombosis and bacterial infection using dual function nitric oxide releasing central venous catheters in a 9day rabbit model. Acta Biomater. 2016;44:304-12.

12. Luo JD, Chen AF. Nitric oxide: a newly discovered function on wound healing. Acta Pharmacol Sin. 2005;26(3):259-64.

13. Murphy MP. Nitric oxide and cell death. Biochimica et Biophysica Acta (BBA) - Bioenergetics. 1999;1411(2):401-14.

14. Hopkins SP, Frost MC. Synthesis and Characterization of Controlled Nitric Oxide Release from S-Nitroso-N-Acetyl-d-Penicillamine Covalently Linked to Polyvinyl Chloride (SNAP-PVC). Bioengineering (Basel). 2018;5(3).

15. Goudie MJ, Brisbois EJ, Pant J, Thompson A, Potkay JA, Handa H. Characterization of an S-nitroso-N-acetylpenicillamine-based nitric oxide releasing polymer from a translational perspective. Int J Polym Mater. 2016;65(15):769-78.

16. Brisbois EJ, Major TC, Goudie MJ, Bartlett RH, Meyerhoff ME, Handa H. Improved hemocompatibility of silicone rubber extracorporeal tubing via solvent swelling-impregnation of S-nitroso-N-acetylpenicillamine (SNAP) and evaluation in rabbit thrombogenicity model. Acta Biomater. 2016;37:111-9.

17. Lautner G, Stringer B, Brisbois EJ, Meyerhoff ME, Schwendeman SP. Controlled light-induced gas phase nitric oxide release from S-nitrosothiol-doped silicone rubber films. Nitric Oxide. 2019;86:31-7.